



Published in final edited form as:

Chem Rev. 2020 June 24; 120(12): 5252–5307. doi:10.1021/acs.chemrev.9b00629.

BIOLOGICAL AND BIOINSPIRED INORGANIC N–N BOND FORMING REACTIONS

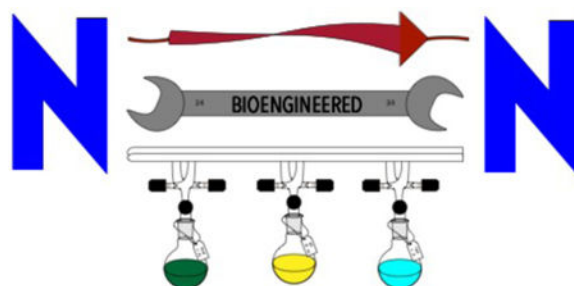
Christina Ferousi, Sean H. Majer, Ida M. DiMucci, Kyle M. Lancaster

Department of Chemistry and Chemical Biology, Baker Laboratory, Cornell University, Ithaca, NY USA 14853

Abstract

The metallobiochemistry underlying the formation of the inorganic N–N-bond-containing molecules nitrous oxide (N_2O), dinitrogen (N_2), and hydrazine (N_2H_4) is essential to the lifestyles of diverse organisms. Similar reactions hold promise as means to use N-based fuels as alternative, carbon-free energy sources. This review discusses research efforts to understand the mechanisms underlying biological N–N bond formation in primary metabolism and how the associated reactions are tied to energy transduction and organismal survival. These efforts comprise studies of both natural and engineered metalloenzymes, as well as synthetic model complexes.

Graphical Abstract



1. Introduction

Nitrogen accesses eight oxidation states. In three of these oxidation states, nitrogen forms simple, isolable compounds bearing N–N bonds: nitrous oxide (N_2O) with N^I , dinitrogen gas (N_2) with N^0 , and hydrazine (N_2H_4) with N^{-II} . Nature has leveraged the energetics underlying the formation and cleavage of these N–N-bond featuring species as key steps in the primary metabolisms of microorganisms exhibiting multiple diverse lifestyles. Invariably, the mechanisms driving these bond formations harness the redox flexibility of transition metal-containing cofactors. Understanding the means by which protein matrices tune transition metal properties for N–N bond formation can potentially deliver insights into the use of N-based fuels, and also can inspire technologies enabling selective heteroatom-heteroatom bond formations. The importance of the latter facet has recently been discussed

at lengths in the context of secondary metabolite biosynthesis and thus will not be covered here.¹ For additional reading on N–N bond containing natural products, the reader is directed to References 2,3. Here we will focus on the metallobiochemistry of N–N bond formation in primary metabolism, discussing the tremendous strides that have been made to understand these processes while also highlighting gaps in our knowledge and the new research opportunities these afford.

Section 2 will describe biological reactions that produce N₂O. N₂O is a linear triatomic molecule that can be drawn with resonance structures featuring either double (N=N) or triple (N≡N) bonds between the nitrogen atoms. N₂O has multiple uses including serving as an oxidant in rocket propellants,⁴ enhancing the performance of internal combustion engines, functioning as a culinary aerosol propellant, or acting as a mild anaesthetic/dissociative.⁵ Industrially, N₂O is produced by the controlled decomposition of ammonium nitrate (NH₄NO₃) to N₂O and H₂O via the following reaction:⁶



Despite its utility, N₂O is a potent greenhouse gas with ca. 300 times the global warming potential of carbon dioxide (CO₂) that has also been shown to be an ozone-depleting agent.⁷ Consequently, its release into the atmosphere is of environmental concern. Currently, most anthropogenic N₂O release is associated with agriculture and land use.⁷ This can be traced in large part to the fact that N₂O is a product of several enzymatic pathways within the biogeochemical nitrogen cycle. N₂O is an intermediate in denitrification produced by nitric oxide (NO)-reducing enzymes, and N₂O has also been shown to be a by-product of biological ammonia (NH₃) oxidation, or nitrification.⁸ NO (or some redox congener thereof) contributes one of N₂O's N-atoms in either case.

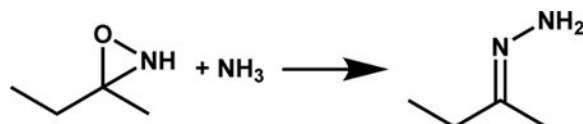
Section 5 will discuss biological reactions that form N₂. N₂ comprises ca. 70% of Earth's atmosphere. Despite this, N is among the most limiting nutrient in any ecosystem.⁹ This is due in part to the inert nature of N₂; N must be rendered bioavailable through cleavage of the homodinuclear triple N≡N bond to generate assimilable species such as ammonia or nitrate (NO₃⁻).^{10–12} The former species can also act as a chemical fuel¹³ for nitrifying microbes and anammox bacteria, while the latter serves as a respiratory electron acceptor for denitrifying bacteria. In either case, the final metabolic product returns N to the atmosphere as a stable, non-toxic gas that can readily re-enter the biogeochemical N cycle. Consequently, reactions that form N₂ are of tremendous interest because they offer a way to harness reduced N-species as clean-burning, carbon-free fuels (e.g. in fuel cell applications)^{14–18} or as a final product for reactions to remediate N pollution.¹⁹

Finally, Section 7 will discuss the metallobiochemistry underlying N₂H₄ formation. This is a particularly exciting, new area of investigation owing to the fact that N₂H₄ was only recently discovered to be a primary metabolite.²⁰ This came as some surprise, because N₂H₄ is a highly reactive compound that, when anhydrous, forms N₂ and H₂O upon contact with air. N₂H₄ and its derivatives are known to be toxic and putatively carcinogenic to mammals. As early as in 1894, the acute toxicity and high mortality rate of this newly discovered

compound was proven via direct administration to dogs.²¹ Ironically, some decades later the organic derivative mono-methylhydrazine was identified in two mycotoxins (gyromitrin and agaritine) that were isolated from edible varieties of mushrooms (*Gyromitra* and *Agaricus* species).^{22–25} Regardless, ample applications make use of its high reducing power and reactivity. Consequently, N_2H_4 is produced on industrial scales. The most recently invented process for N_2H_4 production with industrial significance is the so-called Peroxide or Pechiney–Ugine–Kuhlmann process (Equations 2–5) that was established in the 1970s²⁶ and significantly diverges from the original Raschig route. The world's largest hydrazine hydrate plant currently in use operates under this process.²⁷



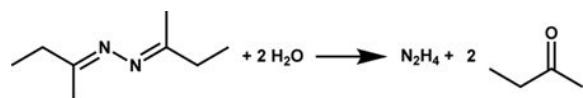
(2)



(3)



(4)



(5)

Among its many uses, N_2H_4 performs exceptionally as a rocket fuel. For example, monopropellant N_2H_4 engines are used in auxiliary power units of military aircraft and for terminal spacecraft descent, such as the Phoenix lander and the Curiosity rover that landed on Mars in 2008 and 2012, respectively.^{28–30} Juno, a NASA space probe, entered Jupiter's orbit in 2016 powered by a bipropellant engine fueled by hydrazine.³¹ As will be discussed in Section 5.2, effectively the same chemistry (albeit carried out in a gentler fashion) is harnessed by anammox bacteria.

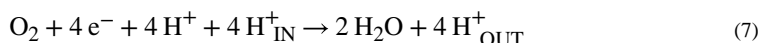
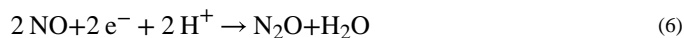
In the case of each N–N-bond bearing species under discussion, the structures and functions of metalloenzymes known to produce these species will be introduced. The state of

understanding of the mechanisms used to forge N–N bonds will be described, with controversies and knowledge gaps highlighted. Where available, advances in understanding contributed from either the preparation and study of both artificial metalloenzymes or model complexes will be covered.

2. N₂O-Forming Enzymes

2.1. Nitric Oxide Reductase (NOR)

2.1.1. Heme Copper Oxygenase (HCO) superfamily—NO reductases (NORs) comprise enzymes within the heme Cu oxidase (HCO) superfamily that catalyze the reductive conversion of NO to N₂O (Equation 6), either as part of prokaryotic denitrification or as a detoxification mechanism.^{32–34} The HCO superfamily is a large and diverse group of integral membrane oxidoreductases involved in aerobic and anaerobic respiration as well as detoxification processes.³⁵ All HCOs share a structurally conserved core catalytic subunit while some also feature secondary subunits that are involved in electron transport or regulation (Figure 1). HCOs are principally classified based on the primary chemical reaction they catalyze, although cross-reactivity has been observed.^{36–39} Cytochrome c oxidases (CcOs), or alternatively termed heme Cu oxygen reductases, couple the four-electron reduction of dioxygen (O₂) (Equation 7) to proton translocation, conserving energy in the form of an electrochemical cross-membrane gradient. This process concludes cellular aerobic respiration (for further reading on CcOs see Reference 40 and references therein). In contrast to CcOs, no NOR homolog characterized thus far has been shown to pump protons across the membrane from the negative to the positive side. However, some NORs are electrogenic since the protons needed for water formation (chemical protons) are taken up from the negative side of the membrane (e.g. cytoplasm).



2.1.2. HCO Active Site Template—The subunit compositions of HCO complexes and the coordination geometries of their active sites are variable, but their catalytic subunits exhibit high overall sequence and structural conservation. All members of the HCO superfamily harbor a binuclear active site and an electron-transfer heme site within their subunit I. The binuclear center (BNC) consists of a five-coordinate, high-spin *b*-heme denoted by a subscript 3, and a non-heme metal. In CcOs, this metal is a Cu ion (Cu_B) that is coordinated by three conserved histidine residues. The side chain of one of these histidines is covalently linked to the aromatic ring of a second-sphere tyrosine that is implicated in electron and proton donation during catalysis (e.g., *ba*₃ oxidase; PDBID: 1XME).⁴¹ NORs, on the contrary, support non-heme Fe ions (Fe_B) and exhibit higher variability in their inner-coordination spheres. A conserved histidine and three variable residues ligate Fe_B, while a second-sphere glutamate, that is suggested to serve as a proton-relay site, is variably present depending on the NOR subfamily (Figure 2).

2.1.3. NOR Classes—Most NORs characterized to date fall within distinct families based on the identity of their physiological electron donor: cytochrome NORs (cNORs) receive electrons from soluble *c*-type cytochromes (cyts) or pseudoazurin,⁴³ while quinone NORs (qNORs) receive electrons from the quinone/quinol pool.⁴⁴ The kinetic properties of different NORs have been studied either in isolated cellular membranes or homogeneous NOR preparations with the use of Clark-type electrodes (see Reference 45 and references therein). Steady-state NOR activity is second order with respect to NO, consistent with the sequential binding of two molecules of NO to the active site. Additionally, NORs have been shown to be inhibited at relatively low NO concentrations (ca. 10 μ M), leading to sigmoidal kinetics.⁴⁶ Genomic identification of putative NORs is based upon the primary structure conservation of subunit I of all members of the HCO superfamily, together with some diagnostic domains and residues specific to the NOR family. The inherent difficulty in purification and crystallization of integral membrane proteins, such as NORs, has presumably led to the scarcity of isolated and structurally resolved representatives of this family. However, based on genomic surveys and structural predictions, three more NOR families have been proposed:⁴⁷ eNOR,⁴⁸ gNOR,^{49,50} and sNOR.^{45,51–53} Distinguishing features of these predicted NOR subfamilies include subunit composition, cofactor identity, and putative electron and proton transfer pathways. Nevertheless, the mechanistic details of the reductive conversion of NO to N₂O are assumed to be conserved within the NOR class.

Recently, the discovery of nitrite-driven anaerobic methane oxidation catalyzed by oxygenic bacteria spurred a hypothesis for an additional member of the NOR class of proteins.⁵⁴ According to a working model for this metabolism, this protein—NO dismutase (NOD)—carries out the redox-neutral conversion of NO into O₂ and dinitrogen (N₂).^{55–57} The putative NOD is predicted to harbor a BNC that conforms to the HCO active site template, and the protein bears some homology to the qNOR family. Sequence substitutions obviate any electron or proton channels towards the BNC, biasing the activity towards dismutation. Studies of this putative NOD enzyme may yield the identification of a unique mechanism for biological N–N bond formation, but the protein has yet to be isolated and characterized.

2.1.4. cNOR Active Site Architecture—The cNORs comprise the first identified and the most studied NOR subfamily, with the first representatives being isolated from *Pseudomonas stutzeri*⁵⁸ and *Paracoccus denitrificans*⁵⁹ ca. 30 years ago. The *Pseudomonas aeruginosa* isolate (PaNOR) has been structurally characterized via a 2.7 Å crystal structure (PDBID: 3OOR)⁶⁰ and serves as a key model for structural and mechanistic studies. The only other deposited structure of a cNOR comes from *Roseobacter denitrificans* (RdNOR) at 2.85 Å resolution (PDBID: 4XYD),⁶¹ while extensive biochemical and spectroscopic studies have been performed on isolated enzymes from *P. denitrificans*, *P. stutzeri*, *Halomonas halodenitrificans*, and *P. aeruginosa* (References^{58,59,62–66} and references below).

cNOR is an integral membrane heterodimeric protein complex that consists of a large catalytic subunit I (NorB; 56 kDa) and a small electron-transfer subunit II (NorC; 17 kDa). The NorB subunit spans the cytoplasmic membrane via 12 α -helices, one of which interacts with the single N-terminal transmembrane helix (TMH) of the NorC subunit. The hydrophilic domain of NorC resides in the periplasmic space and lies over NorB, creating the largest interaction surface between the two subunits (Figure 3). This globular hydrophilic

domain houses a *c*-type heme with histidine and methionine as the axial Fe ligands. The hydrophobic core of NorB harbors a catalytic *b*-type heme (denoted as heme *b*₃) with a single histidine axial ligand, a low-spin *b*-type heme with saturated coordination sites (*bis*-His), and non-heme FeB, that is ligated by three conserved histidine residues and a glutamate (Glu211) (Figure 4). A calcium ion (Ca²⁺) is present at the interface of NorB and NorC and is interacting with the propionates of the two *b*-hemes, a glutamate residue from NorB, a tyrosine and a glycine residue from NorC, and a water molecule. In the fully oxidized resting state, the heme *b*₃ Fe and FeB are kept at a metal-to-metal distance of 3.8 Å by a μ₂-oxo ligand.

In the case of RdNOR, an additional metal ion is bound by three residues of the NorC subunit and it faces the periplasm (Figure 5). X-ray anomalous scattering studies suggested that this metal could be either Cu or Zn,⁶¹ but inductively-coupled plasma mass spectrometry (ICP-MS)⁶⁷ and electron paramagnetic resonance (EPR)⁶⁸ analyses provided further support for the presence of Cu in the isolated protein complex. The 14 Å edge-to-edge distance of this metal ion from the *c*-type heme of the same subunit does not rule out electron transfer, but any such activity is likely to be slow.⁶⁹ Also, the residues coordinating this putative Cu ion are not conserved among cNOR sequences, suggesting that the site may not be essential for the catalytic conversion of NO to N₂O. Its surface-exposed nature raises the possibility of mediating protein-protein interactions. Terasaka and co-workers⁷⁰ probed the hypothesized intracellular association of the NO-forming *cd*₁ nitrite reductase (NiR) and the cNOR from *P. aeruginosa*—two enzymes that carry out sequential catalysis as part of the denitrification process. This study identified a super-complex comprising one *cd*₁ NiR homodimer and two cNOR heterodimers, although a 1:1 ratio of NiR to cNOR appears more physiologically relevant due to the restricted spatial arrangement of the membrane embedded cNOR. Regardless of the stoichiometry of the super-complex, the interface was formed between the heme *c* domain of *cd*₁ NiR and the soluble domain of NorC, possibly implicating the additional metal cofactor of RdNOR in such an interaction *in vivo*. However, a simpler structural role for this additional metal ion cannot be excluded.

2.1.5. cNOR Electron and Proton Transfer—Reductive conversion of NO to N₂O and H₂O requires the input of two electrons and two protons (Equation 6) that need to reach the buried active site cleft that resides within the NorB subunit. Whole-cell studies carried out in the late 1980s suggested that the periplasmic space is the source of the necessary protons for NO reduction,⁷¹ while the NOR-catalyzed reaction was found to be non-electrogenic.⁷² Since then, various independent studies have unambiguously proven that both electrons and protons are supplied from the periplasmic space. Inspection of the PaNOR structure, combined with biochemical data collected over the years, has revealed a likely interprotein pathway for electron transfer (Figure 6a). Cyt *c*₅₅₀ and/or pseudoazurin, the most probable physiological electron donors to cNOR,^{73–75} likely docks on the NorBC complex at the periplasmic hydrophilic domain of NorC in a manner similar to what was recently seen for the mitochondrial CcO.^{76,77} The six-coordinate, low-spin *c*-type heme of the NorC subunit is close enough to this interface to serve as the entry point for the electrons. A histidine and an alanine residue oriented toward the heme *b* propionates could shuttle electrons to the heme *b*₃ either via direct contact of the neighboring methyl groups of

the heme moieties or through a conserved phenylalanine residue. The Ca²⁺ ion identified within the active site pocket presumably plays a structural role in maintaining the necessary protein conformation for efficient electron transfer.

In contrast to CcOs, no proton transfer pathway connecting the active site with the cytoplasm was observed, in agreement with the non-electrogenic nature of cNOR (*vide supra*).^{78,79} Instead, two potential water channels and hydrogen-bonding networks formed by protonatable and/or polar amino acids, leading from the periplasmic side of the membrane to the buried active site, were identified (Figure 6b). The terminal branch of this network is formed by three highly conserved glutamate residues (Glu211, Glu215, and Glu280 in PaNOR structure) that are associated with the catalytic competence of cNOR.^{78,80,81} Structure-based molecular dynamics (MD) simulations further evaluated these putative water channels and brought forward an additional one that is not evident from a static crystal structure and may implicate protein dynamics in gating proton transfer.⁸²

2.1.6. qNOR Active Site Architecture and Electron Transfer Pathways—Two members of the qNOR subfamily have been structurally characterized, one from *Geobacillus stearothermophilus* resolved at 2.5 Å (GsNOR; PDBID: 3AYF),⁴⁴ and another one from *Neisseria meningitidis* (NmNOR; PDBID: 6FWF),⁸³ albeit at much lower resolution (4.5 Å). NO reduction to N₂O at the catalytic center of qNOR is believed to proceed the same way as in cNOR proteins (*vide infra*). However, their cofactor composition together with some minor but crucial changes in the primary structure suggest probable differences in electron and proton transfer pathways within the NOR family.

The qNOR class comprises monomeric integral membrane proteins encoded by the highly conserved *norZ* gene. As evident from primary structure analyses, NorZ is a fusion protein with the first 30% of its sequence aligning to the NorC subunit of cNOR. Although the TMH that is present in NorC is conserved, the CXXCH heme binding motif is missing, and the resolved GsNOR structure revealed the absence of any heme cofactor embedded in the protein.⁴⁴ A large portion of NorZ is homologous to NorB, while an additional TMH brings the total to 14 TMHs for the complete protein (Figure 7). The absence of the *c* heme from the hydrophilic NorC portion of qNOR does not perturb this domain's cyt *c* fold. This is likely because bulky hydrophobic residues take the place of the porphyrin. The absence of the electron entry heme *c* moiety from the periplasmic side of the enzyme is in agreement with previous studies, where purified representatives of the qNOR subfamily could not accept electrons from reduced cyt *c*. Instead, quinol analogs were shown to be suitable electron donors for the catalytic conversion of NO by qNOR.^{84,85} The cocrystal structure of GsNOR with the quinol analog 2-heptyl hydroxyquinoline N-oxide (HQNO) revealed the quinol-binding site of qNOR (PDBID: 3AYG, Figure 8).⁴⁴ A histidine and an aspartate residue together with a second-sphere glutamate (His328, Asp746, and Glu332) position the HQNO molecule within a hydrophobic pocket 10 Å away from the *bis*-His coordinated heme *b*. The latter lies 13.7 Å away from the active site heme *b*₃ that is part of a highly conserved BNC. Adhering to the general HCO template, the BNC of GsNOR consists of a catalytic heme *b*₃ and a non-heme metal that are positioned 4.6 Å apart in the fully oxidized resting state. A water molecule bridges these metals (Figure 9). Anomalous difference Fourier maps of the resolved structure suggested Zn as the non-heme metal (ZnB).

Interestingly, the choice of detergent during NOR purification seemed to affect the identity of the coordinated metal in this position, as shown by ICP atomic emission spectroscopy (AES); homogenous and active preparations of GsNOR were found to contain both Fe_B and Zn_B, whereas in the cases where only Zn_B was detected, the enzyme was inactive.⁴⁴ Atomic absorption spectroscopy on purified and active NmNOR excluded Zn as a metal cofactor, but the low-resolution structure obtained for this protein does not allow for definitive identification of the metal occupying the non-heme site.⁸³ It is unlikely that the Zn_B center corresponds to any physiological state of qNOR- it rather appears to be a purification artifact- but in lieu of any high-resolution qNOR (Fe_B) structure, the GsNOR (Zn_B) serves as a model for qNOR structural observations. Like Fe_B in cNOR, this Zn_B center is coordinated by three invariable histidine residues. However, the fully conserved glutamate in both cNOR and qNOR sequences is moved away from the Zn_B center, in contrast to the cNOR structures where it is the fourth ligand to Fe_B (Glu211 in PaNOR; Glu512 in GsNOR; Glu494 in NmNOR). According to MD simulations, the TMH harboring Glu494 appears flexible enough to imply possible coordination of the glutamate carboxylate to the non-heme metal—either Zn_B or Fe_B—upon slight conformational changes.⁴⁴ Identical to the cNOR structures, a Ca²⁺ ion coordinated by Gly91, Tyr93, Glu429, and the propionates of both hemes is identified within the hydrophobic cavity of the BNC.

2.1.7. NOR Proton Transfer Pathways—The cNOR structures indicated the absence of any proton transfer pathway from the cytoplasmic side of the membrane that would render cNOR electrogenic. Meanwhile, these structures suggested two possible water networks connecting the bulk solvent of the periplasm with the active site. Inspection of the qNOR structure though, concluded that both periplasm-facing channels are probably non-operational, due to structural differences between cNOR and qNOR (Figure 10). In one case, a hydrophobic alanine residue is present in qNOR in place of an aspartate in cNOR that blocks the water network around the interface of the NorB and NorC regions. The other channel is completely absent owing to the different conformation of the C-terminus of the NorC hydrophilic domain.⁸⁶

The fully conserved glutamate residues of the hydrophobic active site cavity (Glu512 and Glu581 in PaNOR) are also present in both qNOR structures and allow for the formation of a water cluster. In contrast to PaNOR though, the only hydrophilic channel identified in qNORs extends from this water cluster towards the cytoplasm and is lined with polar residues (Figure 10B). The cytoplasmic proton entry site of GsNOR appears to be formed by a salt bridge between a lysine and a glutamate residue that were found to be indispensable for catalytic activity based on mutagenesis studies.⁴⁴ Molecular dynamics simulations focused on the water network formed within this channel suggested that this could serve as a catalytic proton transfer pathway that would function according to the Grotthuss mechanism as in all characterized members of the HCO superfamily.^{44,86} In the case of NmNOR, the lysine at the opening of the cytoplasmic water channel is replaced by a serine, but the overall properties of the putative water channel appear conserved. Extensive mutagenesis studies on NmNOR showed that a functional cytoplasmic channel is necessary for complete NO reductase activity, although poor non-heme Fe incorporation in some variants could have also been the reason for the reduced NO reactivity observed.⁸³ More importantly,

reconstitution of purified NmNOR in liposomes and kinetics experiments unambiguously demonstrated that the reductive conversion of NO by NmNOR was coupled to proton translocation across the membrane.⁸³ This finding corroborates the previous hypothesis about the electrogenic nature of qNOR and, based on sequence conservation, supports the possibility of the qNOR subfamily substantially differing from cNOR with regards to intracellular energy conservation.

2.1.8. NOR Catalytic Mechanism—The mechanistic details of the reductive conversion of NO to N₂O by HCO-type NORs are not fully understood, but three hypothetical mechanisms have been extensively scrutinized, both experimentally and computationally: a trans-mechanism and two cis-mechanisms, the cis-heme *b*₃ and the cis-FeB (Scheme 1a). These studies are exclusively focused on cNORs, but the mechanisms for other members of the class are expected to follow suit. Interestingly, spectroscopic studies on the NOR activity of various CcOs suggest yet another mechanism for this class of the HCO superfamily,^{88–90} but this topic is beyond the scope of the current review.

In the resting ferric state, a μ₂-oxo ligand whose presence was validated through detailed assignment⁹¹ of a resonance Raman band at ca. 810 cm⁻¹ as *v*_{as}(Fe–O–Fe) (as = antisymmetric) maintains non-heme FeB and the heme *b*₃ Fe at a close distance. Based on comparisons to model complexes, the resonance Raman data suggested a distance of 3.5 Å, close to the ca. 3.8–3.9 Å determined in the PaNOR crystal structure.⁶⁰ The expected antiferromagnetic coupling of the Fe centers mediated by this bridge offers an explanation for the EPR-silence of the ferric enzyme.^{46,92} In this resting state, the heme *b*₃ Fe is five-coordinate as evidenced by resonance Raman studies,⁹³ indicating that the proximal histidine is dissociated from the heme *b*₃ Fe (Scheme 1b, intermediate 1). The bridging oxo ligand may draw the heme *b*₃ Fe out of the porphyrin plane, facilitating the cleavage of the heme Fe-histidine bond.⁶⁶ Contrasting conclusions were drawn, though, for the *Marinobacter hydrocarbonoclasticus* (formerly *Pseudomonas nautica*) purified NOR (MhNOR)—⁵⁷Fe Mössbauer and EPR data were interpreted as indicative of a low-spin, possibly six-coordinate heme *b*₃.⁹⁴

In one version of the trans mechanism, the μ₂-oxo ligand dissociates upon complete reduction of the protein, with concomitant association of the proximal histidine to the heme *b*₃ Fe (Scheme 1b, intermediate 2). This results in elongation of the distance between the now ferrous centers to 4.2 Å.^{93,95} In the crystal structures of carbon monoxide (CO)- and aldoxime-bound reduced PaNOR (PDBID: 3WFC and 3WFD, respectively), the Fe–Fe distance increases to 4.4 Å, but no other conformational changes are detectable.⁹⁵ The non-heme FeB and the heme *b*₃ Fe then each bind one NO, resulting in the formation of two Fe-nitrosyl species (Scheme 1b, intermediate 3). In an alternative sequence of events, Fe_B is reduced while the heme *b*₃ Fe remains oxidized. It is not until NO binds to both Fe centers that further reduction occurs.⁹⁶ Regardless, the relatively short Fe–Fe distance within the BNC of PaNOR can plausibly accommodate the binding of two NO molecules and likely plays a vital role in the efficiency of the N–N bond formation by arranging the substrate molecules in close proximity to each other.

The heme b_3 Fe-nitrosyl complex has been optically resolved by flow flash photolysis, where it was assigned as the first intermediate of the reaction of *P. denitrificans* cNOR (PdNOR) with NO that occurred within 2 μ s upon photolysis.⁷⁹ The reconstructed spectrum was similar to the reduced myoglobin NO adduct⁹⁷ with a trough at 430 nm and a peak at 410 nm, overall characteristic for ligand binding to reduced high-spin hemes. Time- and temperature-dependent rapid freeze quench (RFQ) EPR studies identified two Fe-nitrosyl signals within 0.5 ms from NO addition.⁶⁶ The $g = 4.0$ signal was assigned to the ferrous FeB–NO species, as it was consistent with the previously reported {FeNO}⁷ systems with the $S = 3/2$ ground state of non-heme Fe proteins and their model complexes.^{66,79,91–94} (The {FeNO}^X nomenclature follows Enemark-Feltham⁹⁸ notation wherein the superscript X denotes the sum of electrons in the metal d -orbital manifold and the electrons in the NO π^* orbitals.) The other signal at g ca. 2.0 exhibited a set of three lines that can be assigned to the hyperfine splitting by the ¹⁴N nucleus ($I = 1$) of the bound NO to a low spin ferrous heme ($g_z = 2.012$, $g_{x,y} = 2.08$, $^{NO}A_z = 1.6$ mT). Therefore, it was assigned as the five-coordinate ferrous heme b_3 –NO species, further supporting the dissociation of histidine from the heme b_3 Fe upon NO binding. The formation of a diiron dinitrosyl has been preceded in synthetic functional models of NOR (see Section 4.1). The subsequent step in the proposed catalytic cycle involves formation of a diiron-bridged hyponitrite ($N_2O_2^{2-}$) complex that has never been observed (Scheme 1b, intermediate 4). This could come about either by the nucleophilic attack of one nitrosyl to the other or via the combination of both nitrosyl species in a radical coupling process.^{46,99,100} Notably, Daskalakis and co-workers¹⁰¹ used UV-Raman spectroscopy to probe a protein-bound $N_2O_2^{2-}$ intermediate during the catalytic cycle of cNOR from *P. denitrificans*, where the heme b_3 Fe was in the ferric state and the $\nu(N-N) = 1332$ cm^{-1} mode was assigned to the N–N stretching vibration of the hyponitrite species.¹⁰²

In the final step of this proposed mechanism, N–O bond cleavage promoted by donation of protons from the solvent leads to N_2O and H_2O release from the NOR active site, resulting in a short-lived species where both Fe centers are in the ferric state and the heme b_3 Fe is ligated by the proximal histidine (Scheme 1b, intermediate 5).⁶⁶ The second turnover (Scheme 1b, intermediates 6–7) proceeds in a manner analogous to the first. Two scenarios could occur to close the cycle: a return to the oxo-bridged diferric (Scheme 1b, intermediate 1) with NO supplying the oxo, or the pathway could traverse an un-bridged diferric intermediate (Scheme 1b, intermediate 8) poised to accept electrons.

Ferrous nitrosyl species are often stable, and this stability could promote off-pathway reactivity during catalysis.^{103–105} Consequently, cis mechanisms have been proposed that exclude the formation of such intermediates. According to one working hypothesis, referred to as the cis-Fe_B mechanism, the non-heme Fe_B is the only substrate-binding site (Scheme 1a), and catalysis proceeds via the formation of a dinitrosyl Fe complex (DNIC). This species is denoted {Fe(NO)₂}⁹. DNICs have been implicated in NO storage as well as mammalian immune response.^{106,107} That such species exist has been supported by the synthesis of [Fe(NO)₂(Im)]₄ (Im = imidazolate), which exhibits an EPR signal near $g = 2.03$ shared by putative biological DNICs.^{108,109} Meanwhile, heme b_3 's proposed roles are some combination of (a) mediating electron transfer, (b) enforcing proper orientation of the FeB-

bound NO molecules, and/or (c) the N–O bond cleavage.¹⁰⁰ Following the formation of the DNIC at the non-heme Fe_B, an Fe_B-bound N₂O₂²⁻ intermediate is hypothesized, followed by subsequent N–O bond cleavage. However, Speelman and co-workers¹¹⁰ contend that N–N bond formation between NO units in an {Fe(NO)₂}⁹ DNIC is highly unfavorable due to the anti-ferromagnetic coupling between each NO and Fe, which causes a parallel alignment of the NO spins. N–N bond formation necessitates antiparallel spin alignment—the spin-flip barrier thus presents a likely origin for the lack of N–N bond formation observed from synthetic DNICs.

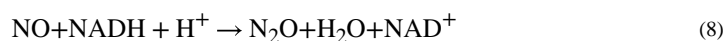
Prevention of the formation of a stable heme *b*₃ {FeNO}⁷ species during the initial step of NO binding to NOR could be achieved by a mixed-valent state of the enzyme, where heme *b*₃ would remain oxidized. Redox titrations of PdNOR determined the reduction potential of heme *b*₃ to be about 200 mV lower than that of Fe_B, making this a plausible relevant state during catalysis.¹¹¹ It should be noted that two independent electrochemical studies on PaNOR and MhNOR homologs determined different values for the formal midpoint potentials of the metal centers. Kato, Yagi, and co-workers¹¹² used spectroelectrochemistry (specifically, surface enhanced infrared spectroscopy) to determine reduction potentials of –0.11 V and –0.44 V vs. the normal hydrogen electrode (NHE) for Fe_B and heme *b*₃, respectively. The latter value was found to occur near the onset of electrocatalytic NO reduction, suggesting that NO reduction was initiated at heme *b*₃ and thus prompting the authors to favor the trans mechanism. Meanwhile, Cordas and co-workers¹¹³ assigned the Fe_B reduction potential at ca. –0.37 V and heme *b*₃ at –0.16 V vs. the saturated calomel electrode (SCE) (–0.129 and +0.081 V vs. NHE, respectively). These findings were used to favor reduction at the Fe_B site and thus, a cis mechanism.

An alternative scenario that would favor exclusive non-heme Fe_B NO binding was described for MhNOR. In this study, complete reduction of all metal centers of MhNOR was necessary for reactivity to occur, and ferrous heme *b*₃ was described as a low-spin center (even at room temperature) with an axial His coordination and a μ₂-oxo (or μ₂-hydroxo) bridge to Fe_B. This six-coordinated ligation state is believed to decrease the heme affinity for NO and, thus, promote binding of NO to the Fe_B instead.⁹⁴ An alternative hypothetical cis mechanism for NO reduction by NORs, the cis-heme *b*₃ mechanism, bears a resemblance to the P450_{nor} mechanism in that it primarily involves a high-spin heme for substrate binding (see Section 2.2, Scheme 2).^{8,114} Resonance Raman studies on the NO reductase activity of *cbb*₃ oxidase from *P. stutzeri* alluded to a similar mechanism by identifying a five-coordinate ferrous heme *b*₃ nitrosyl species ($\nu(\text{N–O}) = 1679 \text{ cm}^{-1}$, $\nu(\text{Fe–NO}) = 524 \text{ cm}^{-1}$) as a catalytic intermediate.¹¹⁵ Computational studies on the NOR catalytic mechanism strongly favor the cis-heme *b*₃ hypothesis based on free energy profiles of putative intermediates and transition states.¹¹⁶ In this mechanism, NO binds to the ferrous heme *b*₃, partially oxidizing it, while the oxygen is coordinated by the ferrous non-heme Fe_B. Although ferrous heme nitrosyl complexes are generally quite stable, density functional theory (DFT) calculations using the dispersion-corrected B3LYP-D3 hybrid density functional^{117,118} predicted this species to be an intermediate in the reaction. The interaction of the non-heme Fe_B with the oxygen atom of NO is suggested to electrostatically polarize the heme-nitrosyl. The metal-bound nitrosyl species is then attacked by a second NO molecule to generate a hyponitrite radical that is asymmetrically bridging the diiron center via double oxygen coordination to the non-heme

FeB.^{116,119} The N₂O₂²⁻-bridged diiron intermediate (Scheme 1b, intermediate 4) implicated in the trans mechanism was calculated to be ca. 30 kcal·mol⁻¹ higher in energy relative to this cis-heme *b*₃ N₂O₂²⁻ intermediate.

2.2. P450nor

2.2.1. P450nor Classification, Structure and Function—According to field experiments, fungal denitrification appears to be the major contributor to global environmental N₂O fluxes.^{120–122} Fungal NORs, unlike prokaryotic NORs, belong to the cyt P450 superfamily of enzymes which are more commonly known for selectively oxidizing C–H bonds.^{123–127} This makes the so-called P450nors a peculiar case of enzymes that evolved from performing monooxygenase activity to reductive chemistry on a substrate (Equation 8).¹²⁸



Shoun and co-workers¹²⁹ reported the first purification of a P450nor enzyme from *Fusarium oxysporum*, wherein they initially observed lipoxygenase activity and similar properties to canonical P450s. Only later did they serendipitously find that this enzyme was actually involved in denitrification, as the enzyme was specifically induced by NO₃⁻ and nitrite (NO₂⁻).¹³⁰

P450nor is a soluble, *b*-heme enzyme that is axially coordinated by a cysteinate ligand, similar to other members of the P450 superfamily. P450nor amino acid sequences share up to 40% and on average 25% identity with other members of the P450 superfamily.¹³¹ Interestingly, fungal P450nor is more closely related to bacterial rather than eukaryotic P450s, and thus P450nor has been proposed to originate from horizontal gene transfer.¹³² P450nors exist in two isoforms that are localized in different parts of the cell. However, their origins appear to stem from different genetic mechanisms. For example, the genome of *Cylindrocarpon tonkinense* encodes for two separate P450nor proteins: P450nor1 (*cyp55A2*, mitochondrial isoform) and P450nor2 (*cyp55A3*, cytoplasmic isoform).^{133,134} In the case of *F. oxysporum*, the two isoforms are derived from the same gene (*cyp55*) but are translated at different initiation codons, one of them in frame with a mitochondrial leader sequence.¹³⁵ The localization of these isoforms also appears to be associated with stereoselectivity for nicotinamide adenine dinucleotide (NADH) or nicotinamide adenine dinucleotide phosphate (NADPH) redox partners: *C. tonkinense* P450nor1 specifically employs NADH while P450nor2 uses both, albeit with higher affinity for NADPH.^{136,137} This specificity has also been linked to the tertiary structures of the enzymes.

The first X-ray crystal structure of P450nor from *F. oxysporum* was reported in 1997 by Park and co-workers (PDBID: 1CL6, Figure 11a).¹³¹ The overall protein fold does not deviate dramatically from canonical cyt P450 monooxygenases. However, the distal pocket of the heme has a few interesting rearrangements to the P450 protein scaffold: The *F*- and *G*-helices (per cyt P450 nomenclature) and the loop between them show significant thermal motion, which is common to P450 enzymes. This region has been implicated as a substrate channel and thus plausibly expected to be highly dynamic. However, unlike canonical

P450s, the P450nor structure shows the *F*- and *G*-helices oriented in a “flipped up” conformation which allows for a significantly more solvent-exposed heme pocket. A similar difference in solvent access is noticeable with the relative orientation of the *B*'-helix, a structural element which has been implicated in the aforementioned NADH/NADPH selectivity (Figure 11b).¹³⁷ It was postulated by Park and co-workers¹³¹ that these “open” features of the tertiary structure allow either NADH or NADPH to participate in NO reduction by entering the distal pocket during catalysis.

Key features of P450nor are its direct binding and redox interactions with the NADH/NADPH cofactor.^{128,138} The NADH/NADPH binds in the distal pocket through global conformational changes and participation with multiple amino acid side chains. Upon NADH/NADPH entry, the *F*-helix closes off the distal pocket by a movement of ca. 3 Å, engulfing the cofactor.¹³⁹ Two arginine residues (Arg64 and Arg174; numbering as in *F. oxysporum* P450nor) to a positively charged cluster which aids in binding and specifically binds to one of the co-substrate pyrophosphates.¹³⁶ Another essential residue is a conserved threonine (Thr243) on the distal *I*-helix. This residue forms a hydrogen-bonding network with a carbonyl oxygen of the main chain (Ala239) via two water molecules, and it has been implicated in proton shuttling.¹³¹ A follow-up study by Okamoto and co-workers¹⁴⁰ found that when the conserved Thr243 was mutated to hydrophobic residues the catalytic activity was significantly reduced. These authors attributed this to a disruption of the hydrogen-bonding network at the distal *I*-helix. This is partly true: while acting as a proton-relay may be one role of Thr243, it clearly also (along with the peptide-nitrogen from Gly240) orients the NADH/NADPH properly during catalysis by hydrogen bonding with the carbonyl moiety of the nicotinamide ring.¹³⁹ This, in concert with one of the propionate arms of the porphyrin and a serine residue (Ser286), imposes constraints on the cofactor dynamics and positions the pro-*R* side of the C4-hydrogens to face the substrate. Currently, the proton relay in this system is proposed to be composed of the distal Ser286 and an aspartate (Asp393) that appear to be essential for maintaining the hydrogen-bonding network of solvent molecules in the pocket.^{136,137,141–143}

2.2.2. P450nor Mechanism—Fungal P450nors are distinguished from bacterial NOR enzymes (see Section 2.1) by their mediation of efficient catalysis ($\sim 1200 \text{ s}^{-1}$ at 10°C for *F. oxysporum*) at a *single* metal cofactor rather than employing two metal centers as with bacterial NORs or flavodiiron proteins (FDPs) (*vide infra*, Section 2.5) (Scheme 2).¹⁴⁴ Resting P450nor exists in a low-spin, ferric state with a Soret UV-vis absorption maximum at 415 nm and a $\text{Fe}^{\text{II/III}}$ reduction potential of -0.307 V vs. NHE.^{144–146} The EPR spectrum obtained at 5 K of the resting ferric enzyme exhibits a minor high-spin ($g = 7.97, 4.12, 1.75$) and a dominant low-spin ($g = 2.44, 2.26, 1.91$) component.¹⁴⁷ ^{57}Fe Mössbauer data also support a low-spin assignment for the ferric resting state ($E_{\text{q}} = -2.96 \text{ mm}\cdot\text{s}^{-1}$, $\delta = 0.32 \text{ mm}\cdot\text{s}^{-1}$).¹⁴⁸ The resting enzyme binds NO with a high on-rate ($2.6 \times 10^7 \text{ M}^{-1}\cdot\text{s}^{-1}$ for *F. oxysporum*) forming a well-studied six-coordinate, ferric nitrosyl $\{\text{FeNO}\}^6$ species with a Soret maximum at 431 nm.^{144,149} The ^{57}Fe Mössbauer spectrum of the $\{\text{FeNO}\}^6$ reveals a decreased isomer shift ($\delta = 0.15 \text{ mm}\cdot\text{s}^{-1}$) with a quadrupole splitting of $E_{\text{q}} = 1.31 \text{ mm}\cdot\text{s}^{-1}$, consistent with a diamagnetic species.¹⁴⁸ Importantly, this $\{\text{FeNO}\}^6$ complex likely oxidizes the NO upon coordination and has been described as having a $\text{Fe}^{\text{II}}\text{-NO}^+$ ground-state

electronic configuration wherein the nitrosonium ion (NO^+) is bent and poised for nucleophilic attack. This bent geometry has been observed crystallographically in the P450nor from *F. oxysporum*. The Fe–N–O angle is 161° , significantly deviating from a linear geometry.¹⁴² However, this geometry may also have been the result of photoreduction of the $\{\text{FeNO}\}^6$ to the $\{\text{FeNO}\}^7$ during synchrotron data collection. A more recent study using X-ray free electron laser data collection provided more robust structural data which also supported a bent geometry at the $\{\text{FeNO}\}^6$ ($\angle_{\text{FeNO}} = 158^\circ$).¹⁵⁰ The *trans*-effect from the axial thiolate induces the NO ligand to bend and weakens both the Fe–NO and N–O by a mixing with the $d_{z^2}-\sigma_n$ and $d_{xz}-\pi^*_{\text{NO}}$ orbitals (Figure 12). The strong donation from the thiolate pushes the $d_{z^2}-\sigma_n$ to higher energy and increases admixture with the $d_{xz}-\pi^*_{\text{NO}}$.^{98,151–156} Praneeth and co-workers¹⁵⁷ noted that while one could envision the $\{\text{FeNO}\}^6$ species assuming a low-spin $\text{Fe}^{3+}-\text{NO}^\cdot$ configuration (ca. $1 \text{ kcal}\cdot\text{mol}^{-1}$ higher in energy), the bent geometry of the NO moiety is not an intrinsic quality of this assignment.

Canonical P450s undergo one-electron reduction events via a redox partner (either ferredoxin reductase/ferredoxin in the case of bacterial/mitochondrial P450 or flavin adenine dinucleotide (FAD)/flavin mononucleotide (FMN) as with eukaryotic P450).^{127,149} One of the key features distinguishing P450nors from other P450s are their ability to accept electrons directly from a precisely positioned NADH/NADPH molecule via hydride transfer (H^-), a physiologically rare redox reaction considering that heme cofactors are typically one-electron redox centers that interact with a mediating redox partner. It was shown by Shiro and co-workers¹⁴⁴ that the $\{\text{FeNO}\}^6$ species from the P450nor of *F. oxysporum* is able to react with NADH rapidly with a rate constant of ca. $1 \times 10^6 \text{ M}^{-1} \text{ s}^{-1}$ at 10°C . Subsequent investigations by Oshima and co-workers¹³⁹ provided structural evidence to support the contention that the $\{\text{FeNO}\}^6$ species undergoes reduction via direct hydride (H^-) transfer from the NADH to form a nitroxyl (HNO) adduct, $\{\text{FeHNO}\}^8$.¹³⁹ These authors crystallized P450nor with an unreactive NADH analogue (nicotinic acid adenine dinucleotide, NAAD) to demonstrate that a hydrogen atom on the C4 position is ca. $1.9\text{--}2.0 \text{ \AA}$ away from the NO^+ (when compared to the structure of the nitrosyl adduct structure from the same organism) (Figure 13). The nicotinic acid ring is appropriately positioned at the heme active site by the aforementioned conserved Thr243, porphyrin propionate, and peptide nitrogen of a glycine residue (Gly240).^{139,140,143}

Further experimental evidence in support of direct hydride transfer to the $\{\text{FeNO}\}^6$ is the accumulation of a 444 nm intermediate (*vide infra*) when using an exogenous H^- -donor such as sodium borohydride. Daiber and co-workers¹⁵⁸ reported kinetic isotope effects for the reaction with monodeutero, C4 NADH of 2.7 and 1.1 for the *R*- and *S*-stereoisomers, respectively. This finding suggests that hydride transfer is both stereoselective and rate-limiting.¹⁵⁸ A wealth of computational studies also support this reactivity of the $\{\text{FeNO}\}^6$.^{143,153,159} Synthetic $\{\text{FeNO}\}^6$ porphyrin complexes have also been observed to undergo direct hydride transfer at the nitrosyl nitrogen.^{160,161} Currently P450nor is the only known member of the P450 superfamily to exhibit this redox behavior. Presumably, the product of this reaction would be a transient $\text{Fe}^{2+}-\text{HNO}$. There is no spectroscopic evidence for this heme–HNO intermediate in P450nor, but there is precedent for its existence based on the surprisingly stable $\text{Fe}^{2+}-\text{HNO}$ species in myoglobin models.^{162,163} The HNO

intermediate presumably remains sufficiently basic to be protonated by the bulk solvent in the distal heme pocket, yielding a hydroxylamide which has been dubbed Intermediate I.
143,144,148,153,158

Intermediate I is the apparent accumulating species under stopped-flow, steady-state turnover conditions with a signature Soret maximum at 444 nm and having a lifetime of ca. 100 ms (Figure 14).^{144,164} The Fe–HNO adduct is believed to undergo a single protonation step. Analogous to the conjugate base of compound II (Fe⁴⁺-hydroxide) in cyt P450 monooxygenase mechanisms, the basicity of the HNO ligand is likely enhanced by the strong electron-donating ability of the cysteine thiolate ligand axially coordinated to the Fe.^{153,165–169} While it has been proposed that the proton is donated from nearby solvent molecules, it has also been suggested that the protein scaffold plays this role. Riplinger and Neese¹⁴³ suggested in a computational study that a nearby aspartate (Asp 393 in *F. oxysporum*) donates a proton to the {FeHNO},⁸ in accordance with experimental data.
131,139,141,142

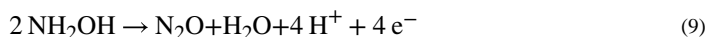
Both the oxidation state of the Fe and the protonation state of the hydroxylamide species in Intermediate I remain under debate. Due to the short-lived nature of Intermediate I, it remains difficult to scrutinize these parameters experimentally. Obayashi and co-workers¹⁶⁴ offered the first characterization of this species via mixed-flow resonance Raman spectroscopy. They reported that the oxidation state of the macrocycle remains constant during Intermediate I formation, obviating storage of electrons by the porphyrin.¹⁷⁰ They also noted a 10 cm⁻¹ isotope shift sensitive to ¹⁴N/¹⁵N NO-labeling at 596/586 cm⁻¹ and concluded that this species cannot be assigned as $\nu(\text{Fe}=\text{N})$, which typically appear at 700–900 cm⁻¹.¹⁷¹ Rather, they assigned this as an $\nu(\text{Fe}-\text{NO})$ stretching mode. Based on their findings, they suggested that the two-electron reduction does not proceed via H⁻-transfer, but rather the NO unit accumulates the negative charge as a Fe^{II}-NO⁻, with the N-atom remaining deprotonated. More recent kinetics, structural, and theoretical evidence disputes this conclusion; H⁻-transfer to the N-atom of the {FeNO}⁶ appears to be the actual path during P450_{nor} catalysis (*vide supra*) and the source of this isotopically sensitive Raman shift remains unclear. Recent investigations into the nature of Intermediate I have focused on the presumption of the Fe²⁺-HNO and its protonation state.

Intermediate I plausibly exists as one of two valence tautomers: one structure features an Fe⁴⁺-NHOH⁻ species while the other structure is Fe³⁺-NHOH[•] (Scheme 2). Computational investigations have probed which of these two tautomers is the most likely, and these studies have also scrutinized the mechanism by which Intermediate I reacts with the second equivalent of NO. One study by Vincent and co-workers¹⁷² proposed that Intermediate I exists as Fe⁴⁺-NHOH⁻, which then binds the second NO and dissociates free hyponitrous acid (H₂N₂O₂) that rapidly decomposes to the enzymatic products. Lehnert and co-workers¹⁵³ have also suggested that Fe⁴⁺-NHOH⁻ is on path, but contend that the H₂N₂O₂ remains bound to the Fe. The NO donates an electron to loosely bind to the NHOH, reducing the formal Fe⁴⁺, followed by an exergonic proton transfer (ca. -16.5 kcal·mol⁻¹) from the bound nitrogen to the neighboring oxygen, resulting in a cyclic [Fe³⁺-N₂O₂H₂] transition state.

A spectroscopic and computational investigation by Riplinger and co-workers,¹⁴⁸ however, caused these authors to favor the Fe³⁺-NHOH* configuration for Intermediate I. Using a combination of magnetic circular dichroism (MCD) and ⁵⁷Fe Mössbauer spectroscopies, the authors concluded that Intermediate I must be a diamagnetic, *S* = 0 species. MCD spectra obtained in the steady-state upon treatment of the {FeNO}⁶ with NADH reveal no discernable features at 445 nm, suggesting that Intermediate I is diamagnetic. This was further supported by both ⁵⁷Fe Mössbauer and EPR spectroscopy; under similar conditions a sharp quadrupole doublet (*E*_q = 1.96 mm·s⁻¹, *d* = 0.24 mm·s⁻¹) was observed as well as barren EPR spectrum. These findings were consistent with reported model complexes competent for NO reduction,¹⁷³ and importantly suggest that Intermediate I likely does not exist as Fe⁴⁺. Thorough computational modelling of this system using both closed shell and broken symmetry DFT methods showed an acceptable comparison to experimental spectroscopic data.¹⁴⁸ The authors concluded that the {FeNO}⁶ species is reduced by NADH in a two-state reaction wherein a spin-inversion participates in the rate-limiting step.¹⁷⁴ The nascent HNO is quickly protonated and cannot be observed experimentally. The second protonation via the distal Asp393 results in a Fe³⁺-NHOH* diradical wherein one spin centered on the N-atom of the NHOH adduct antiferromagnetically couples to the low-spin ferric center, consistent with the experimentally observed diamagnetism. The N–N bond is formed by a spin-recoupling pathway, forming either a Fe³⁺-N₂O₂²⁻, -HN₂O₂⁻, or -H₂N₂O₂ intermediate, which decomposes to release N₂O and H₂O.^{143,148,153} Recent synthetic models produced by Lehnert and co-workers^{175–177} have provided precedent for these final proposed intermediates (see Section 4.1).

2.3. Cytochrome (Cyt) P460

2.3.1. Cyt P460 Classification, Structure, and Function—Cyt P460s are soluble, homodimeric enzymes that catalyze hydroxylamine (NH₂OH) oxidation to N₂O (Equation 9) without producing net reducing equivalents for cellular respiration.¹⁷⁸ In stark contrast to NORs, cyt P460s carry out oxidative rather than reductive reactions to produce N₂O.



Cyt P460 homologs are encountered in genomes of metabolically diverse microorganisms including Proteobacteria, Planctomycetes, Bacteroidetes, Acidobacteria, and methanotrophs^{179–181} and are now recognized to comprise an entire family of *c*-type cytochromes.¹⁸⁰ The first example was purified from the archetypal ammonia oxidizing bacterium (AOB) *Nitrosomonas europaea* by Erickson and Hooper,¹⁸² albeit erroneously assigned at the time. Cyt P460s are commonly found in AOB and are, therefore, associated with the biogeochemical process of nitrification, *i.e.* the complete oxidation of ammonia to NO₃⁻ catalyzed by aerobic AOB^{183–186} and ammonia oxidizing archaea (AOA),^{186–188} nitrite oxidizing bacteria (NOB),^{183,189,190} and complete ammonia oxidizing (comammox) bacteria.^{191,192} Further, they provide a direct enzymatic link between the metabolism of nitrifying organisms and environmental N₂O emissions.^{13,178,193}

Cyt P460s represent a large family of *c*-type cytochromes closely related to proteobacterial cytochromes.¹⁸⁰ They are small homodimeric proteins comprised of ca. 17 kDa monomers

which each bear a single *mono*-His-ligated, *c*-heme cofactor in each subunit that is covalently bound to the polypeptide chain through a canonical CXXCH binding cassette (Figure 16a). The overall protein fold of each monomer is very similar to cytochrome β , and it has been recently suggested by Adams and co-workers¹⁹⁴ that cyt β evolved from cyt P460. While both of these proteins support *c*-hemes, the heme P460 cofactors of cyt P460s are distinguished from standard *c*-hemes such that, in addition to the two thioether linkages, they support an additional covalent C–N cross-link at the 13'-*meso* carbon position by a lysine residue (Figure 15b).^{195,196}

The eponymous heme P460 cofactor derives its name from the position of its Soret near 460 nm in the ferrous state. All known P460 cofactors are *c*-type hemes which support additional covalent attachments to amino acid side chains. Such “non-canonical” cross-links appear to be a hallmark modification of heme enzymes involved in aerobic and anaerobic ammonia oxidation (e.g. hydroxylamine oxidoreductase (HAO) and hydrazine dehydrogenase (HDH, see section 5.2)).^{197,198} Hydrazine synthase (HZS, see section 7.1) also supports an additional Cys-heme cross-link at one of its cofactors, but this has not been designated as a heme P460 at this time (*vide infra*). The cyt P460 cofactor is closely related to the active site of the metabolic AOB enzyme HAO. HAO is similarly competent for NH₂OH oxidation and features a heme P460 active site of slightly different architecture.^{197,199} The HAO P460, rather than being covalently attached at one point by a lysine residue, is attached at two points by a tyrosine residue: One C–C attachment is between a Tyr carbon and the heme 5'-*meso* carbon, while the other attachment is between the phenolic oxygen and an adjacent pyrrole α -carbon (Figure 16b).^{197,199} The HAO cofactor also exhibits a far greater degree of ruffling compared to cyt P460, perhaps due to the nature of its cross-link. This can be quantified using the normal-coordinate structural decomposition method to describe out-of-plane deviations from heme planarity (Figure 16c).^{200,201} One observes that the B1u coefficient (ruffling) of the ferric P460 cofactors is much greater for *N. europaea* HAO compared to cyt P460, which experiences a higher degree of B2u (saddling) deformation. These contortions may, in part, explain the different reactivities observed for these two enzymes. While both enzymes contain heme P460 cofactors and catalyze the oxidation of NH₂OH to NO, their subsequent chemical mechanisms are distinct from each other and fulfill different roles for nitrifiers.^{178,202,203}

Functional cyt P460 bearing the intact heme-Lys cross-link can be recombinantly expressed and purified from heterologous hosts, implicating autocatalysis but at least excluding the necessity of AOB-specific chaperone proteins.^{204,205} Further, site-directed mutagenesis studies of cyt P460 have revealed cross-link formation occurs uniquely with Lys. The mechanism by which the cyt P460 cross-link forms remains unknown, although some reports have speculated in other systems it proceeds through a radical cross-coupling via a Compound I pathway.^{204,206–208} The role of the cyt P460 heme-Lys cross-link in catalysis remains an area of inquiry. Site-directed mutagenesis studies indicate that the heme-Lys cross-link is required for NH₂OH oxidation, although the reason for this requirement is uncertain. An evidentially-substantiated role is to impart rigidity to the cofactor and to avoid NO-dependent axial-His dissociation during catalysis.¹⁰⁴ One proposal suggests that these cross-links disrupt the π -conjugation of the porphyrin and distort the planarity of the macrocycle. This in turn controls the degree of ruffling at the cofactor, which has been

shown to tune the cofactor reduction potential.^{209,210} Another possibility is that the cross-link positions the cofactor within an appropriate distance to essential second-sphere residues which participate in the redox catalysis (*vide infra*).

2.3.2. Cyt P460 Mechanism—For at least 30 years, the oxidation of NH_2OH to NO_2^- by AOB was thought to proceed via a single enzymatic process. This presumed four-electron oxidation would produce the NO_2^- that is the terminal metabolic product of NH_3 oxidation by AOB. This was largely based on activity assays of HAO.^{202,211,212} The major product of aerobic NH_2OH oxidation was indeed NO_2^- , but consistently substoichiometric with respect to NH_2OH (maximum of 60% conversion). The remainder was attributed to the formation of NO_3^- and trace amounts of N_2O .^{202,211} However, under anaerobic conditions these reactions only produced mixtures of NO and N_2O , implicating the necessity of O_2 activation for NO_2^- formation.²⁰² These results were attributed to incomplete NH_2OH oxidation, forming reactive NO and HNO intermediates, the latter product undergoing homocoupling to form N_2O . This model accounted for the products observed but could not explain the origins of O-atoms in assay products. Isotopic ^{18}O -labeling showed the two O-atoms of NO_2^- from AOB are derived from two different sources: O_2 and H_2O .²¹³ This obviates an O_2 -dependent step during NH_2OH oxidation, as the O-atom in this molecule originates from the activation of O_2 by ammonia monooxygenase.²¹⁴ Taken together, these data suggest that an O-atom from H_2O is incorporated during AOB metabolism downstream from NH_2OH oxidation, which is at odds with the apparent O_2 -dependence of HAO catalysis.

Due to the similar nature of their cofactors, the cyt P460 and HAO reactions with NH_2OH were anticipated to proceed by a similar mechanism. However, a recent mechanistic study of *N. europaea* cyt P460 led to a revision of this enzyme's reaction chemistry and, by extension, of bacterial nitrification. Under anaerobic turnover conditions, the enzymatic product of NH_2OH oxidation by cyt P460 is N_2O —no NO_2^- is formed.¹⁷⁸ Kinetics supported by spectroscopic characterization of reaction intermediates has yielded a working mechanism for NH_2OH oxidation by cyt P460 (Scheme 3). The catalytic cycle begins with the resting Fe^{3+} form of the enzyme. The as-isolated ferric enzyme demonstrates a high-spin $S = 5/2$ rhombic EPR signal with g values of 6.57, 5.09 and 1.97 and its UV-vis absorption spectrum has a characteristically broad Soret band at 440 nm with a shoulder at ca. 414 nm (Figure 17, Figure 18a). This species binds NH_2OH with a modest equilibrium dissociation constant (K_D) of 9 mM, forming a stable, low-spin $S = 1/2$ Fe^{3+} - NH_2OH adduct that persists indefinitely in the absence of an oxidant (Figure 17, Figure 18b).

Treatment of the Fe^{3+} - NH_2OH adduct with diverse oxidants promotes a formal three-electron, three-proton oxidation. The first identified intermediate species is the two-electron oxidation product, a six-coordinate ferrous nitrosyl. This $\{\text{FeNO}\}^7$ species can also be generated by shunt experiments with exogenous HNO donors such as Angeli's salt ($\text{Na}_2\text{N}_2\text{O}_3$). The $\{\text{FeNO}\}^7$ has a characteristic $S = 1/2$ EPR signal ($g = 2.01, 2.03, 2.10$) that demonstrates hyperfine coupling contribution from the ^{14}N -nucleus from the NO (^{14}N A = 50, 57, 45 MHz). This initial oxidation presumably proceeds through a proton-coupled electron transfer (PCET) pathway, but the exact steps involved have not been investigated in detail. Caranto and co-workers¹⁷⁸ suggest that since cyt P460 is catalytically competent with

both formally one- and two-electron oxidants, the reaction likely proceeds via rapid one-electron, one-proton steps.

The six-coordinate $\{\text{FeNO}\}^7$ species undergoes a facile one-electron oxidation to form a kinetically stable $\{\text{FeNO}\}^6$. Under steady-state turnover conditions, the $\{\text{FeNO}\}^6$ is the only observed Fe-nitrosyl intermediate that accumulates. This species has a characteristic Soret maximum at 455 nm and is X-band EPR-silent (Figure 17, Figure 18c). It can be generated by exogenous NO addition and persists indefinitely in the absence of O_2 . What is peculiar in the cyt P460 case is the $\{\text{FeNO}\}^6$ species is kinetically stable. Traditionally, ferric nitrosyls are unstable compounds which often undergo rapid autoreduction.^{215–217} Some aspects regarding protein structure may shed light onto this apparent stability. A reasonable comparison can be made with the NO-delivery protein, nitrophorin (NP). NPs are proteins found in the saliva of blood-sucking insects such as *Rhodnius prolixus* which release NO and induce vasodilation. NPs are *b*-heme proteins that exhibit a high degree of ruffling, similar to cyt P460. Additionally, both ferric nitrosyls are stable against autoreduction. The structure of one variant, NP-4, reveals a highly exposed distal heme pocket which, upon NO-binding, undergoes dramatic conformational changes which close the pocket, packing hydrophobic groups and expelling water molecules in the process.²¹⁸ Subsequent high-resolution structures also revealed that the heme-ruffling increases upon NO-binding (Figure 16c) with a significantly bent geometry at the ligand ($\angle_{\text{FeNO}} = 156^\circ$).²¹⁶ It has been proposed that these dynamics act in concert to enhance stability of the $\{\text{FeNO}\}^6$ by protecting the NO and modulating the electronic structure. However, X-ray crystallography on ferric nitrosyls often results in partial photoreduction, which convolutes the distinction between the $\{\text{FeNO}\}^6$ and $\{\text{FeNO}\}^7$ structures and their structural parameters.¹⁵⁰

As with P450nor (see 2.2), the electronic ground-state of a NP or cyt P460 $\{\text{FeNO}\}^6$ can be formulated with one of three possible limiting configurations: $\text{Fe}^{2+}\text{-NO}^+$, $\text{Fe}^{3+}\text{-NO}^*$, or $\text{Fe}^{4+}\text{-NO}^-$. It has been suggested by Walker²¹⁵ that significant ruffling at a heme cofactor stabilizes the $\{\text{FeNO}\}^6$ in the $\text{Fe}^{3+}\text{-NO}^*$ state; ruffling at the low-spin Fe^{3+} heme drives a $(d_{xy})^2(d_{xz}, d_{yz})^3$ to a $(d_{xz}, d_{yz})^4(d_{xy})^1$ electronic ground-state configuration. The single electron in the d_{xy} orbital is orthogonal to the $\text{NO } \pi^*$, and thus cannot overlap. This results in a diradical, antiferromagnetically coupled system. However, as noted by Praneeth and co-workers,¹⁵⁷ the spectroscopic and structural properties of the NP $\{\text{FeNO}\}^6$ are virtually identical to other model complexes and proteins which have been assigned an $\text{Fe}^{2+}\text{-NO}^+$ electronic ground-state. The stability of the $\text{Fe}^{3+}\text{-NO}^*$ may be at play in the cyt P460 $\{\text{FeNO}\}^6$ but requires additional studies to investigate the electronic structure of this reactive intermediate.

During the rate-determining step, nucleophilic attack by a second equivalent of NH_2OH on the $\{\text{FeNO}\}^6$ results in the stoichiometric formation of N_2O under anaerobic conditions. Under aerobic conditions the reaction forms a ca. 50/50 stoichiometric mixture of NO_2^- and N_2O , suggesting that the $\{\text{FeNO}\}^6$ intermediate is labile, allowing free NO to react with O_2 .²¹⁹ Experiments in which the shunted $\{\text{FeNO}\}^6$ is treated with $^{14}\text{N}/^{15}\text{N}$ -labeled NH_2OH revealed that the $\{\text{FeNO}\}^6$ reacts in a bimolecular fashion with NH_2OH ; the N–N bond is formed between the nitrosyl and a second equivalent of NH_2OH . It is uncertain whether the

first or second equivalent of NH_2OH , which is turned over, contributes the O-atom in the final N–N product. Similar to the initial oxidation step, the formation of N_2O presumably proceeds via a PCET pathway, although the exact steps of how this N–N bond is formed remain elusive. Plausibly, this proceeds via nucleophilic attack of NH_2OH on the $\{\text{FeNO}\}^6$, which can be viewed as having appreciable nitrosonium (NO^+) character. N_2O is released, followed by rapid oxidation of an unobserved, putative Fe^{2+} intermediate to the resting ferric enzyme to complete the cycle.

2.3.3. Secondary Coordination Sphere Effects in Cyt P460 Catalysis—The cyt P460 catalytic cycle involves selective oxidation of NH_2OH to NO , followed by the nucleophilic attack of NH_2OH on a $\{\text{FeNO}\}^6$ intermediate. The production of N_2O likely involves PCET and thus poses the necessity for a proton relay to be present to allow catalysis. Indeed, selective redox catalysis of N-oxides in biomimetic compounds have required proton-responsive moieties in the second-coordination sphere.^{220–224} A relatively recent X-ray structure of an HAO from the anaerobic ammonia oxidizing (annamox) bacterium *Kueneenia stuttgartiensis* soaked in NH_2OH revealed distal hydrogen-bonding partners: Asp291 and His292.²²⁵ Theoretical studies of HAO have also implicated these second-sphere moieties.^{226,227} Upon examination of the available X-ray crystal structures of cyt P460s, similar features of the P460 active sites emerge.

A recent crystal structure of cyt P460 from the nitrifier *Nitrosomonas* sp. AL212 published by Smith and Lancaster¹⁹⁶ allowed for a comparison of distinct P460 active sites. The AL212 active site conserves the inner-sphere of the *mono*-His *c*-heme. However, this protein is inactive for NH_2OH oxidation. One modification of this enzyme compared to the *N. europaea* variant (NeP460) proved to be key to shutting down catalysis. In the NeP460 structure, a distal glutamate residue (Glu97) is oriented toward the distal substrate binding pocket. This residue is replaced in the AL212 variant by an alanine (Ala131) (Figure 19).

In the initial report of the AL212 structure,¹⁹⁶ it was noted that this enzyme is *inactive* with respect to NH_2OH oxidation. While capable of generating the observed intermediates from the NeP460 cycle via shunt experiments, the AL212 variant is incapable of any redox chemistry under similar NH_2OH turnover conditions.¹⁹⁶ Follow-up mutagenesis and crystallographic work with AL212 cyt P460 variants revealed that the secondary coordination sphere plays an essential role with respect to NH_2OH oxidation.²²⁸ While WT AL212 cyt P460 is not competent for NH_2OH oxidation, incorporation of a glutamate at position 131 (Ala131Glu) and thus installing a secondary coordination sphere similar to NeP460, restored ca. half of the catalytic activity observed for NeP460, allowing the variant to yield expected stoichiometric amounts of N_2O (Figure 20). Importantly, mutation of this position to a glutamine (Ala131Gln) did not restore catalytic activity, implicating a basic residue as necessary to shuttle protons away from the NH_2OH adduct during turnover. These mutations seemed to have little effect on the reduction potentials of the heme cofactor, nor did they dramatically affect the K_D for NH_2OH or NO . Together these findings underscore the necessity of precisely positioning residues in the protein scaffold to enable selective oxidation of NH_2OH by cyt P460.

The crystallographic study that supported this mutagenesis work shed light on additional participants within the secondary coordination sphere of cyt P460 and their dynamics during substrate binding. A comparison of the crystal structures of AL212 cyt P460 A131E and A131Q, as well as the former soaked with NO and the later with NH₂OH, revealed a highly dynamic substrate binding pocket with respect to the second-coordination sphere (Figure 21). These structures revealed a distal phenylalanine residue (Phe76) that moves in concert with the basic residue at position 131 upon ligand coordination. The two apparent conformations of Phe76 can perhaps be explained by the following rationale: the “swung in” conformation is operative when no substrate is present and the “swung out” species when substrate is bound. When considering the ferric EPR spectra, this hypothesis seems plausible. Multiple variants of cyt P460 yield two-component high-spin ferric, rhombic EPR signals. Interestingly, the relative populations of the two components change dramatically depending on the substitution at the 131 position. With bulkier sidechains occupying the 131 position, the EPR signal exhibits more contribution from the axial component, which presumably occupies the “swung out” position. One may view this Phe76 as a mode of outer-sphere gating during catalysis, which may shield the reactive, on-path nitrosyl species from undesired side-reactions with O₂ or H₂O/OH⁻ much like the {FeNO}⁶ of NP (*vide infra*). How these outer coordination sphere dynamics manifest themselves spectroscopically and enzymatically remains a field of inquiry.

2.4. Cyt *c*₅₅₄ (C554)

2.4.1. C554 Structure, Function, and Electrochemical Characterization—Cyt *c*₅₅₄ (C554) is a small, ca. 26 kDa monomeric tetraheme protein ubiquitous in AOB. 184,229–231 First purified by Yamanaka and Shinra,²³² the soluble protein was presumed to play a role in electron transfer during NH₂OH oxidation by HAO since C554 was observed to undergo reduction during turnover conditions and capable of delivering reducing equivalents to the monoheme cyt *c*₅₅₂. While Yamanaka and Shinra²³² originally proposed C554 had two hemes, this was later corrected by Andersson and co-workers²³³ to four *c*-type hemes which form two magnetically interacting pairs. A recent proteomics study showed that C554 is relatively highly expressed by AOB (ca. 0.5–1.7% of total protein content).²³⁴ Taken together, these data have led researchers to propose that C554 is the physiological redox partner of HAO and is an essential component of primary AOB metabolism.

The genome for *N. europaea* encodes three copies of the gene for C554, and C554 is contained in the gene cluster that also encodes HAO.^{235,236} C554 bears no significant sequence homology to any other protein (including other tetraheme proteins), and is considered to be in its own class.²³⁶ Andersson and co-workers²³³ noted that C554 could bind small molecules (i.e. NO, CO, cyanide (CN⁻)) at an open Fe coordination site. However, this apparent ligand binding has been subsequently disputed (*vide infra*).^{230,237}

An X-ray crystal structure (Figure 22) reported by Iverson and co-workers²³⁸ confirmed that C554 contains four *c*-hemes (labeled I-IV, based on primary structure beginning at the N-terminus), one of which is five-coordinate (heme II). The distal pocket of heme II, where ligand binding plausibly occurs, is surrounded by three bulky, hydrophobic residues:

Thr154, Pro155 and Phe156. The three remaining heme sites are coordinately saturated by two axial histidines each. Heme I is ligated by the Nd-atom of a histidine sidechain (His102), while the Ne-atom participates in a hydrogen-bond with a nearby glutamate. This is a rare example of this binding mode reported in a heme protein. Electrostatic modelling of the overall protein structure along with the structure of HAO show complimentary surface charges to facilitate binding between the apparent redox partners.²³⁸

Another observation concerns the C554 heme packing motif and its relation to other multiheme proteins. The heme-heme distances within each pair (heme I/III and heme IV/II) are relatively short (ca. 9.5 Å) and result in an observed weak exchange-coupling (J ca. -0.5 cm^{-1} , $H = -2J\mathbf{S}_1\cdot\mathbf{S}_2$) between the cofactors.²³⁷ This coupling can make deconvolution of C554's spectroscopic properties quite challenging. Despite the lack of sequence identity, the heme packing motif appears to be nearly superimposable to the arrangement of hemes of HAO and cyt *c* NiR. This may suggest a common ancestry between these three enzymes, which is curious considering their dramatically different roles in AOB metabolism.
199,230,239,240

C554 has been a workhorse system in protein electrochemistry. It was initially shown by Arciero and co-workers²⁴¹ that the four hemes exhibit reduction potentials of -0.276 , -0.147 V, and a degenerate $+0.047$ V (vs. NHE) on the basis of potentiometric measurements. Further resolution of these potentials via redox titrations in tandem with both parallel and perpendicular mode EPR measurements mapped these reduction potentials to each heme (IV, III, and (II & I), respectively), with hemes I and II having the identical set of reduction potentials.²³⁷ Using protein-film voltammetry Pulcu and co-workers²⁴² were able to assign reduction potentials to each heme site individually, but reach a different conclusion. Rather than observing a degenerate reduction potential at hemes I and II, they assign six-coordinate, low-spin heme I at $+0.050$ V vs. NHE and high-spin five-coordinate heme II with a reduction potential of $+0.032$ V. The other two hemes were in close agreement to the previously reported potentials: heme III at -0.183 V and heme IV at -0.283 V. The authors speculated that C554 is tuned to perform two-electron reduction at its high potential sites.

Indeed, C554's role as a two-electron redox partner of HAO was previously suggested by rapid mixing kinetics experiments, with the apparent stoichiometry of two electrons per NH_2OH turnover.²⁴³ These showed that the high-potential heme pair (I & II) of C554, under single-turnover experiments, would accept two electrons from HAO. The five-coordinate, high-spin heme would accept the first equivalent at rates faster than the time of manual mixing (>100 s^{-1}), followed by a second reduction at the six-coordinate low-spin heme at a ca. 10–30-fold slower rate. These rate constants were either in agreement with or faster than the observed reduction of HAO by NH_2OH , further implicating C554 as a physiological electron acceptor for HAO. It was also observed that under multiple-turnover conditions, the rates of reduction for both hemes I and II decreased when the C554 concentration was raised above that of HAO. This, with the apparent dependence on ionic strength under both single- and multiple-turnover conditions, suggests that HAO and C554 form a tight electrostatic complex. In summary, C554 likely positions heme I towards HAO under turnover conditions, which is followed by rapid intramolecular electron transfer to heme II.

2.4.2. Putative C554 NOR Activity—Knocking out Cu-containing nitrite reductase (NirK) in *N. europaea*, does not preclude the organism from producing a significant amount of N₂O.²⁴⁴ This led to the hypothesis that NO reduction must be playing a role in the formation of N₂O from nitrifying organisms, so called “nitrifier denitrification.”^{193,234} Indeed, knock out experiments in which the NorB homolog in *N. europaea* is disrupted retained N₂O production (albeit diminished) and NO tolerance.^{245,246} This prompted the proposal that some additional biotic pathway is operative implicating an undiscovered NOR (*vide infra*).

Many studies dispute the ability of C554 to bind exogenous ligands despite structural evidence of an open coordination site.^{230,237} However, Upadhyay and co-workers²⁴⁷ reported that C554 exhibits significant NOR activity. They observed transient NO-binding at heme II, leading the authors to suggest that C554 can potentially act as a catalyst for NO reduction. The authors noted that the fully reduced protein exhibits only small changes in the ⁵⁷Fe Mössbauer or UV-visible spectra upon treatment with NO. However, C554 will bind to NO in the semi-reduced state. In the semi-reduced state, the high-spin, five-coordinate heme II and low-spin, six-coordinate heme I are in the ferrous state, while the remaining hemes III and IV are low-spin ferric. Addition of NO to the semi-reduced protein results in a diminished heme II signal in the ⁵⁷Fe Mössbauer spectrum ($\delta = 0.98 \text{ mm}\cdot\text{s}^{-1}$, $E_Q = 2.2 \text{ mm}\cdot\text{s}^{-1}$) and the appearance of a new diamagnetic doublet ($\delta = 0.23 \text{ mm}\cdot\text{s}^{-1}$, $E_Q = 1.53 \text{ mm}\cdot\text{s}^{-1}$) (Species X in Figure 24a). Heme II in the high-spin ferrous state will bind NO to form a {FeNO}⁷. The apparent diamagnetic character of the ⁵⁷Fe Mössbauer spectrum originates from the spin-interaction from the high-spin ferric heme IV; the low-spin {FeNO}⁷ at heme II ($S = 1/2$) will interact with the low-spin, ferric heme IV ($S = 1/2$). The {FeNO}⁷ center was resolved in the X- and Q-band EPR spectra. C554 reduced in the presence of NH₂OH and catalytic HAO resulted in new signals at $g = 2.4, 1.73, 1.46$ (X-band) and $g = 2.4, 1.85$ (Q-band), which when simulated are consistent with reported {FeNO}⁷ species. Similarly, the electrochemically semi-reduced C554 shows EPR signals from heme III ($g = 3.24$ and 2.2) and a broad signal from heme IV ($g = 3.6$). Treatment with one equivalent of NO results in the disappearance of the heme IV signal, along with the concomitant formation of new signals at $g = 2.4, 1.7$ and 1.5 . Addition of a second equivalent of NO results in EPR features consistent with the fully oxidized C554.

The electronic absorption spectra also support some interaction between the semi-reduced C554 and NO: The authors observed the immediate loss of intensity of the low-spin Fe²⁺ (heme I) UV-vis absorption bands at 420, 554 and 524 nm and a complete loss of the high-spin Fe²⁺ (heme II) band at 430 nm (Figure 23). Kinetic measurements under single-turnover conditions suggest an NO-turnover rate of $>16 \text{ s}^{-1}$, on the same order of magnitude of other reported NORs. The semi-reduced C554 {FeNO}⁷ is reported to be stable to stoichiometric NO, but decomposes in excess NO. This suggests a bimolecular reaction between the {FeNO}⁷ and free NO.²⁴⁷

While there is evidence C554 can bind NO, there is a lack of support for the claim that C554 can act as an NO-reductase; the authors indirectly associate observed oxidation events of the {FeNO}⁷ with the reaction of NO. NO is extremely sensitive under reducing conditions and can react with even trace amounts of O₂.^{248,249} A recent report by McGarry and Pacheco²⁵⁰

addressed these concerns and suggested that C554 can reversibly bind NO, but cannot perform NOR catalysis. They, unlike Upadhyay co-workers,²⁴⁷ did not observe rapid oxidation at heme I, nor loss of the {FeNO}⁷ signal at heme II upon excess NO addition. They also found that the oxidation state of the protein (*i.e.* half- or fully-reduced) did not dramatically impact the rate constant for NO binding ($3,000 \pm 140 \text{ M}^{-1}\cdot\text{s}^{-1}$). This finding suggests that C554 cannot turnover multiple NO molecules, and thus is unlikely to function as a NOR. It is worth noting that neither of these studies provide evidence of N₂O formation, which could provide a compelling argument in either case. Further, much of this work proceeded under the presumption that NO was neither the enzymatic product of HAO nor an obligate intermediate in AOB metabolism.²⁰³ This would undoubtedly convolute the conditions of previous experiments wherein NH₂OH/HAO turnover was used to reduce C554. While the NOR activity of C554 is disputed, there remains the unanswered question of the role of C554's apparent NO-binding properties and the complete extent to which it participates in nitrification energy transduction.

2.5. Flavo-diiron Proteins (FDPs)

2.5.1. FDP Classification, Structure and Function—FDPs are a family of soluble, cytoplasmic proteins which contain non-heme, sulfur-free diiron sites with nearby FMN cofactors. These proteins occur in all domains of life which thrive in anaerobic (or micro-aerobic) environments, including Bacteria, Archaea, and a few protozoa.^{251–256} The first reported isolation of an FDP was from Chen and co-workers,²⁵⁷ who reported an isolate from *Desulfovibrio gigas* that was able to couple *in vitro* O₂ reduction to NADH oxidation, potentially serving as an O₂-scavenger (Equation 10).



Indeed, it has been shown for several organisms that FDP expression is upregulated in oxidative conditions.^{252,258} Ensuing studies of FDPs have provided evidence that they also serve as NO reductases.

FDPs can be classified into nine distinct classes (A-I).^{259,260} Class A FDPs represent the common protein domains between all these classes and are widespread among prokaryotes.^{261,262} These include the N-terminal metallo-β-lactamase domain that houses the diiron active site and the C-terminal FMN binding (flavodoxin) domain of each subunit. The remaining classes are differentiated by additional C-terminal domains. Class B (or flavorubredoxin) and Class D feature a rubredoxin (Rb) C-terminal domain, the latter possessing a “short type” Rb. Class C (from bacterial and eukaryotic oxygenic phototrophs), G and H (from Firmicutes) FDPs only vary in the number of Rb-domains they support and are characterized by a flavin oxidoreductase (Flv) domain. These three classes are noteworthy because they apparently support all of the necessary redox partners to couple NADH/NADPH oxidation to O₂ and/or NO reduction; regeneration of the FMNH₂ requires additional redox partners such as NADH/NADPH:flavin oxidoreductase and/or NADH:Rb oxidoreductase and Rb.^{251,262} Class E FDPs (from Clostridiales) support a putative FeS-binding domain and Class F (from Clostridiales and some protozoa) have a NADH:Rb oxidoreductase domain, but lack the Flv domain. Finally, Class I FDPs may exist and are

unique in that they appear to be fused to a desulfiredoxin-like domain along with a neelaredoxin, diiron superoxide reductase (SOR) domain.

The presence of the diiron active site in FDPs was unprecedented, and was revealed only by the first reported crystal structure of the FDP isolated from *D. gigas*.²⁶³ Since then, many structures have been reported and corroborate the universal presence of diiron sites (Figure 24).^{264–267} In each case, the two Fe atoms are ca. 3.2–3.4 Å apart. With one exception, the Fe inner coordination spheres are highly conserved, comprising four histidines, an aspartate, and a glutamate. The Fe centers are bridged by a carboxylate ligand from a conserved aspartate and, in frozen solution, by one or two μ_2 -hydroxo ligands in the ferrous and ferric states, respectively.²⁶⁸ The one exception occurs in *D. gigas*, where one of the four histidines is replaced by a water molecule. Site-directed mutagenesis studies on this FDP variant reveal, however, that the presence or absence of this His residue does not significantly affect either the O₂ reductase (O₂R) or NOR activities.²⁶⁷

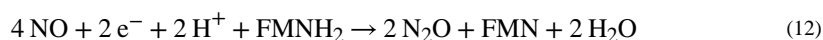
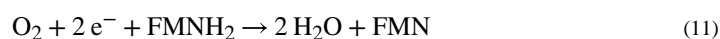
Another feature common to all FDP active sites is a proximal FMN cofactor ca. 4 Å away from the diiron site. While the diiron site and FMN molecule are ca. 40 Å apart within a single subunit, the homodimeric quaternary structure orients the two redox sites near each other in a “head-to-tail” fashion. Namely the C-terminal end of one subunit, which houses the FMN cofactor, accompanies the N-terminal end of the other subunit which supports the diiron site (Figure 24b).

There are multiple lines of experimental evidence in support of the hypothesis that FDPs facilitate a reductive pathway to relieve O₂ stress.^{254,269} However, a study by Gardner and co-workers²⁷⁰ demonstrated clear genetic evidence that linked NO-scavenging to FDP-containing gene clusters in *Escherichia coli*. They proposed that FDPs, along with flavohemoglobins (NO oxidases), could open both anaerobic and aerobic detoxification pathways for *E. coli* under nitrosative/oxidative stress. The NOR activity of the *E. coli* FDP variant was confirmed *in vitro* with recombinantly expressed protein by Gomes and co-workers.²⁵⁶ Additionally, another *in vitro* study of an FDP from the obligate anaerobe *Moorella thermoacetica* showed both NOR and O₂R activity, with the former being more efficient.²⁷¹

Interestingly, there is some variability in FDP catalytic performance on each substrate. The FDP variants from *M. thermoacetica*, *D. gigas*, and *Desulfovibrio vulgaris* demonstrate similar O₂R and NOR activities.^{271–273} However, some FDPs show substrate preference.²⁶⁰ The secondary coordination sphere appears to be a factor in this selectivity among FDP variants. A mutagenesis study on the O₂-reducing FDP from the protozoan *Entamoeba histolytica* (EhFdp1) showed that point mutations influenced this preference. Attempting to emulate the active site of the NO-reducing variant from *E. coli*, two residues were identified that impart this bias. By mutating a distal lysine residue to an aspartate (Lys53Asp) and a tyrosine to a serine (Tyr271Ser), NOR activity increased 20-fold while inactivating the enzyme for O₂ turnover.²⁷⁴

2.5.2. FDP Mechanism—To drive either O₂ or NO reduction, the FDP catalytic cycle begins in the reduced, diferrous state. In this fully reduced state, the FMN harbors an

additional two reducing equivalents (FMNH₂). It is worth noting that the two reactions differ markedly in the number of turnovers per cycle by the number of electrons available for catalysis. Namely, O₂ reduction will turn over one molecule of O₂ with four electrons (Equation 11), while four molecules of NO can be reduced to two N₂O molecules under the same conditions (Equation 12).



While many details of the O₂R activity of FDPs are beyond the scope of this review, the chemical mechanism is worth discussing if only to compare to the NOR mechanism. Frederick and co-workers²⁷⁵ performed kinetics experiments on a bacterial FDP from *Treponema denticola*, wherein they showed, under single-turnover experiments with the fully reduced [2Fe²⁺ : FMNH₂] and O₂, the rapid concomitant formation of an intermediate with UV-vis absorption maxima at 462 and 650 nm. The feature at 462 nm is attributed to the FMN, while the 650 nm intermediate is assigned as a *cis*-μ-1,2-peroxodiferric intermediate in accord with other similar enzyme intermediates.^{276,277} This intermediate, upon further reduction from the two electrons supplied by the FMNH₂ cofactor, forms H₂O and generates the fully oxidized [2Fe³⁺ : FMN] species. It is worth noting that, *in vitro*, a number of FDPs from various organisms have been reported to become irreversibly inactivated after O₂ reduction.^{264,266,271,272,274,275} However, this may not be an issue *in vivo* where the partial pressure of O₂ is likely much lower and prolonged air exposure is unlikely.^{278,279}

FDPs are isolated in a diferric state, as demonstrated by Silaghi-Dumitrescu and co-workers²⁷¹ by obtaining ⁵⁷Fe Mössbauer data on the *M. thermoacetica* protein. Under low applied magnetic field conditions (50 mT), the ⁵⁷Fe Mössbauer spectrum shows two Fe centers each with unique coordination environments. Under high applied magnetic field (8 T), the as-isolated FDP spectrum exhibits a larger quadrupole splitting, suggestive of diamagnetism ($\delta_1 = \delta_2 = 0.49 \pm 0.02 \text{ mm}\cdot\text{s}^{-1}$, $E_{Q1} = -0.69 \pm 0.03 \text{ mm}\cdot\text{s}^{-1}$, $E_{Q2} = 0.97 \pm 0.03 \text{ mm}\cdot\text{s}^{-1}$). The EPR spectrum supports this, showing a weak resonance from adventitious Fe at $g = 4.3$ and a narrow peak at $g = 2.01$, presumably from a small amount of semi-reduced FMN (semiquinone). Together, these data suggest the two Fe centers of the active site are antiferromagnetically coupled, mediated by the bridging solvent molecule, consistent with the reported crystal structure.^{263,271,280}

NOR mechanistic hypotheses (See Section 2.1) also invoke fully reduced enzyme [2Fe²⁺ : FMNH₂] as the catalytically relevant resting state for production of N₂O.^{271,281} Silaghi-Dumitrescu and co-workers²⁷¹ established the stoichiometry of the FDP NOR activity, showing 1 mol NADH oxidized:2 mol NO consumed, presumably forming N₂O. Their initial kinetics scheme suggested that the two-electron reduced enzyme would sequentially bind two NO molecules and reductively couple them to form N₂O as well as the diferric protein, similar to models adopted for bacterial heme/non-heme respiratory NORs.⁴⁶ The

various proposals for the FDP NOR mechanism all make the diferrous assumption, wherein two NO molecules are consumed in a committed step to form N₂O and proton transfer is rate limiting.²⁷⁸ The three most commonly discussed mechanistic proposals (Scheme 4) are the hyponitrite pathway (hyp), the super-reduced (sr) pathway, and the diferrous-dinitrosyl (diFeNO) pathway.

The hyp pathway largely originates from a computational study by Blomberg and co-workers.²⁸² Similar to models employed for NORs (see Section 2.1), this mechanism supposes pre-equilibrium formation of a Fe²⁺{FeNO}⁷ species. The nitrosyl bridges the two irons in a $\mu\text{-}\eta^1(\text{O})\text{:}\eta^1(\text{N})$ fashion. This intermediate is subsequently attacked by the second NO, forming the N–N bond through a N₂O₂²⁻ adduct. This mechanism suggests that only one Fe atom participates in NO binding, while the other Fe stabilizes N₂O₂²⁻. Moreover, the N–N bond is formed before any PCET event and is, conceivably, reversible. The Fe³⁺–($\mu\text{-N}_2\text{O}_2^{2-}$)–Fe³⁺ intermediate then decays during the rate-determining step to form N₂O, returning to diferrous enzyme. Interestingly, this proposal forgoes any need for the FMN cofactor, and this can be viewed as one of its idiosyncrasies when considering the lack of appreciable NOR activity between similar diiron sites and NO without FMN cofactors.
283–285

On the other hand, the proposed sr and diFeNO mechanisms take a much different approach in describing the FDP NOR activity.^{278,286} In the sr scenario, the Fe²⁺{FeNO}⁷ binds a second NO at the second Fe, forming a diferrous dinitrosyl species, [{FeNO}⁷]₂. The reduced FMNH₂ then sequentially could add two reducing equivalents and two protons to the diiron site in a rate-determining step, forming a [2{Fe(HNO)}⁸ : FMN] that rapidly dimerizes to form N₂O and water. The diFeNO proposal takes a different pathway from the sr mechanism. Rather than the FMNH₂ providing additional electrons to the [{FeNO}⁷]₂ intermediate, the diferrous-dinitrosyl generates N₂O and the diferrous site, the key distinction being that the FMNH₂ serves to regenerate the diferrous site, which is poised to bind and turn over another two equivalents of NO.

In principle, the presence/absence of the FMN cofactor should differentiate between the two pathways that require FMNH₂ participation (sr, diFeNO) and the hyp pathway which forgoes any additional reduction from FMNH₂. An investigation by Hayashi and co-workers,²⁸¹ using a recombinantly expressed, deflavinated FDP from *T. maritima* revealed that the diferrous FDP, when treated with one equivalent of NO, yields a Fe²⁺{FeNO}⁷ species. This species, a common intermediate in all three proposed mechanisms, was verified by various spectroscopic methods. Upon treatment with one equivalent of NO, the diferrous protein turns yellow, exhibiting a UV-vis absorption spectrum characterized by peaks at 420, 455 and 638 nm assigned as ligand-to-metal charge transfer (LMCT) bands. The EPR spectrum of the diferrous protein is silent due to antiferromagnetic coupling between the two Fe²⁺ sites. Hayashi and co-workers²⁸¹ observed that a broad axial $S = 1/2$ feature centered at $g \approx 2$ forms following the addition of one equivalent of NO. They rationalized that the Fe³⁺ ($S = 5/2$) binds and antiferromagnetically couples to NO⁻ ($S = 1$), yielding a $S = 3/2$ {FeNO}⁷. This fragment then couples to the presumably bridged Fe²⁺ ($S = 2$) site, resulting in the observed $S = 1/2$ signal in the EPR spectrum. A similar spin-coupling scheme has been

observed in the NO adduct of hemerythrin^{287,288} as well as a model complex of a diiron mononitrosyl reported by Jana and co-workers.²⁸⁹ Further addition of NO yields a mixture of products. Up to 70% of the diiron sites are competent for formation of N₂O with concomitant conversion to diferric protein, as verified by Fourier-transform infrared (FTIR) spectroscopy. The remaining 30% of enzyme forms an intriguing diferrous-dinitrosyl species in which the two $S = 3/2$ {FeNO}⁷ centers are magnetically uncoupled as revealed by an EPR spectrum centered at $g \approx 4$. The apparent uncoupling of these two sites is intriguing when one considers the similar diiron sites of other proteins when treated with NO, such as the R2 protein of ribonucleotide reductase, which demonstrates a magnetically coupled, EPR silent [{FeNO}⁷]₂.^{283,284} While the authors concluded that the Fe²⁺-{FeNO}⁷ is an intermediate in the NOR mechanism, there is insufficient evidence to distinguish between the three proposed pathways. In a subsequent study by Hayashi and co-workers,²⁸⁸ the authors carried out a similar set of spectroscopic measurements on the native flavinated protein. Similar results were observed for the native FDP NO adduct species, and resonance Raman spectroscopy revealed an unusually low value for the NO stretching frequency. The value obtained for this NO adduct species was $\nu(\text{NO}) = 1681 \text{ cm}^{-1}$, ca. 100 cm^{-1} lower than expected for comparable proteins and synthetic compounds. This can be attributed to an exceptionally electron rich NO-adduct and can be assumed to have the limiting Fe³⁺-NO⁻ configuration. The authors also rationalize that the remaining Fe²⁺ atom activates this intermediate, populating the π^* NO-orbital and weakening the N=O bond. Taken together, these data support the hyp mechanism. However, they do not completely explain the previously observed ca. 30% of de-flavinated enzyme that forms [{FeNO}⁷]₂.

Two follow-up studies by Caranto and co-workers^{286,290} employed rapid-mixing experiments with the FDP from *T. maritima* to support the assertion that the [{FeNO}⁷]₂ intermediate is on-path with N₂O formation and returns to the diferric enzyme. Treatment of the fully reduced [2Fe²⁺ : FMNH₂] with substoichiometric NO resulted in UV-vis absorption features consistent with the nearly quantitative formation of the mononitrosyl, as encountered with the de-flavinated protein. No features of the oxidized FMN cofactor were observed, and minimal signal from the semiquinone $S = 1/2$ EPR signal suggest that, at least upon the formation of Fe²⁺{FeNO}⁷, the FMN cofactor remains reduced. The authors assigned this [Fe²⁺{FeNO}⁷ : FMNH₂] as the first intermediate in the cycle. Titrating the fully reduced enzyme with NO in tandem with ⁵⁷Fe Mössbauer spectroscopy confirmed this assignment. The signal attributed to the diferrous protein ($\delta = 1.15 \text{ mm}\cdot\text{s}^{-1}$, $E_Q = 2.39 \text{ mm}\cdot\text{s}^{-1}$) diminishes with concomitant formation of two new quadrupole doublets with equal areas. One signal is assigned as an Fe²⁺ center of the Fe²⁺{FeNO}⁷ ($\delta = 1.12 \text{ mm}\cdot\text{s}^{-1}$, $E_Q = 1.98 \text{ mm}\cdot\text{s}^{-1}$) while the other corresponds unambiguously to the {FeNO}⁷ ($\delta = 0.67 \text{ mm}\cdot\text{s}^{-1}$, $E_Q = 1.53 \text{ mm}\cdot\text{s}^{-1}$).^{284,287,291}

Rapid-mixing UV-vis experiments with excess NO indicated an initial rapid phase occurring within 130 ms and that was followed by a lag phase which occurs over 120 s. A quantitative analysis of these spectra were indicative of an additional {FeNO}⁷ species operative in addition to the Fe²⁺{FeNO}⁷, but before any significant oxidation of the FMNH₂ cofactor. ⁵⁷Fe Mössbauer data collected under similar time courses corroborated this observation and served as evidence for a transient $S = 0$ species assigned as an [{FeNO}⁷]₂ (Figure 25). The

dinitrosyl was only observed over the 0.2 to 2 s time course. RFQ samples scrutinized by low- and high-field ^{57}Fe Mössbauer revealed that this intermediate could be best described as an antiferromagnetic exchange pair of equivalent $\{\text{FeNO}\}^7 S = 3/2$ centers with an exchange energy $J = 40 \text{ cm}^{-1}$, consistent with an oxo- or hydroxo-bridged center.²⁸⁰ The steady-state activity data were also fit to the Michaelis-Menten expression, which yielded $K_m = 1 \text{ mM}$ and $k_{\text{cat}} = 0.6 \text{ s}^{-1}$. These parameters along with observations from the RFQ EPR time course suggest that the first equivalent of NO binds with much higher affinity than the second.

This comprehensive mechanistic study by Caranto and co-workers²⁸⁶ lays out the following scheme for the FDR NOR mechanism (Scheme 5). The diferrous protein, $[2\text{Fe}^{2+} : \text{FMNH}_2]$, rapidly binds the first equivalent of NO on the sub-millisecond scale to yield the $[\text{Fe}^{2+} \{\text{FeNO}\}^7 : \text{FMNH}_2]$. This species reacts with a second equivalent of NO over 100 ms to form the diferrous dinitrosyl prior to any oxidation of the FMNH₂. Over the course of ca. 2 min the $[2\{\text{FeNO}\}^7 : \text{FMNH}_2]$ couples the two NO molecules to the first equivalent of N₂O in the rate-determining step to yield the $[2\text{Fe}^{3+} : \text{FMNH}_2]$. This species does not accumulate due to facile electron transfer from the FMNH₂. The diferrous site is regenerated as $[2\text{Fe}^{2+} : \text{FMN}]$, and the cycle repeats again to yield a second equivalent of N₂O.

These findings are at odds with the sr mechanism. In the absence of an exogenous reductant, the sr mechanism limits N₂O production to only one mol per turnover. However, the observation of the four-electron oxidation of the FDP with five equivalents of NO suggests that the FMN cofactor instead regenerates the diferrous site. Further, the same diFeNO pathway was implicated in the deflavinated form of the enzyme; the observation of the $[\{\text{FeNO}\}^7]_2$ and its competence for N₂O formation without FMNH₂ is in disagreement with the sr pathway.²⁹⁰

While Caranto and co-workers²⁸⁶ make the compelling case for the accumulation of the $[\{\text{FeNO}\}^7]_2$, there remains the possibility that the N–N bond is formed through a transient $\text{N}_2\text{O}_2^{2-}$ intermediate. This would require the cleavage of only one of the two substrate N–O bonds. The authors note that neither the formation of the $[\{\text{FeNO}\}^7]_2$ nor the oxidation of the FMNH₂ with excess NO show an appreciable isotope effect in D₂O. This would imply that any proton transfer must necessarily occur after the rate-determining step. This may implicate the formation of the N–N bond via a short-lived $\text{N}_2\text{O}_2^{2-}$ ligand that is then protonated to release N₂O.

Weitz and co-workers²⁹² further characterized the $\text{Fe}^{2+}\{\text{FeNO}\}^7$ and $[\{\text{FeNO}\}^7]_2$ intermediates. Using a combination of EPR, ^{57}Fe Mössbauer and DFT methods, the authors conclude that the first NO binds to the proximal Fe (closest to the FMN cofactor), resulting in an exchange coupling constant of $J = 17 \text{ cm}^{-1}$ (Hex = $\mathcal{S}_1 \bullet \mathcal{S}_2$). This is significantly lower than the previously reported J -value for the diferrous protein ($J = 32 \text{ cm}^{-1}$) and is attributed to the $\text{Fe}^{3+}\text{--}\text{Fe}^{2+}$ exchange interaction mediated by the semi-bridging NO.^{268,288} Upon binding of a second equivalent of NO, this value increases dramatically to 60 cm^{-1} , attributed to spin-coupling between the Fe and NO within the $\{\text{FeNO}\}^7$ centers and, possibly, a $^-\text{ON}\cdots\text{NO}^-$ exchange interaction prior to N–N bond formation. The increase in the J -value in the $[\{\text{FeNO}\}^7]_2$ species is consistent with results observed for synthetic model

complexes.^{293,294} The combination of experimental data and DFT also supported the retention of at least one μ_2 -hydroxo ligand between the two Fe centers during turnover which may have significant implications in catalysis; the bridge may impart essential proximity between the two NO molecules and be necessary for N_2O formation.

3. Bioengineered N_2O Forming Reactions

Tremendous advances have been recently made in repurposing extant biological scaffolds for otherwise non-native reactivity.²⁹⁵ This powerful approach can be used to engender novel reactivity to enzymes—for example, directed evolution of P450 enzymes has led to impressive feats such as enzymatic Si–C bond formation.²⁹⁶ Alternatively, rational design can be used to teach old enzymes new tricks.²⁹⁷ In this latter context, imbuing proteins with novel reactivity affords a means to apply otherwise intractable experimental tools to understand biological reactivity. Germane to the present discussion, the O_2 -carrying heme protein myoglobin (Mb) has been adapted to NOR reactivity via engineering a non-heme metal (M_B) site above its natural heme *b* site. Metalation of this site with Fe generated a construct termed “ $Fe_B Mb$ ” (Figure 26a).²⁹⁸ This offered a starting point to probe the role of MB identity, heme macrocycle composition, and second-sphere coordination (Figure 26b) over the efficacy of NO reduction to N_2O .²⁹⁹ Using this approach, Sabuncu and co-workers³⁰⁰ could show that a semi-reduced, one-electron pathway is a viable route to N_2O generation by HCO-type NOR enzymes—substitution of Fe_B by Zn_B did not abolish the ability to produce N_2O .

4. Bioinspired N_2O Forming Reactions

4.1. Iron

4.1.1. Diiron—Among the earliest purpose-built diiron model complexes relevant to N_2O formation was a carboxylate-bridged non-heme diiron dinitrosyl complex, $[Fe_2(Et-HPTB)(O_2CPh)](BF_4)$ (Et-HPTB = *N,N,N',N'*-tetrakis-(*N*-ethyl-2-benzimidazolylmethyl)-2-hydroxy-1,3-diaminopropane) (Figure 27a).³⁰¹ Formation of this species was achieved by addition of NO to $[Fe_2(Et-HPTB)(O_2CPh)](BF_4)_2$. While this binding mode mimics the manner in which certain non-heme Fe proteins, including ribonucleotide reductase³⁰² and oxyhemerythrin³⁰³ bind NO, the species ultimately formed is not competent for N_2O formation. It was not until 2008 that the first *functional* diiron model for NOR was reported.³⁰⁴ This model is based upon a bifunctional ligand “L” bearing a heme (MH) and a MB coordination site. The diferrous ($LFe^{2+}H/Fe^{2+}B$) (Figure 27b) adduct of this ligand is synthesized by reaction of LFe^{2+} with one equivalent of $Fe(OTf)_2MeCN$ (OTf = triflate) in tetrahydrofuran (THF) at room temperature under N_2 . Addition of NO results in formation of an intermediate that is consistent with an $LFe^{3+}-NO/Fe^{3+}-OH$ and production of nearly quantitative N_2O . Further investigation into the intermediates formed during this transformation suggests that an $LFeH^{2+}/FeB^{2+}-NO$ species is formed upon initial addition of NO at -80 °C.³⁰⁵ Upon warming to -40 °C, a second intermediate is formed. Resonance Raman data obtained for this species revealed a peak at 1366 cm^{-1} , shifted 8 cm^{-1} from the 1358 cm^{-1} seen for the $LFeH^{2+}/FeB^{2+}-NO$ species. This shift in the porphyrin ν_4 band indicates NO binding at the FeH^{2+} site and suggests an $\{FeNO\}^7$ unit. Upon warming to

room temperature, the $\text{LFe}^{3+}\text{H-NO/Fe}^{3+}\text{B-OH}$ is formed. Reaction of this same species in dimethylformamide (DMF) results in formation of a *bis*-nitrosyl species, but no formation of N_2O was observed. Additionally, the analogous $\text{LZnH}^{2+}/\text{FeB-NO}$ species shows no NO dissociation at room temperature. Combined, these results support a *trans* mechanism (*vide supra*) where NO first binds at the Fe_B site, followed by NO binding at the Fe_H site, resulting in N_2O formation and a diferric product.

A stable $\text{N}_2\text{O}_2^{2-}$ -bridged Fe porphyrin complex was later reported and proposed as a model for NOR.³⁰⁶ This species, $[(\text{OEP})\text{Fe}]_2(\mu\text{-N}_2\text{O}_2)$ (OEP = octaethylporphyrin) (Figure 27c), displays a *trans*-bridging $\text{N}_2\text{O}_2^{2-}$ ligand bound to each Fe via the $\text{h}^1\text{-O}$ binding mode. Addition of HCl to a solution of $[(\text{OEP})\text{Fe}]_2(\mu\text{-N}_2\text{O}_2)$ in toluene resulted in near quantitative formation of N_2O as evidenced by headspace IR spectroscopy. The mechanism of this formation was hypothesized to occur through attack of H^+ on one of the O atoms in the N_2O_2 followed by cleavage of the O–N bond and subsequent formation of N_2O .

A bridged diiron porphyrin $\text{N}_2\text{O}_2^{2-}$ complex, $[(\text{OEP-CH}_2)\text{Fe}]_2(\text{h}^1, \text{h}^1\text{-ONNO})$ (Figure 27d), was reported to produce N_2O from $\text{N}_2\text{O}_2^{2-}$ without the need for H^+ .³⁰⁷ Generation of this species was carried out by treatment of $[(\text{OEP-CH}_2)\text{Fe}]_2(\mu\text{-O})$ with sulfuric acid (H_2SO_4) followed by addition of $\text{H}_2\text{N}_2\text{O}_2$. The resulting product was unstable in the absence of $\text{H}_2\text{N}_2\text{O}_2$, however, and decomposition notably resulted in the re-formation of starting complex $[(\text{OEP-CH}_2)\text{Fe}]_2(\mu\text{-O})$ and formation of N_2O gas as evidenced by headspace IR. The ability of this species to produce N_2O without addition of acid, in contrast to the $[(\text{OEP})\text{Fe}]_2(\mu\text{-N}_2\text{O}_2)$ species discussed above, was attributed to the Fe–Fe distances of 3.4 Å vs. 6.7 Å for the $[(\text{OEP-CH}_2)\text{Fe}]_2(\mu\text{-O})$ and $[(\text{OEP})\text{Fe}]_2(\mu\text{-N}_2\text{O}_2)$ species, respectively. The 3.4 Å distance falls much closer to those reported for biological systems, such as the *P. aeruginosa* NOR with Fe–Fe distances ca. 3.8 Å.

The first flavodiiron NO model competent for N_2O formation was reported in 2013.³⁰⁸ This model, $[\text{Fe}_2(\text{BPMP})(\text{OPr})(\text{NO})_2](\text{BPh}_4)_2$ (BPMP = 2,6-*bis*[(2-pyridylmethyl)amino)methyl]-4-methylphenol) (Figure 28a), produces nearly quantitative N_2O formation following two-electron reduction. Formation of this species is achieved by addition of $[\text{Fe}_2(\text{BPMP})(\text{OPr})](\text{BPh}_4)_2$ to form a diiron dinitrosyl motif where each Fe center is coordinated by two pyridine units and a single NO with bridging phenolate and propionate groups, resulting in pseudo-octahedral geometry. This species does not mediate NO reduction and, thus, N_2O formation in solution, which is analogous to previous reports by Feig and co-workers²⁹³ as well as the dinitrosyl adducts of methane monooxygenase²⁸⁵ and ribonucleotide reductase.²⁸⁴ However, upon two-electron reduction of the species, either chemically or electrochemically, rapid production of N_2O was observed, lending credence to the previously suggested *sr* mechanism for FDPs (Section 2.5.2). Importantly, the monomeric analogues $[\text{Fe}(\text{BMPA-PhO}^{\text{Me,CH}_2\text{Cl}})(\text{NO})](\text{OTf})$ (Figure 28b) and $[\text{Fe}(\text{BMPA-PhO}^{\text{tBu,tBu}})(\text{NO})](\text{OTf})$ (Figure 28b) (BMPA-PhO = *N*-(2-methyl-(2-chloromethyl)-6-methylphenolate)-*N,N*-*bis*-(2-pyridylmethyl)amine)) did not generate N_2O upon reduction, demonstrating the importance of the diiron structure for N_2O formation. Further mechanistic studies showed that this species also undergoes rapid and quantitative N_2O production through the addition of a single electron, following the “semi-reduced” pathway.²⁹⁴ Furthermore, through the use of spectroelectrochemistry and stopped-flow measurements

coupled with gas-headspace IR, solution IR and UV-vis absorption spectroscopy it was determined that the initial product is an $\text{Fe}^{2+}\text{Fe}^{3+}$ species that disproportionates over time to $[\text{Fe}(\text{BPMP})(\text{OPr})_2]^+$ and a ferric product. This further supports the semi-reduced pathway—which requires only one electron for N_2O formation—over the sr pathway. Computational studies showed that the breaking of the Fe–NO π interactions and the partial transfer of an electron from the metal center to NO were the two major barriers for N–N bond formation.³⁰⁹ This result supports the contention that the two-electron reduced species should have the lowest barrier for N–N bond formation since the electron transfer is largely complete. Surprisingly, the one-electron reduced species has a comparably low activation barrier which was justified by a decrease in the $\text{Fe}_2\text{–NO}_2$ π -bonding allowing activation of that unit. These results further support the assertion that reduction of the diiron core is necessary for N_2O formation.

The $[\text{Fe}_2(\text{N-Et-HPTB})(\text{O}_2\text{CPh})(\text{NO})_2](\text{BF}_4)_2$ species, comprising two $\{\text{FeNO}\}^7$ units with identical coordination environments, was later revisited.³¹⁰ It was shown to undergo formation of N_2O under illumination with white light at 15 K, which is suggested to proceed by initial formation of a caged-in dissociated NO that can react with the diiron complex to form N_2O under further illumination. Due to the low temperature required for reactivity and no observed change in the rate of N_2O at low concentrations of complex, an intramolecular process was proposed to be most favorable. Studies at room temperature further inform the mechanism, suggesting a putative intermediate in the form of a metastable nitroxyl-like mononitrosyl complex that undergoes side-on electrophilic attack by the second NO species to produce transient $\text{N}_2\text{O}_2^{2-}$ complexes that decay to form N_2O . While light activation is not required in FDPs for N_2O formation, the formation of the HNO and $\text{N}_2\text{O}_2^{2-}$ intermediates could inform the mechanism through which NO reduction proceeds.

The mononitrosyl diiron species $[\text{Fe}_2(\text{N-Et-HPTB})(\text{NO})(\text{DMF})_3](\text{BF}_4)_3$ (Figure 28c) mediates reduction of NO to N_2O .²⁸⁹ This species is synthesized by allowing $[\text{Fe}_2(\text{N-Et-HPTB})(\text{CH}_3\text{COS})](\text{BF}_4)_2$ to react with nitrosonium tetrafluoroborate (NOBF_4). Structural characterization revealed a previously unprecedented mononitrosyl diferrous unit with one Fe center coordinated by NO and DMF, and the other coordinated by two DMF molecules. In accord with previous accounts, this species does not generate N_2O spontaneously in solution.^{285,308,311} However, upon either electrochemical reduction or treatment with cobaltocene at room temperature, nearly quantitative formation of N_2O was observed. Formation of N_2O was monitored by IR spectroelectrochemistry experiments that showed N_2O formation with no detectable intermediates, as well as no release of coordinated DMF upon product formation. While the exact mechanism of N_2O formation by this species is not established, two pathways were proposed. One pathway involves reaction between two molecules of the initial reduced $[\text{Fe}^{2+}\{\text{FeNO}\}^8]$ product through N–N coupling and N–O cleavage assisted by hydrogen-bonding interactions. Alternatively, disproportionation of two $[\text{Fe}^{2+}\{\text{FeNO}\}^8]$ units to one unit each of $[\text{Fe}^{2+}]_2$ and $[\{\text{FeNO}\}^8]_2$ could yield N_2O .

An additional model complex, $[\text{Fe}_2(\text{Py}_2\text{PhO}_2)\text{MP}(\text{OPr})_2](\text{OTf})$ (where two of the pyridine groups in the BPMP ligand used previously are replaced with phenolate groups; Figure 28d), is competent for formation of N_2O and does so directly without formation of a nitrosyl intermediate.³¹² Furthermore, product formation was observed in the absence of acid, ruling

out the requirement for the formation of H₂O as the driving force of the reaction. This suggested instead that this is supplied by formation of a stable μ -oxo diferric species. Additionally, addition of acetic acid followed by cobaltocene to the product resulted in regeneration of the active species, which would subsequently produce an additional equivalent of N₂O from NO. This result is pertinent to the biological proposal that FDPs mediate N₂O formation through direct metal-mediated NO reduction without the involvement of the flavin cofactor.²⁸⁶

4.1.2. Mono-iron—The simple Fe nitrosyl, nitroprusside dianion [Fe(CN)₅NO]²⁻, has long been known to form N₂O following treatment with reagents such as azide (N₃⁻) and NH₂OH.³¹³ The latter reaction likely proceeds in a manner analogous of the N–N bond forming step of cyt P460 catalysis (see Section 2.3) where NH₂OH attacks the electrophilic heme {FeNO}⁶.¹⁷⁸ Additional Fe species competent for N₂O formation through nucleophilic substrate attack have also been reported.³¹⁴ The reaction of [(OEP)Fe-(NO)(5-methylimidazole)]OTf (Figure 29a) with sodium azide (NaN₃) in THF/DMF (4:1) produces N₂O as determined by IR spectroscopy. Having ¹⁵N labeled NO in the Fe starting complex results in production of ¹⁴N¹⁵NO.

Additional mononuclear Fe species have since been reported to produce N₂O as minor products after reaction with NO or nitrogen dioxide (NO₂) through electrocatalytic reduction. The first was [Fe(H₂O)(TPPS)]³⁺ (TPPS = *meso-tetrakis*(*p*-sulfonatophenyl)porphine) (Figure 29b) which produced N₂O as a minor product from reaction with NO.³¹⁵ Shortly after, [Fe(H₂O)(TMPyP)]⁵⁺ (TMPyP = *meso-tetrakis*(*N*-methyl-4-pyridyl)porphine) (Figure 29c) was reported to reduce NO₂⁻ to N₂O and NH₃.³¹⁶ It was then shown that multielectron NO₂⁻ reduction activity could be imparted into polytungstates by replacing one of the W sites with an Fe site (Figure 29d).³¹⁷ Investigation of an additional porphyrin species Fe(PP)Cl (PP = protoporphyrin) (Figure 29e), immobilized in an electropolymerized film, revealed that N₂O formation proceeds through initial formation of the nitrosyl complex Fe(NO⁺)(PP)(Cl) followed by a multielectron step forming N₂O.³¹⁸ This series of one-electron reductions at an Fe porphyrin supports the notion that Fe nitrosyl complexes are key intermediates in multielectron reductions in cyt *cd1* NiR.

N₂O₂²⁻ has also been observed as an intermediate in the reduction of NO at a mononuclear Fe site in studies of an Fe²⁺-MOF (MOF = metal-organic framework) (Figure 29f) with an Fe coordination sphere consisting of four O atoms in a trigonal pyramidal geometry.³¹⁹ Treatment of this species with NO produced an {FeNO}⁷ species which, if left at room temperature under an NO atmosphere, proceeded to decay through disproportionation of NO, first to a Fe³⁺-N₂O₂²⁻ product followed by release of N₂O and formation of a Fe³⁺-NO₂⁻ product.

A metastable nonheme {FeNO}⁸ species was recently reported to generate N₂O.³²⁰ This species, [Fe(NO)(N₃PyS)] (N₃PyS = 2-[[di-2-pyridinylmethyl](2-pyridinylmethyl)amino]methyl]-benzenethiol) (Figure 29g), is generated through the one-electron reduction of the previously described [Fe(NO)(N₃PyS)]BF₄. If left in solution at room temperature, the {FeNO}⁸ species undergoes a gradual color change from purple to

red-orange. Analysis of the headspace by gas chromatography revealed formation of N₂O in a 54% yield assuming a self-decay mechanism involving reaction of two isolated {FeNO}⁸ monomers. Importantly, the {FeNO}⁷ species produces no N₂O, highlighting the need for reduction before N–N bond formation. Although the Fe-containing product was not determined, NMR data were consistent with the presence of multi-iron clusters. Product formation in the presence of acid was greatly decreased, suggesting the mechanism does not proceed through initial release of HNO, but rather through reduction of the active species.

4.2. Copper

4.2.1. Dicopper—Despite the early prevalence of studies on Cu–NO chemistry,^{321–324} the first crystallographically characterized examples were reported fairly recently. The first, [Cu₂(XYL-O⁻)(NO)]²⁺ (XYL = 2,6-*bis*[(*bis*(2-pyridylethyl)amino)methyl]-phenol) (Figure 30a), was a Cu₂–NO species that upon decomposition produced N₂O and an Cu²⁺–O–Cu²⁺ product.³²⁵ Several additional dicopper species were later shown to perform this same reaction, resulting in N₂O and the Cu₂O product.³²⁶

Reductive coupling of NO by a yttrium-dicopper core was reported by Lionetti and co-workers.³²⁷ A solution of LYCu₃ (Figure 30b) was exposed to gaseous NO at –78 °C. After 6 hours, a metal-bound N₂O₂²⁻ species was observed. Further reduction of N₂O to N₂ was hypothesized. Isotope labeling experiments suggest that after N₂O is produced, it can be further reduced by the remaining Cu sites to N₂.

The first Cu-only system competent for stoichiometric NO reduction was reported by Wijeratne and co-workers.³²⁸ [Cu¹⁺(tmpa)(MeCN)](B(C₆F₅)₄) (tmpa = *tris*(2-pyridylmethyl)amine) was treated with excess NO in MeOH, resulting in a color change from yellow to green. EPR of the green species was diagnostic of an *S* = 1/2 system with a d₂₂ ground state, consistent with a single Cu²⁺ in trigonal bipyramidal geometry. Titration experiments suggest a 1:1 NO to Cu stoichiometry. Crystallization of this species revealed the N₂O₂²⁻ complex [{Cu²⁺(tmpa)}₂(μ-N₂O₂²⁻)](B(C₆F₅)₄)₂ (Figure 30c). This stability of this species is solvent-dependent. Upon addition of excess THF to a solution of this N₂O₂²⁻ species in MeOH, disproportionation of the N₂O₂²⁻ takes place, resulting in formation of N₂O, NO₂⁻, and Cu¹⁺(tmpa) in a 1:1:2 stoichiometry.

Conversion of NO₂⁻ to N₂O has been reported for a Cu²⁺Cu¹⁺ center, [Cu₂(Py₄DMB)(MeCN)₂](B(C₆F₅)₄)₂ (Py₄DMB = 1,2-*bis*(di(pyridine-2-yl)methoxy)benzene) (Figure 30d).³²⁹ Treatment of the Cu²⁺Cu¹⁺ species with three equivalents of NO resulted in loss of N₂O and formation of an unprecedented formally μ-oxo, μ-nitrosyl formally Cu²⁺Cu³⁺ complex, [Cu₂(Py₄DMB)(μ-O)(μ-NO)](B(C₆F₅)₄)₂. This latter species can also be prepared from treatment of the Cu¹⁺Cu¹⁺ species with NO. This structure suggests coupling of two {CuNO}¹¹ motifs resulting in formation of N₂O and the presumed [Cu²⁺–O–Cu²⁺]²⁺ species, which subsequently reacts with an additional equivalent of NO.

4.2.2. Monocopper—The first monomeric Cu–NO species, a pseudotetrahedral [HB(t-Bupz)₃CuNO] (t-Bupz = 3-*tert*-butylpyrazole) (Figure 31a) was shown to be stable for weeks in solution, but showed loss of NO upon purging with argon or vacuum.³³⁰ Re-addition of NO restored the original spectrum, implicating reversible NO binding.³³¹ Later,

two additional Cu species supported by substituted trispyrazolylborate (Tp) ligands (*tris*(3,5-dimethyl)-pyrazol-1-yl)hydroborate ($\text{Tp}^{\text{CH}_3, \text{CH}_3}\text{Cu}(\text{NO})$) and (*tris*(3,5-diphenyl)-pyrazol-1-yl)hydroborate ($\text{Tp}^{\text{Ph}, \text{Ph}}\text{Cu}(\text{NO})$) (Figure 31b) were thoroughly characterized, and they were shown to be competent for N_2O production.^{332,333} Treatment of the later-characterized Cu^{1+} complexes of *tris*(3-(trifluoromethyl)-5-methylpyrazol-1-yl)hydroborate ($\text{Tp}^{\text{CF}_3, \text{CH}_3}\text{Cu}(\text{CH}_3\text{CN})$) and *tris*(3-mesitylpyrazol-1-yl)hydroborate ($\text{Tp}^{\text{Ms}, \text{H}}\text{Cu}(\text{THF})$) with NO, yields mononuclear mononitrosyl complexes (Figure 31c) as evidenced by IR and UV-vis absorption spectroscopies.³³⁴ Further treatment with NO results in decomposition of these species and formation of the $\text{Cu}^{2+}\text{-NO}_2^-$ species, in contrast to formation of μ -oxo species as reported for the early dicopper systems. Additional studies of this class of Cu compounds showed that increased steric hinderance and electron withdrawal of the supporting ligand slows NO disproportionation. Consistent with this driving force, mechanistic studies show attack of a second, electrophilic NO molecule on the initial and reversibly-formed Cu–NO adduct is the rate-limiting step.³³⁴ Mechanistic investigation into this class of compounds by DFT further supported the formation of a *trans*-Cu(ONNO) unit followed by an (NO)₃ unit bound to the Cu with the original N–Cu bond and a new O–Cu bond, which subsequently decays to form N_2O and the Cu(ONO) product,³³⁵ consistent with crystallized species.³³⁰ It should be noted that more recent studies of the (*tris*(3,tert-butyl-5-isopropyl)-pyrazol-1-yl)hydroborate ($\text{Tp}^{\text{tBu}, \text{iPr}}$) species, $\text{Tp}^{\text{tBu}, \text{iPr}}\text{Cu}(\text{NO})$, and $[\text{Tp}^{\text{tBu}, \text{iPr}}\text{Cu}(\text{NO})]\text{ClO}_4$ revealed end on NO binding modes in synthetic Cu–NO species. However, evaluation of EPR parameters from these model species provide a probe for determining Cu–N–O angles and binding modes in enzymatic systems of interest.³³⁶

The Cu-hydroperoxo compound (BA = *tris*-2-pyridylmethylamine with one pyridine decorated with-N(H)CH₂C₆H₅) was reported to react with NO in acetone to form a NO_3^- -bound complex as evidenced by gas chromatography and electrospray ionization-MS, implying a change in geometry from trigonal bipyramidal to square pyramidal (Figure 31d).³³⁷ Investigation into the mechanism of this transformation supported formation of an $^-\text{OON}=\text{O}$ intermediate species formed from nucleophilic attack of the hydroperoxo ligand, followed by release of a proton, formation of Cu^{1+} and isomerization of the peroxyxynitrite to form NO_3^- . The nascent Cu^{1+} species further reacts with NO to form N_2O .

4.2.3. Heme-Copper—Binary mixtures of heme and Cu complexes as well as molecular heme/Cu models have been employed in a variety of systems to study O₂ binding or reductive coupling.^{338–341} The first molecular binuclear heme/Cu assembly competent for NO coupling was reported by Kim and co-workers.³⁴² These authors were able to deliver stoichiometric amounts of NO using their previously reported³³⁸ $(^6\text{L})\text{Fe}(\text{NO})_2$ species as an NO donor. Addition of $[\text{Cu}^{1+}(\text{MeCN})_4]\text{B}(\text{C}_6\text{F}_5)_4$ and two equivalents of acid to stoichiometric amounts of this Fe species results in formation of N_2O in 80% yield as well as a $\text{Fe}^{3+}/\text{Cu}^{2+}$ (Figure 32a) product, suggesting a transformation similar to those seen in NOR enzymes (see Section 2.1) had taken place. The Cu ion plays a critical role in this transformation as evidenced by a lack of reaction and release of NO when the Cu species is removed from the reaction. Without the presence of acid, the resulting product is the heme-nitrosyl Cu–NO₂⁻ complex.

Wang and co-workers³⁴³ later applied the same concept to coupling of NO with a discrete heme and Cu system (Figure 32b). The Fe heme complex $(F_8)Fe^{3+}(NO)_2$ is generated by bubbling NO through either a solution of $(F_8)Fe^{2+}$ or $(F_8)Fe^{2+}(NO)$. Addition of $[(tmpa)Cu^I(MeCN)](ClO_4)$ and two equivalents of acid results in formation of the Fe^{3+} species, Cu^{2+} , N_2O , and H_2O . No reaction was observed when $(F_8)Fe(NO)_2$ was treated with acid. In the absence of acid, a disproportionation occurs resulting in the $(F_8)Fe(NO)$ species, along with products $[(tmpa)Cu^{2+}(NO_2^-)]^+$, $[(tmpa)Cu^{2+}(solvent)]^+$ and N_2O in a 1:2:1 ratio. The mechanism proposed is attack of the Cu^{1+} complex ($[(tmpa)Cu^{1+}(MeCN)]^+$) on the NO ligand in $F_8Fe(NO)_2$, releasing NO that can then attack the binuclear heme- Fe^{2+} - $(NO)-Cu^{1+}$ species yielding a $N_2O_2^{2-}$ -type species. Subsequent protonation, electron transfer from Cu, and NO cleavage would yield N_2O , H_2O as well as the heme- Fe^{3+} and Cu^{2+} species observed.

4.3. Nickel

While examples of biological systems competent for N–N bond formation containing Ni have not yet been realized, synthetic systems that may offer insight into analogous Fe- and Cu-mediated biological mechanisms have been reported since the mid-1900s, although the transformation was not initially investigated in depth.³⁴⁴ Wright and co-workers³⁴⁵ reported a Ni species, $[Ni(NO)(CH_3NO_2)_3][PF_6]$ (Figure 33a) that they synthesized via reaction of $NOPF_6$ with excess Ni powder in CH_3NO_2 in the presence of NiI_2 . Byproducts of this reaction include N_2O , which was initially suggested to be formed via a Ni-mediated NO coupling. $[Ni(NO)(bpy)_2][PF_6]$ ($bpy = 2,2'$ -bipyridine) (Figure 33b) was later reported to form N_2O via an initial rearrangement to $[Ni(\kappa^2-O_2N_2)(bpy)]$ and $[Ni(NO)(bpy)_3](PF_6)_2$ followed by subsequent reaction of $H(acac)$ ($acac = acetylacetonate$) with $[Ni(\kappa^2-O_2N_2)(bpy)]$.³⁴⁶ Further mechanistic studies on this transformation were carried out to differentiate between NO^-/NO^- , NO^-/NO^* , or NO^-/NO^+ coupling.³⁴⁷ Results of these studies precluded involvement of free NO in the formation of N_2O as mediated by $[Ni(NO)(bpy)_2][PF_6]$. Moreover, treatment of $[Ni(NO)(bpy)_2][PF_6]$ with $[Ni(NO)(bpy)][PF_6]$ resulted in isolation of $\{[(bpy)-Ni(\kappa^2-O_2N_2)]\eta^1:\eta^1 N,N\{[Ni(NO)(bpy)]_2\}[PF_6]_2$, a trimetallic Ni complex that features the $N_2O_2^{2-}$ fragment, $(bpy)-Ni(\kappa^2-O_2N_2)$, capped by two $[Ni(NO)(bpy)]^+$ groups. These combined results support a mechanism driven by NO^-/NO^- coupling.

In 2016, Ghosh and co-workers³⁴⁸ investigated the competence of Ni^{2+} for NO reduction. Treatment of the Ni^{2+} species L_2NiCl_2 ($L = bis(2\text{-ethyl-4-methylimidazol-5-yl})methane$) (Figure 33c) with two equivalents of NO produced the $[L_2Ni^I(NO)]Cl$ species. Further treatment of this species with two additional equivalents of NO results in formation of the $[L_2Ni^{2+}(NO_2)]Cl$, release of N_2O and formation of a Ni^{2+} -nitrito complex. While this is an example of NO disproportionation, which is not operative in biological systems, the Ni^{2+} reactivity towards NO still highlights Ni^{2+} as a potential starting point for N_2O formation.

It has been hypothesized that spin density at the N atom of a metal-nitrosyl as well the formation of a side-on M–NO conformation may facilitate N–N bond formation.³⁵⁰ Investigation of a low coordinate M–NO species that could accommodate both side-on NO and *cis*- $N_2O_2^{2-}$ ligands, specifically $(^iPr_2NNF_6)Ni(NO)$ ($(^iPr_2NNF_6 = 1,1,1,5,5,5\text{-Hexafluoro-2-(2,6-diisopropyl)phenylamino-4-(2,6-diisopropyl)phenyliminopent-2-ene}$

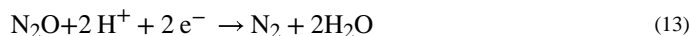
(Figure 33d), which exhibits a trigonal-planar Ni center with an end-on nitrosyl ligand, provides some evidence to support this claim. However, treatment of either end-on or side-on M–NO species with NO results in facile N–N coupling and formation of $\{[\text{Ni}(\kappa^2\text{-O}_2\text{N}_2)]\}^-$ species which release N_2O upon protonation. In both cases the complexes possess a significant amount of unpaired electron density at the nitrosyl N atom. Corresponding $\{\text{Ni}(\text{NO})\}^{10}$ species show no N_2O formation, highlighting the notion that electron density at the nitrosyl N atom is the likely driving force for this transformation.

A dinickel dihydride complex $[\text{KL}(\text{Ni-H})_2]^{349}$ (Figure 33e) was recently reported to facilitate two electron reductive coupling of NO resulting in formation of an N,O bridging cis-hyponitrite complex. Crystallographic studies of this species revealed the two Ni centers to display square-planar geometry, consistent with a low spin Ni^{2+} and the presence of a dianionic hyponitrite ligand. Further treatment of this species with NO or a proton source results in formation of N_2O and the μ -hydroxo complex. The isolation of an on-path hyponitrite intermediate will inform mechanistic transformations of biological NO reduction.

5. N_2 -Forming Enzymes

5.1. Nitrous Oxide Reductase (N_2OR)

5.1.1. N_2OR Background—Reduction of N_2O to N_2 is a strongly exergonic reaction ($G^0 = -339.5 \text{ kJ}\cdot\text{mol}^{-1}$) but rather kinetically inert under standard conditions due to its high activation energy ($G^0 = 250 \text{ kJ}\cdot\text{mol}^{-1}$).³⁵¹ The nitrogenase protein complex^{352,353} as well as a multicopper oxidase from a thermophilic archaeon³⁵⁴ have been reported to catalyze N_2O reduction *in vitro*. However, the only biological catalyst whose primary reactivity is the reductive conversion of N_2O to N_2 (Equation 13) is the soluble multicopper N_2O reductase enzyme (N_2OR or NosZ) that is encountered in all domains of life.³⁵⁵ N_2OR is predominantly associated with the multistep process of denitrification, i.e. the anaerobic respiration of NO_2^- or NO_3^- to N_2 , although the environmental abundance and diversity of non-denitrifying microorganisms harboring nosZ genes was recently appreciated.³⁵⁶



N_2OR is a soluble 130-kDa homodimeric multicopper protein complex that is encoded by the highly conserved nosZ gene. The latter is always found within the so-called nos gene cluster that includes six or seven accessory genes (nosRZDFYL[X]). The corresponding gene products have been implicated in expression, regulation, and biological assembly of a functional N_2OR holoprotein (References^{355,357,358} and references therein). In close proximity to the nos cluster there are usually genes coding for electron carrier proteins, e.g. c-type cytochromes or type-1 Cu proteins, that might act as electron donors for the biological reduction of N_2O to N_2 .³⁵⁹

Although NosZ (sometimes referred to as Z-type N_2OR) is encoded by the highly conserved nosZ gene, genomic investigations have identified an atypical nosZ open reading frame (NosZ clade II) that is well distributed among Bacteria and Archaea. The NosZ clade II

amino acid sequences display only up to 50% similarity to the NosZ clade I representatives and lack some active-site residues that are fully conserved among clade I members. This suggests possible structural and/or mechanistic variations among N₂ORs.³⁵⁹ Whole-cell N₂O consumption studies on bacterial strains harboring *nosZ* clade II gene clusters have detected measurable N₂O reductase activities,³⁶⁰ and in a comparative kinetics study, clade II exhibited 5- to 100-fold higher affinity for N₂O compared to clade I.³⁶¹ Another noteworthy difference between the two NosZ clades is the composition and arrangement of their *nos* gene clusters.³⁵⁹ Most interestingly, some but not all NosZ clade II sequences have an extended C-terminus that includes a cyt *c* domain with a single heme *c* binding motif (sometimes encountered as cNosZ).³⁶² In the single report available of the biochemical characterization of any cNosZ representative, the isolated protein from *Wolinella succinogenes* was, indeed, shown to harbor a *c*-type heme, as evidenced by UV/vis absorption and AES, as well as polyacrylamide gel electrophoresis (PAGE) heme staining, and exhibited substantial N₂OR activity without the necessity for activation (*vide infra*).³⁶³ Heterologous expression of the active *Geobacillus thermodenitrificans* clade II NosZ,³⁶⁴ lacking the heme binding motif, demonstrated that the *c*-heme cofactor is likely involved in electron transfer to the cNosZ enzymes but it is not necessary for efficient catalysis by clade II NosZ proteins.

5.1.2. N₂OR Active site architecture—To date, there are four crystal structures available for the clade I NosZ protein complex isolated by native organisms (*M. hydrocarbonoclasticus* (MhN₂OR), PDBID: 1QNI; *P. denitrificans* (PdN₂OR), PDBID: 1FWX; *Achromobacter cycloclastes* (AcN₂OR), PDBID: 2IWF; *P. stutzeri* (PsN₂OR), PDBID: 3SBP), one structure of the apoprotein as the result of recombinant expression (*Shewanella denitrificans* (SdN₂OR), PDBID: 5I5M), and two structures of the recombinantly expressed PsN₂OR holoprotein (rPsN₂OR-form I, PDBID: 6RL0; rPsN₂OR-form II, PDBID: 6RKZ). After pressurization of the PsN₂OR crystals with N₂O gas, an additional structure was obtained, where an N₂O molecule was found within the active site pocket of the enzyme, albeit not within bonding distances to the metal centers (PDBID: 3SBR). This structure will be hereafter referred to as the N₂O-associated PsN₂OR.

All structures present a tight head-to-tail homodimer with a dimerization interface consisting of conserved residues and accounting for about 25% of the surface area of each subunit (Figure 34).³⁶⁵ Each monomer consists of two domains that each bind a Cu center. The N-terminal seven-bladed β-propeller harbors the Cu_Z tetranuclear center and the C-terminal cupredoxin-like fold incorporates the Cu_A binuclear redox center.³⁵⁸ The two Cu centers within one subunit are more than 40 Å apart, but the arrangement of the complex is such that the Cu_A site of one subunit lies ca. 10 Å away from the Cu_Z center of the other. This structural arrangement yields two active sites per complex and precludes functionality of a monomeric N₂OR.

Cu_A is a binuclear Cu center, similar to the one present in cytochrome *c* oxidases,^{366,367} that is found within a loop of the cupredoxin fold at the C-terminus of NosZ. Two fully conserved Cys residues are the bridging ligands of the two Cu ions that lie 2.5 Å apart (Figure 35a). Each Cu is additionally coordinated by a fully conserved His, while Cu_{A1} is also bound to a Met S_δ and Cu_{A2} to the backbone carbonyl oxygen of a tryptophan residue.

The PsN₂OR structure revealed a slightly different conformation for the Cu_{A1}-ligating His,³⁶⁸ which was also seen in the structures of both rPsN₂OR-form I and rPsN₂OR-form II.³⁵⁷ His583 (numbering as in PsN₂OR) is rotated away from the Cu_A center and interacts with the neighboring Ser550 and Asp575 via hydrogen-bonding, resulting in a more planar arrangement for Cu_A with respect to the sulfur atoms of the bridging cysteines and Met629 (Figure 35b). Interestingly, in the N₂O-associated PsN₂OR structure, His583 is swung inwards, resulting in a Cu_A geometry identical to all other N₂OR structures obtained thus far.

The biologically unique tetranuclear [4Cu:1S] Cu_Z metal center resides in the center of the N-terminal β-propeller domain of NosZ. The four Cu atoms are coordinated by seven fully conserved histidine residues and a μ₄-sulfido ligand (S₁), resulting in the shape of a distorted tetrahedron for the Cu_Z cluster (Figure 36). The ligating His residues participate in a hydrogen-bonding network that involves neighboring residues, solvent molecules, and a protein-bound chloride ion. The latter is hydrogen-bonded to the histidine residue that coordinates the Cu_{Z1} atom (His392; numbering as in PdN₂OR), an observation that led to the hypothesis that the bound chloride might not only serve a structural role, but also influence the reduction potential of that Cu ion.^{369,370} DFT calculations suggest a crucial role for the complex network of hydrogen bonds around the Cu_Z center that determines the orientation of the imidazole rings of the coordinating histidines. Without these structural constraints, the Cu_Z cluster would assume a different geometry that would preclude substrate binding (Figure 37).³⁷¹

All N₂OR structures revealed the presence of additional ligands for the Cu_{Z1} and Cu_{Z4} ions, although there are discrepancies about their nature (Figure 38). In MhN₂OR the electron density maps accommodated the modelling of a solvent-derived ligand on the Cu_{Z1}/Cu_{Z4} open edge (hydroxo or aqua)^{369,372} as was also the case for PdN₂OR,³⁷⁰ whereas in AcN₂OR Cu_{Z1} and Cu_{Z4} atoms are ligated by hydroxide and water, respectively.³⁷³ Remarkably, the iodide-bound structure of AcN₂OR³⁷³ exhibited the same Cu_Z coordination (Figure 38) as was later shown for both the native,³⁷⁴ and the recombinantly expressed PsN₂OR's.³⁵⁷ In the latter structures, a sulfur atom was modelled as the bridging ligand for Cu_{Z1} and Cu_{Z4}, resulting in a [4Cu:2S] Cu_Z cluster, whose physiological relevance is currently under debate (*vide infra*). To differentiate between the two Cu_Z forms observed thus far, the [4Cu:1S] cluster is denoted by an asterisk (Cu_Z*), while Cu_Z represents the form with the S_{Z2} ligand. It is noteworthy that the isolation of Cu_Z*-containing N₂OR homologs has been associated with the presence of O₂ and the presumed irreversible loss of the labile S_{Z2} ligand.³⁷⁵ However, the aerobic isolation of the Cu_Z-containing MhN₂OR³⁷⁶ and rPsN₂OR-form I³⁵⁷ called this hypothesis into question. So far, the reasons for the variable identity of the Cu_{Z1}-Cu_{Z4} μ₂-ligand remain unknown, and so do the ramifications for enzyme activity.

Next to the two Cu centers, N₂OR appears to also bind two additional cations as is evident in all available structures. Although the electron density at the interface of the two monomers has been inconsistently assigned to either a Ca²⁺ (in MhN₂OR, PdN₂OR, and AcN₂OR) or a potassium (K⁺) ion (in PsN₂OR), the cation identified within the N-terminal β-propeller domain is undoubtedly shown to be a Ca²⁺. A structural study on the non-metallated

SdN₂OR suggested a crucial role for this Ca²⁺, and that it is presumably incorporated into the protein complex after the *in vivo* metallation events.³⁷⁷ Ca²⁺ binding was shown to confer structural rigidity to the protein complex by bringing the two domains of each subunit closer to each other and, thus, securing the Cu_A-binding cleft of N₂OR. This was further supported by the inability to reconstitute the Cu_A center after the addition of calcium to the apoprotein, which was possible before that addition.³⁷⁷ The same study also demonstrated that, apart from the three flexible loops that appeared disordered before Ca²⁺ addition, the rest of the apoprotein aligned very well with the structures of the holoprotein, indicating that the protein scaffold heavily predetermines the coordination geometries of the Cu centers in N₂OR.

5.1.3. Cu_A and Cu_Z Electronic Structures—Since the first isolation of an N₂OR,³⁷⁸ several studies have been focused on the biochemical and spectroscopic characterization of this metalloenzyme and have all reached the consensus that N₂OR exists in different forms *in vitro*. These forms are often named by the color of the isolated enzyme or using Latin numerals. The basic characteristics of these forms are presented here in Table 1. More relevant details will be discussed further below in the context of the catalytic mechanism of N₂O reduction. For a thorough description of the spectroscopic and catalytic properties of the different N₂OR forms, the reader is referred to a comprehensive review compiled by Pauleta and co-workers.³⁵⁸

Prior to the first crystal structure of an N₂OR that was obtained in the end of the 20th century,^{369,372} many spectroscopic studies were focused on determining the stoichiometry of the metal centers. Although some of the suggested models might have been proven inaccurate by now, all these studies contributed to the deconvolution of the spectroscopic signatures of the holoprotein. UV-vis absorption and EPR spectroscopies have been key approaches used to characterize N₂OR metal centers, although additional spectroscopic techniques, such as resonance Raman, CD, MCD, and X-ray absorption (XAS) have also been used.^{379–385}

The binuclear Cu_A center exhibits minimum variation in its coordination geometry (Figure 35) and its electronic structure is reasonably well understood.^{386–388} Cu_A has so far been observed in two distinct oxidation states with a midpoint potential of about +0.260 V (vs. NHE).³⁸⁹ In its oxidized form, it is found in a mixed-valent [Cu_{A1}^{1.5+}: Cu_{A2}^{1.5+}] state with a net charge of +3 and an $S = 1/2$ spin state,³⁷⁵ similar to some HCOs.^{366,390} In UV-vis absorption spectra of holoproteins, oxidized Cu_A contributes absorption maxima at 480, 525–540, and 800 nm (Figure 39). The single unpaired electron that is fully delocalized over both Cu nuclei gives rise to a narrow seven-line hyperfine splitting in the g_{\parallel} region of EPR spectra, characteristic of two nuclear spins $I_{\text{Cu}} = 3/2$.³⁹¹

Based on partial reduction of N₂OR isolates—ascorbate can selectively reduce the Cu_A center³⁹²—studies on Cu_Z-deficient variants,^{393,394} and simulations of the separate Cu centers' contributions,³⁷⁵ the UV-vis absorption subspectra of the Cu_Z center have been confidently determined. The Cu_Z center contributes UV-vis absorption features with maxima at 550 and 650 nm that are attributed to $S \rightarrow \text{Cu}$ LMCT transitions involving Cu 3*d* and S 3*p* orbitals.³⁹⁵ The Cu_Z* center contains only the 650 nm feature, indicating that the origin

of the 550 nm band is the S_{Z2} atom, while the 650 nm band only disappears once the Cu_Z^* center is reduced by methyl viologen.³⁶⁸ Based on spectroscopic studies and DFT calculations, the spin state of Cu_Z^* has been assigned as $S = 1/2$, with the spin density partially delocalized over the four Cu atoms and the μ_4 -sulfido ligand.^{382,383} Participation of the sulfide ligand in the redox active molecular orbital has been confirmed by sulfur K-edge XAS, which estimates ca. 15–22% participation of S 3p.³⁸⁴ Delocalized spin density, even more widely distributed, has also been described for the $[1Cu_Z^{2+} : 3Cu_Z^{1+}]$ redox state of Cu_Z ,³⁹⁶ leading to the premise that the electron delocalization over the Cu_Z center contributes to a low reorganization energy of the redox processes during the catalytic cycle of N_2OR .³⁸⁴

5.1.4. Intermolecular Electron Transfer Involving N_2OR —Based on kinetics and spectroscopic studies, both type-1 Cu proteins and *c*-type cytochromes have been shown to donate electrons to different N_2OR homologs *in vitro*, and this flexibility is presumed to be exploited *in vivo* as well.^{74,75,385} So far, cyt *c552* and pseudoazurin have been clearly identified as the physiological electron donors for MhN_2OR and AcN_2OR , respectively,^{397,398} while other N_2OR homologs seem to interact with either. Although the exact binding interface and the electron transfer pathways are not yet elucidated, protein-protein docking simulations have predicted the interacting geometries between different N_2OR homologs and their corresponding physiological electron donors.³⁹⁹ A negatively-charged patch on the surface of N_2OR has been identified as the recognition site for the transient complex, while the main interactions once the complex is formed are hydrophobic.^{397,399} The distance between the electron donor metal center and the electron-accepting Cu_A is ca. 15 Å in all cases, and a few highly conserved residues (Pro, His, Asp, and Leu) are the most likely candidates to form an electron ladder from the surface entry point to the Cu_A center,^{397,398,400} similar to other transient electron transfer complexes.^{401,402}

The different geometries of the Cu_A site observed in the obtained structures (*vide supra*) could be indicating a possible conformational switch operative during catalysis.^{368,375} While the imidazole side chain of His583 (numbering as in PsN_2OR) is rotated away from Cu_A in the resting PsN_2OR structures, it was found to coordinate Cu_A in the N_2O -associated PsN_2OR . Electron transfer from Cu_A to Cu_Z was also observed only after binding of N_2O .³⁶⁸ Cu_A could be envisaged as a molecular gate that controls the electron transfer from the external donor to the Cu_Z center. Once N_2O is present within the binding pocket of N_2OR , His583 ligates Cu_A , possibly also regulating its reduction potential,³⁹⁸ and thus, allows its reduction and subsequent intramolecular electron transfer to Cu_Z . This would be in line with the observation of *Paracoccus pantotrophus* N_2OR reducing N_2O only after the formation of a complex with the electron-donating cyt *c552*,³⁸⁵ and would explain the prediction that electron transfer is the rate-limiting step in the catalytic cycle of N_2OR at physiological pH.^{371,375,397}

5.1.5. N_2OR Substrate Binding and Catalysis—Kinetics studies performed on different N_2OR homologs have yielded varying kinetics parameters,⁴⁰³ although in most cases the spectrophotometric assay developed by Kristjansson and Hollocher⁴⁰⁴ was used, where the strong reductant methyl viologen is the artificial electron donor for N_2O

reduction. These discrepancies can be, at least partially, attributed to the precarious nature of the Cu_Z cluster. Cu_Z is considerably affected by the experimental procedures used for isolation with regards to its structural coordination, redox state, and catalytic competence. The observed variability of the Cu_{Z1}/Cu_{Z4} μ₂-ligand identity seemingly determines both its redox flexibility and catalytic competence (*vide infra*).

Cu_Z* is always isolated in the [1Cu_Z²⁺ : 3Cu_Z¹⁺] state, which is redox inert under mild conditions and essentially inactive. *In vitro* reductive activation to the so-called sr, UV/vis- and EPR-silent, diamagnetic, [4Cu_Z¹⁺] state^{397,405–409} is necessary and sufficient for catalysis that proceeds with turnover rates of 4–300 s⁻¹ depending on the nature of the reductant used.³⁹⁷ This reductive activation process was not only shown to be quite slow, with a rate constant $k = 0.07 \text{ min}^{-1}$,⁴⁰⁸ but also required strong reducing conditions (methyl viologen: $E'^{\circ} = -0.440 \text{ V vs. NHE}$ ⁴¹⁰) that are most probably not available *in vivo*.⁴⁰⁹ As a result, the [1Cu²⁺ : 3Cu¹⁺] Cu_Z* state has been assumed to be non-physiological and the prevailing perception of N₂O reduction by N₂ORs involves the super-reduced Cu_Z* site (Scheme 6).

The coordination of a substrate molecule is assumed to happen at the Cu_{Z1}/Cu_{Z4} edge, as was shown for the iodide-bound inhibited AcN₂OR.³⁷³ According to DFT calculations performed by Ghosh and co-workers,⁴⁰⁸ the lowest-energy structure for the N₂O-bound inactive [1Cu_Z²⁺ : 3Cu_Z¹⁺] Cu_Z* resting state is in a linear N end-on fashion, which is very similar to the gas-phase structure of N₂O. In contrast, the super-reduced Cu_Z* center preferably binds N₂O in a μ₂-1,3 bridging mode resulting in a bent geometry, where the Cu_{Z1}-N and Cu_{Z4}-O interactions are stronger compared to the N-N and N-O bonds.³⁷¹ This strong back-bonding from Cu_{Z1} and Cu_{Z4} would compensate for the large deformation energy of the N₂O ligand and, therefore, activate the otherwise kinetically inert N₂O molecule for both direct and proton-assisted N-O bond cleavage.^{371,382} Hydrogen-bonding between the O atom of N₂O and the side chain of a neighboring conserved lysine is presumably assisting in the stabilization of this coordination by lowering the activation energy even more.³⁷¹ Bar-Nahum and co-workers⁴¹¹ suggested a different mode for substrate binding to the Cu_{Z1}/Cu_{Z4} edge, that is in a μ₂-1,1-O coordination, while another computational study concluded that terminal O end-on binding of N₂O is yet another possibility that would lead to the same μ₂-oxo coordination upon dissociation of N₂.⁴¹²

In any case, two-electron transfer from Cu_Z, with or without concomitant protonation of the N₂O oxygen atom, could then induce N-O bond cleavage. This would lead to the dissociation of N₂ and leave the Cu_Z center at the two-hole intermediate ([2Cu²⁺ : 2Cu¹⁺]) that is presumably short-lived and, thus, has never been observed. Subsequent protonation and single electron transfer from the Cu_A center would result to the Cu_Z⁰ intermediate that is at the [1Cu_Z²⁺ : 3Cu_Z¹⁺] redox state and either has an aquo ligand to Cu_{Z1}⁴¹³ or a terminal Cu_{Z4}-hydroxo ligand.⁴¹⁴ Fast two-electron reduction, possibly through super-exchange pathways involving the μ₄-sulfido ligand, would return to the catalytically competent [4Cu_Z¹⁺] redox state.

In the absence of reductant, Cu_Z⁰ was shown to decay *in vitro* to the inactive resting Cu_Z* state with a rate constant of $k = 0.3 \text{ min}^{-1}$.⁴¹³ This inactivation process does not involve any

redox transitions, but it exhibits pH dependence. Specifically, it proceeds faster at basic pH, implicating a protonation/deprotonation event.⁴¹³ The Cu_{Z1}/Cu_{Z4}-bridging water has been implicated in this process based on the premise that cupric μ_2 -hydroxo ligands exhibit lower reduction potentials compared to their aqua counterparts.^{397,413,415} This suggests that, upon deprotonation of the Cu_{Z1}/Cu_{Z4}-bridging ligand, the midpoint potential of Cu_Z is lowered and, therefore, the center cannot be easily re-reduced to return to the active [4Cu²⁺] state. Instead, the center decays to the inactive Cu_Z* state. Deprotonation of the Cu_{Z1}/Cu_{Z4}-bridging water during the catalytic cycle could also lead to slower intramolecular electron transfer between Cu_A and Cu_Z and, therefore, to lower catalytic rates as has been observed before when cyt c552 was used as an electron donor for N₂O reduction by MhN₂OR.³⁹⁷ Detailed computational, spectroscopic, and kinetics studies have shown that proton concentration has multiple effects on both the reductive activation and the catalytic activity of N₂OR, albeit the mechanistic details are poorly understood.^{416–418} N₂OR seems to retain its catalytic competence over a wide pH range but it does exhibit complex pH dependence that is attributed to conformational changes around the Cu centers. Next to the Cu_{Z1}/Cu_{Z4} μ_2 -ligand, a lysine residue near the Cu_{Z1}/Cu_{Z4} edge has also been suggested to influence the pH-dependent behavior of N₂OR. The protonated lysine, that could H-bond to the Cu_{Z1}/Cu_{Z4} μ_2 -hydroxo ligand, would increase the redox potential of the Cu_Z center and, thus, promote its reductive activation to the [4Cu¹⁺] state.⁴¹⁸

All of the mechanistic studies mentioned above have been based on the [4Cu-1S] Cu_Z* center architecture that contains a μ_2 -water (or -hydroxo) ligand in the Cu_{Z1}/Cu_{Z4} edge, without accounting for the S_{Z2} ligand of the Cu_Z center.^{357,368,374,419} In the N₂O-associated PsN₂OR structure, N₂O is positioned in a linear side-on manner within a structurally defined cleft between Cu_Z and Cu_A that is formed by Phe621, Met627, and the Cu_A-ligating His626 (Figure 40). The O atom of N₂O is oriented towards a solvent-filled cavity while the N end is within about 3.5 Å from the Cu_Z site. The observed distances between N₂O and Cu_Z suggest weak interactions that would not allow substrate activation and, thus, conformational changes around both Cu clusters would have to occur before any catalytic event takes place.³⁸⁹ Although the Cu_Z site architecture was only recently structurally resolved, it can be confidently concluded in hindsight that few Cu_Z-containing N₂OR homologs have been isolated over the previous years, although the identity of the Cu_{Z1}/Cu_{Z4} μ_2 -ligand was not known at the time. These species could never reach the super-reduced state, even after prolonged incubation with excess reductant,^{392,419} and exhibited very low steady-state turnover rates (up to 106-fold lower compared to fully reduced Cu_Z*) under physiological conditions.^{357,376,380,381,389,399,419–422} Presently, the super-reduced [4Cu¹⁺] state of the Cu_Z* center is the only species that has exhibited substantial kinetic competency during steady-state turnover conditions,⁴¹⁹ and the physiological relevance of the μ_2 -S_{Z2} ligand of the Cu_Z center still awaits investigation.

5.2. Hydrazine Dehydrogenase (HDH)

The other known enzyme that produces N₂ under physiological conditions is the massive, 1.7 MDa multiheme protein complex HDH.^{20,423,424} HDH completes the final step of anammox metabolism (anammox,²⁰ *vide infra*) process by carrying out the following reaction:



Via this process, HDH emits a purported 50% of N_2 returned to the atmosphere to close the biogeochemical nitrogen cycle. HDH is a paralog of HAO (see Section 2.3). Its three-dimensional structure was recently determined through a combination of X-ray crystallography and cryoelectron microscopy.⁴²³ The complex is roughly cube shaped and is comprised of two subunits α and β in an $(\alpha_3)_8\beta_{12}$ arrangement (Figure 41a). The α subunits are octaheme proteins like the subunits of HAO complexes, with each bearing eight *c*-hemes. Of these, seven are coordinatively-saturated hemes expected to participate in an extensive electron transfer network, while the eighth has a labile coordination site and thus likely to be the active site for N_2H_4 oxidation (Figure 41b). The extensive electron transfer network is hypothesized to be vital to storage and delivery of the many low-potential reducing equivalents liberated during catalysis.

The catalytic *c* heme is a P460-like cofactor that, in addition to HAO-like heme-Tyr cross-links and two canonical *c*-heme thioethers, also bears a third heme-Cys cross-link (Figure 41b). Distal His and Asp residues likely mediate a combination of substrate orientation/binding as well as proton transfer. A plausible mechanism for N_2H_4 oxidation by HDH devised by Maalcke and co-workers⁴²⁴ is given in Scheme 7. Curiously, HDH is inhibited by both NH_2OH and NO. Given the profound complexity of the HDH complex, scrutinizing this mechanistic hypothesis will need to draw heavily on the efforts of computational and synthetic chemists.

6. Bioinspired N_2 -forming Reactions

Bar-Nahum and co-workers⁴¹¹ reported a tri-Cu disulfide cluster (Figure 42a) that was competent for reduction of N_2O to N_2 . Their proposed mechanism for this species includes formation of a dicopper complex which reduces N_2O via an O bridged transition state. Johnson and co-workers⁴²⁵ later reported a model bearing Cu_Z 's full complement of four Cu centers: $[(\mu_2\text{-dppa})_4\text{Cu}_4(\mu_4\text{-S})](\text{PF}_6)_2$ (dppa = *bis*(diphenylphosphino)-amine) (Figure 42b). This model featured an asymmetric core, where the fourth Cu is significantly displaced from the others, closely resembling Cu_Z^* . Although this species was not reactive towards N_2O , treatment with NaN_3 , which is isoelectronic to N_2O , at room temperature produced a mixture of compounds including $[\text{Cu}_3(\mu^3\text{-S})]$ and $[(\mu^2\text{-dppa})_3\text{Cu}_3(\mu^3\text{-N}_3)_2](\text{PF}_6)$. The $[(\mu^2\text{-dppa})_3\text{Cu}_3(\mu^3\text{-N}_3)_2](\text{PF}_6)$ showed a characteristic IR vibration at 2046 cm^{-1} and the obtained crystal structure showed N_3^- binding in an end-on fashion, which contrasts the proposed side on binding of N_2O in Cu_Z^* .³⁷¹ Later, Jayarathne and co-workers⁴²⁶ explored bimetallic N-heterocyclic carbene species and their reactivity toward N_2O . One species, (IMes)CuFp, (IMes = *N,N'*-bis(2,4,6-trimethylphenyl)imidazol-2-ylidene; Fp = Fe(cyclopentadienyl)(CO)₂) (Figure 42c) was shown to produce stoichiometric formation of N_2 by gas chromatography/mass spectrometry (GC-MS). Reactivity of this species towards N_2O is unique in that the later, more electronegative, less oxophilic metal serves as the acidic site. More typically, N_2O reactivity in synthetic systems is the domain of highly oxophilic or azophilic metal centers that do not perform catalytic turnover.⁴²⁷⁻⁴³⁰ Treatment

of this species with triphenylphosphine (PPh₃) produced triphenylphosphine oxide (OPPh₃), suggesting an intermediate containing a bifunctionally activated N₂O adduct capable of donating its O atom to PPh₃. A Cu₄(μ₄-S) (Figure 42d) species was later reported that was stable in the [2 Cu¹⁺ : 2 Cu²⁺] form⁴³¹ as well as the reduced [3 Cu¹⁺ : Cu²⁺].⁴³² The [3 Cu¹⁺ : Cu²⁺] species was shown to be competent for reduction of N₂O, producing N₂ and the [2 Cu¹⁺ : 2 Cu²⁺] species, completing the cycle (for the first time) as a mimic for reduction of N₂O by the Cu_Z* site. DFT calculations on a truncated structure of Cu₄(μ₄-S) suggest high levels of covalency in the Cu–S bonds, implicating that S may be involved in the oxidation step.

Recently, a Ni species was described to be competent for reduction of NO₃⁻ to N₂.¹⁹ A Ni–NO₃⁻ species (PNP)Ni(ONO₂) (PNP = (N[2-PⁱPr₂-4-Me-C₆H₃]₂) (Figure 42e) was prepared by treatment of [(PNP)Ni](OTf) with NaNO₂. The coordination sphere around the Ni consists of the PNP ligand and one of the oxygens from the NO₃⁻ group in square planar geometry. This species is competent for O atom transfer to CO—addition of CO to a solution of (PNP)Ni(ONO₂) results in formation of (PNP)Ni(NO). Intermediates expected along this path include the Ni-nitrito or Ni-nitro species. Reaction of (PNP)NiCl with NaNO₂ produces (PNP)Ni(NO₂), which exhibits identical ³¹P NMR and IR signals to the intermediate trapped along the reaction pathway. To continue along the denitrification sequence, treatment of (PNP)Ni(NO) with two equivalents of NO results in N₂O formation, as evidenced by headspace GC and formation of the (PNP)Ni(NO₂) species. Furthermore, addition of N₂O directly to (PNP)Ni(NO) results in formation of N₂ after 36 hours. This species represents the first transformation of NO₃⁻ to N₂ by a single reaction site, where the driving force for the reaction comes from CO, which serves as the acceptor of the O atoms. However, the authors note that each step in the transformation proceeds through a vastly different mechanism. Transformation from NO₃⁻ to NO₂⁻ requires a bimetallic mechanism, followed by the Ni-nitro readily affording the Ni-nitrosyl and CO₂. Removal of the last oxygen requires addition of NO, although the final species can also act as an oxygen acceptor producing NO₂ and N₂.

7. N₂H₄-Forming Enzymes

7.1. Hydrazine Synthase (HZS)

7.1.1. HZS Background—Although N₂H₄ had already been recognized as a potent toxin and an industrially valuable compound, it was not until the very end of the 20th century that it was identified as a biological intermediate.⁴³³ To date, anammox is the only known biological process that exploits the reducing power of N₂H₄ for energy conservation and anabolic purposes.⁴³⁴ In this case, N₂H₄ synthesis relies on the combination of two compounds with different nitrogen oxidation states, NO and NH₃, and is catalyzed by the heterotrimeric protein complex HZS. HZS catalyzes N₂H₄ synthesis from NO and NH₄⁺ *in vitro*, albeit with a rate of 20 nmol·h⁻¹·mg⁻¹ protein that accounts for about 1% of the *in vivo* turnover.⁴³⁵ Curiously, HZS activity is only observed in a coupled assay where the produced N₂H₄ is enzymatically converted to N₂ by HDH (see Section 5.2), supplying the former with the necessary electrons. Although the use of artificial electron donors might account for the slow conversion observed, the possibility of a metabolic supercomplex that is

essential for HZS activity and is disrupted upon purification cannot not be excluded. Immunogold localization studies have not identified such a complex, neither any direct association of HZS to the energized membrane of anammox bacteria,⁴³⁶ but formation of transient catabolic macromolecular assemblies has been previously observed in prokaryotes.^{437,438}

7.1.2. HZS Active Site Architecture—*K. stuttgartiensis* is the most studied anammox species to date and is also the source of the single crystallographically resolved structure of HZS at 2.7 Å (PDBID: 5C2V).⁴³⁹ HZS crystallized as a crescent-shaped dimer of heterotrimers (($\alpha\beta\gamma$)₂) of ca. 330 kDa size but, according to the current understanding, the catalytic protomer is the $\alpha\beta\gamma$ heterotrimer (Figure 43). In accord with genomic predictions,^{440,441} subunits α and γ harbor two *c*-type hemes each, with one heme per subunit being *bis*-His coordinate (hemes α II and γ II). The other two heme centers are five-coordinate and exhibit a few oddities with regards to their inner coordination spheres (Figure 44).

In heme α I the histidine residue (His587) of the typical CXXCH heme binding motif is rotated away from the heme Fe and the hydroxyl group of a highly conserved tyrosine (Tyr591) is the proximal ligand instead. His587 is bound to a Zn²⁺ ion with an atypical coordination sphere⁴⁴² that includes direct interaction with a propionate group of heme α I.

Heme γ I is proximally coordinated by the histidine of the corresponding heme binding motif (His106) and distally by a solvent molecule that is hydrogen bonded to Asp168. Remarkably, apart from the two covalent attachments to the cysteines of the binding motif (Cys102 and Cys105), heme γ I features an additional covalent bond to the protein that is formed between the C₁ porphyrin methyl group and the S γ sulfur atom of Cys165 of the same subunit. The edge-to-edge distance between the two hemes of the γ subunit is 15 Å, and a conserved histidine (His144) is positioned between them.

7.1.3. HZS Catalytic Mechanism—Based on preliminary biochemical and spectroscopic data combined with analyses of the 2.7 Å crystal structure of HZS, a working hypothesis for the catalytic mechanism of biological hydrazine synthesis has been suggested.⁴³⁹ According to the working model (Figure 45), the HZS heterotrimer serves as the catalytic monomer and N₂H₄ synthesis proceeds via two half reactions, facilitated by the two five-coordinate *c*-type hemes and a branched tunneling system consisting of metal ions and polar residues. NO enters the protein complex through a presumed substrate channel that connects the protein surface to heme γ I. Electrons from the external electron donor enter the complex at heme γ II and are shuttled to heme γ I via His144. With the input of three protons from the solvent reaching heme γ I via the conserved Asp168, the nitrosyl complex undergoes a three-electron reduction to NH₂OH at the first active site of HZS (heme γ I). This plausibly could be the microscopic reverse of the oxidation of NH₂OH by heme P460 enzymes (see Section 2.3).

Examination of the HZS structure revealed an intraprotein tunneling system that traverses the catalytic heterotrimer and, thus, connects hemes γ I and α I. This offers a means for the intramolecular intermediate of HZS, i.e. NH₂OH, to diffuse to the second active site (α I). A 15-amino-acid-long loop of the β -subunit (β 245–260), harboring a conserved glutamate

(Glu253) that binds a magnesium (Mg^{2+}) ion, could be regulating the transport of the intermediate. The modelled heme αI - NH_2OH adduct predicted coordination of NH_2OH with its N atom bound to the heme Fe in a hydrophobic cleft that would minimize electrostatic shielding of the partial positive charge on the nitrogen.

A small branch of the identified tunneling system that reaches heme αI from the proximal side is the assumed entry point of the second substrate of HZS, NH_3 , which would predominantly be in its protonated form *in vivo*.⁴⁴³ An acid/base reaction that would yield ammonia might be taking place at the Zn site, before NH_3 would then attack the nitrogen of NH_2OH , producing N_2H_4 through comproportionation. However, this umpolung reactivity necessitates considerable electronic perturbation of NH_2OH . Although this could possibly be achieved through binding to a metallocofactor, this has yet to be experimentally or computationally investigated.

Curiously, activity assays performed on HZS purified from another anammox species (*Brocadia sinica*) showed production of N_2H_4 *in vitro* from NH_4^+ and NH_2OH but not from NH_4^+ and NO ,⁴⁴⁴ raising considerations about possible differences among anammox bacteria with regards to their mechanism for N_2H_4 synthesis. However, the high sequence conservation among HZS homologs weakens any argument in favor of *in vivo* mechanistic differences and points towards experimental limitations in understanding this unique enzyme.

7.1.4. HZS Electron Transfer—The genes coding for the HZS subunits (Kuste2859–Kuste2861 or KSMBR1_3601–KSMBR1_3603) are highly conserved among anammox bacteria, and so are three other genes (Kuste2854–Kuste2856 or KSMBR1_3596–KSMBR1_3598) that are usually found within the same gene cluster and upstream of the HZS catalytic genes.⁴³⁴ Kuste2854 codes for a soluble tetraheme *c*-type cyt that is present in the proteome of *K. stuttgartiensis*⁴³⁵ and has been implicated in electron transfer to HZS.⁴⁴⁵ Kuste2855 and Kuste2856 code for a membrane-anchored and an integral membrane protein, respectively, and their corresponding gene products have been identified in the membrane complexome analysis of the same bacterium.⁴⁴⁶ Based on their genomic context and their expression levels these gene products have been speculated to constitute the dedicated electron transfer module (ETM) that would shuttle the necessary electrons from the quinone pool towards N_2H_4 synthesis, possibly though without contributing to energy conservation.^{434,446}

The membrane-bound part of the ETM consists of a membrane-anchored heptaheme *c*-type cyt (Kuste2855) and an integral membrane protein harboring six TMH (Kuste2856). The latter exhibits significant homology to the *b*-heme-containing γ subunit (FdnI) of menaquinone-dependent formate dehydrogenase (FDH-N), which couples periplasmic formate oxidation to menaquinone reduction.⁴⁴⁷ By analogy, Kuste2856 could work in reverse and couple menaquinol oxidation to *b*-heme reduction. The generated electrons would then be shuttled to the *c*-hemes of Kuste2855, that would subsequently reduce the soluble electron carrier, *i.e.* Kuste2854. The latter would be the direct electron donor to HZS (Figure 46).⁴⁴⁸

Based on their surface-exposed position within the protein complex, both six-coordinate hemes of HZS (α II and γ II) could serve as entry points for electrons. However, the electrostatic surface properties around heme γ II are in agreement with cyt *c* binding sites (negatively charged patch), and heme α II appears redox isolated. The closest redox center to heme α II is heme α I and their edge-to-edge distance is too long for single-step electron transfer on the timescale of catalysis (31 Å).⁴⁴⁹ Thus, the most likely scenario of electron transfer involves docking of Kuste2854 on the γ -subunit side of the catalytic complex and shuttling electrons to heme γ II.

8. Bioinspired N₂H₄-Forming Reactions

Because N₂H₄ was only recently discovered to be an obligate metabolic intermediate, there are no synthetic models for HZS to date. However, synthetic efforts have been made towards studying nitrogenase, in which N₂H₄ is proposed as an intermediate.^{450–453} Synthesis of N₂H₄ from NH₃ has also been reported in the context of NH₃-bearing ice in the solar system^{454,455}, as well as numerous accounts of N₂H₄ formation from electron or laser induced studies of NH₃, NO₂ and NO₃.^{456–458} Yet, none of these systems approach the mechanism used by nature to make the highly energetic metabolite N₂H₄. Consequently, the recent discovery and characterization of HZS highlights an area of synthetic opportunity that should spur future efforts.

9. Summary and Conclusions

Nature forms N₂O via the reaction of NO (or one of its redox congeners) with either additional NO or with NH₂OH. In the HCO- and FDP-type NORs, much evidence points toward the necessity of two redox-active Fe-centers to produce N₂O via coupling of two equivalents of NO, although in engineered systems NORs as well as in P450nor, a single redox-active metal appears sufficient. Thus, it remains unclear whether a single type of mechanism is operative in the binuclear Fe NORs, or whether differential tuning of either metal site through second-sphere effects favors alternative mechanisms among the binuclear NORs. Meanwhile, comproportionation of NH₂OH with NO (likely NO⁺) by cyt P460s affords another route to N₂O. Such a reaction necessarily involves careful proton and electron management, although the sequence of events promoting and following N–N bond formation remains to be elucidated.

Considerable opportunities remain concerning research into biological N₂-forming reactions. HDH is a remarkably complex metalloprotein that is effectively impervious to even element-selective spectroscopies. Here, clever modeling chemistry could afford new catalysts that could confer control over the highly exergonic oxidation of N₂H₄, potentially serving as electrode materials or mediators in N-based fuel cells. Likewise, resolving the ambiguities in the relationships between Cu-cluster oxidation states and competence for O-atom transfer from N₂O could inspire new technologies to remediate atmospheric contamination by this potent and persistent greenhouse gas.

Perhaps the least is known about the mechanism underlying biological N₂H₄ formation, although recognition that this molecule has relevance to primary metabolism has come about

very recently. Some parallel can be drawn between the chemistry of HZS and NH_2OH oxidizing heme P460 enzymes, namely that N_2H_4 likely proceeds via comproportionation of N-species. However, the current hypothesis that two nucleophiles (NH_2OH and NH_3) combine to make N_2H_4 demands considerable electronic perturbation mediated by the metallocofactors involved. Progress on this front, demands improved preparative methods for HZS that yield active enzyme, but in the meantime synthetic inorganic chemists can ply their trade to realize a functional model for this very enigmatic N–N-bond forming reaction.

Acknowledgments

We gratefully acknowledge Dr. Samantha N. MacMillan and Prof. Jonathan D. Caranto for assistance with the preparation of this review and for valuable discussions. K.M.L. gratefully acknowledges the Alfred P. Sloan Foundation, the US Department of Energy Office of Science (DE-SCSC0013997), and the National Institute of General Medical Sciences (R35GM124908) for support of his laboratory's research into chemistry germane to the biogeochemical nitrogen cycle. C.F. is a Fellow of the Dreyfus Postdoctoral Program in Environmental Chemistry; K.M.L. is a mentor in the same program. S.H.M. is a National Science Foundation Graduate Research Fellow.

Author Information

13.

Christina Ferousi received a Diploma degree in Biology from National and Kapodistrian University of Athens in Athens, Greece. She then obtained her Ph.D. from the Department of Environmental Microbiology of Radboud University in Nijmegen, the Netherlands, where she worked on *c*-type cytochromes from anammox bacteria. She is currently a Postdoctoral Fellow at Cornell University as part of the Dreyfus Program in Environmental Chemistry, studying the enzymology of nitrification. She hates lemons.

Sean H. Majer was born and raised in Buffalo, New York. He attended Vassar College where he received a B.A. in Chemistry with a minor in Art History. At Vassar, he worked in the laboratory of Joseph M. Tanski where he studied the asymmetric alkylation of imines with Group IV organometallic catalysts. He is currently an NSF Graduate Research Fellow at Cornell University. His current research focuses on the bioinorganic chemistry of microbial nitrification, specifically the heme enzymes involved in NH_2OH oxidation. When not in lab, he is often found playing trivia or picking up heavy things at the gym.

Ida M. DiMucci is currently a Ph.D. candidate at Cornell University. She was raised in Conneaut Lake, a tiny tourist town in Northwestern, PA. She then obtained her B.S. in Chemistry from Gettysburg College where she worked with Dr. Lucas B. Thompson evaluating the potential for gold nanoparticles to act as drug delivery systems. Her current research focus involves investigating the electronic structure of late high-valent transition metal species. When not working on her computer or at a synchrotron, Ida can be found watching Grey's Anatomy with her cats or hiking the Adirondacks.

Kyle M. Lancaster earned a Bachelor of Arts in Molecular Biology at Pomona College, where he studied the redox enzymology and sulfur metabolism of the hyperthermophilic archaeon *Pyrococcus furiosus* with E.J. Crane, III. As an NSF Graduate Research Fellow at the California Institute of Technology, he became a card-carrying bioinorganic spectroscopist thanks to the mentorship of Harry B. Gray and Jack Richards. After

completing his Ph.D. studying electronic structures and electron transfer mechanisms of not-particularly-blue Cu proteins, Kyle moved to Cornell University to deepen his knowledge of X-ray spectroscopies under the guidance of Serena DeBeer. Kyle is now an Associate Professor in the Department of Chemistry and Chemical Biology at Cornell, where he and his group leverage spectroscopic, computational, synthetic, and biochemical methods to understand transition metal (bio)catalysis relevant to energy transduction and C/N–H bond activations.

List of Abbreviations

10.

acac	acetylacetonate
ACN₂OR	Achromobacter cycloclastes
AES	atomic emission spectroscopy
ANAMMOX	anaerobic ammonium oxidizing bacteria
AOB	ammonia oxidizing bacteria
BMPA-PhO	<i>N</i> -(2-methyl-(2-chloromethyl-6-methylphenolate))- <i>N,N</i> -bis-(2-pyridylmethyl)amine)
BNC	binuclear center
BPMP	2,6- <i>bis</i> [<i>bis</i> (2-pyridylmethyl)amino)methyl]-4-methylphenol
BPMP	2,6- <i>bis</i> [<i>bis</i> (2-pyridylmethyl)amino)methyl]-4-methylphenol
BPY	2,2'-bipyridine
Ca²⁺	calcium ion
Cco	cytochrome <i>c</i> oxidase
CN⁻	Cyanide
cNO	cytochrome nitric oxide reductase
CO	carbon monoxide
CO₂	carbon dioxide
Cyt	cytochrome
DFT	density functional theory
DiFeNO	diferrous dinitrosyl
DMF	dimethylformamide
DNIC	dinitrosyl iron complex

dppa	<i>bis</i> (diphenylphosphino)-amine
EPR	electron paramagnetic resonance spectroscopy
Et-HPTB	<i>N,N,N',N'</i> - <i>tetrakis</i> -(<i>N</i> -ethyl-2-benzimidazolylmethyl)-2-hydroxy-1,3-diaminopropane)
FAD	flavin adenine dinucleotide
FDPS	flavodiiron proteins
Flv	flavin oxidoreductase
FMN	flavin mononucleotide
Fp	Fe(cyclopentadienyl)(CO) ₂
FTIR	Fourier-transform infrared spectroscopy
H⁻	Hydride
H₂N₂O₂	hyponitrous acid
H₂SO₄	sulfuric acid
HAO	hydroxylamine oxidoreductase
HCO	heme copper oxidase
HDH	hydrazine dehydrogenase
hyp	hyponitrite pathway
HZS	hydrazine synthase
ICP-MS	inductively-coupled plasma mass spectrometry
ImH	imidazolate
iPr₂NNF₆	1,1,1,5,5,5-Hexafluoro-2-(2,6-diisopropyl)phenylamino-4-(2,6-diisopropyl)phenyliminopent-2-ene
K_D	equilibrium dissociation constant
LMCT	ligand-to-metal charge transfer
MD	molecular dynamics
MhN₂OR	Marinobacter hydrocarbonoclasticus nitrous oxide reductase
MhNOR	Marinobacter hydrocarbonoclasticus nitric oxide reductase
MOF	metal-organic framework
N₂	Dinitrogen
N₂H₄	Hydrazine

N₂O	nitrous oxide
N₂O₂²⁻	Hyponitrite
N₂OR	nitrous oxide reductase
N₃⁻	Azide
N₃PyS	2-[[[(di-2-pyridinylmethyl)(2-pyridinylmethyl)amino]methyl]-benzenethiol
Na₂N₂O₃	Angeli's Salt
NAAD	nicotinic acid adenine dinucleotide
NADH	nicotinamide adenine dinucleotide
NADPH	nicotinamide adenine dinucleotide phosphate
NAN₃	sodium azide
NeP460	<i>Nitrosomonas europaea</i> cytochrome P460
NH₂OH	hydroxylamine
NH₃	Ammonia
NH₄NO₃	ammonium nitrate
NHE	normal hydrogen electrode
NIR	<i>cdI</i> nitrite reductase
NirK	Cu-containing nitrite reductase
NmNOR	<i>Neisseria meningitidis</i> nitric oxide reductase
NO	nitric oxide
NO⁺	nitrosonium
NO₂	nitrogen dioxide
NO₂⁻	Nitrite
NO₃⁻	Nitrate
NOBF₄	tetrafluoroborate
NOD	NO dismutase
NOR	nitric oxide reductases
NP	Nitrophorin
O₂	Dioxygen

O₂R	dioxygen reductase
OEP	octaethylporphyrin
OEP	octaethylporphyrin
OTF	Triflate
PAGE	polyacrylamide gel electrophoresis
PaNOR	<i>Pseudomonas aeruginosa</i> nitric oxide reductases
PCET	proton-coupled electron transfer
PdN₂OR	<i>Paracoccus denitrificans</i> nitrous oxide reductase
PdNOR	<i>Paracoccus denitrificans</i> nitric oxide reductases
PNP	(<i>N</i> [2-PiPr ₂ -4-Me-C ₆ H ₃] ₂)
PP	protoporphyrin
PsN₂OR	<i>Pseudomonas stutzeri</i> nitrous oxide reductase
Py₄DMB	1,2- <i>bis</i> (di(pyridine-2-yl)methoxy)benzene
qNOR	quinone-dependent nitrous oxide reductase
RB	Rubredoxin
RdNOR	<i>Roseobacter denitrificans</i> nitric oxide reductases
RFQ	rapid freeze quench
SCE	saturated calomel electrode
Sr	super-reduced
t-Bupz	3-tert-butylpyrazole
THF	tetrahydrofuran
TMH	transmembrane helix
tmpa	<i>tris</i> (2-pyridylmethyl)amine
TMPyP	<i>meso-tetrakis</i> (<i>N</i> -methyl-4-pyridyl)porphine
Tp	trispyrazolylborate
TPPS	<i>meso-tetrakis</i> (<i>p</i> -sulfonatophenyl)porphine
XYL	2,6- <i>bis</i> [(<i>bis</i> (2-pyridylethyl)amino)methyl]-phenol

12. References

- (1). Waldman AJ; Ng TL; Wang P; Balskus EP Heteroatom–Heteroatom Bond Formation in Natural Product Biosynthesis. *Chem. Rev* 2017, 117, 5784–5863. [PubMed: 28375000]
- (2). Le Goff G; Ouazzani J Natural Hydrazine-Containing Compounds: Biosynthesis, Isolation, Biological Activities and Synthesis. *Bioorg. Med. Chem* 2014, 22, 6529–6544. [PubMed: 25456382]
- (3). Caranto JD The Emergence of Nitric Oxide in the Biosynthesis of Bacterial Natural Products. *Curr. Opin. Chem. Biol* 2019, 49, 130–138. [PubMed: 30640032]
- (4). Goddard RH Rocket Apparatus US 1102653, 1914.
- (5). Sneader W *Drug Discovery: A History*; John Wiley & Sons, 2005.
- (6). Parmon VN; Panov GI; Uriarte A; Noskov AS Nitrous Oxide in Oxidation Chemistry and Catalysis: Application and Production. *Catal. Today* 2005, 100, 115–131.
- (7). Ravishankara AR; Daniel JS; Portmann RW Nitrous Oxide (N₂O): The Dominant Ozone-Depleting Substance Emitted in the 21st Century. 2009, 326, 123–125.
- (8). Lehnert N; Dong HT; Harland JB; Hunt AP; White CJ Reversing Nitrogen Fixation. *Nat. Rev. Chem* 2018, 2, 278–289.
- (9). Chen JG; Crooks RM; Seefeldt LC; Bren KL; Bullock RM; Darensbourg MY; Holland PL; Hoffman B; Janik MJ; Jones AK et al. Beyond Fossil Fuel–Driven Nitrogen Transformations. *Science* 2018, 360, eaar6611. [PubMed: 29798857]
- (10). Canfield DE; Glazer AN; Falkowski PG The Evolution and Future of Earth’s Nitrogen Cycle. *Science* 2010, 330, 192–196. [PubMed: 20929768]
- (11). Hoffman BM; Lukoyanov D; Yang Z-Y; Dean DR; Seefeldt LC Mechanism of Nitrogen Fixation by Nitrogenase: The Next Stage. *Chem. Rev* 2014, 114, 4041–4062. [PubMed: 24467365]
- (12). Thamdrup B New Pathways and Processes in the Global Nitrogen Cycle. *Annu. Rev. Ecol. Evol. Syst* 2012, 43, 407–428.
- (13). Lancaster KM; Caranto JD; Majer SH; Smith MA Alternative Bioenergy: Updates to and Challenges in Nitrification Metalloenzymology. *Joule* 2018, 2, 421–441.
- (14). Zott M; Garrido-Barros P; Peters JC Electrocatalytic Ammonia Oxidation Mediated by a Polypyridyl Iron Catalyst. *ACS Catalysis* 2019, 9, 10101–10108.
- (15). Bhattacharya P; Heiden ZM; Chambers GM; Johnson SI; Bullock RM; Mock MT Catalytic Ammonia Oxidation to Dinitrogen by Hydrogen Atom Abstraction. *Angew. Chem. Int. Ed* 2019, 131, 11744–11750.
- (16). Habibzadeh F; Miller SL; Hamann TW; Smith MR Homogeneous Electrocatalytic Oxidation of Ammonia to N₂ under Mild Conditions. *Proc. Natl. Acad. Sci. U.S.A* 2019, 116, 2849–2853. [PubMed: 30655346]
- (17). Najafian A; Cundari TR Computational Mechanistic Study of Electro-Oxidation of Ammonia to N₂ by Homogenous Ruthenium and Iron Complexes. *J. Phys. Chem. A* 2019, 123, 7973–7982. [PubMed: 31454245]
- (18). Nakajima K; Toda H; Sakata K; Nishibayashi Y Ruthenium-Catalysed Oxidative Conversion of Ammonia into Dinitrogen. *Nature Chem* 2019, 11, 702–709. [PubMed: 31341266]
- (19). Gwak J; Ahn S; Baik MH; Lee Y One Metal Is Enough: A Nickel Complex Reduces Nitrate Anions to Nitrogen Gas. *Chem. Sci* 2019, 10, 4767–4774. [PubMed: 31160953]
- (20). Kartal B; Maalcke WJ; de Almeida NM; Cirpus I; Gloerich J; Geerts W; Op den Camp HJM; Harhangi HR; Janssen-Megens EM; Francoijs K-J et al. Molecular Mechanism of Anaerobic Ammonium Oxidation. *Nature* 2011, 479, 127–130. [PubMed: 21964329]
- (21). Underhill FP; Kleiner IS The Influence of Hydrazine Upon Intermediary Metabolism in the Dog. *J. Biol. Chem* 1908, 4, 165–178.
- (22). Toth B; Erickson J Cancer Induction in Mice by Feeding of the Uncooked Cultivated Mushroom of Commerce *Agaricus Bisporus*. *Cancer Res* 1986, 46, 4007–4011. [PubMed: 3731070]
- (23). List PH; Luft P Gyromitrin, Das Gift Der Frühjahrsorchel. 16. Mitt. Über Pilzinhaltstoffe. *Arch. Pharm* 1968, 301, 294–305.

- (24). List PH; Luft P Nachweis Und Gehaltsbestimmung Von Gyromitrin in Frischen Lorcheln 19. Mitt. Über Pilzinhaltstoffe. Arch. Pharm 1969, 302, 143–146.
- (25). Pyysalo H Some New Toxic Compounds in False Morels, *Gyromitra Esculenta*. Naturwissenschaften 1975, 62, 395. [PubMed: 1238907]
- (26). Schirmann J-P; Combroux J; Delavarenne Serge Y Method For Preparing Azines And Hydrazones US 3972878 A, 1976.
- (27). Arkema. Arkema consolidates its Hydrazine Hydrate and Derivatives activity at its Lannemezan industrial facility <https://www.arkema.com/en/media/news/news-details/Arkema-consolidates-its-Hydrazine-Hydrate-and-Derivatives-activity-at-its-Lannemezan-industrial-facility/> (accessed on April 20, 2019).
- (28). NASA Phoenix Mars Mission. Phoenix Mars Lander Is Silent, New Image Shows Damage <http://phoenix.lpl.arizona.edu/> (accessed on April 20, 2019).
- (29). Plemmons DH; Mehta M; Clark BC; Kounaves SP; Peach LL Jr.; Renno NO; Tamppari L; Young SMM Effects of the Phoenix Lander Descent Thruster Plume on the Martian Surface. J. Geophys. Res.-Planet 2008, 113.
- (30). Mizukami MB, Todd J; Baker Raymond S. In NASA Jet Propulsion Laboratory, 2013.
- (31). Laboratory, N. J. P. Jupiter Orbit Insertion (accessed on April 20, 2019).
- (32). Zumft WG Nitric Oxide Reductases of Prokaryotes with Emphasis on the Respiratory, Heme-Copper Oxidase Type. J. Inorg. Biochem 2005, 99, 194–215. [PubMed: 15598502]
- (33). Bell LC; Ferguson SJ Nitric and Nitrous Oxide Reductases Are Active under Aerobic Conditions in Cells of *Thiosphaera pantotropha*. Biochem. J 1991, 273, 423–427. [PubMed: 1846742]
- (34). Philippot L; Hallin S; Schloter M Ecology of Denitrifying Prokaryotes in Agricultural Soil. In Advances in Agronomy; Academic Press: Cambridge, MA, 2007; Vol. 96; pp 249–305.
- (35). Sousa FL; Alves RJ; Ribeiro MA; Pereira-Leal JB; Teixeira M; Pereira MM The Superfamily of Heme-Copper Oxygen Reductases: Types and Evolutionary Considerations. Biochim. Biophys. Acta 2012, 1817, 629–637. [PubMed: 22001780]
- (36). Giuffrè A; Stubauer G; Sarti P; Brunori M; Zumft WG; Buse G; Soulimane T The Heme-Copper Oxidases of *Thermus thermophilus* Catalyze the Reduction of Nitric Oxide: Evolutionary Implications. Proc Natl Acad Sci U S A 1999, 96, 14718–14723. [PubMed: 10611279]
- (37). Flock U; Watmough NJ; Ädelroth P Electron/Proton Coupling in Bacterial Nitric Oxide Reductase During Reduction of Oxygen. Biochemistry 2005, 44, 10711–10719. [PubMed: 16060680]
- (38). Salomonsson L; Reimann J; Tosha T; Krause N; Gonska N; Shiro Y; Adelroth P Proton Transfer in the Quinol-Dependent Nitric Oxide Reductase from *Geobacillus stearothermophilus* During Reduction of Oxygen. Biochim. Biophys. Acta 2012, 1817, 1914–1920. [PubMed: 22538294]
- (39). Bhagi-Damodaran A; Reed JH; Zhu Q; Shi Y; Hosseinzadeh P; Sandoval BA; Harnden KA; Wang S; Sponholtz MR; Mirts EN et al. Heme Redox Potentials Hold the Key to Reactivity Differences between Nitric Oxide Reductase and Heme-Copper Oxidase. Proc. Natl. Acad. Sci. U.S.A 2018, 115, 6195–6200. [PubMed: 29802230]
- (40). Lyons JA; Hilbers F; Caffrey M Structure and Function of Bacterial Cytochrome c Oxidases. In Cytochrome Complexes: Evolution, Structures, Energy Transduction, and Signaling; Cramer WA; Kallas T Eds.; Springer: Netherlands, Dordrecht, 2016; Vol. 96; pp 307–329.
- (41). Hunsicker-Wang LM; Pacoma RL; Chen Y; Fee JA; Stout CD A Novel Cryoprotection Scheme for Enhancing the Diffraction of Crystals of Recombinant Cytochrome ba3 Oxidase from *Thermus thermophilus*. Acta Crystallogr. Sect. D. Biol. Crystallogr 2005, 61, 340–343. [PubMed: 15735345]
- (42). Reimann J; Jetten MS; Keltjens JT Metal Enzymes in “Impossible” Microorganisms Catalyzing the Anaerobic Oxidation of Ammonium and Methane. Met. Ions Life Sci 2015, 15, 257–313. [PubMed: 25707470]
- (43). Thorndycroft FH; Butland G; Richardson DJ; Watmough NJ A New Assay for Nitric Oxide Reductase Reveals Two Conserved Glutamate Residues Form the Entrance to a Proton-Conducting Channel in the Bacterial Enzyme. Biochem. J 2007, 401, 111–119. [PubMed: 16961460]

- (44). Matsumoto Y; Tosha T; Pislakov AV; Hino T; Sugimoto H; Nagano S; Sugita Y; Shiro Y Crystal Structure of Quinol-Dependent Nitric Oxide Reductase from *Geobacillus stearothermophilus*. *Nat. Struct. Mol. Biol* 2012, 19, 238–245. [PubMed: 22266822]
- (45). Al-Attar S; de Vries S An Electrogenic Nitric Oxide Reductase. *FEBS Lett* 2015, 589, 2050–2057. [PubMed: 26149211]
- (46). Girsch P; de Vries S Purification and Initial Kinetic and Spectroscopic Characterization of NO Reductase from *Paracoccus denitrificans*. *Biochim. Biophys. Acta* 1997, 1318, 202–216. [PubMed: 9030265]
- (47). Hemp J; Gennis RB Diversity of the Heme-Copper Superfamily in Archaea: Insights from Genomics and Structural Modeling. *Results Probl. Cell. Differ* 2008, 45, 1–31.
- (48). Murali R Studies on the Cytochrome bd-Type Oxygen Reductase Superfamily and the Discovery of a Novel Nitric Oxide Reductase Ph.D. Dissertation, University of Illinois, Urbana-Champaign, IL, 2016.
- (49). Sievert SM; Scott KM; Klotz MG; Chain PS; Hauser LJ; Hemp J; Hugler M; Land M; Lapidus A; Larimer FW et al. Genome of the Epsilonproteobacterial Chemolithoautotroph *Sulfurimonas denitrificans*. *Appl. Environ. Microbiol* 2008, 74, 1145–1156. [PubMed: 18065616]
- (50). Welte CU; Rasigraf O; Vaksmaa A; Versantvoort W; Arshad A; Op den Camp HJ; Jetten MS; Luke C; Reimann J Nitrate- and Nitrite-Dependent Anaerobic Oxidation of Methane. *Environ. Microbiol. Rep* 2016, 8, 941–955. [PubMed: 27753265]
- (51). Stein LY; Arp DJ; Berube PM; Chain PS; Hauser L; Jetten MS; Klotz MG; Larimer FW; Norton JM; Op den Camp HJ et al. Whole-Genome Analysis of the Ammonia-Oxidizing Bacterium, *Nitrosomonas europaea* C91: Implications for Niche Adaptation. *Environ. Microbiol* 2007, 9, 2993–3007. [PubMed: 17991028]
- (52). Heylen K; Keltjens J Redundancy and modularity in membrane-associated dissimilatory nitrate reduction in *Bacillus*. *Front. Microbiol* 2012, 3, article number 371.
- (53). Cho CM-H; Yan T; Liu X; Wu L; Zhou J; Stein LY Transcriptome of a *Nitrosomonas europaea* Mutant with a Disrupted Nitrite Reductase Gene (NirK). *Appl. Environ. Microbiol* 2006, 72, 4450–4454. [PubMed: 16751567]
- (54). Ettwig KF; Butler MK; Le Paslier D; Pelletier E; Mangenot S; Kuypers MMM; Schreiber F; Dutilh BE; Zedelius J; de Beer Det al. Nitrite-Driven Anaerobic Methane Oxidation by Oxygenic Bacteria. *Nature* 2010, 464, 543–548. [PubMed: 20336137]
- (55). Ettwig KF; Speth DR; Reimann J; Wu ML; Jetten MS; Keltjens JT Bacterial Oxygen Production in the Dark. *Front. Microbiol* 2012, 3, 273. [PubMed: 22891064]
- (56). Reimann J; Jetten MS; Keltjens JT Metal enzymes in “impossible” microorganisms catalyzing the anaerobic oxidation of ammonium and methane. In *Sustaining Life on Planet Earth: Metalloenzymes Mastering Dioxygen and Other Chewy Gases; Metal Ions in Life Sciences 2015*; Springer: Switzerland, 2015; pp 257–313.
- (57). Zhang Y; Ma A; Liu W; Bai Z; Zhuang X; Zhuang G The Occurrence of Putative Nitric Oxide Dismutase (Nod) in an Alpine Wetland with a New Dominant Subcluster and the Potential Ability for a Methane Sink. *Archaea* 2018, 2018, 6201541. [PubMed: 30532656]
- (58). Heiss B; Frunzke K; Zumft WG Formation of the N-N Bond from Nitric Oxide by a Membrane-Bound Cytochrome Bc Complex of Nitrate-Respiring (Denitrifying) *Pseudomonas stutzeri*. *J. Bacteriol* 1989, 171, 3288–3297. [PubMed: 2542222]
- (59). Carr GJ; Ferguson SJ The Nitric Oxide Reductase of *Paracoccus denitrificans*. *Biochem. J* 1990, 269, 423–429. [PubMed: 2167070]
- (60). Hino T; Matsumoto Y; Nagano S; Sugimoto H; Fukumori Y; Murata T; Iwata S; Shiro Y Structural Basis of Biological N₂O Generation by Bacterial Nitric Oxide Reductase. *Science* 2010, 330, 1666–1670. [PubMed: 21109633]
- (61). Crow A; Matsuda Y; Arata H; Oubrie A Structure of the Membrane-Intrinsic Nitric Oxide Reductase from *Roseobacter denitrificans*. *Biochemistry* 2016, 55, 3198–3203. [PubMed: 27185533]
- (62). Hoglen J; Hollocher TC Purification and Some Characteristics of Nitric Oxide Reductase-Containing Vesicles from *Paracoccus denitrificans*. *J. Biol. Chem* 1989, 264, 7556–7563. [PubMed: 2708379]

- (63). Kastrau DH; Heiss B Fau - Kroneck PM; Kroneck Pm Fau - Zumft WG; Zumft WG Nitric Oxide Reductase from *Pseudomonas stutzeri*, a Novel Cytochrome bc Complex. Phospholipid Requirement, Electron Paramagnetic Resonance and Redox Properties. *Eur. J. Biochem* 1994, 222, 293–303. [PubMed: 8020468]
- (64). Sakurai T; Nakashima S; Kataoka K; Seo D; Sakurai N Diverse NO Reduction by *Halomonas halodenitrificans* Nitric Oxide Reductase. *Biochem. Biophys. Res. Commun* 2005, 333, 483–487. [PubMed: 15950940]
- (65). Sakurai T; Sakurai N; Matsumoto H; Hirota S; Yamauchi O Roles of Four Iron Centers in *Paracoccus halodenitrificans* Nitric Oxide Reductase. *Biochem. Biophys. Res. Commun* 1998, 251, 248–251. [PubMed: 9790940]
- (66). Kumita H; Matsuura K; Hino T; Takahashi S; Hori H; Fukumori Y; Morishima I; Shiro Y No Reduction by Nitric-Oxide Reductase from Denitrifying Bacterium *Pseudomonas aeruginosa*: Characterization of Reaction Intermediates That Appear in the Single Turnover Cycle. *J. Biol. Chem* 2004, 279, 55247–55254. [PubMed: 15504726]
- (67). Matsuda Y; Inamori K; Osaki T; Eguchi A; Watanabe A; Kawabata S; Iba K; Arata H Nitric Oxide-Reductase Homologue That Contains a Copper Atom and Has Cytochrome c-Oxidase Activity from an Aerobic Phototrophic Bacterium *Roseobacter denitrificans*. *J. Biochem* 2002, 131, 791–800. [PubMed: 12038974]
- (68). Matsuda Y; Uchida T; Hori H; Kitagawa T; Arata H Structural Characterization of a Binuclear Center of a Cu-Containing No Reductase Homologue from *Roseobacter denitrificans*: EPR and Resonance Raman Studies. *Biochim. Biophys. Acta* 2004, 1656, 37–45. [PubMed: 15136157]
- (69). Gray HB; Winkler JR Long-Range Electron Transfer. *Proc. Natl. Acad. Sci. U.S.A* 2005, 102, 3534–3539. [PubMed: 15738403]
- (70). Terasaka E; Yamada K; Wang PH; Hosokawa K; Yamagiwa R; Matsumoto K; Ishii S; Mori T; Yagi K; Sawai H et al. Dynamics of Nitric Oxide Controlled by Protein Complex in Bacterial System. *Proc. Natl. Acad. Sci. U.S.A* 2017, 114, 9888–9893. [PubMed: 28847930]
- (71). Shapleigh JP; Payne WJ Nitric Oxide-Dependent Proton Translocation in Various Denitrifiers. *J. Bacteriol* 1985, 163, 837–840. [PubMed: 3928599]
- (72). Bell LC; Richardson DJ; Ferguson SJ Identification of Nitric Oxide Reductase Activity in *Rhodobacter Capsulatus*: The Electron Transport Pathway Can Either Use or Bypass Both Cytochrome c2 and the Cytochrome bc1 Complex. *J. Gen. Microbiol* 1992, 138, 437–443. [PubMed: 1317404]
- (73). Carr GJ; Page MD; Ferguson SJ The Energy-Conserving Nitric-Oxide-Reductase System in *Paracoccus denitrificans*. *Eur. J. Biochem* 1989, 179, 683–692. [PubMed: 2920732]
- (74). Koutný M; Kura I; Tesák R; Turánek J; Van Spanning RJM Pseudoazurin Mediates Periplasmic Electron Flow in a Mutant Strain of *Paracoccus denitrificans* Lacking Cytochrome c550. *FEBS Lett* 1999, 448, 157–159. [PubMed: 10217431]
- (75). Moir JWB; Ferguson SJ Properties of a *Paracoccus denitrificans* Mutant Deleted in Cytochrome c550 Indicate That a Copper Protein Can Substitute for This Cytochrome in Electron Transport to Nitrite, Nitric Oxide and Nitrous Oxide 1994, 140, 389–397.
- (76). Shimada S; Shinzawa-Itoh K; Baba J; Aoe S; Shimada A; Yamashita E; Kang J; Tateno M; Yoshikawa S; Tsukihara T Complex Structure of Cytochrome c-Cytochrome c Oxidase Reveals a Novel Protein-Protein Interaction Mode. *EMBO J* 2017, 36, 291–300. [PubMed: 27979921]
- (77). Flock U; Thorndycroft FH; Matorin AD; Richardson DJ; Watmough NJ; Adelroth P Defining the Proton Entry Point in the Bacterial Respiratory Nitric-Oxide Reductase. *J. Biol. Chem* 2008, 283, 3839–3845. [PubMed: 18056717]
- (78). Reimann J; Flock U; Lepp H; Honigsmann A; Adelroth P A Pathway for Protons in Nitric Oxide Reductase from *Paracoccus denitrificans*. *Biochim. Biophys. Acta* 2007, 1767, 362–373. [PubMed: 17466934]
- (79). Hendriks JHM; Jasaitis A; Saraste M; Verkhovskiy MI Proton and Electron Pathways in the Bacterial Nitric Oxide Reductase. *Biochemistry* 2002, 41, 2331–2340. [PubMed: 11841226]
- (80). Butland G; Spiro S; Watmough NJ; Richardson DJ Two Conserved Glutamates in the Bacterial Nitric Oxide Reductase Are Essential for Activity but Not Assembly of the Enzyme. *J. Bacteriol* 2001, 183, 189–199. [PubMed: 11114916]

- (81). Flock U; Lachmann P; Reimann J; Watmough NJ; Ädelroth P Exploring the Terminal Region of the Proton Pathway in the Bacterial Nitric Oxide Reductase. *J. Inorg. Biochem* 2009, 103, 845–850. [PubMed: 19332356]
- (82). Pislakov AV; Hino T; Shiro Y; Sugita Y Molecular Dynamics Simulations Reveal Proton Transfer Pathways in Cytochrome c-Dependent Nitric Oxide Reductase. *PLoS Comput. Biol* 2012, 8, e1002674. [PubMed: 22956904]
- (83). Gonska N; Young D; Yuki R; Okamoto T; Hisano T; Antonyuk S; Hasnain SS; Muramoto K; Shiro Y; Tosha T et al. Characterization of the Quinol-Dependent Nitric Oxide Reductase from the Pathogen *Neisseria Meningitidis*, an Electrogenic Enzyme. *Sci. Rep* 2018, 8, 3637. [PubMed: 29483528]
- (84). Cramm R; Pohlmann A; Friedrich B Purification and Characterization of the Single-Component Nitric Oxide Reductase from *Ralstonia Eutropha* H16. *FEBS Lett* 1999, 460, 6–10. [PubMed: 10571051]
- (85). de Vries S; Strampraad MJ; Lu S; Moenne-Loccoz P; Schroder I Purification and Characterization of the Mqh2:No Oxidoreductase from the Hyperthermophilic Archaeon *Pyrobaculum aerophilum*. *J. Biol. Chem* 2003, 278, 35861–35868. [PubMed: 12799376]
- (86). Tosha T; Shiro Y Crystal Structures of Nitric Oxide Reductases Provide Key Insights into Functional Conversion of Respiratory Enzymes. *IUBMB Life* 2013, 65, 217–226. [PubMed: 23378174]
- (87). Petrek M; Otyepka M; Banas P; Kosinova P; Koca J; Damborsky J Caver: A New Tool to Explore Routes from Protein Clefts, Pockets and Cavities. *BMC Bioinformatics* 2006, 7, 316. [PubMed: 16792811]
- (88). Varotsis C; Ohta T; Kitagawa T; Soulimane T; Pinakoulaki E The Structure of the Hyponitrite Species in a Heme Fe-Cu Binuclear Center. *Angew. Chem. Int. Ed* 2007, 46, 2210–2214.
- (89). Ohta T; Soulimane T; Kitagawa T; Varotsis C Nitric Oxide Activation by *caa3* Oxidoreductase from *Thermus thermophilus*. *Phys. Chem. Chem. Phys* 2015, 17, 10894–10898. [PubMed: 25820937]
- (90). Pinakoulaki E; Koutsoupakis C; Stavrakis S; Aggelaki M; Papadopoulos G; Daskalakis V; Varotsis C Structural Dynamics of Heme–Copper Oxidases and Nitric Oxide Reductases: Time-Resolved Step-Scan Fourier Transform Infrared and Time-Resolved Resonance Raman Studies. *J. Raman Spectrosc* 2005, 36, 337–349.
- (91). Moënné-Loccoz P; Richter O-MH; Huang H.-w.; Wasser IM; Ghiladi RA; Karlin KD; de Vries S Nitric Oxide Reductase from *Paracoccus denitrificans* Contains an Oxo-Bridged Heme/Non-Heme Diiron Center. *J. Am. Chem. Soc* 2000, 122, 9344–9345.
- (92). Cheesman MR; Zumft WG; Thomson AJ The MCD and EPR of the Heme Centers of Nitric Oxide Reductase from *Pseudomonas stutzeri*: Evidence That the Enzyme Is Structurally Related to the Heme-Copper Oxidases. *Biochemistry* 1998, 37, 3994–4000. [PubMed: 9521721]
- (93). Moënné-Loccoz P; de Vries S Structural Characterization of the Catalytic High-Spin Heme b of Nitric Oxide Reductase: A Resonance Raman Study. *J. Am. Chem. Soc* 1998, 120, 5147–5152.
- (94). Timoteo CG; Pereira AS; Martins CE; Naik SG; Duarte AG; Moura JJ; Tavares P; Huynh BH; Moura I Low-Spin Heme b(3) in the Catalytic Center of Nitric Oxide Reductase from *Pseudomonas nautica*. *Biochemistry* 2011, 50, 4251–4262. [PubMed: 21452843]
- (95). Sato N; Ishii S; Sugimoto H; Hino T; Fukumori Y; Sako Y; Shiro Y; Tosha T Structures of Reduced and Ligand-Bound Nitric Oxide Reductase Provide Insights into Functional Differences in Respiratory Enzymes. *Proteins* 2014, 82, 1258–1271. [PubMed: 24338896]
- (96). Hino T; Nagano S; Sugimoto H; Tosha T; Shiro Y Molecular Structure and Function of Bacterial Nitric Oxide Reductase. *Biochim. Biophys. Acta* 2012, 1817, 680–687. [PubMed: 22001779]
- (97). Wang B; Shi Y; Tejero J; Powell SM; Thomas LM; Gladwin MT; Shiva S; Zhang Y; Richter-Addo GB Nitrosyl Myoglobins and Their Nitrite Precursors: Crystal Structural and Quantum Mechanics and Molecular Mechanics Theoretical Investigations of Preferred Fe–NO Ligand Orientations in Myoglobin Distal Pockets. *Biochemistry* 2018, 57, 4788–4802. [PubMed: 29999305]
- (98). Enemark JH; Feltham RD Principles of Structure, Bonding, and Reactivity for Metal Nitrosyl Complexes. *Coord. Chem. Rev* 1974, 13, 339–406.

- (99). Berto TC; Xu N; Lee SR; McNeil AJ; Alp EE; Zhao J; Richter-Addo GB; Lehnert N Characterization of the Bridged Hyponitrite Complex {[Fe(OEP)]₂(μ-N₂O₂)}: Reactivity of Hyponitrite Complexes and Biological Relevance. *Inorg. Chem* 2014, 53, 6398–6414. [PubMed: 24971721]
- (100). Moenne-Loccoz P Spectroscopic Characterization of Heme Iron-Nitrosyl Species and Their Role in NO Reductase Mechanisms in Diiron Proteins. *Nat. Prod. Rep* 2007, 24, 610–620. [PubMed: 17534533]
- (101). Daskalakis V; Ohta T; Kitagawa T; Varotsis C Structure and Properties of the Catalytic Site of Nitric Oxide Reductase at Ambient Temperature. *Biochim. Biophys. Acta* 2015, 1847, 1240–1244. [PubMed: 26140941]
- (102). Pinakoulaki E; Gemeinhardt S; Saraste M; Varotsis C Nitric-Oxide Reductase. Structure and Properties of the Catalytic Site from Resonance Raman Scattering. *J. Biol. Chem* 2002, 277, 23407–23413. [PubMed: 11971903]
- (103). Zhao Y; Brandish PE; Ballou DP; Marletta MA A Molecular Basis for Nitric Oxide Sensing by Soluble Guanylate Cyclase. *Proc. Natl. Acad. Sci. U.S.A* 1999, 96, 14753–14758. [PubMed: 10611285]
- (104). Vilbert AC; Caranto JD; Lancaster KM Influences of the Heme-Lysine Crosslink in Cytochrome P460 over Redox Catalysis and Nitric Oxide Sensitivity. *Chem. Sci* 2018, 9, 368–379. [PubMed: 29629106]
- (105). Praneeth VKK; Näther C; Peters G; Lehnert N Spectroscopic Properties and Electronic Structure of Five- and Six-Coordinate Iron(II) Porphyrin No Complexes: Effect of the Axial N-Donor Ligand. *Inorg. Chem* 2006, 45, 2795–2811. [PubMed: 16562937]
- (106). Drapier J; Pellat C; Henry Y Generation of EPR-Detectable Nitrosyl-Iron Complexes in Tumor Target Cells Cocultured with Activated Macrophages. *J. Biol. Chem* 1991, 266, 10162–10167. [PubMed: 1645341]
- (107). Vanin AF Endothelium-Derived Relaxing Factor Is a Nitrosyl Iron Complex with Thiol Ligands. *FEBS Lett* 1991, 289, 1–3. [PubMed: 1893995]
- (108). Wang X; Sundberg EB; Li L; Kantardjieff KA; Herron SR; Lim M; Ford PC A Cyclic Tetra-Nuclear Dinitrosyl Iron Complex [Fe(NO)₂(Imidazolate)]₄: Synthesis, Structure and Stability. *Chem. Commun* 2005, 477–479.
- (109). Lancaster J; Hibbs J Epr Demonstration of Iron-Nitrosyl Complex Formation by Cytotoxic Activated Macrophages. *Proc. Natl. Acad. Sci. U.S.A* 1990, 87, 1223–1227. [PubMed: 2153975]
- (110). Speelman AL; Zhang B; Silakov A; Skodje KM; Alp EE; Zhao J; Hu MY; Kim E; Krebs C; Lehnert N Unusual Synthetic Pathway for an {Fe(NO)₂}₉ Dinitrosyl Iron Complex (DNIC) and Insight into DNIC Electronic Structure via Nuclear Resonance Vibrational Spectroscopy. *Inorg. Chem* 2016, 55, 5485–5501. [PubMed: 27203448]
- (111). Gronberg KL; Roldan MD; Prior L; Butland G; Cheesman MR; Richardson DJ; Spiro S; Thomson AJ; Watmough NJ A Low-Redox Potential Heme in the Dinuclear Center of Bacterial Nitric Oxide Reductase: Implications for the Evolution of Energy-Conserving Heme-Copper Oxidases. *Biochemistry* 1999, 38, 13780–13786. [PubMed: 10529222]
- (112). Kato M; Nakagawa S; Toshi T; Shiro Y; Masuda Y; Nakata K; Yagi I Surface-Enhanced Infrared Absorption Spectroscopy of Bacterial Nitric Oxide Reductase under Electrochemical Control Using a Vibrational Probe of Carbon Monoxide. *J. Phys. Chem. Lett* 2018, 9, 5196–5200. [PubMed: 30141632]
- (113). Cordas CM; Duarte AG; Moura JJ; Moura I Electrochemical Behaviour of Bacterial Nitric Oxide Reductase-Evidence of Low Redox Potential Non-Heme FeB Gives New Perspectives on the Catalytic Mechanism. *Biochim. Biophys. Acta* 2013, 1827, 233–238. [PubMed: 23142527]
- (114). Blomberg LM; Blomberg MR; Siegbahn PE A Theoretical Study on Nitric Oxide Reductase Activity in a ba₃-Type Heme-Copper Oxidase. *Biochim. Biophys. Acta* 2006, 1757, 31–46. [PubMed: 16375849]
- (115). Pinakoulaki E; Stavrakis S; Urbani A; Varotsis C Resonance Raman Detection of a Ferrous Five-Coordinate Nitrosylheme b₃ Complex in Cytochrome cbb₃ Oxidase from *Pseudomonas stutzeri*. *J. Am. Chem. Soc* 2002, 124, 9378–9379. [PubMed: 12167025]

- (116). Blomberg MR Can Reduction of NO to N₂O in Cytochrome c Dependent Nitric Oxide Reductase Proceed through a Trans-Mechanism? *Biochemistry* 2017, 56, 120–131. [PubMed: 27959492]
- (117). Becke AD Density-Functional Thermochemistry. III. The Role of Exact Exchange. *J. Chem. Phys* 1993, 98, 5648–5652.
- (118). Grimme S; Antony J; Ehrlich S; Krieg H A Consistent and Accurate Ab Initio Parametrization of Density Functional Dispersion Correction (DFT-D) for the 94 Elements H-Pu. *J. Chem. Phys* 2010, 132, 154104. [PubMed: 20423165]
- (119). Blomberg MR; Siegbahn PE Mechanism for N₂O Generation in Bacterial Nitric Oxide Reductase: A Quantum Chemical Study. *Biochemistry* 2012, 51, 5173–5186. [PubMed: 22680334]
- (120). Laughlin RJ; Stevens RJ Evidence for Fungal Dominance of Denitrification and Codenitrification in a Grassland Soil. *Soil Sci. Soc. Am. J* 2002, 66, 1540–1548.
- (121). Crenshaw CL; Lauber C; Sinsabaugh RL; Stavely LK Fungal Control of Nitrous Oxide Production in Semiarid Grassland. *Biogeochemistry* 2008, 87, 17–27.
- (122). Wankel SD; Ziebis W; Buchwald C; Charoenpong C; De Beer D; Dentinger J; Xu Z; Zengler K Evidence for Fungal and Chemodenitrification Based N₂O Flux from Nitrogen Impacted Coastal Sediments. *Nat. Commun* 2017, 8, 15595. [PubMed: 28580932]
- (123). Shaik S; Cohen S; Wang Y; Chen H; Kumar D; Thiel W P450 Enzymes: Their Structure, Reactivity, and Selectivity - Modeled by QM/MM Calculations. *Chem. Rev* 2010, 110, 949–1017. [PubMed: 19813749]
- (124). McQuarters AB; Wolf MW; Hunt AP; Lehnert N 1958–2014: After 56 Years of Research, Cytochrome P450 Reactivity Is Finally Explained. *Angew. Chem. Int. Ed* 2014, 53, 4750–4752.
- (125). Denisov IG; Makris TM; Sligar SG; Schlichting I Structure and Chemistry of Cytochrome P450. *Chem. Rev* 2005, 105, 2253–2278. [PubMed: 15941214]
- (126). Lewis JC; Coelho PS; Arnold FH Enzymatic Functionalization of Carbon-Hydrogen Bonds. *Chem. Soc. Rev* 2011, 40, 2003–2021. [PubMed: 21079862]
- (127). Guengerich FP Mechanisms of Cytochrome P450-Catalyzed Oxidations. *ACS Catal* 2018, 8, 10964–10976. [PubMed: 31105987]
- (128). Nakahara K; Tanimoto T; Hatano KI; Usuda K; Shoun H Cytochrome P-450 55a1 (P-450dnir) Acts as Nitric Oxide Reductase Employing NADH as the Direct Electron Donor. *J. Biol. Chem* 1993, 268, 8350–8355. [PubMed: 8463342]
- (129). Shoun H; Sudo Y; Seto Y; Beppu T Purification and Properties of a Cytochrome P-450 of a Fungus, *Fusarium oxysporum*. *J. Biochem* 1983, 94, 1219–1229. [PubMed: 6654854]
- (130). Shoun H; Suyama W; Yasui T Soluble, Nitrate/Nitrite-Inducible Cytochrome P-450 of the Fungus, *Fusarium oxysporum*. *FEBS Lett* 1989, 244, 11–14. [PubMed: 2924900]
- (131). Park S-Y; Shimizu H; Adachi S-I; Nakagawa A; Tanaka I; Nakahara K; Shoun H; Obayashi E; Nakamura H; Iizuka T et al. Crystal Structure of Nitric Oxide Reductase Cytochrome P-450nor from *Fusarium oxysporum*. *Nat. Struct. Biol* 1997, 4, 827–832. [PubMed: 9334748]
- (132). Kizawa H; Tomura D; Oda M; Fukamizu A; Hoshino T; Gotoh O; Yasui T; Shoun H Nucleotide Sequence of the Unique Nitrate/Nitrite-Inducible Cytochrome P-450 cDNA from *Fusarium oxysporum*. *J. Biol. Chem* 1991, 266, 10632–10637. [PubMed: 2037602]
- (133). Kudo T; Tomura D; Liu DL; Dai XQ; Shoun H Two Isozymes of P450nor of *Cylindrocarpum tonkinense*: Molecular Cloning of the Cdnas and Genes, Expressions in the Yeast, and the Putative Nad(P)H-Binding Site. *Biochimie* 1996, 78, 792–799. [PubMed: 9010609]
- (134). Usuda K; Toritsuka N; Matsuo Y; Kim DH; Shoun H Denitrification by the Fungus *Cylindrocarpum tonkinense*: Anaerobic Cell Growth and Two Isozyme Forms of Cytochrome P-450nor. *Appl. Environ. Microbiol* 1995, 61, 883–889. [PubMed: 7793922]
- (135). Nakahara K; Shoun H N-Terminal Processing and Amino Acid Sequence of Two Isoforms of Nitric Oxide Reductase Cytochrome P450nor from *Fusarium oxysporum*. *J. Biochem* 1996, 120, 1082–1087. [PubMed: 9010754]
- (136). Kudo T; Takaya N; Park SY; Shiro Y; Shoun H A Positively Charged Cluster Formed in the Heme-Distal Pocket of Cytochrome P450nor Is Essential for Interaction with NADH. *J. Biol. Chem* 2001, 276, 5020–5026. [PubMed: 11076941]

- (137). Zhang L; Kudo T; Takaya N; Shoun H The B' Helix Determines Cytochrome P450nor Specificity for the Electron Donors NADH and NADPH. *J. Biol. Chem* 2002, 277, 33842–33847. [PubMed: 12105197]
- (138). Umemura M; Su F; Takaya N; Shiro Y; Shoun H D88a Mutant of Cytochrome P450nor Provides Kinetic Evidence for Direct Complex Formation with Electron Donor NADH. *Eur. J. Biochem* 2004, 271, 2887–2894. [PubMed: 15233785]
- (139). Oshima R; Fushinobu S; Su F; Zhang L; Takaya N; Shoun H Structural Evidence for Direct Hydride Transfer from NADH to Cytochrome P450nor. *J. Mol. Biol* 2004, 342, 207–217. [PubMed: 15313618]
- (140). Okamoto N; Imai Y; Shoun H; Shiro Y Site-Directed Mutagenesis of the Conserved Threonine (Thr243) of the Distal Helix of Fungal Cytochrome P450nor. *Biochemistry* 1998, 37, 8839–8847. [PubMed: 9636024]
- (141). Shimizu H; Park SY; Lee DS; Shoun H; Shiro Y Crystal Structures of Cytochrome P450nor and Its Mutants (Ser286→Val, Thr) in the Ferric Resting State at Cryogenic Temperature: A Comparative Analysis with Monooxygenase Cytochrome P450s. *J. Inorg. Biochem* 2000, 81, 191–205. [PubMed: 11051564]
- (142). Shimizu H; Obayashi E; Gomi Y; Arakawa H; Park SY; Nakamura H; Adachi SI; Shoun H; Shiro Y Proton Delivery in No Reduction by Fungal Nitric-Oxide Reductase. Cryogenic Crystallography, Spectroscopy, and Kinetics of Ferric-NO Complexes of Wild-Type and Mutant Enzymes. *J. Biol. Chem* 2000, 275, 4816–4826. [PubMed: 10671516]
- (143). Riplinger C; Neese F The Reaction Mechanism of Cytochrome P450 No Reductase: A Detailed Quantum Mechanics/Molecular Mechanics Study. *ChemPhysChem* 2011, 12, 3192–3203. [PubMed: 22095732]
- (144). Shiro Y; Fujii M; Iizuka T; Adachi S-I; Tsukamoto K; Nakahara K; Shoun H Spectroscopic and Kinetic Studies on Reaction of Cytochrome P450nor with Nitric Oxide. *J. Biol. Chem* 1995, 270, 1617–1623. [PubMed: 7829493]
- (145). Obayashi E; Tsukamoto K; Adachi SI; Takahashi S; Nomura M; Iizuka T; Shoun H; Shiro Y Unique Binding of Nitric Oxide to Ferric Nitric Oxide Reductase from *Fusarium oxysporum* Elucidated with Infrared, Resonance Raman, and X-Ray Absorption Spectroscopies. *J. Am. Chem. Soc* 1997, 119, 7807–7816.
- (146). Singh UP; Obayashi E; Takahashi S; Iizuka T; Shoun H; Shiro Y The Effects of Heme Modification on Reactivity, Ligand Binding Properties and Iron-Coordination Structures of Cytochrome P450nor. *Biochim. Biophys. Acta* 1998, 1384, 103–111. [PubMed: 9602081]
- (147). Shiro Y; Fujii M; Isogai Y; Adachi SI; Iizuka T; Obayashi F; Makino R; Nakahara K; Shoun H Iron-Ligand Structure and Iron Redox Property of Nitric Oxide Reductase Cytochrome P450nor from *Fusarium Oxysporum*: Relevance to Its No Reduction Activity. *Biochemistry* 1995, 34, 9052–9058. [PubMed: 7619804]
- (148). Riplinger C; Bill E; Daiber A; Ullrich V; Shoun H; Neese F New Insights into the Nature of Observable Reaction Intermediates in Cytochrome P450 No Reductase by Using a Combination of Spectroscopy and Quantum Mechanics/Molecular Mechanics Calculations. *Chem. Eur. J* 2014, 20, 1602–1614. [PubMed: 24453075]
- (149). Shoun H; Fushinobu S; Jiang L; Kim SW; Wakagi T Fungal Denitrification and Nitric Oxide Reductase Cytochrome P450nor. *Philos. Trans. R. Soc. London, Ser B* 2012, 367, 1186–1194. [PubMed: 22451104]
- (150). Tosha T; Nomura T; Nishida T; Saeki N; Okubayashi K; Yamagiwa R; Sugahara M; Nakane T; Yamashita K; Hirata K et al. Capturing an Initial Intermediate During the P450nor Enzymatic Reaction Using Time-Resolved XFEL Crystallography and Caged-Substrate. *Nat. Commun* 2017, 8.
- (151). Hoffmann R; M-l Chen M; Thorn DL Qualitative Discussion of Alternative Coordination Modes of Diatomic Ligands in Transition Metal Complexes. *Inorg. Chem* 1977, 16, 503–511.
- (152). Paulat F; Lehnert N Electronic Structure of Ferric Heme Nitrosyl Complexes with Thiolate Coordination. *Inorg. Chem* 2007, 46, 1547–1549. [PubMed: 17286401]

- (153). Lehnert N; Praneeth VKK; Paulat F Electronic Structure of Iron(II)–Porphyrin Nitroxyl Complexes: Molecular Mechanism of Fungal Nitric Oxide Reductase (P450nor). *J. Comput. Chem* 2006, 27, 1338–1351. [PubMed: 16788909]
- (154). Soldatova AV; Ibrahim M; Olson JS; Czernuszewicz RS; Spiro TG New Light on NO Bonding in Fe(III) Heme Proteins from Resonance Raman Spectroscopy and DFT Modeling. *J. Am. Chem. Soc* 2010, 132, 4614–4625. [PubMed: 20218710]
- (155). Hunt AP; Lehnert N The Thiolate Trans Effect in Heme {FeNO}6 Complexes and Beyond: Insight into the Nature of the Push Effect. *Inorg. Chem* 2019.
- (156). Xu N; Goodrich LE; Lehnert N; Powell DR; Richter-Addo GB Preparation of the Elusive [(Por)Fe(NO)(O-Ligand)] Complex by Diffusion of Nitric Oxide into a Crystal of the Precursor. *Angew. Chem. Int. Ed* 2013, 52, 3896–3900.
- (157). Praneeth VKK; Paulat F; Berto TC; George SDB; Näther C; Sulok CD; Lehnert N Electronic Structure of Six-Coordinate Iron(III)-Porphyrin NO Adducts: The Elusive Iron(III)-NO(Radical) State and Its Influence on the Properties of These Complexes. *J. Am. Chem. Soc* 2008, 130, 15288–15303. [PubMed: 18942830]
- (158). Daiber A; Nauser T; Takaya N; Kudo T; Weber P; Hultschig C; Shoun H; Ullrich V Isotope Effects and Intermediates in the Reduction of NO by P450nor. *J. Inorg. Biochem* 2002, 88, 343–352. [PubMed: 11897349]
- (159). Krámos B; Menyhárd DK; Oláh J Direct Hydride Shift Mechanism and Stereoselectivity of P450nor Confirmed by QM/MM Calculations. *J. Phys. Chem. B* 2012, 116, 872–885. [PubMed: 22148861]
- (160). Abucayon EG; Khade RL; Powell DR; Shaw MJ; Zhang Y; Richter-Addo GB Over or Under: Hydride Attack at the Metal Versus the Coordinated Nitrosyl Ligand in Ferric Nitrosyl Porphyrins. *Dalton Trans* 2016, 45, 18259–18266. [PubMed: 27801456]
- (161). Abucayon EG; Khade RL; Powell DR; Zhang Y; Richter-Addo GB Hydride Attack on a Coordinated Ferric Nitrosyl: Experimental and DFT Evidence for the Formation of a Heme Model–HNO Derivative. *J. Am. Chem. Soc* 2016, 138, 104–107. [PubMed: 26678216]
- (162). Lin R; Farmer PJ The HNO Adduct of Myoglobin: Synthesis and Characterization. *J. Am. Chem. Soc* 2000, 122, 2393–2394.
- (163). Farmer PJ; Sulc F Coordination Chemistry of the HNO Ligand with Hemes and Synthetic Coordination Complexes. *J. Inorg. Biochem* 2005, 99, 166–184. [PubMed: 15598500]
- (164). Obayashi E; Takahashi S; Shiro Y Electronic Structure of Reaction Intermediate of Cytochrome P450nor in Its Nitric Oxide Reduction. *J. Am. Chem. Soc* 1998, 120, 12964–12965.
- (165). Green MT; Dawson JH; Gray HB Oxoiron (IV) in Chloroperoxidase Compound II Is Basic: Implications for P450 Chemistry. *Science* 2004, 304, 1653–1656. [PubMed: 15192224]
- (166). Onderko EL; Silakov A; Yosca TH; Green MT Characterization of a Selenocysteine-Ligated P450 Compound I Reveals Direct Link between Electron Donation and Reactivity. *Nature Chem* 2017, 9, 623. [PubMed: 28644466]
- (167). Yosca TH; Rittle J; Krest CM; Onderko EL; Silakov A; Calixto JC; Behan RK; Green MT Iron(IV)Hydroxide pKa and the Role of Thiolate Ligation in C–H Bond Activation by Cytochrome P450. *Science* 2013, 342, 825–829. [PubMed: 24233717]
- (168). Krest CM; Onderko EL; Yosca TH; Calixto JC; Karp RF; Livada J; Rittle J; Green MT Reactive Intermediates in Cytochrome P450 Catalysis. *J. Biol. Chem* 2013, 288, 17074–17081. [PubMed: 23632017]
- (169). Goodrich LE; Paulat F; Praneeth VKK; Lehnert N Electronic Structure of Heme-Nitrosyls and Its Significance for Nitric Oxide Reactivity, Sensing, Transport, and Toxicity in Biological Systems. *Inorg. Chem* 2010, 49, 6293–6316. [PubMed: 20666388]
- (170). Spiro T; Li X-Y Resonance Raman Spectroscopy of Metalloporphyrins. In *Biological Applications of Raman Spectroscopy*, TG S, Ed.; Wiley & Sons Inc.: New York, NY 1988; Vol. 3, pp 1–37.
- (171). Wagner WD; Nakamoto K Resonance Raman Spectra of Nitridoiron (V) Porphyrin Intermediates Produced by Laser Photolysis. *J. Am. Chem. Soc* 1989, 111, 1590–1598.
- (172). Vincent MA; Hillier IH; Ge J How Is N–N Bond Formation Facilitated by P450 NO Reductase? A DFT Study. *Chem. Phys. Lett* 2005, 407, 333–336.

- (173). Suzuki N; Higuchi T; Urano Y; Kikuchi K; Uchida T; Mukai M; Kitagawa T; Nagano T First Synthetic No– Heme– Thiolate Complex Relevant to Nitric Oxide Synthase and Cytochrome P450nor. *J. Am. Chem. Soc* 2000, 122, 12059–12060.
- (174). Schröder D; Shaik S; Schwarz H Two-State Reactivity as a New Concept in Organometallic Chemistry. *Acc. Chem. Res* 2000, 33, 139–145. [PubMed: 10727203]
- (175). Goodrich LE; Roy S; Alp EE; Zhao J; Hu MY; Lehnert N Electronic Structure and Biologically Relevant Reactivity of Low-Spin {FeNO}8 Porphyrin Model Complexes: New Insight from a bis-Picket Fence Porphyrin. *Inorg. Chem* 2013, 52, 7766–7780. [PubMed: 23746143]
- (176). McQuarters AB; Wirgau NE; Lehnert N Model Complexes of Key Intermediates in Fungal Cytochrome P450 Nitric Oxide Reductase (P450nor). *Curr. Opin. Chem. Biol* 2014, 19, 82–89. [PubMed: 24658055]
- (177). McQuarters AB; Blaesi EJ; Kampf JW; Alp EE; Zhao J; Hu M; Krebs C; Lehnert N Synthetic Model Complex of the Key Intermediate in Cytochrome P450 Nitric Oxide Reductase. *Inorg. Chem* 2019, 58, 1398–1413. [PubMed: 30623648]
- (178). Caranto JD; Vilbert AC; Lancaster KM *Nitrosomonas europaea* Cytochrome P460 Is a Direct Link between Nitrification and Nitrous Oxide Emission. *Proc. Natl. Acad. Sci. U.S.A* 2016, 113, 14704–14709. [PubMed: 27856762]
- (179). Zahn JA; Duncan C; DiSpirito AA Oxidation of Hydroxylamine by Cytochrome P-460 of the Obligate Methylophilic Methylococcus capsulatus Bath. *J. Bacteriol* 1994, 176, 5879–5887. [PubMed: 7928947]
- (180). Elmore BO; Bergmann DJ; Klotz MG; Hooper AB Cytochromes P460 and c' -Beta; a New Family of High-Spin Cytochromes c. *FEBS Lett* 2007, 581, 911–916. [PubMed: 17292891]
- (181). Bergmann DJ; Zahn JA; Hooper AB; DiSpirito AA Cytochrome P460 Genes from the Methanotroph Methylococcus capsulatus Bath. *J. Bacteriol* 1998, 180, 6440–6445. [PubMed: 9851984]
- (182). Erickson RH; Hooper AB Preliminary Characterization of a Variant CO-Binding Heme Protein from *Nitrosomonas*. *Biochim. Biophys. Acta* 1972, 275, 231–244. [PubMed: 5077861]
- (183). Winogradsky S On the Nitrifying Organisms. *Ann. Inst. Pasteur* 1890, 110, 1013–1016.
- (184). Hooper AB; Vannelli T; Bergmann DJ; Arciero DM Enzymology of the Oxidation of Ammonia to Nitrite by Bacteria. *Antonie van Leeuwenhoek* 1997, 71, 59–67. [PubMed: 9049018]
- (185). Kozłowski JA; Kits KD; Stein LY Comparison of Nitrogen Oxide Metabolism among Diverse Ammonia-Oxidizing Bacteria. *Front. Microbiol* 2016, article number 7.
- (186). Kozłowski JA; Stieglmeier M; Schleper C; Klotz MG; Stein LY Pathways and Key Intermediates Required for Obligate Aerobic Ammonia-Dependent Chemolithotrophy in Bacteria and Thaumarchaeota. *ISME J* 2016, 10, 1836–1845. [PubMed: 26882267]
- (187). Könneke M; Bernhard AE; de La Torre JR; Walker CB; Waterbury JB; Stahl DA Isolation of an Autotrophic Ammonia-Oxidizing Marine Archaeon. *Nature* 2005, 437, 543–546. [PubMed: 16177789]
- (188). Francis CA; Beman JM; Kuypers MMM New Processes and Players in the Nitrogen Cycle: The Microbial Ecology of Anaerobic and Archaeal Ammonia Oxidation. *ISME J* 2007, 1, 19–27. [PubMed: 18043610]
- (189). Winogradsky S Contributions à la Morphologie des Organismes de la Nitrification. *Arch. Sci. Biol. (St. Petersb.)* 1892, 1, 88–137.
- (190). Daims H; Lückner S; Wagner M A New Perspective on Microbes Formerly Known as Nitrite-Oxidizing Bacteria. *Trends Microbiol* 2016, 24, 699–712. [PubMed: 27283264]
- (191). Daims H; Lebedeva EV; Pjevac P; Han P; Herbold C; Albertsen M; Jehmlich N; Palatinszky M; Vierheilig J; Bulaev A et al. Complete Nitrification by *Nitrospira* Bacteria. *Nature* 2015, 528, 504–509. [PubMed: 26610024]
- (192). van Kessel MA; Speth DR; Albertsen M; Nielsen PH; Op den Camp HJ; Kartal B; Jetten MS; Lucker S Complete Nitrification by a Single Microorganism. *Nature* 2015, 528, 555–559. [PubMed: 26610025]
- (193). Stein LY Surveying N₂O-Producing Pathways in Bacteria. *Methods Enzymol* 2011, 486, 131–152. [PubMed: 21185434]

- (194). Adams HR; Krewson C; Vardanega JE; Fujii S; Moreno T; Chicano; Sambongi Y; Svistunenko D; Paps J; Andrew CR et al. One Fold, Two Functions: Cytochrome P460 and Cytochrome: C'-B from the Methanotroph *Methylococcus capsulatus* (Bath). *Chem. Sci* 2019, 10, 3031–3041. [PubMed: 30996884]
- (195). Pearson AR; Elmore BO; Yang C; Ferrara JD; Hooper AB; Wilmot CM The Crystal Structure of Cytochrome P460 of *Nitrosomonas europaea* Reveals a Novel Cytochrome Fold and Heme - Protein Cross-Link. *Biochemistry* 2007, 46, 8340–8349. [PubMed: 17583915]
- (196). Smith MA; Lancaster KM The Eponymous Cofactors in Cytochrome P460s from Ammonia-Oxidizing Bacteria Are Iron Porphyrinoids Whose Macrocycles Are Dibasic. *Biochemistry* 2018, 57, 334–343. [PubMed: 29211462]
- (197). Cedervall P; Hooper AB; Wilmot CM Structural Studies of Hydroxylamine Oxidoreductase Reveal a Unique Heme Cofactor and a Previously Unidentified Interaction Partner. *Biochemistry* 2013, 52, 6211–6218. [PubMed: 23952581]
- (198). Dietl A; Ferousi C; Maalcke WJ; Menzel A; De Vries S; Keltjens JT; Jetten MSM; Kartal B; Barends TRM The Inner Workings of the Hydrazine Synthase Multiprotein Complex. *Nature* 2015, 527, 394–397. [PubMed: 26479033]
- (199). Igarashi N; Moriyama H; Fujiwara T; Fukumori Y; Tanaka N The 2.8 Å Structure of Hydroxylamine Oxidoreductase from a Nitrifying Chemoautotrophic Bacterium, *Nitrosomonas europaea*. *Nat. Struct. Biol* 1997, 4, 276–284. [PubMed: 9095195]
- (200). Jentzen W; Song X-Z; Shelnett JA Structural Characterization of Synthetic and Protein-Bound Porphyrins in Terms of the Lowest-Frequency Normal Coordinates of the Macrocycle. *J. Phys. Chem. B* 1997, 101, 1684–1699.
- (201). Graves AB; Graves MT; Liptak MD Measurement of Heme Ruffling Changes in Mhud Using Uv-Vis Spectroscopy. *J. Phys. Chem. B* 2016, 120, 3853.
- (202). Hooper AB; Terry KR Hydroxylamine Oxidoreductase of *Nitrosomonas*. Production of Nitric Oxide from Hydroxylamine. *Biochim. Biophys. Acta* 1979, 571, 12–20. [PubMed: 497235]
- (203). Caranto JD; Lancaster KM Nitric Oxide Is an Obligate Bacterial Nitrification Intermediate Produced by Hydroxylamine Oxidoreductase. *Proc. Natl. Acad. Sci. U.S.A* 2017, 114, 8217–8222. [PubMed: 28716929]
- (204). Lin YW Structure and Function of Heme Proteins Regulated by Diverse Post-Translational Modifications. *Arch. Biochem. Biophys* 2018, 641, 1–30. [PubMed: 29407792]
- (205). Bergmann DJ; Hooper AB Cytochrome P460 of *Nitrosomonas Europaea*: Formation of the Heme- Lysine Cross-Link in a Heterologous Host and Mutagenic Conversion to a Non-Cross-Linked Cytochrome C'. *Eur. J. Biochem* 2003, 270, 1935–1941. [PubMed: 12709052]
- (206). Yan DJ; Yuan H; Li W; Xiang Y; He B; Nie CM; Wen GB; Lin YW; Tan X How a Novel Tyrosine-Heme Cross-Link Fine-Tunes the Structure and Functions of Heme Proteins: A Direct Comparative Study of L29H/F43Y Myoglobin. *Dalton Trans* 2015, 44, 18815–18822. [PubMed: 26458300]
- (207). Metcalfe CL; Ott M; Patel N; Singh K; Mistry SC; Goff HM; Raven EL Autocatalytic Formation of Green Heme: Evidence for H₂O₂-Dependent Formation of a Covalent Methionine-Heme Linkage in Ascorbate Peroxidase. *J. Am. Chem. Soc* 2004, 126, 16242–16248. [PubMed: 15584761]
- (208). Cheng HM; Yuan H; Wang XJ; Xu JK; Gao SQ; Wen GB; Tan X; Lin YW Formation of Cys-Heme Cross-Link in K42C Myoglobin under Reductive Conditions with Molecular Oxygen. *J. Inorg. Biochem* 2018, 182, 141–149. [PubMed: 29477977]
- (209). Liptak MD; Wen X; Bren KL NMR and DFT Investigation of Heme Ruffling: Functional Implications for Cytochrome c. *J. Am. Chem. Soc* 2010, 132, 9753–9763. [PubMed: 20572664]
- (210). Kleingardner JG; Levin BD; Zoppellaro G; Andersson KK; Elliott SJ; Bren KL Influence of Heme c Attachment on Heme Conformation and Potential. *J. Biol. Inorg. Chem* 2018, 23, 1073–1083. [PubMed: 30143872]
- (211). Rees MK Studies of the Hydroxylamine Metabolism of *Nitrosomonas Europaea*. I. Purification of Hydroxylamine Oxidase. *Biochemistry* 1968, 7, 353–366. [PubMed: 5758552]

- (212). Hooper AB; Nason A Characterization of Hydroxylamine-Cytochrome C Reductase from the Chemoautotrophs *Nitrosomonas europaea* and *Nitrosocystis oceanus*. *J. Biol. Chem* 1965, 240, 4044–4057. [PubMed: 5842070]
- (213). Andersson KK; Hooper AB O₂ and H₂O Are Each the Source of One O in NO₂⁻ Produced from NH₃ by *Nitrosomonas*: ¹⁵N-NMR Evidence. *FEBS Lett* 1983, 164, 236–240.
- (214). Hollocher TC; Tate ME; Nicholas DJ Oxidation of Ammonia by *Nitrosomonas europaea*. Definite ¹⁸O-Tracer Evidence That Hydroxylamine Formation Involves a Monooxygenase. *J. Biol. Chem* 1981, 256, 10834–10836. [PubMed: 7287737]
- (215). Walker FA Nitric Oxide Interaction with Insect Nitrophorins and Thoughts on the Electron Configuration of the {FeNO}₆ Complex. *J. Inorg. Biochem* 2005, 99, 216–236. [PubMed: 15598503]
- (216). Roberts SA; Weichsel A; Qiu Y; Shelnutt JA; Walker FA; Montfort WR Ligand-Induced Heme Ruffling and Bent NO Geometry in Ultra-High-Resolution Structures of Nitrophorin 4. *Biochemistry* 2001, 40, 11327–11337. [PubMed: 11560480]
- (217). Ding XD; Weichsel A; Andersen JF; Kh Shokhireva T; Balfour C; Pierik AJ; Averill BA; Montfort WR; Ann Walker F Nitric Oxide Binding to the Ferri- and Ferroheme States of Nitrophorin 1, a Reversible NO-Binding Heme Protein from the Saliva of the Blood-Sucking Insect, *Rhodnius prolixus*. *J. Am. Chem. Soc* 1998, 121, 128–138.
- (218). Weichsel A; Andersen JF; Roberts SA; Montfort WR Nitric Oxide Binding to Nitrophorin 4 Induces Complete Distal Pocket Burial. *Nat. Struct. Biol* 2000, 7, 551–554. [PubMed: 10876239]
- (219). Ford PC Reactions of NO and Nitrite with Heme Models and Proteins. *Inorg. Chem* 2010, 49, 6226–6239. [PubMed: 20666383]
- (220). Warren JJ; Mayer JM Moving Protons and Electrons in Biomimetic Systems. *Biochemistry* 2015, 54, 1863–1878. [PubMed: 25742166]
- (221). Tutusaus O; Ni C; Szymczak NK A Transition Metal Lewis Acid/Base Triad System for Cooperative Substrate Binding. *J. Am. Chem. Soc* 2013, 135, 40.
- (222). Cioncoloni G; Roger I; Wheatley PS; Wilson C; Morris RE; Sproules S; Symes MD Proton-Coupled Electron Transfer Enhances the Electrocatalytic Reduction of Nitrite to NO in a Bioinspired Copper Complex. *ACS Catal* 2018, 8, 5070–5084.
- (223). Cheung PM; Burns KT; Kwon YM; Deshayes MY; Aguayo KJ; Oswald VF; Seda T; Zakharov LN; Kowalczyk T; Gilbertson JD Hemilabile Proton Relays and Redox Activity Lead to {FeNO}_x and Significant Rate Enhancements in NO₂⁻ Reduction. *J. Am. Chem. Soc* 2018, 140, 17040–17050. [PubMed: 30427681]
- (224). Borovik AS Bioinspired Hydrogen Bond Motifs in Ligand Design: The Role of Noncovalent Interactions in Metal Ion Mediated Activation of Dioxigen. *Acc. Chem. Res* 2005, 38, 54–61. [PubMed: 15654737]
- (225). Maalcke WJ; Dietl A; Marritt SJ; Butt JN; Jetten MSM; Keltjens JT; Barends TRM; Kartal B Structural Basis of Biological NO Generation by Octaheme Oxidoreductases. *J. Biol. Chem* 2014, 289, 1228–1242. [PubMed: 24302732]
- (226). Attia AAA; Silaghi-Dumitrescu R Computational Investigation of the Initial Two-Electron, Two-Proton Steps in the Reaction Mechanism of Hydroxylamine Oxidoreductase. *J. Phys. Chem. B* 2014, 118, 12140–12145. [PubMed: 25277374]
- (227). Fernández ML; Estrin DA; Bari SE Theoretical Insight into the Hydroxylamine Oxidoreductase Mechanism. *J. Inorg. Biochem* 2008, 102, 1523–1530. [PubMed: 18336913]
- (228). Smith MA; Majer SH; Vilbert AC; Lancaster KM Controlling a Burn: Outer-Sphere Gating of Hydroxylamine Oxidation by a Distal Base in Cytochrome P460. *Chem. Sci* 2019, 10, 3756–3764. [PubMed: 31015919]
- (229). Whittaker M; Bergmann D; Arciero D; Hooper AB Electron Transfer During Oxidation of Ammonia by the Chemolithotrophic Bacterium *Nitrosomonas europaea*. *Biochim. Biophys. Acta* 2000, 1459, 346–355. [PubMed: 11004450]
- (230). Iverson TM; Hendrich MP; Arciero DM; Hooper AB; Rees DC Cytochrome c554. In *Handbook of Metalloproteins*, John Wiley & Sons: Chichester, UK, 2001; Vol. 1; pp 136–146.
- (231). Hooper AB; Arciero D; Bergmann D; Hendrich MP The Oxidation of Ammonia as an Energy Source in Bacteria. *Advances in Photosynthesis and Respiration* 2005, 16, 121–147.

- (232). Yamanaka T; Shinra M Cytochrome c-552 and Cytochrome c-554 Derived from Nitrosomonas europaea: Purification, Properties, and Their Function in Hydroxylamine Oxidation. *J. Biochem* 1974, 75, 1265–1273. [PubMed: 4372235]
- (233). Andersson KK; Lipscomb JD; Valentine M; Münck E; Hooper AB Tetraheme Cytochrome C-554 from Nitrosomonas europaea. Heme-Heme Interactions and Ligand Binding. *J. Biol. Chem* 1986, 261, 1126–1138. [PubMed: 3003055]
- (234). Zorz JK; Kozlowski JA; Stein LY; Strous M; Kleiner M Comparative Proteomics of Three Species of Ammonia-Oxidizing Bacteria. *Front. Microbiol* 2018, 9, 1–15. [PubMed: 29403456]
- (235). Mctavish H; Laquier F; Arciero D; Logan M; Mundfrom G; Fuchs JA; Hooper AB Multiple Copies of Genes Coding for Electron Transport Proteins in the Bacterium Nitrosomonas europaea. *J. Bacteriol* 1993, 175, 2445–2447. [PubMed: 8385668]
- (236). Bergmann DJ; Arciero DM; Hooper AB Organization of the HAO Gene Cluster of Nitrosomonas europaea: Genes for Two Tetraheme c Cytochromes. *J. Bacteriol* 1994, 176, 3148–3153. [PubMed: 8195067]
- (237). Upadhyay AK; Petasis DT; Arciero DM; Hooper AB; Hendrich MP Spectroscopic Characterization and Assignment of Reduction Potentials in the Tetraheme Cytochrome c554 from Nitrosomonas europaea. *J. Am. Chem. Soc* 2003, 125, 1738–1747. [PubMed: 12580599]
- (238). Iverson TM; Arciero DM; Hsu BT; Logan MSP; Hooper AB; Rees DC Heme Packing Motifs Revealed by the Crystal Structure of the Tetra-Heme Cytochrome c554 from Nitrosomonas europaea. *Nat. Struct. Biol* 1998, 5, 1005–1012. [PubMed: 9808046]
- (239). Iverson TM; Arciero DM; Hooper AB; Rees DC High-Resolution Structures of the Oxidized and Reduced States of Cytochrome c554 from Nitrosomonas europaea. *J. Biol. Inorg. Chem* 2001, 6, 390–397. [PubMed: 11372197]
- (240). Einsle O; Messerschmidt A; Stach P; Bourenkov GP; Bartunik HD; Huber R; Kroneck PMH Structure of Cytochrome c Nitrite Reductase. *Nature* 1999, 400, 476–480. [PubMed: 10440380]
- (241). Arciero DM; Collins MJ; Hooper AB; Collins MJ; Haladjian J; Bianco P Resolution of the Four Hemes of Cytochrome c554 from Nitrosomonas europaea by Redox Potentiometry and Optical Spectroscopy. *Biochemistry* 1991, 30, 11459–11465. [PubMed: 1660303]
- (242). Pulcu GS; Elmore BL; Arciero DM; Hooper AB; Elliott SJ Direct Electrochemistry of Tetraheme Cytochrome c554 from Nitrosomonas europaea: Redox Cooperativity and Gating. *J. Am. Chem. Soc* 2007, 129, 1838–1839. [PubMed: 17263529]
- (243). Arciero DM; Hooper AB; Balny C Spectroscopic and Rapid Kinetic Studies of Reduction of Cytochrome C554 by Hydroxylamine Oxidoreductase from Nitrosomonas europaea. *Biochemistry* 1991, 30, 11466–11472. [PubMed: 1660304]
- (244). Beaumont HJE; Hommes NG; Sayavedra-Soto LA; Arp DJ; Arciero DM; Hooper AB; Westerhoff HV; Van Spanning RJM Nitrite Reductase of Nitrosomonas europaea Is Not Essential for Production of Gaseous Nitrogen Oxides and Confers Tolerance to Nitrite. *J. Bacteriol* 2002, 184, 2557–2560. [PubMed: 11948173]
- (245). Beaumont HJE; Van Schooten B; Lens SI; Westerhoff HV; Van Spanning RJM Nitrosomonas europaea Expresses a Nitric Oxide Reductase During Nitrification. *J. Bacteriol* 2004, 186, 4417–4421. [PubMed: 15205449]
- (246). Schmidt I; van Spanning RJM; Jetten MSM Denitrification and Ammonia Oxidation by Nitrosomonas europaea Wild-Type, and NirK- and NorB-Deficient Mutants. *Microbiology* 2004, 150, 4107–4114. [PubMed: 15583163]
- (247). Upadhyay AK; Hooper AB; Hendrich MP NO Reductase Activity of the Tetraheme Cytochrome c554 of Nitrosomonas europaea. *J. Am. Chem. Soc* 2006, 128, 4330–4337. [PubMed: 16569009]
- (248). Lewis RS; Deen WM Kinetics of the Reaction of Nitric Oxide with Oxygen in Aqueous Solutions. *Chem. Res. Toxicol* 1994, 7, 568–574. [PubMed: 7981422]
- (249). Lim MD; Lorkovi IM; Ford PC The Preparation of Anaerobic Nitric Oxide Solutions for the Study of Heme Model Systems in Aqueous and Nonaqueous Media: Some Consequences of NO_x Impurities. *Methods Enzymol* 2005, 396, 3–17. [PubMed: 16291216]
- (250). McGarry JM; Pacheco AA Upon Further Analysis, Neither Cytochrome c554 from Nitrosomonas europaea nor Its F156A Variant Display NA Reductase Activity, Though Both

- Proteins Bind Nitric Oxide Reversibly. *J. Biol. Inorg. Chem* 2018, 23, 861–878. [PubMed: 29946979]
- (251). Wasserfallen A; Ragetti S; Jouanneau Y; Leisinger T A Family of Flavoproteins in the Domains Archaea and Bacteria. *Eur. J. Biochem* 1998, 254, 325–332. [PubMed: 9660187]
- (252). Vicente JB; Tran V; Pinto L; Teixeira M; Singh U A Detoxifying Oxygen Reductase in the Anaerobic Protozoan *Entamoeba histolytica*. *Eukaryot Cell* 2012, 11, 1112–1118. [PubMed: 22798391]
- (253). Mills PC; Rowley G; Spiro S; Hinton JC; Richardson DJ A Combination of Cytochrome c Nitrite Reductase (NrfA) and Flavorubredoxin (NorV) Protects *Salmonella enterica* Serovar Typhimurium against Killing by NO in Anoxic Environments. *Microbiology* 2008, 154, 1218–1228. [PubMed: 18375814]
- (254). Le Fourn C; Brasseur G; Brochier-Armanet C; Pieulle L; Brioukhanov A; Ollivier B; Dolla A An Oxygen Reduction Chain in the Hyperthermophilic Anaerobe *Thermotoga maritima* Highlights Horizontal Gene Transfer between Thermococcales and Thermotogales. *Environ. Microbiol* 2011, 13, 2132–2145. [PubMed: 21366819]
- (255). Thorgersen MP; Stirrett K; Scott RA; Adams MW Mechanism of Oxygen Detoxification by the Surprisingly Oxygen-Tolerant Hyperthermophilic Archaeon, *Pyrococcus furiosus*. *Proc. Natl. Acad. Sci. U.S.A* 2012, 109, 18547–18552. [PubMed: 23093671]
- (256). Gomes CM; Giuffre A; Forte E; Vicente JB; Saraiva LM; Brunori M; Teixeira M A Novel Type of Nitric-Oxide Reductase. *Escherichia coli* Flavorubredoxin. *J. Biol. Chem* 2002, 277, 25273–25276. [PubMed: 12101220]
- (257). Chen L; Liu MY; LeGall J; Fareleira P; Santos H; Xavier AV Rubredoxin Oxidase, a New Flavo-Hemo-Protein, Is the Site of Oxygen Reduction to Water by the “Strict Anaerobe” *Desulfovibrio gigas*. *Biochem. Biophys. Res. Commun* 1993, 193, 100–105. [PubMed: 8503894]
- (258). Le Fourn C; Fardeau ML; Ollivier B; Lojou E; Dolla A The Hyperthermophilic Anaerobe *Thermotoga maritima* Is Able to Cope with Limited Amount of Oxygen: Insights into Its Defence Strategies. *Environ. Microbiol* 2008, 10, 1877–1887. [PubMed: 18397308]
- (259). Romao CV; Vicente JB; Borges PT; Frazao C; Teixeira M The Dual Function of Flavodiiron Proteins: Oxygen and/or Nitric Oxide Reductases. *J. Biol. Inorg. Chem* 2016, 21, 39–52. [PubMed: 26767750]
- (260). Martins MC; Romão CV; Folgosa F; Borges PT; Frazão C; Teixeira M How Superoxide Reductases and Flavodiiron Proteins Combat Oxidative Stress in Anaerobes. *Free Radic. Biol. Med* 2019, 140, 36–60. [PubMed: 30735841]
- (261). Saraiva LM; Vicente JB; Teixeira M The Role of the Flavodiiron Proteins in Microbial Nitric Oxide Detoxification. *Adv. Microb. Physiol* 2004, 49, 77–129. [PubMed: 15518829]
- (262). Goncalves VL; Saraiva LM; Teixeira M Gene Expression Study of the Flavodi-Iron Proteins from the Cyanobacterium *Synechocystis* sp. Pcc6803. *Biochem. Soc. Trans* 2011, 39, 216–218. [PubMed: 21265776]
- (263). Frazão C; Silva G; Gomes CM; Matias P; Coelho R; Sieker L; Macedo S; Liu MY; Oliveira S; Teixeira M et al. Structure of a Dioxygen Reduction Enzyme from *Desulfovibrio gigas*. *Nat. Struct. Biol* 2000, 7, 1041–1045. [PubMed: 11062560]
- (264). Silaghi-Dumitrescu R; Kurtz DM; Ljungdahl LG; Lanzilotta WN X-Ray Crystal Structures of *Moorella thermoacetica* FprA. Novel Diiron Site Structure and Mechanistic Insights into a Scavenging Nitric Oxide Reductase. *Biochemistry* 2005, 44, 6492–6501. [PubMed: 15850383]
- (265). Di Matteo A; Scandurra FM; Testa F; Forte E; Sarti P; Brunori M; Giuffre A The O₂-Scavenging Flavodiiron Protein in the Human Parasite *Giardia intestinalis*. *J. Biol. Chem* 2008, 283, 4061–4068. [PubMed: 18077462]
- (266). Seedorf H; Hagemeyer CH; Shima S; Thauer RK; Warkentin E; Ermler U Structure of Coenzyme F₄₂₀H₂ Oxidase (FprA), a Di-Iron Flavoprotein from Methanogenic Archaea Catalyzing the Reduction of O₂ to H₂O. *FEBS J* 2007, 274, 1588–1599. [PubMed: 17480207]
- (267). Fang H; Caranto JD; Mendoza R; Taylor AB; Hart PJ; Kurtz DM Jr. Histidine Ligand Variants of a Flavo-Diiron Protein: Effects on Structure and Activities. *J. Biol. Inorg. Chem* 2012, 17, 1231–1239. [PubMed: 22990880]

- (268). Weitz AC; Giri N; Caranto JD; Kurtz DM; Bominaar EL; Hendrich MP Spectroscopy and DFT Calculations of a Flavo-Diiron Enzyme Implicate New Diiron Site Structures. *J. Am. Chem. Soc* 2017, 139, 12009–12019. [PubMed: 28756660]
- (269). Das A; Coulter ED; Kurtz DM Jr.; Ljungdahl LG Five-Gene Cluster in *Clostridium thermoaceticum* Consisting of Two Divergent Operons Encoding Rubredoxin Oxidoreductase-Rubredoxin and Rubrerythrin-Type a Flavoprotein- High-Molecular-Weight Rubredoxin. *J. Bacteriol* 2001, 183, 1560–1567. [PubMed: 11160086]
- (270). Gardner AM; Helmick RA; Gardner PR Flavorubredoxin, an Inducible Catalyst for Nitric Oxide Reduction and Detoxification in *Escherichia coli*. *J. Biol. Chem* 2002, 277, 8172–8177. [PubMed: 11751865]
- (271). Silaghi-Dumitrescu R; Coulter ED; Das A; Ljungdahl LG; Jameson GN; Huynh BH; Kurtz DM Jr. A Flavodiiron Protein and High Molecular Weight Rubredoxin from *Moorella thermoacetica* with Nitric Oxide Reductase Activity. *Biochemistry* 2003, 42, 2806–2815. [PubMed: 12627946]
- (272). Silaghi-Dumitrescu R; Kim YN; Viswanathan R; Kurtz DM A Flavo-Diiron Protein from *Desulfovibrio Vulgaris* with Oxidase and Nitric Oxide Reductase Activities. Evidence for an In Vivo Nitric Oxide Scavenging Function. *Biochemistry* 2005, 44, 3572–3579. [PubMed: 15736966]
- (273). Rodrigues R; Vicente JB; Felix R; Oliveira S; Teixeira M; Rodrigues-Pousada C *Desulfovibrio gigas* Flavodiiron Protein Affords Protection against Nitrosative Stress in Vivo. *J. Bacteriol* 2006, 188, 2745–2751. [PubMed: 16585735]
- (274). Goncalves VL; Vicente JB; Pinto L; Romao CV; Frazao C; Sarti P; Giuffre A; Teixeira M Flavodiiron Oxygen Reductase from *Entamoeba histolytica*: Modulation of Substrate Preference by Tyrosine 271 and Lysine 53. *J. Biol. Chem* 2014, 289, 28260–28270. [PubMed: 25151360]
- (275). Frederick RE; Caranto JD; Masitas CA; Gebhardt LL; MacGowan CE; Limberger RJ; Kurtz DM Jr. Dioxygen and Nitric Oxide Scavenging by *Treponema denticola* Flavodiiron Protein: A Mechanistic Paradigm for Catalysis. *J. Biol. Inorg. Chem* 2015, 20, 603–613. [PubMed: 25700637]
- (276). Pereira AS; Small W; Krebs C; Tavares P; Edmondson DE; Theil EC; Huynh BH Direct Spectroscopic and Kinetic Evidence for the Involvement of a Peroxodiferric Intermediate During the Ferroxidase Reaction in Fast Ferritin Mineralization. *Biochemistry* 1998, 37, 9871–9876. [PubMed: 9665690]
- (277). Vu VV; Emerson JP; Martinho M; Kim YS; Munck E; Park MH; Que L Jr. Human Deoxyhypusine Hydroxylase, an Enzyme Involved in Regulating Cell Growth, Activates O₂ with a Nonheme Diiron Center. *Proc. Natl. Acad. Sci. U.S.A* 2009, 106, 14814–14819. [PubMed: 19706422]
- (278). Kurtz JDM Flavo-Diiron Enzymes: Nitric Oxide or Dioxygen Reductases? *Dalton Trans* 2007, 4115–4121.
- (279). Wildschut JD; Lang RM; Voordouw JK; Voordouw G Rubredoxin:Oxygen Oxidoreductase Enhances Survival of *Desulfovibrio vulgaris* Hildenborough under Microaerophilic Conditions. *J. Bacteriol* 2006, 188, 6253–6260. [PubMed: 16923892]
- (280). Solomon EI; Brunold TC; Davis MI; Kemsley JN; Lee SK; Lehnert N; Neese F; Skulan AJ; Yang YS; Zhou J Geometric and Electronic Structure/Function Correlations in Non-Heme Iron Enzymes. *Chem. Rev* 2000, 100, 235–350. [PubMed: 11749238]
- (281). Hayashi T; Caranto JD; Wampler DA; Kurtz DM; Moënné-Loccoz P Insights into the Nitric Oxide Reductase Mechanism of Flavodiiron Proteins from a Flavin-Free Enzyme. *Biochemistry* 2010, 49, 7040–7049. [PubMed: 20669924]
- (282). Blomberg LM; Blomberg MR; Siegbahn PE Theoretical Study of the Reduction of Nitric Oxide in an a-Type Flavoprotein. *J. Biol. Inorg. Chem* 2007, 12, 79–89. [PubMed: 16957917]
- (283). Lu S; Libby E; Saleh L; Xing G; Bollinger JM; Moënné-Loccoz P Characterization of NO Adducts of the Diiron Center in Protein R2 of *Escherichia coli* Ribonucleotide Reductase and Site-Directed Variants; Implications for the O₂ Activation Mechanism. *J. Biol. Inorg. Chem* 2004, 9, 818–827. [PubMed: 15311337]

- (284). Haskin CJ; Ravi N; Lynch JB; Münck E; Que L Reaction of NO with the Reduced R2 Protein of Ribonucleotide Reductase from *Escherichia coli*. *Biochemistry* 1995, 34, 11090–11098. [PubMed: 7669766]
- (285). Coufal DE; Tavares P; Pereira AS; Hyunh BH; Lippard SJ Reactions of Nitric Oxide with the Reduced Non-Heme Diiron Center of the Soluble Methane Monooxygenase Hydroxylase. *Biochemistry* 1999, 38, 4504–4513. [PubMed: 10194372]
- (286). Caranto JD; Weitz A; Hendrich MP; Kurtz DM The Nitric Oxide Reductase Mechanism of a Flavo-Diiron Protein: Identification of Active-Site Intermediates and Products. *J. Am. Chem. Soc* 2014, 136, 7981–7992. [PubMed: 24828196]
- (287). Nocek JM; Kurtz DM; Debrunner P; Xia Y-M; Sage JT; Shiemke AK; Sanders-Loehr J; Loehr TM Nitric Oxide Adducts of the Binuclear Iron Site of Hemerythrin. *Biochemistry* 1988, 27, 1014–1024. [PubMed: 3365363]
- (288). Hayashi T; Caranto JD; Matsumura H; Kurtz DM; Moëne-Loccoz P Vibrational Analysis of Mononitrosyl Complexes in Hemerythrin and Flavodiiron Proteins: Relevance to Detoxifying NO Reductase. *J. Am. Chem. Soc* 2012, 134, 6878–6884. [PubMed: 22449095]
- (289). Jana M; Pal N; White CJ; Kupper C; Meyer F; Lehnert N; Majumdar A Functional Mononitrosyl Diiron(II) Complex Mediates the Reduction of NO to N2O with Relevance for Flavodiiron No Reductases. *J. Am. Chem. Soc* 2017, 139, 14380–14383. [PubMed: 28953388]
- (290). Caranto JD; Weitz A; Giri N; Hendrich MP; Kurtz DM A Diferrous-Dinitrosyl Intermediate in the N2O-Generating Pathway of a Deflavinated Flavo-Diiron Protein. *Biochemistry* 2014, 53, 5631–5637. [PubMed: 25144650]
- (291). Arciero DM; Lipscomb JD; Huynh BH; Kent TA; Munck E EPR and Mossbauer Studies of Protocatechuate 4,5-Dioxygenase. *J. Biol. Chem* 1983, 258, 14981–14991. [PubMed: 6317682]
- (292). Weitz AC; Giri N; Frederick RE; Kurtz DM; Bominaar EL; Hendrich MP Spectroscopy and DFT Calculations of Flavo-Diiron Nitric Oxide Reductase Identify Bridging Structures of NO-Coordinated Diiron Intermediates. *ACS Catal* 2018, 8, 11704–11715. [PubMed: 31263628]
- (293). Feig AL; Becker M; Schindler S; van Eldik R; Lippard SJ Mechanistic Studies of the Formation and Decay of Diiron(III) Peroxo Complexes in the Reaction of Diiron(II) Precursors with Dioxygen. *Inorg. Chem* 1996, 35, 2590–2601. [PubMed: 11666474]
- (294). White CJ; Speelman AL; Kupper C; Demeshko S; Meyer F; Shanahan JP; Alp EE; Hu M; Zhao J; Lehnert N The Semireduced Mechanism for Nitric Oxide Reduction by Non-Heme Diiron Complexes: Modeling Flavodiiron Nitric Oxide Reductases. *J. Am. Chem. Soc* 2018, 140, 2562–2574. [PubMed: 29350921]
- (295). Schwizer F; Okamoto Y; Heinisch T; Gu Y; Pellizzoni MM; Lebrun V; Reuter R; Köhler V; Lewis JC; Ward TR Artificial Metalloenzymes: Reaction Scope and Optimization Strategies. *Chem. Rev* 2017, 118, 142–231. [PubMed: 28714313]
- (296). Kan SJ; Lewis RD; Chen K; Arnold FHJS Directed Evolution of Cytochrome c for Carbon–Silicon Bond Formation: Bringing Silicon to Life 2016, 354, 1048–1051.
- (297). Lu Y; Yeung N; Sieracki N; Marshall NM Design of Functional Metalloproteins. *Nature* 2009, 460, 855. [PubMed: 19675646]
- (298). Sigman JA; Kwok BC; Lu Y From Myoglobin to Heme-Copper Oxidase: Design and Engineering of a CuB Center into Sperm Whale Myoglobin. *J. Am. Chem. Soc* 2000, 122, 8192–8196.
- (299). Bhagi-Damodaran A; Petrik I; Lu Y Using Biosynthetic Models of Heme-Copper Oxidase and Nitric Oxide Reductase in Myoglobin to Elucidate Structural Features Responsible for Enzymatic Activities 2016, 56, 773–790.
- (300). Sabuncu S; Reed JH; Lu Y; Moëne-Loccoz P Nitric Oxide Reductase Activity in Heme–Nonheme Binuclear Engineered Myoglobins through a One-Electron Reduction Cycle. *J. Am. Chem. Soc* 2018, 140, 17389–17393. [PubMed: 30512937]
- (301). Feig AL; Bautista MT; Lippard SJ A Carboxylate-Bridged Non-Heme Diiron Dinitrosyl Complex. *Inorg. Chem* 1996, 35, 6892–6898. [PubMed: 11666858]
- (302). Stubbe J; Nocera DG; Yee CS; Chang MC Radical Initiation in the Class I Ribonucleotide Reductase: Long-Range Proton-Coupled Electron Transfer? *Chem. Rev* 2003, 103, 2167–2201. [PubMed: 12797828]

- (303). Stenkamp RE; Sieker LC; Jensen LH; McCallum JD; Sanders-Loehr J Active Site Structures of Deoxyhemerythrin and Oxyhemerythrin. *Proc. Natl. Acad. Sci. U.S.A* 1985, 82, 713. [PubMed: 3856224]
- (304). Collman JP; Yang Y; Dey A; Decreau RA; Ghosh S; Ohta T; Solomon EI A Functional Nitric Oxide Reductase Model. *Proc. Natl. Acad. Sci. U.S.A* 2008, 105, 15660–15665. [PubMed: 18838684]
- (305). Collman JP; Dey A; Yang Y; Decreau RA; Ohta T; Solomon EI Intermediates Involved in the Two Electron Reduction of NO to N₂O by a Functional Synthetic Model of Heme Containing Bacterial NO Reductase. *J. Am. Chem. Soc* 2008, 130, 16498–16499. [PubMed: 19049449]
- (306). Xu N; Campbell AL; Powell DR; Khandogin J; Richter-Addo GB A Stable Hyponitrite-Bridged Iron Porphyrin Complex. *J. Am. Chem. Soc* 2009, 131, 2460–2461. [PubMed: 19191487]
- (307). Xu N; Abucayon EG; Powell DR; Richter-Addo GB A Bridged Di-Iron Porphyrin Hyponitrite Complex as a Model for Biological N₂O Production from Hyponitrite. *Nitric Oxide* 2016, 52, 16–20. [PubMed: 26529479]
- (308). Zheng S; Berto TC; Dahl EW; Hoffman MB; Speelman AL; Lehnert N The Functional Model Complex [Fe₂(BPMP)(OPr)(NO)₂](BPh₄)₂ Provides Insight into the Mechanism of Flavodiiron NO Reductases. *J. Am. Chem. Soc* 2013, 135, 4902–4905. [PubMed: 23472831]
- (309). Van Stappen C; Lehnert N Mechanism of N-N Bond Formation by Transition Metal-Nitrosyl Complexes: Modeling Flavodiiron Nitric Oxide Reductases. *Inorg. Chem* 2018, 57, 4252–4269. [PubMed: 29608298]
- (310). Jiang Y; Hayashi T; Matsumura H; Do LH; Majumdar A; Lippard SJ; Moëne-Loccoz P Light-Induced N₂O Production from a Non-Heme Iron-Nitrosyl Dimer. *J. Am. Chem. Soc* 2014, 136, 12524–12527. [PubMed: 25158917]
- (311). Haskin CJ; Ravi N; Lynch JB; Munck E; Que L Jr. Reaction of No with the Reduced R2 Protein of Ribonucleotide Reductase from Escherichia Coli. *Biochemistry* 1995, 34, 11090–11098. [PubMed: 7669766]
- (312). Dong HT; White CJ; Zhang B; Krebs C; Lehnert N Non-Heme Diiron Model Complexes Can Mediate Direct NO Reduction: Mechanistic Insight into Flavodiiron NO Reductases. *J. Am. Chem. Soc* 2018, 140, 13429–13440. [PubMed: 30220202]
- (313). Wolfe SK; Andrade C; Swinehart J Kinetic Studies of the Pentacyanonitrosylferrate (2-) Azide and Hydroxylamine Reactions. *Inorg. Chem* 1974, 13, 2567–2572.
- (314). Abucayon EG; Powell DR; Richter-Addo GB Carbon-Nitrogen and Nitrogen-Nitrogen Bond Formation from Nucleophilic Attack at Coordinated Nitrosyls in Fe and Ru Heme Models. *J. Am. Chem. Soc* 2017, 139, 9495–9498. [PubMed: 28648069]
- (315). Barley MH; Meyer TJ Electrocatalytic Reduction of Nitrite to Ammonia Based on a Water-Soluble Iron Porphyrin. *J. Am. Chem. Soc* 1986, 108, 5876–5885. [PubMed: 22175344]
- (316). Barley MH; Rhodes MR; Meyer TJ Electrocatalytic Reduction of Nitrite to Nitrous Oxide and Ammonia Based on the N-Methylated, Cationic Iron Porphyrin Complex [Fe^{III}(H₂O)(TMPyP)]⁵⁺. *Inorg. Chem* 1987, 26, 1746–1750.
- (317). Toth JE; Anson FC Electrocatalytic Reduction of Nitrite and Nitric Oxide to Ammonia with Iron-Substituted Polyoxotungstates. *J. Am. Chem. Soc* 1989, 111, 2444–2451.
- (318). Younathan JN; Wood KS; Meyer TJ Electrocatalytic Reduction of Nitrite and Nitrosyl by Iron(III) Protoporphyrin IX Dimethyl Ester Immobilized in an Electropolymerized Film. *Inorg. Chem* 1992, 31, 3280–3285.
- (319). Brozek CK; Miller JT; Stoian SA; Dinc M NO Disproportionation at a Mononuclear Site-Isolated Fe²⁺ Center in Fe²⁺-MOF-5. *J. Am. Chem. Soc* 2015, 137, 7495–7501. [PubMed: 25988850]
- (320). Confer AM; McQuilken AC; Matsumura H; Moenne-Loccoz P; Goldberg DP A Nonheme, High-Spin {FeNO}₈ Complex That Spontaneously Generates N₂O. *J. Am. Chem. Soc* 2017, 139, 10621–10624. [PubMed: 28749673]
- (321). Fraser RTM; Dasent WE The Composition of the Nitric Oxide Complexes of Cupric Halides. *J. Am. Chem. Soc* 1960, 82, 348–351.
- (322). Mercer M; Fraser RTM Formation and Dissociation of Copper(II) Nitrosyl Complexes in Non-Aqueous Solvents. *J. Inorg. Nucl. Chem* 1963, 25, 525–534.

- (323). Doyle MP; Siegfried B; Hammond JJ Oxidative Deamination of Primary Amines by Copper Halide Nitrosyls. The Formation of Geminal Dihalides. *J. Am. Chem. Soc* 1976, 98, 1627–1629.
- (324). Yordanov ND; Terziev V Studies on the Intermolecular Interactions of Metal Chelate Complexes. I. Spectroscopic Study on the Interaction of Copper(II) Chelate Complexes with NO. *Inorg. Chim. Acta* 1982, 58, 213–216.
- (325). Paul PP; Tyeklár Z; Farooq A; Karlin KD; Liu S; Zubieta J Isolation and X-Ray Structure of a Dinuclear Copper-Nitrosyl Complex. *J. Am. Chem. Soc* 1989, 112, 2430–2432.
- (326). Paul PP; Karlin KD Functional Modeling of Copper Nitrite Reductases: Reactions of NO₂⁻ or NO with Copper(I) Complexes. *J. Am. Chem. Soc* 1991, 113, 6331–6332.
- (327). Lionetti D; de Ruiter G; Agapie T A Trans-Hyponitrite Intermediate in the Reductive Coupling and Deoxygenation of Nitric Oxide by a Tricopper-Lewis Acid Complex. *J. Am. Chem. Soc* 2016, 138, 5008–5011. [PubMed: 27028157]
- (328). Wijeratne GB; Hematian S; Siegler MA; Karlin KD Copper(I)/NO(g) Reductive Coupling Producing a Trans-Hyponitrite Bridged Dicopper(II) Complex: Redox Reversal Giving Copper(I)/NO(g) Disproportionation. *J. Am. Chem. Soc* 2017, 139, 13276–13279. [PubMed: 28820592]
- (329). Tao W; Bower JK; Moore CE; Zhang S Dicopper μ -Oxo, μ -Nitrosyl Complex from the Activation of NO or Nitrite at a Dicopper Center. *J. Am. Chem. Soc* 2019, 141, 10159–10164. [PubMed: 31244169]
- (330). Tolman WB A Model for the Substrate Adduct of Copper Nitrite Reductase and Its Conversion to a Novel Tetrahedral Copper(II) Triflate Complex. *Inorg. Chem* 1991, 30, 4877–4880.
- (331). Carrier SM; Ruggiero CE; Tolman WB Synthesis and Structural Characterization of a Mononuclear Copper Nitrosyl Complex. *J. Am. Chem. Soc* 1992, 114, 4407–4408.
- (332). Ruggiero CE; Carrier SM; Antholine WE; Whittaker JW; Cramer CJ; Tolman WB Synthesis and Structural and Spectroscopic Characterization of Mononuclear Copper Nitrosyl Complexes: Models for Nitric Oxide Adducts of Copper Proteins and Copper-Exchanged Zeolites. *J. Am. Chem. Soc* 1993, 115, 11285–11298.
- (333). Ruggiero CE; Carrier SM; Tolman WB Reductive Disproportionation of NO Mediated by Copper Complexes: Modeling N₂O Generation by Copper Proteins *Angew. Chem. Int. Ed* 1994, 33, 895–897.
- (334). Schneider JL; Carrier SM; Ruggiero CE Jr., V. G. Y.; Tolman WB Influences of Ligand Environment on the Spectroscopic Properties and Disproportionation Reactivity of Copper-Nitrosyl Complexes. *J. Am. Chem. Soc* 1998, 120, 11408–11418.
- (335). Metz S N₂O Formation Via Reductive Disproportionation of NO by Mononuclear Copper Complexes: A Mechanistic DFT Study. *Inorg. Chem* 2017, 56, 3820–3833. [PubMed: 28291346]
- (336). Fujisawa K; Tateda A; Miyashita Y; Okamoto K; Paulat F; Praneeth VKK; Merkle A; Lehnert N Structural and Spectroscopic Characterization of Mononuclear Copper(I) Nitrosyl Complexes: End-on versus Side-on Coordination of NO to Copper(I). *J. Am. Chem. Soc* 2008, 130, 1205–1213. [PubMed: 18179210]
- (337). Kim S; Siegler MA; Karlin KD Peroxynitrite Chemistry Derived from Nitric Oxide Reaction with a Cu(II)-OOH Species and a Copper Mediated NO Reductive Coupling Reaction. *Chem. Commun* 2014, 50, 2844–2846.
- (338). Chufan EE; Puiu SC; Karlin KD Heme-Copper/Dioxygen Adduct Formation, Properties, and Reactivity. *Acc. Chem. Res* 2007, 40, 563–572. [PubMed: 17550225]
- (339). Ghiladi RA; Ju TD; Lee D-H; Moëne-Loccoz P; Kaderli S; Neuhold Y-M; Zuberbuhler AD; Woods AS; Cotter RJ; Karlin KD Formation and Characterization of a High-Spin Heme-Copper Dioxygen (Peroxo) Complex. *J. Am. Chem. Soc* 1999, 121, 9885–9886.
- (340). Chufan EE; Mondai B; Thirumanavelan; Kim E; Rube ND Reactivity Studies on Fe(III)-(O₂)⁻-Cu(II) Compounds: Influence of the Ligand Architecture and Copper Ligand Denticity. *Inorg. Chem* 2007, 46, 6382–6394. [PubMed: 17616124]
- (341). Kim E; Chufan EE; Kamaraj K; Karlin KD Synthetic Models for Heme-Copper Oxidases. *Chem. Rev* 2004, 104, 1077. [PubMed: 14871150]

- (342). Wang J; Schopfer MP; Sarjeant AAN; Karlin KD Heme-Copper Assembly Mediated Reductive Coupling of Nitrogen Monoxide (-NO). *J. Am. Chem. Soc* 2009, 131, 450–451. [PubMed: 19099478]
- (343). Wang J; Schopfer MP; Puiu SC; Sarjeant AA; Karlin KD Reductive Coupling of Nitrogen Monoxide (*NO) Facilitated by Heme/Copper Complexes. *Inorg. Chem* 2010, 49, 1404–1419. [PubMed: 20030370]
- (344). Hieber W; Nast R Über Stickoxydverbindungen von Nickel[I]- und Eisen [I]-halogeniden. *Z. Anorg. Allg. Chem* 1940, 244, 23–47.
- (345). Wright AM; Wu G; Hayton TW Late-Metal Nitrosyl Cations: Synthesis and Reactivity of [Ni(NO)(MeNO₂)₃][PF₆]. *Inorg. Chem* 2011, 50, 11746–11753. [PubMed: 22032412]
- (346). Wright AM; Wu G; Hayton TW Formation of N₂O from a Nickel Nitrosyl: Isolation of the cis-[N₂O]₂ Intermediate. *J. Am. Chem. Soc* 2012, 134, 9930–9933. [PubMed: 22676289]
- (347). Wright AM; Zaman HT; Wu G; Hayton TW Mechanistic Insights into the Formation of N₂O by a Nickel Nitrosyl Complex. *Inorg. Chem* 2014, 53, 3108–3116. [PubMed: 24597563]
- (348). Ghosh S; Deka H; Dangat YB; Saha S; Gogoi K; Vanka K; Mondal B Reductive Nitrosylation of Nickel(II) Complex by Nitric Oxide Followed by Nitrous Oxide Release. *Dalton Trans* 2016, 45, 10200–10208. [PubMed: 27230278]
- (349). Ferretti E; Dechert S; Demeshko S; Holthausen MC; Meyer F Reductive Nitric Oxide Coupling at a Dinickel Core: Isolation of a Key Cis-Hyponitrite Intermediate en route to N₂O Formation. *Angew. Chem. Int. Ed. Engl* 2019, 58, 1705–1709. [PubMed: 30516873]
- (350). Kundu S; Phu PN; Ghosh P; Kozimor SA; Bertke JA; Stieber SCE; Warren TH Nitrosyl Linkage Isomers: NO Coupling to N₂O at a Mononuclear Site. *J. Am. Chem. Soc* 2019, 141, 1415–1419. [PubMed: 30599509]
- (351). Banks RGS; Henderson RJ; Pratt JM Reactions of Nitrous Oxide with Some Transition-Metal Complexes. *Chem. Commun* 1967, 387–388.
- (352). Jensen BB, J.; Burriss RH N₂O as a Substrate and as a Competitive Inhibitor of Nitrogenase. *Biochemistry* 1986, 25, 1083–1088. [PubMed: 3516213]
- (353). Christiansen J; Seefeldt LC; Dean DR Competitive Substrate and Inhibitor Interactions at the Physiologically Relevant Active Site of Nitrogenase. *J. Biol. Chem* 2000, 275, 36104–36107. [PubMed: 10948195]
- (354). Fernandes AT; Damas JM; Todorovic S; Huber R; Baratto MC; Pogni R; Soares CM; Martins LO The Multicopper Oxidase from the Archaeon *Pyrobaculum aerophilum* Shows Nitrous Oxide Reductase Activity. *FEBS J* 2010, 277, 3176–3189. [PubMed: 20597980]
- (355). Philippot L Denitrifying Genes in Bacterial and Archaeal Genomes. *Biochim. Biophys. Acta* 2002, 1577, 355–376. [PubMed: 12359326]
- (356). Jones CM; Spor A; Brennan FP; Breuil M-C; Bru D; Lemanceau P; Griffiths B; Hallin S; Philippot L Recently Identified Microbial Guild Mediates Soil N₂O Sink Capacity. *Nat. Clim. Change* 2014, 4, 801–805.
- (357). Zhang L; Wust A; Prasser B; Muller C; Einsle O Functional Assembly of Nitrous Oxide Reductase Provides Insights into Copper Site Maturation. *Proc. Natl. Acad. Sci. U.S.A* 2019, 116, 12822–12827. [PubMed: 31189605]
- (358). Pauleta SR; Dell'Acqua S; Moura I Nitrous Oxide Reductase. *Coord. Chem. Rev* 2013, 257, 332–349.
- (359). Sanford RA; Wagner DD; Wu Q; Chee-Sanford JC; Thomas SH; Cruz-Garcia C; Rodriguez G; Massol-Deya A; Krishnani KK; Ritalahti K Met al. Unexpected Nondenitrifier Nitrous Oxide Reductase Gene Diversity and Abundance in Soils. *Proc. Natl. Acad. Sci. U.S.A* 2012, 109, 19709–19714. [PubMed: 23150571]
- (360). Payne WJ; Grant MA; Shapleigh J; Hoffman P Nitrogen Oxide Reduction in *Wolinella succinogenes* and *Campylobacter* Species. *J. Bacteriol* 1982, 152, 915–918. [PubMed: 7130133]
- (361). Yoon S; Nissen S; Park D; Sanford RA; Löffler FE Nitrous Oxide Reduction Kinetics Distinguish Bacteria Harboring Clade I NosZ from Those Harboring Clade II NosZ. *Appl. Environ. Microbiol* 2016, 82, 3793–3800. [PubMed: 27084012]

- (362). Simon J; Einsle O; Kroneck PM; Zumft WG The Unprecedented Nos Gene Cluster of Wolinella succinogenes Encodes a Novel Respiratory Electron Transfer Pathway to Cytochrome c Nitrous Oxide Reductase. FEBS Lett 2004, 569, 7–12. [PubMed: 15225600]
- (363). Teraguchi S; Hollocher TC Purification and Some Characteristics of a Cytochrome c-Containing Nitrous Oxide Reductase from Wolinella succinogenes. J. Biol. Chem 1989, 264, 1972–1979. [PubMed: 2536696]
- (364). Liu X; Gao C; Zhang A; Jin P; Wang L; Feng L The Nos Gene Cluster from Gram-Positive Bacterium Geobacillus thermodenitrificans NG80–2 and Functional Characterization of the Recombinant NosZ. FEMS Microbiol. Lett 2008, 289, 46–52. [PubMed: 19054093]
- (365). Zumft WG; Kroneck PM Respiratory Transformation of Nitrous Oxide (N₂O) to Dinitrogen by Bacteria and Archaea. Adv. Microb. Physiol 2007, 52, 107–227. [PubMed: 17027372]
- (366). Kroneck PM; Antholine WA; Riester J; Zumft WG The Nature of the Cupric Site in Nitrous Oxide Reductase and of CuA in Cytochrome c Oxidase. FEBS Lett 1989, 248, 212–213. [PubMed: 2542087]
- (367). Kroneck PM; Antholine WE; Kastrau DH; Buse G; Steffens GC; Zumft WG Multifrequency EPR Evidence for a Bimetallic Center at the CuA Site in Cytochrome c Oxidase. FEBS Lett 1990, 268, 274–276. [PubMed: 2166686]
- (368). Pomowski A; Zumft WG; Kroneck PM; Einsle O N₂O Binding at a [4Cu:2S] Copper-Sulphur Cluster in Nitrous Oxide Reductase. Nature 2011, 477, 234–237. [PubMed: 21841804]
- (369). Brown K; Tegoni M; Prudencio M; Pereira AS; Besson S; Moura JJ; Moura I; Cambillau C A Novel Type of Catalytic Copper Cluster in Nitrous Oxide Reductase. Nat. Struct. Biol 2000, 7, 191–195. [PubMed: 10700275]
- (370). Haltia T; Brown K; Tegoni M; Cambillau C; Saraste M; Mattila K; Djinovic-Carugo K Crystal Structure of Nitrous Oxide Reductase from Paracoccus denitrificans at 1.6 Å Resolution. Biochem. J 2003, 369, 77–88. [PubMed: 12356332]
- (371). Gorelsky SI; Ghosh S; Solomon EI Mechanism of N₂O Reduction by the μ -S Tetranuclear Cu₂Z Cluster of Nitrous Oxide Reductase. J. Am. Chem. Soc 2006, 128, 278–290. [PubMed: 16390158]
- (372). Brown K; Djinovic-Carugo K; Haltia T; Cabrilo I; Saraste M; Moura JJ; Moura I; Tegoni M; Cambillau C Revisiting the Catalytic Cu₂Z Cluster of Nitrous Oxide (N₂O) Reductase. Evidence of a Bridging Inorganic Sulfur. J. Biol. Chem 2000, 275, 41133–41136. [PubMed: 11024061]
- (373). Paraskevopoulos K; Antonyuk SV; Sawers RG; Eady RR; Hasnain SS Insight into Catalysis of Nitrous Oxide Reductase from High-Resolution Structures of Resting and Inhibitor-Bound Enzyme from Achromobacter cycloclastes. J. Mol. Biol 2006, 362, 55–65. [PubMed: 16904686]
- (374). Pomowski A; Zumft WG; Kroneck PM; Einsle O Crystallization of Purple Nitrous Oxide Reductase from Pseudomonas stutzeri. Acta Crystallogr. Sect. F Struct. Biol. Cryst. Commun 2010, 66, 1541–1543.
- (375). Wust A; Schneider L; Pomowski A; Zumft WG; Kroneck PM; Einsle O Nature's Way of Handling a Greenhouse Gas: The Copper-Sulfur Cluster of Purple Nitrous Oxide Reductase. Biol. Chem 2012, 393, 1067–1077. [PubMed: 23096349]
- (376). Dell'Acqua S; Pauleta SR; Moura JJ; Moura I Biochemical Characterization of the Purple Form of Marinobacter hydrocarbonoclasticus Nitrous Oxide Reductase. Philos. Trans. R. Soc. Lond. B Biol. Sci 2012, 367, 1204–1212. [PubMed: 22451106]
- (377). Schneider LK; Einsle O Role of Calcium in Secondary Structure Stabilization During Maturation of Nitrous Oxide Reductase. Biochemistry 2016, 55, 1433–1440. [PubMed: 26885878]
- (378). Matsubara T; Iwasaki H A New-Type of Copper-Protein from Alcaligenes faecalis. J. Biochem 1972, 71, 747–750. [PubMed: 5042462]
- (379). Farrar JA; Thomson AJ; Cheesman MR; Dooley DM; Zumft WG A Model of the Copper Centres of Nitrous Oxide Reductase (Pseudomonas stutzeri). Evidence from Optical, EPR and MCD Spectroscopy. FEBS Lett 1991, 294, 11–15. [PubMed: 1660405]
- (380). Farrar JA; Zumft WG; Thomson AJ CuA and CuZ Are Variants of the Electron Transfer Center in Nitrous Oxide Reductase. Proc. Natl. Acad. Sci. U.S.A 1998, 95, 9891–9896. [PubMed: 9707571]

- (381). Alvarez ML; Ai J; Zumft W; Sanders-Loehr J; Dooley D Characterization of the Copper–Sulfur Chromophores in Nitrous Oxide Reductase by Resonance Raman Spectroscopy: Evidence for Sulfur Coordination in the Catalytic Cluster. *J. Am. Chem. Soc* 2001, 123, 576–587. [PubMed: 11456570]
- (382). Chen P; Cabrito I; Moura J; Moura I; Solomon EI Spectroscopic and Electronic Structure Studies of the M₄-Sulfide Bridged Tetranuclear Cu₂ Cluster in N₂O Reductase: Molecular Insight into the Catalytic Mechanism. *J. Am. Chem. Soc* 2002, 124, 10497–10507. [PubMed: 12197752]
- (383). Chen P; DeBeer George S; Cabrito I; Antholine WE; Moura JJ; Moura I; Hedman B; Hodgson KO; Solomon EI Electronic Structure Description of the μ_4 Sulfide Bridged Tetranuclear Cu₂ Center in N₂O Reductase. *J. Am. Chem. Soc* 2002, 124, 744–745. [PubMed: 11817937]
- (384). Chen P; Gorelsky SI; Ghosh S; Solomon EI N₂O Reduction by the μ_4 -Sulfide-Bridged Tetranuclear Cu₂ Cluster Active Site. *Angew. Chem. Int. Ed* 2004, 43, 4132–4140.
- (385). Rasmussen T; Brittain T; Berks BC; Watmough NJ; Thomson AJ Formation of a Cytochrome c-Nitrous Oxide Reductase Complex Is Obligatory for N₂O Reduction by *Paracoccus pantotrophus*. *Dalton Trans* 2005, 3501–3506. [PubMed: 16234931]
- (386). Gamelin DR; Randall DW; Hay MT; Houser RP; Mulder TC; Canters GW; De Vries S; Tolman WB; Lu Y; Solomon EI Spectroscopy of Mixed-Valence Cu₂-Type Centers: Ligand-Field Control of Ground-State Properties Related to Electron Transfer. *J. Am. Chem. Soc* 1998, 120, 5246–5263.
- (387). Gorelsky SI; Xie X; Chen Y; Fee JA; Solomon EI The Two-State Issue in the Mixed-Valence Binuclear Cu₂ Center in Cytochrome c Oxidase and N₂O Reductase. *J. Am. Chem. Soc* 2006, 128, 16452–16453. [PubMed: 17177365]
- (388). Leguto AJ; Smith MA; Morgada MN; Zitare UA; Murgida DH; Lancaster KM; Vila AJ Dramatic Electronic Perturbations of Cu₂ Centers Via Subtle Geometric Changes. *J. Am. Chem. Soc* 2018, 141, 1373–1381.
- (389). Rasmussen T; Berks BC; Butt JN; Thomson AJ Multiple Forms of the Catalytic Centre, Cu₂, in the Enzyme Nitrous Oxide Reductase from *Paracoccus pantotrophus*. *Biochem. J* 2002, 364, 807–815. [PubMed: 12049645]
- (390). Neese F; Kroneck P; Zumft WG; Antholine WE The Purple Mixed-Valence Cu₂ Center in Nitrous-Oxide Reductase: EPR of the Copper-63-, Copper-65-, and Both Copper-65- and [15N]Histidine-Enriched Enzyme and a Molecular Orbital Interpretation. *J. Am. Chem. Soc* 1996, 118, 8692–8699.
- (391). Kroneck PM; Antholine WA; Riester J; Zumft WG The Cupric Site in Nitrous Oxide Reductase Contains a Mixed-Valence [Cu(II),Cu(I)] Binuclear Center: A Multifrequency Electron Paramagnetic Resonance Investigation. *FEBS Lett* 1988, 242, 70–74. [PubMed: 2849565]
- (392). Riester J; Zumft WG; Kroneck PMH Nitrous Oxide Reductase from *Pseudomonas stutzeri*. *Eur. J. Biochem* 1989, 178, 751–762. [PubMed: 2536326]
- (393). Dooley DM; McGuirl MA; Rosenzweig AC; Landin JA; Scott RA; Zumft WG; Devlin F; Stephens PJ Spectroscopic Studies of the Copper Sites in Wild-Type *Pseudomonas stutzeri* N₂O Reductase and in an Inactive Protein Isolated from a Mutant Deficient in Copper-Site Biosynthesis. *Inorg. Chem* 1991, 30, 3006–3011.
- (394). Charnock JM; Dreusch A; Korner H; Neese F; Nelson J; Kannt A; Michel H; Garner CD; Kroneck PM; Zumft WG Structural Investigations of the Cu₂ Centre of Nitrous Oxide Reductase from *Pseudomonas stutzeri* by Site-Directed Mutagenesis and X-ray Absorption Spectroscopy. *Eur. J. Biochem* 2000, 267, 1368–1381. [PubMed: 10691974]
- (395). Solomon EI Spectroscopic Methods in Bioinorganic Chemistry: Blue to Green to Red Copper Sites. *Inorg. Chem* 2006, 45, 8012–8025. [PubMed: 16999398]
- (396). Oganessian VS; Rasmussen T; Fairhurst S; Thomson AJ Characterisation of [Cu₂S], the Catalytic Site in Nitrous Oxide Reductase, by EPR Spectroscopy. *Dalton Trans* 2004, 996–1002. [PubMed: 15252678]
- (397). Dell'acqua S; Pauleta SR; Monzani E; Pereira AS; Casella L; Moura JJ; Moura I Electron Transfer Complex between Nitrous Oxide Reductase and Cytochrome c₅₅₂ from *Pseudomonas*

- nautica: Kinetic, Nuclear Magnetic Resonance, and Docking Studies. *Biochemistry* 2008, 47, 10852–10862. [PubMed: 18803407]
- (398). Fujita K; Hirasawa-Fujita M; Brown DE; Obara Y; Ijima F; Kohzuma T; Dooley DM Direct Electron Transfer from Pseudoazurin to Nitrous Oxide Reductase in Catalytic N₂O Reduction. *J. Inorg. Biochem* 2012, 115, 163–173. [PubMed: 22910335]
- (399). Dell'acqua S; Moura I; Moura JJ; Pauleta SR The Electron Transfer Complex between Nitrous Oxide Reductase and Its Electron Donors. *J. Biol. Inorg. Chem* 2011, 16, 1241–1254. [PubMed: 21739254]
- (400). Mattila K; Haltia T How Does Nitrous Oxide Reductase Interact with Its Electron Donors?--a Docking Study. *Proteins* 2005, 59, 708–722. [PubMed: 15822112]
- (401). Kukimoto M; Nishiyama M; Ohnuki T; Turley S; Adman ET; Horinouchi S; Beppu T Identification of Interaction Site of Pseudoazurin with Its Redox Partner, Copper-Containing Nitrite Reductase from *Alcaligenes faecalis* S-6. *Protein Eng* 1995, 8, 153–158. [PubMed: 7630886]
- (402). Pauleta SR; Guerlesquin F; Goodhew CF; Devreese B; Van Beeumen J; Pereira AS; Moura I; Pettigrew GW *Paracoccus pantotrophus* Pseudoazurin Is an Electron Donor to Cytochrome c Peroxidase. *Biochemistry* 2004, 43, 11214–11225. [PubMed: 15366931]
- (403). Solomon EI; Heppner DE; Johnston EM; Ginsbach JW; Cirera J; Qayyum M; Kieber-Emmons MT; Kjaergaard CH; Hadt RG; Tian L Copper Active Sites in Biology. *Chem. Rev* 2014, 114, 3659–3853. [PubMed: 24588098]
- (404). Kristjansson JK; Hollocher TC First Practical Assay for Soluble Nitrous Oxide Reductase of Denitrifying Bacteria and a Partial Kinetic Characterization. *J. Biol. Chem* 1980, 255, 704–707. [PubMed: 7356639]
- (405). Kristjansson JK; Hollocher TC Partial Purification and Characterization of Nitrous Oxide Reductase from *Paracoccus denitrificans*. *Curr. Microbiol* 1981, 6, 247–251.
- (406). Snyder SW; Hollocher TC Purification and Some Characteristics of Nitrous Oxide Reductase from *Paracoccus denitrificans*. *J. Biol. Chem* 1987, 262, 6515–6525. [PubMed: 3032972]
- (407). Prudêncio M; Pereira AS; Tavares P; Besson S; Cabrito I; Brown K; Samyn B; Devreese B; Van Beeumen J; Rusnak F et al. Purification, Characterization, and Preliminary Crystallographic Study of Copper-Containing Nitrous Oxide Reductase from *Pseudomonas nautica* 617. *Biochemistry* 2000, 39, 3899–3907. [PubMed: 10747777]
- (408). Ghosh S; Gorelsky SI; Chen P; Cabrito I; Moura JJ; Moura I; Solomon EI Activation of N₂O Reduction by the Fully Reduced μ -4-Sulfide Bridged Tetranuclear Cu₂Z Cluster in Nitrous Oxide Reductase. *J. Am. Chem. Soc* 2003, 125, 15708–15709. [PubMed: 14677937]
- (409). Chan JM; Bollinger JA; Grewell CL; Dooley DM Reductively Activated Nitrous Oxide Reductase Reacts Directly with Substrate. *J. Am. Chem. Soc* 2004, 126, 3030–3031. [PubMed: 15012115]
- (410). Michaelis L; Hill ES The Viologen Indicators. *J. Gen. Physiol* 1933, 16, 859–873. [PubMed: 19872744]
- (411). Bar-Nahum I; Gupta AK; Huber SM; Ertem MZ; Cramer CJ; Tolman WB Reduction of Nitrous Oxide to Dinitrogen by a Mixed Valent Tricopper-Disulfido Cluster. *J. Am. Chem. Soc* 2009, 131, 2812–2814. [PubMed: 19206272]
- (412). Ertem MZ; Cramer CJ; Himo F; Siegbahn PE N–O Bond Cleavage Mechanism(s) in Nitrous Oxide Reductase. *J. Biol. Inorg. Chem* 2012, 17, 687–698. [PubMed: 22434248]
- (413). Dell'Acqua S; Pauleta SR; Paes de Sousa PM; Monzani E; Casella L; Moura JJ; Moura I A New Cu₂Z Active Form in the Catalytic Reduction of N₂O by Nitrous Oxide Reductase from *Pseudomonas nautica*. *J. Biol. Inorg. Chem* 2010, 15, 967–976. [PubMed: 20422435]
- (414). Johnston EM; Carreira C; Dell'Acqua S; Dey SG; Pauleta SR; Moura I; Solomon EI Spectroscopic Definition of the Cu₂Z Degrees Intermediate in Turnover of Nitrous Oxide Reductase and Molecular Insight into the Catalytic Mechanism. *J. Am. Chem. Soc* 2017, 139, 4462–4476. [PubMed: 28228011]
- (415). Torelli S; Belle C; Gautier-Luneau I; Pierre JL; Saint-Aman E; Latour JM; Le Pape L; Luneau D Ph-Controlled Change of the Metal Coordination in a Dicopper(II) Complex of the Ligand H-

- BPMP: Crystal Structures, Magnetic Properties, and Catecholase Activity. *Inorg. Chem* 2000, 39, 3526–3536. [PubMed: 11196811]
- (416). Fujita K; Chan JM; Bollinger JA; Alvarez ML; Dooley DM Anaerobic Purification, Characterization and Preliminary Mechanistic Study of Recombinant Nitrous Oxide Reductase from *Achromobacter Cycloclastes*. *J. Inorg. Biochem* 2007, 101, 1836–1844. [PubMed: 17681606]
- (417). Fujita K; Dooley DM Insights into the Mechanism of N₂O Reduction by Reductively Activated N₂O Reductase from Kinetics and Spectroscopic Studies of pH Effects. *Inorg. Chem* 2007, 46, 613–615. [PubMed: 17257001]
- (418). Ghosh S; Gorelsky SI; George SD; Chan JM; Cabrito I; Dooley DM; Moura JJ; Moura I; Solomon EI Spectroscopic, Computational, and Kinetic Studies of the μ_4 -Sulfide-Bridged Tetranuclear CuZ Cluster in N₂O Reductase: pH Effect on the Edge Ligand and Its Contribution to Reactivity. *J. Am. Chem. Soc* 2007, 129, 3955–3965. [PubMed: 17352474]
- (419). Johnston EM; Dell'Acqua S; Ramos S; Pauleta SR; Moura I; Solomon EI Determination of the Active Form of the Tetranuclear Copper Sulfur Cluster in Nitrous Oxide Reductase. *J. Am. Chem. Soc* 2014, 136, 614–617. [PubMed: 24364717]
- (420). Wunsch P; Herb M; Wieland H; Schiek UM; Zumft WG Requirements for CuA and Cu-S Center Assembly of Nitrous Oxide Reductase Deduced from Complete Periplasmic Enzyme Maturation in the Nondenitrifier *Pseudomonas putida*. *J. Bacteriol* 2003, 185, 887–896. [PubMed: 12533464]
- (421). Wunsch P; Zumft WG Functional Domains of Nosr, a Novel Transmembrane Iron-Sulfur Flavoprotein Necessary for Nitrous Oxide Respiration. *J. Bacteriol* 2005, 187, 1992–2001. [PubMed: 15743947]
- (422). Coyle CL; Zumft WG; Kroneck PM; Korner H; Jakob W Nitrous Oxide Reductase from Denitrifying *Pseudomonas perfectomarina*. Purification and Properties of a Novel Multicopper Enzyme. *Eur. J. Biochem* 1985, 153, 459–467. [PubMed: 3000778]
- (423). Akram M; Dietl A; Mersdorf U; Prinz S; Maalcke W; Keltjens J; Ferousi C; de Almeida NM; Reimann J; Kartal BA 192-Heme Electron Transfer Network in the Hydrazine Dehydrogenase Complex. *Sci. Adv* 2019, 5, eaav4310. [PubMed: 31001586]
- (424). Maalcke WJ; Reimann J; de Vries S; Butt JN; Dietl A; Kip N; Mersdorf U; Barends TR; Jetten MS; Keltjens JT Characterization of Anammox Hydrazine Dehydrogenase, a Key N₂-Producing Enzyme in the Global Nitrogen Cycle. *J. Biol. Chem* 2016, 291, 17077–17092. [PubMed: 27317665]
- (425). Johnson BJ; Lindeman SV; Mankad NP Assembly, Structure, and Reactivity of Cu₄S and Cu₃S Models for the Nitrous Oxide Reductase Active Site, CuZ*. *Inorg. Chem* 2014, 53, 10611–10619. [PubMed: 25211396]
- (426). Jayarathne U; Parmelee SR; Mankad NP Small Molecule Activation Chemistry of Cu–Fe Heterobimetallic Complexes toward CS₂ and N₂O. *Inorg. Chem* 2014, 53, 7730–7737. [PubMed: 24979669]
- (427). Chadeayne AR; Wolczanski PT; Lobkovsky EB The Course of (R₂R'SiO)₃TaCl₂ (R = tBu, R' = H, Me, Ph, tBu (silox)); R = iPr, R' = tBu, iPr) Reduction Is Dependent on Siloxide Size *Inorg. Chem* 2004, 43, 3421–3432. [PubMed: 15154804]
- (428). Baranger AM; Hanna TA; Bergman RG Transfer of Oxygen and Sulfur from Organic Molecules to a Zr–Ir Bond. Evidence for an Unusually Rapid Atom Abstraction Reaction. *J. Am. Chem. Soc* 1995, 117, 10041–10046.
- (429). Laplaza CE; Odom AL; Davis WM; Cummins CC; Protasiewicz JD Cleavage of the Nitrous Oxide NN Bond by a Tris(Amido)Molybdenum(III) Complex. *J. Am. Chem. Soc* 1995, 117, 4999–5000.
- (430). Vaughan GA; Hillhouse GL; Rheingold AL Syntheses, Structures, and Reactivities of Unusual Four-Membered Metallacycles Formed in Insertion Reactions of N:N:O, N:N:Nr, and N:N:Cr₂ with (h⁵-C₅Me₅)₂Zr(C₂Ph₂). *J. Am. Chem. Soc* 1990, 112, 7994–8001.
- (431). Johnson BJ; Antholine WE; Lindeman SV; Mankad NP A Cu₄s Model for the Nitrous Oxide Reductase Active Sites Supported Only by Nitrogen Ligands. *Chem. Commun* 2015, 51, 11860–11863.

- (432). Johnson BJ; Antholine WE; Lindeman SV; Graham MJ; Mankad NP A One-Hole Cu₄S Cluster with N₂O Reductase Activity: A Structural and Functional Model for CuZ. *J. Am. Chem. Soc* 2016, 138, 13107–13110. [PubMed: 27685680]
- (433). van de Graaf AA, de Bruijn P, Robertson LA, Jetten MSM; Kuenen JG Metabolic Pathway of Anaerobic Ammonium Oxidation on the Basis of ¹⁵N Studies in a Fluidized Bed Reactor. *Microbiology* 1997, 2415–2421.
- (434). Kartal B; de Almeida NM; Maalcke WJ; Op den Camp HJ; Jetten MS; Keltjens JT How to Make a Living from Anaerobic Ammonium Oxidation. *FEMS Microbiol. Rev* 2013, 37, 428–461. [PubMed: 23210799]
- (435). Kartal B; Maalcke WJ; de Almeida NM; Cirpus I; Gloerich J; Geerts W; Op den Camp HJ; Harhangi HR; Janssen-Megens EM; Francoijs KJet al. Molecular Mechanism of Anaerobic Ammonium Oxidation. *Nature* 2011, 479, 127–130. [PubMed: 21964329]
- (436). de Almeida NM; Neumann S; Mesman RJ; Ferousi C; Keltjens JT; Jetten MS; Kartal B; van Niftrik L Immunogold Localization of Key Metabolic Enzymes in the Anammoxosome and on the Tubule-Like Structures of *Kuenenia stuttgartiensis*. *J. Bacteriol* 2015, 197, 2432–2441. [PubMed: 25962914]
- (437). Milenkovic D; Blaza JN; Larsson NG; Hirst J The Enigma of the Respiratory Chain Supercomplex. *Cell Metab* 2017, 25, 765–776. [PubMed: 28380371]
- (438). Borrero-de Acuna JM; Timmis KN; Jahn M; Jahn D Protein Complex Formation During Denitrification by *Pseudomonas Aeruginosa*. *Microb. Biotechnol* 2017, 10, 1523–1534. [PubMed: 28857512]
- (439). Dietl A; Ferousi C; Maalcke WJ; Menzel A; de Vries S; Keltjens JT; Jetten MS; Kartal B; Barends TR The Inner Workings of the Hydrazine Synthase Multiprotein Complex. *Nature* 2015, 527, 394–397. [PubMed: 26479033]
- (440). Strous M; Pelletier E; Manganot S; Rattei T; Lehner A; Taylor MW; Horn M; Daims H; Bartol-Mavel D; Wincker P et al. Deciphering the Evolution and Metabolism of an Anammox Bacterium from a Community Genome. *Nature* 2006, 440, 790–794. [PubMed: 16598256]
- (441). Frank J; Lucker S; Vossen R; Jetten MSM; Hall RJ; Op den Camp HJM; Anvar SY Resolving the Complete Genome of *Kuenenia stuttgartiensis* from a Membrane Bioreactor Enrichment Using Single-Molecule Real-Time Sequencing. *Sci. Rep* 2018, 8, 4580. [PubMed: 29545612]
- (442). Auld DS Zinc Coordination Sphere in Biochemical Zinc Sites. *Biometals* 2001, 14, 271–313. [PubMed: 11831461]
- (443). Van Der Star WRL; Dijkema C; De Waard P; Picioreanu C; Strous M; van Loosdrecht MCM An Intracellular Ph Gradient in the Anammox Bacterium *Kuenenia stuttgartiensis* as Evaluated by ³¹P NMR. *Appl. Microbiol. Biotechnol* 2010, 86, 311–317. [PubMed: 19862513]
- (444). Oshiki M; Ali M; Shinyako-Hata K; Satoh H; Okabe S Hydroxylamine-Dependent Anaerobic Ammonium Oxidation (Anammox) by “*Candidatus Brocadia sinica*”. *Environ. Microbiol* 2016, 18, 3133–3143. [PubMed: 27112128]
- (445). Ferousi C; Lindhoud S; Baymann F; Hester ER; Reimann J; Kartal B Discovery of a Functional, Contracted Heme-Binding Motif within a Multiheme Cytochrome. *J. Biol. Chem* 2019.
- (446). de Almeida NM; Wessels HJCT; de Graaf RM; Ferousi C; Jetten MSM; Keltjens JT; Kartal B Membrane-Bound Electron Transport Systems of an Anammox Bacterium: A Complexome Analysis. *Biochim. Biophys. Acta* 2016, 1857, 1694–1704. [PubMed: 27461995]
- (447). Jormakka M; Tornroth S; Byrne B; Iwata S Molecular Basis of Proton Motive Force Generation: Structure of Formate Dehydrogenase-N. *Science* 2002, 295, 1863–1868. [PubMed: 11884747]
- (448). Kartal B; Keltjens JT Anammox Biochemistry: A Tale of Heme C Proteins. *Trends Biochem. Sci* 2016, 41, 998–1011. [PubMed: 27669648]
- (449). Moser CC; Chobot SE; Page CC; Dutton PL Distance Metrics for Heme Protein Electron Tunneling. *Biochim. Biophys. Acta* 2008, 1777, 1032–1037. [PubMed: 18471429]
- (450). Hazari N Homogeneous Iron Complexes for the Conversion of Dinitrogen into Ammonia and Hydrazine. *Chem. Soc. Rev* 2010, 39, 4044–4056. [PubMed: 20571678]
- (451). Nesbit MA; Oyala PH; Peters JC Characterization of the Earliest Intermediate of Fe–N₂ Protonation: CW and Pulse EPR Detection of an Fe–NNH Species and Its Evolution to Fe–NNH₂. *J. Am. Chem. Soc* 2019, 141, 8116–8127. [PubMed: 31046258]

- (452). Kober E; Janas Z; Jezierska J Oxidation of 1-Methyl-1-Phenylhydrazine with Oxidovanadium(V)-Salan Complexes: Insight into the Pathway to the Formation of Hydrazine by Vanadium Nitrogenase. *Inorg. Chem* 2016, 55, 10888–10898. [PubMed: 27754662]
- (453). Gu NX; Ung G; Peters JC Catalytic Hydrazine Disproportionation Mediated by a Thiolate-Bridged Vfe Complex. *Chem. Commun* 2019, 55, 5363–5366.
- (454). Zheng W; Jewitt D; Osamura Y; Kaiser RI Formation of Nitrogen and Hydrogen-Bearing Molecules in Solid Ammonia and Implications for Solar System and Interstellar Ices. *Astrophys. J* 2008, 674, 1242–1250.
- (455). Shulenberger KE; Zhu JL; Tran K; Abdullahi S; Belvin C; Lukens J; Peeler Z; Mullikin E; Cumberbatch HM; Huang Jet al. Electron-Induced Radiolysis of Astrochemically Relevant Ammonia Ices. *ACS Earth Space Chem* 2019, 3, 800–810.
- (456). Andersen WH; Zwolinski BJ; Parlin RB Hydrazine from Ammonia in a High Frequency Discharge Method. *Ind. Eng. Chem* 1959, 51, 527–530.
- (457). Färber M; Huisken F Intracuster Reactions: The Formation of Hydrazine Complexes from Ammonia Clusters Following Ar Excimer Laser Excitation. *J. Chem. Phys* 1996, 104, 4865–4868.
- (458). De D; Englehardt JD; Kalu EE Electroreduction of Nitrate and Nitrite Ion on a Platinum-Group-Metal Catalyst-Modified Carbon Fiber Electrode. *J. Electrochem. Soc* 2000, 147, 4573–4579.

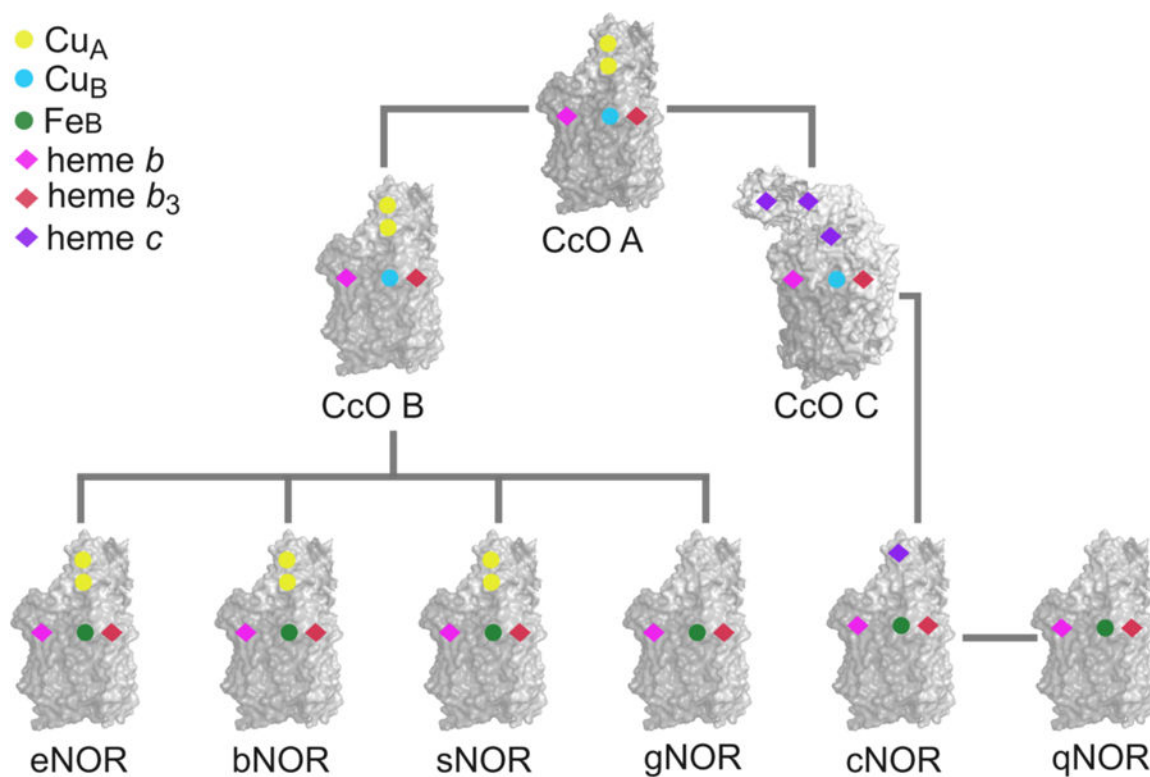
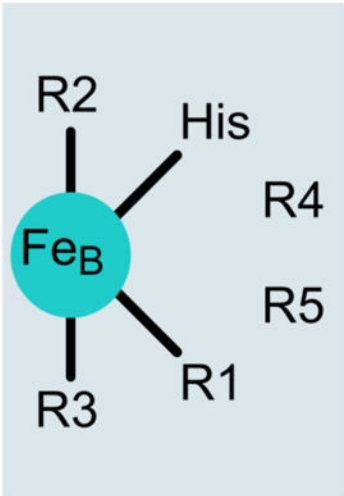


Figure 1.

Cofactor composition of the different classes within the heme Cu oxidase (HCO) superfamily. All members of the HCO superfamily harbor an electron transfer *b*-type heme and a binuclear center that consists of heme b_3 and a non-heme metal that could either be a Cu or an Fe ion (Cu_B and Fe_B , respectively). Additional electron transfer metal centers might also be present, depending on the protein class. PDBIDs: 3HB3 for cytochrome *c* oxidase (CcO) A; 1EHK for CcO B; 3MK7 for CcO C; 3O0R for all nitric oxide reductase (NOR) classes.



	R1	R2	R3	R4	R5
cNOR	His	His	Glu	Glu	Glu
qNOR	His	His	Glu	Glu	Glu
sNOR	His	His	Asn	Tyr	X
gNOR	Asp	His	Asp	Leu	Glu
NOD	His	Asn	Tyr	Glu	Gln

Figure 2.

Ligand identities of the FeB center of different NOR subfamilies. A conserved histidine and three variable residues ligate the NOR FeB center, and a second-sphere glutamate is present in some NOR subfamilies. R1 to R5 denote the different first- and second-sphere residues under discussion and the amino acid variations found in either characterized or putative NOR subfamilies are specified in the table to the right. R5 in sNOR is variable. Adapted by permission from Reference 42. Copyright 2015, Springer Nature.

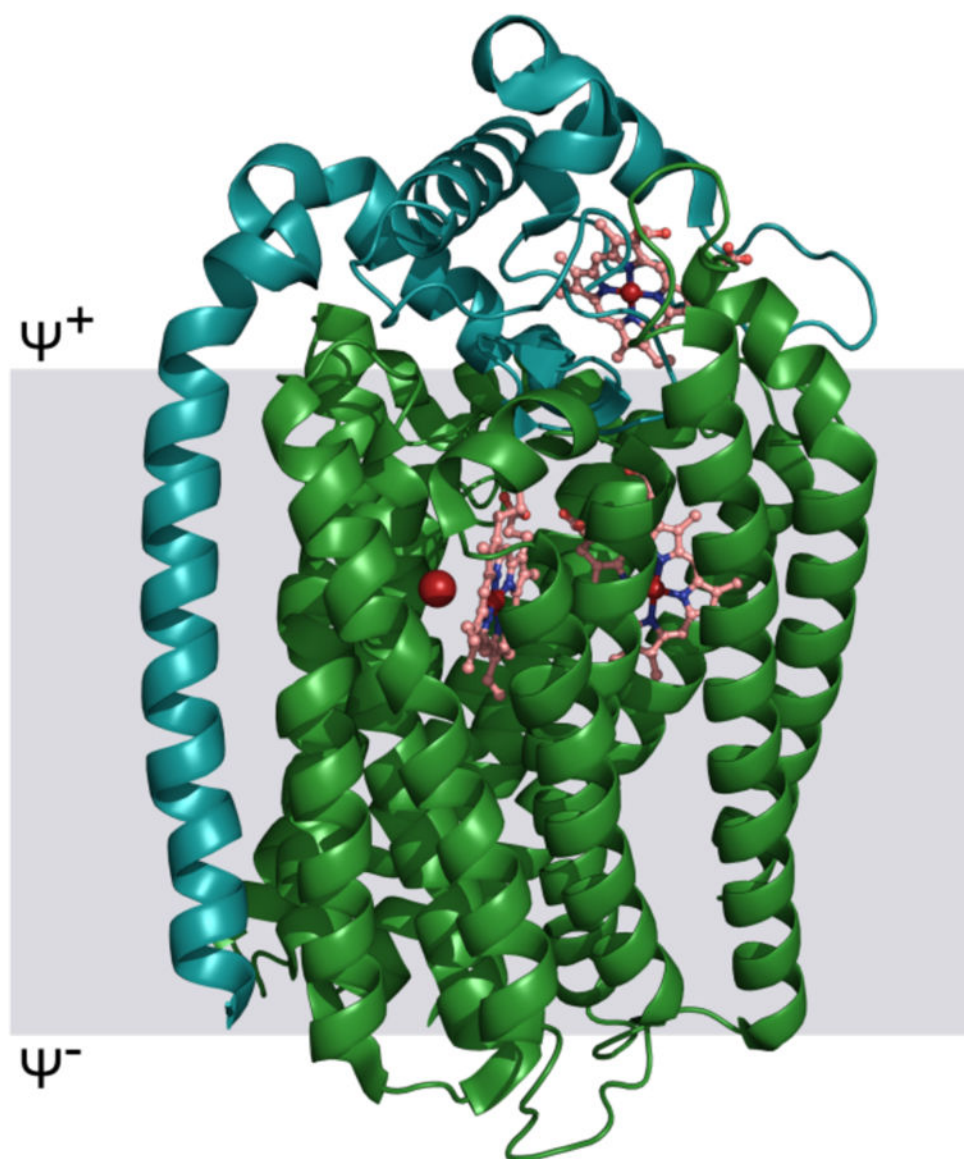


Figure 3. Cartoon representation of the cNOR protein complex from *Pseudomonas aeruginosa* (PaNOR) viewed parallel to the membrane. The NorB subunit is shown in green and the NorC in teal. Heme cofactors are represented as salmon sticks. Fe_B is shown as a ruby red sphere. PDBID: 3O0R.

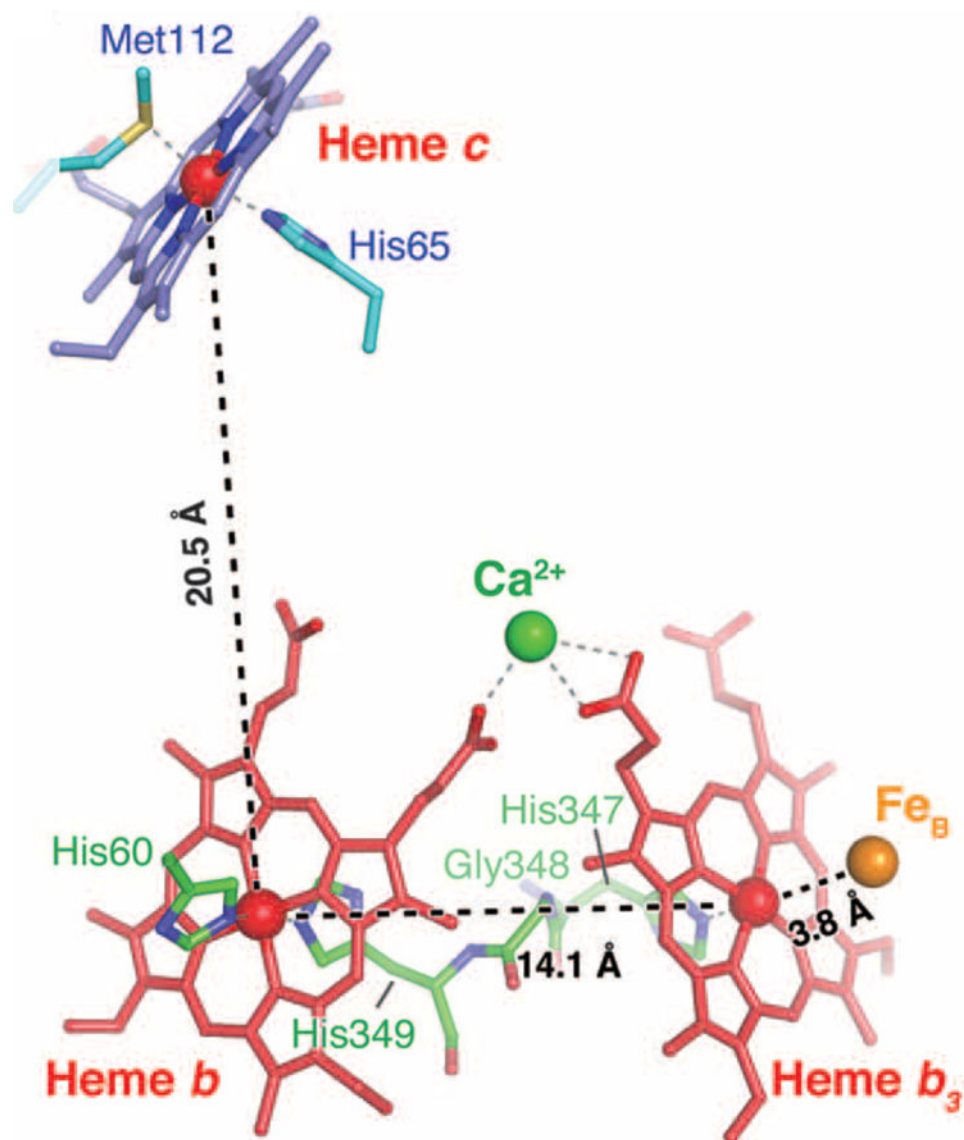


Figure 4. Metal center arrangement in PaNOR. Distances between the redox centers are shown. Heme cofactors, amino acid ligands for metals, and Gly348 are shown as stick models. Fe_B, and Ca are shown as orange and green spheres, respectively. PDBID: 3O0R. Reprinted with permission from Reference 60. Copyright AAAS.

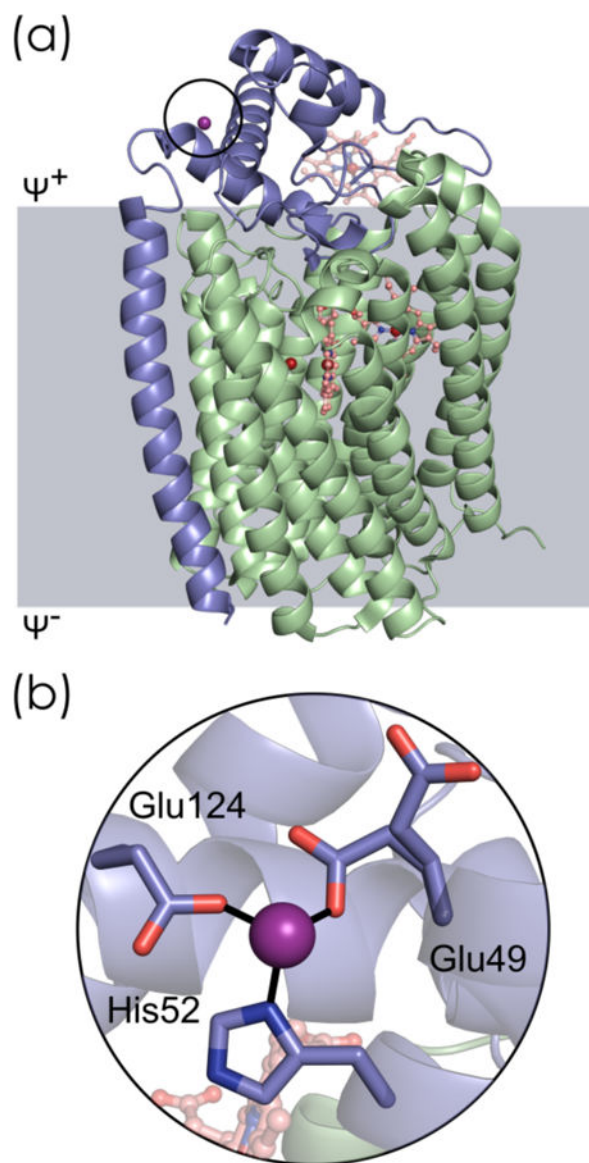


Figure 5. Structure of cNOR from *Roseobacter denitrificans* (RdNOR). (a) Cartoon representation of the RdNOR protein complex viewed parallel to the membrane. The NorB subunit is shown in green and the NorC in blue. Heme cofactors are represented as salmon sticks. Fe_B is shown as a red sphere. (b) Close-up of the extra, unidentified metal ion and its coordination sphere. The extra metal ion identified in the NorC subunit of RdNOR is represented as a purple sphere. PDBID: 4XYD.

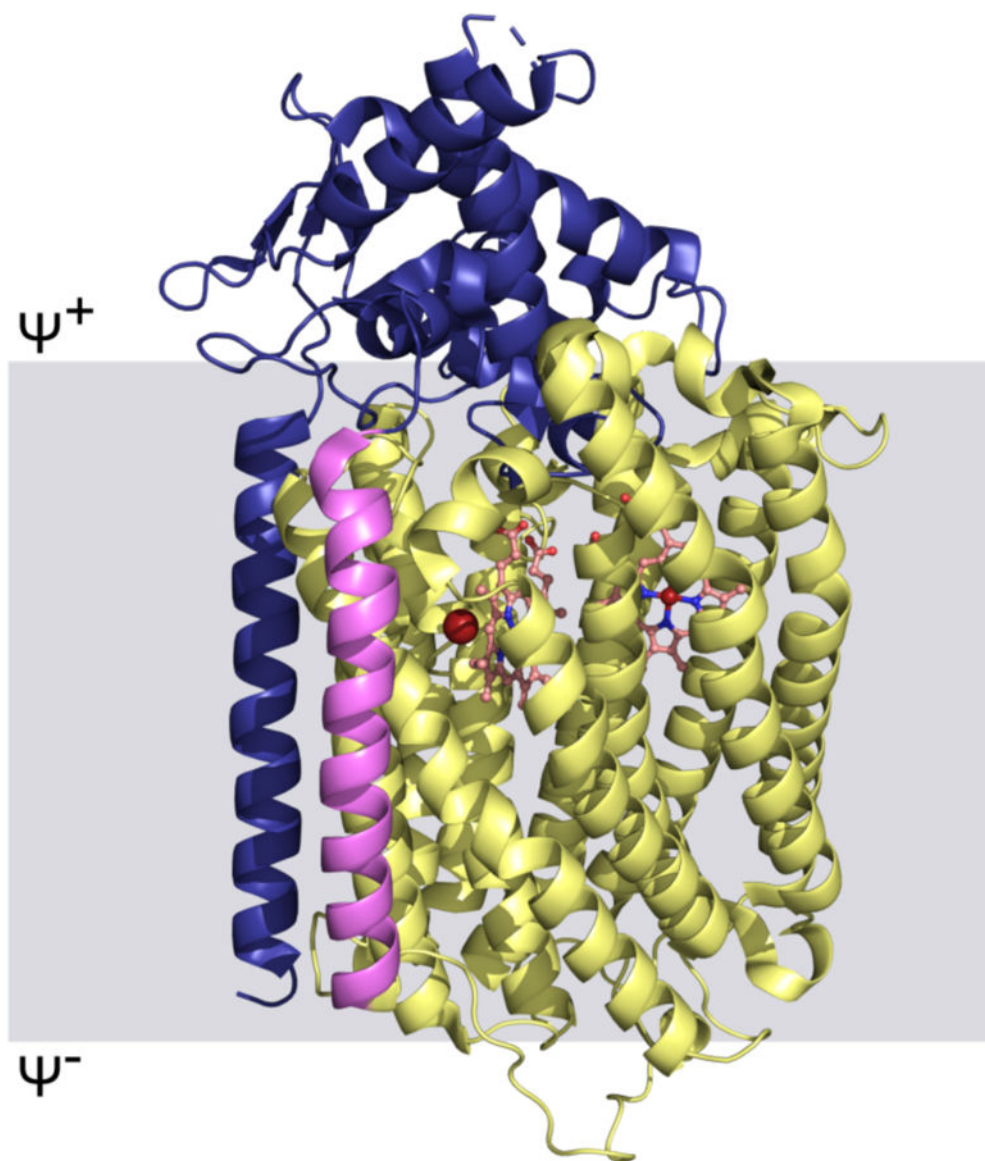


Figure 7. Structure of the qNOR from *Geobacillus stearothermophilus* (GsNOR). Cartoon representation of the GsNOR protein viewed parallel to the membrane. GsNOR is a monomeric protein comprising two main domains that are homologous to the NorB (yellow) and NorC (blue) subunits of cNOR, respectively. The additional transmembrane helix found in the GsNOR crystal structure is colored pink. Heme cofactors are shown as salmon sticks. FeB is shown as a red sphere. PDBID: 3AYF.

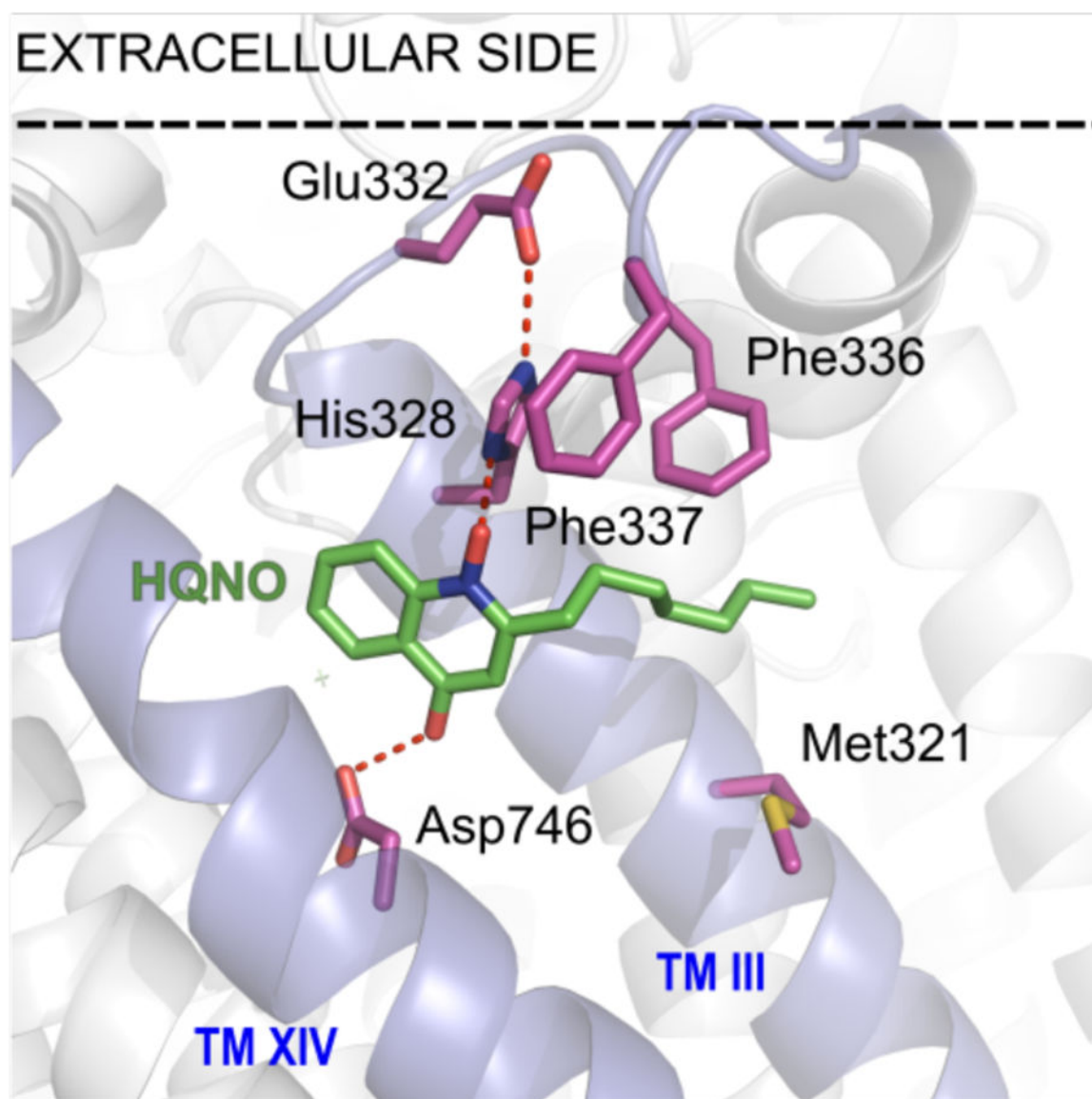


Figure 8. Menaquinol binding site in GsNOR. The quinol analog 2-heptyl hydroxyquinoline N-oxide (HQNO) is observed at the protein surface of the membrane-spanning region close to the extracellular side, which is indicated by the black dashed line. Sidechains of residues involved in the interaction with HQNO are shown as magenta sticks. Hydrogen-bonding interactions are observed between HQNO and polar residues His328 and Asp746. Met321, Phe336, and Phe337 show a hydrophobic interaction with the tail of HQNO. The hydrogen bond network involving HQNO, His328, and Glu322 could function as a proton release pathway from menaquinol to the extracellular side when menaquinol is oxidized. TM = transmembrane region. PDBID: 3AYG. Adapted from Reference 44.

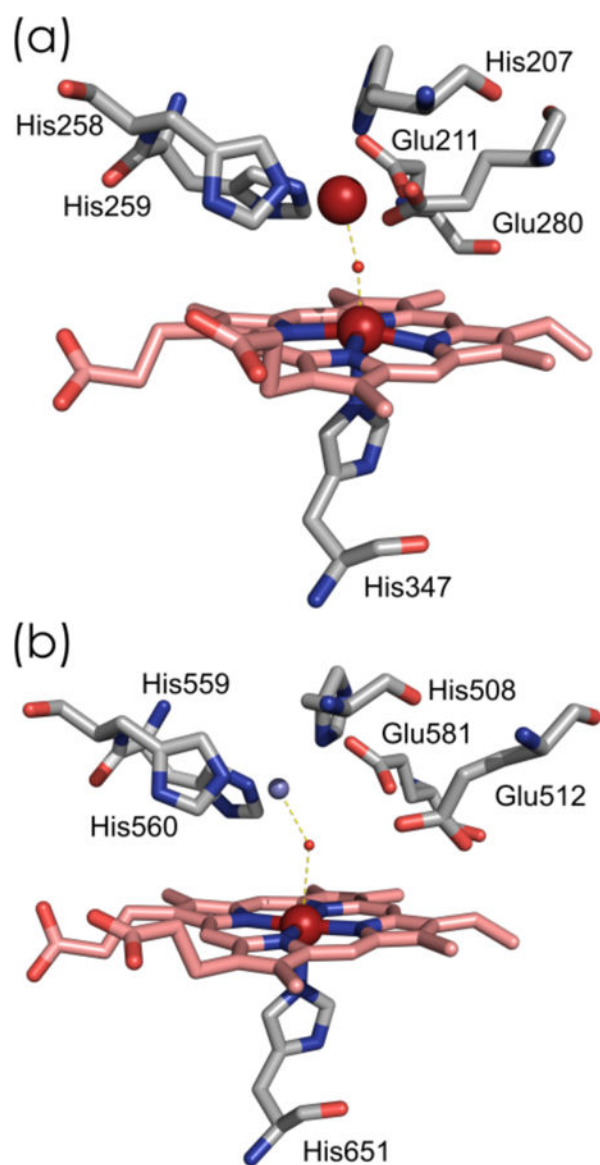


Figure 9. Binuclear catalytic centers of PaNOR (a) and GsNOR (b). Heme *b*₃ is shown as salmon sticks. Fe_B in PaNOR is shown as a red sphere, while Zn_B in GsNOR is shown as a periwinkle sphere. Water molecules are shown as small red spheres. PaNOR PDBID: 3O0R, GsNOR PDBID: 3AYF.

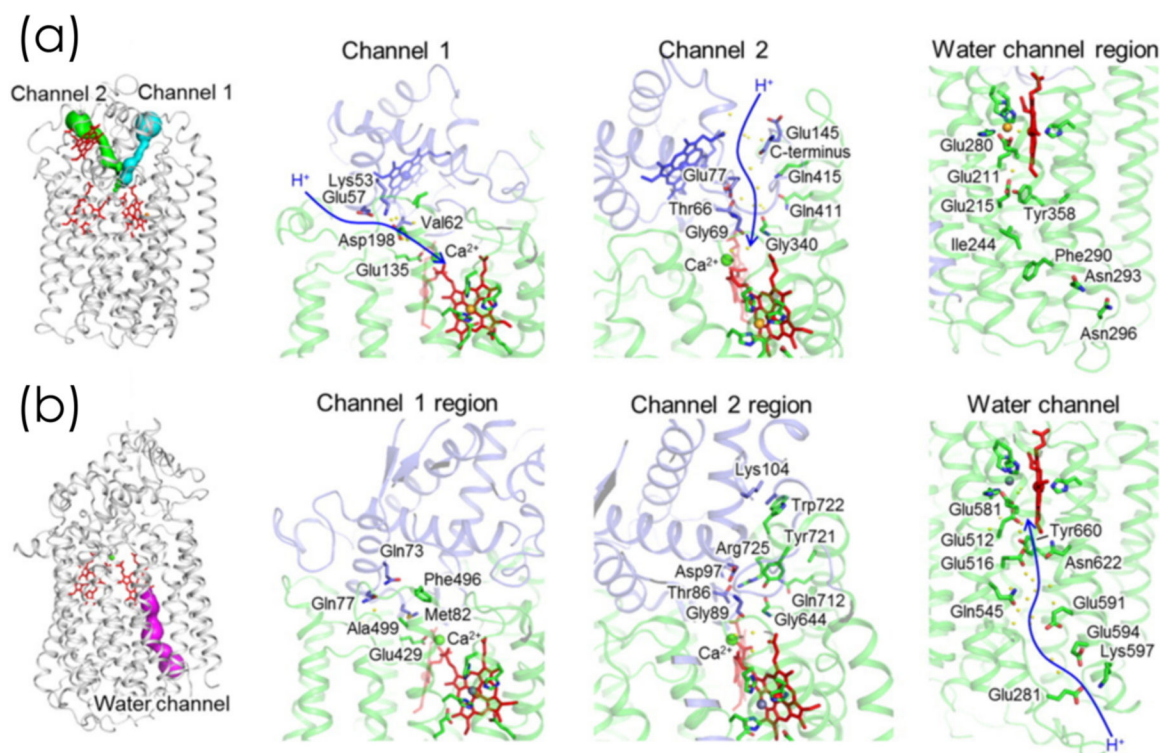


Figure 10.

Comparison of the proposed proton transfer pathways in cNOR (A) and qNOR (B).

Calculation of pathways connecting the buried protein cavities to the outside solvent using Caver⁸⁷ identified two hydrophilic cavities from the outside of the membrane in cNOR (channels 1 (cyan) and 2 (green)) as potential proton transfer pathways, whereas no such cavity from the outside of the membrane was identified in qNOR. Instead, there is a water-containing hydrophilic cavity, designated as a water channel, from the inside of the membrane in qNOR (magenta). Enlarged panels are for the comparison of the proposed proton transfer pathways and corresponding regions in cNOR and qNOR. (A) PaNOR, PDBID: 3O0R. (B) GsNOR, PDBID: 3AYF. Reprinted with permission from Reference 86. Copyright John Wiley & Sons, Inc.

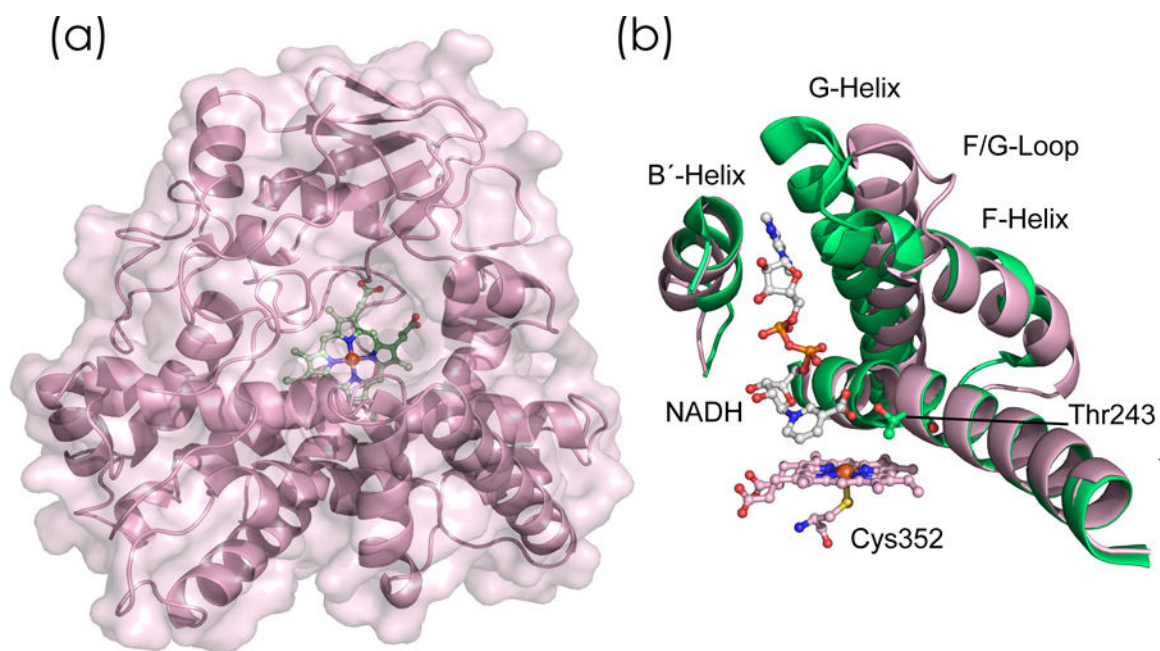


Figure 11.

(a) X-ray crystal structure of P450nor complexed with NO (ligand not shown) from *F. oxysporum* (PDBID: 1CL6, pink) and (b) structural alignment of P450nor complexed with nicotinic acid adenine dinucleotide (NAAD) (PDBID: 1XQD, green). Hydrogen atoms have been omitted for clarity. Relevant secondary structure elements are labeled, along with the conserved Thr243 and axial ligand Cys352.

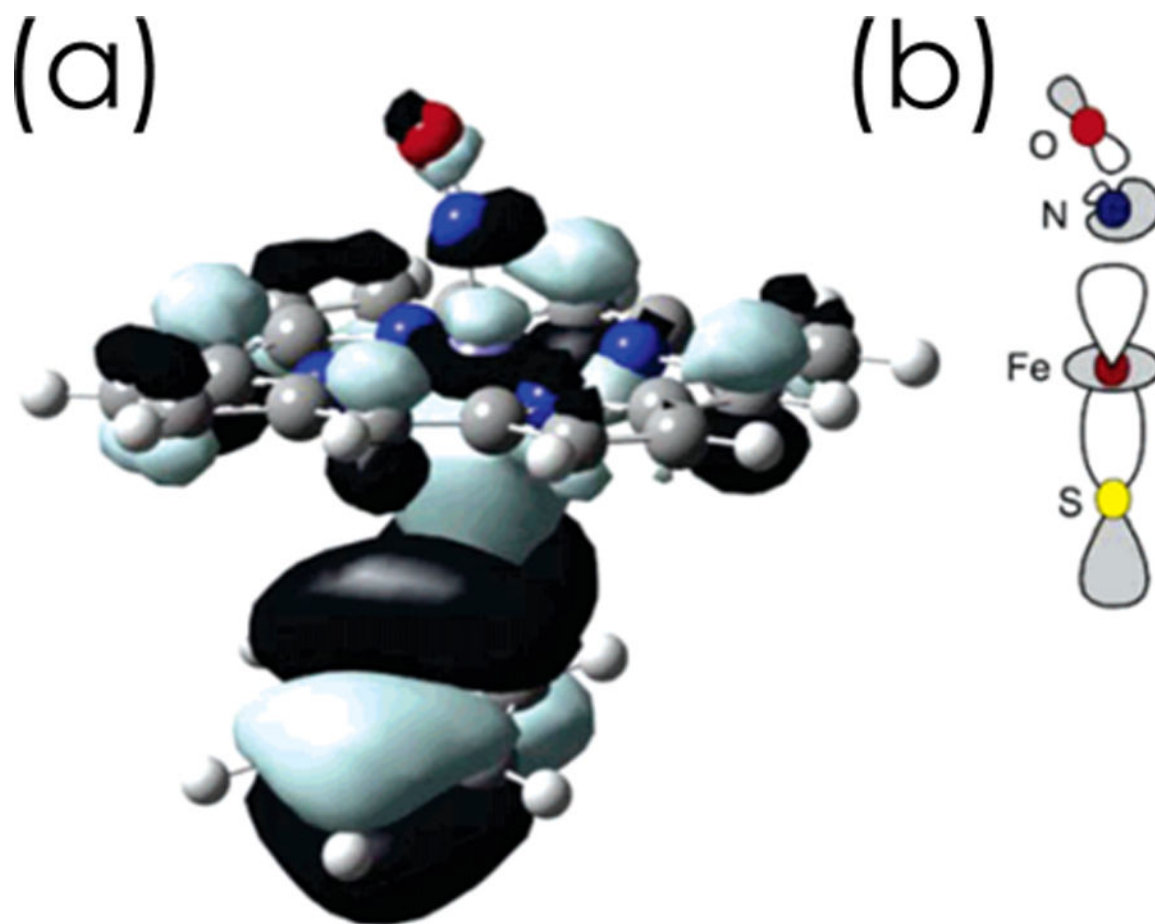


Figure 12.

(a) Contour plot and (b) clarified schematic representations of molecular orbital interaction in a Fe-porphine model complex with thiophenolate and NO axial ligands. This interaction has been implicated in the bent geometry of the axial NO ligand and the observed weakening of the Fe-NO and N-O bonds. The Fe-thiolate s-bond can donate into the σ^* -orbital of the NO via the d_{z^2}/d_{xy} orbitals on Fe, which are antibonding with respect to the Fe-NO and N-O bonds. Geometry optimizations of the model complex were carried out using Gaussian 03 at a BP86 level of theory with a TZVP basis set. Single-point energies were calculated using the ORCA software package using the B3LYP hybrid density functional. Reprinted with permission from Reference ¹⁵². Copyright 2007 American Chemical Society.

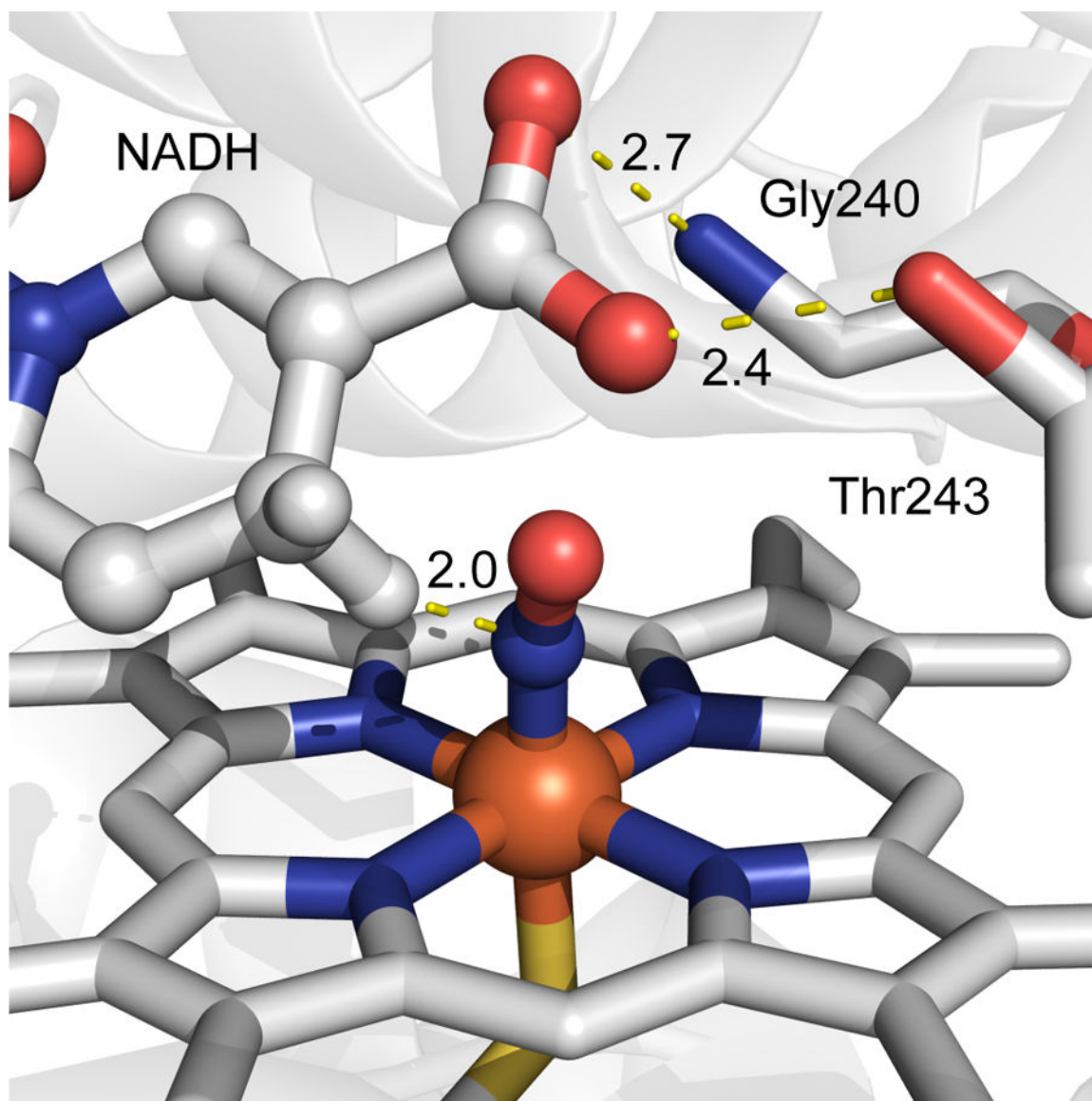


Figure 13.

Structural overlay of P450nor complexed with NO and nicotinic NAAD (+NO PDBID: 1CL6; +NAAD PDBID: 1XQD). Also shown are two residues responsible for properly orienting the NAAD ring. Both the side chain of Thr243 and peptide nitrogen of Gly240 participate in hydrogen bond interactions with the cofactor. Hydrogen atoms are omitted for clarity, except the two hydrogens shown at the C4 position on the NAAD. These are shown to highlight both the stereoselectivity and proximity for the Pro-R hydride towards the N-atom of the NO ligand. All measured distances are reported in Ångstroms (Å).

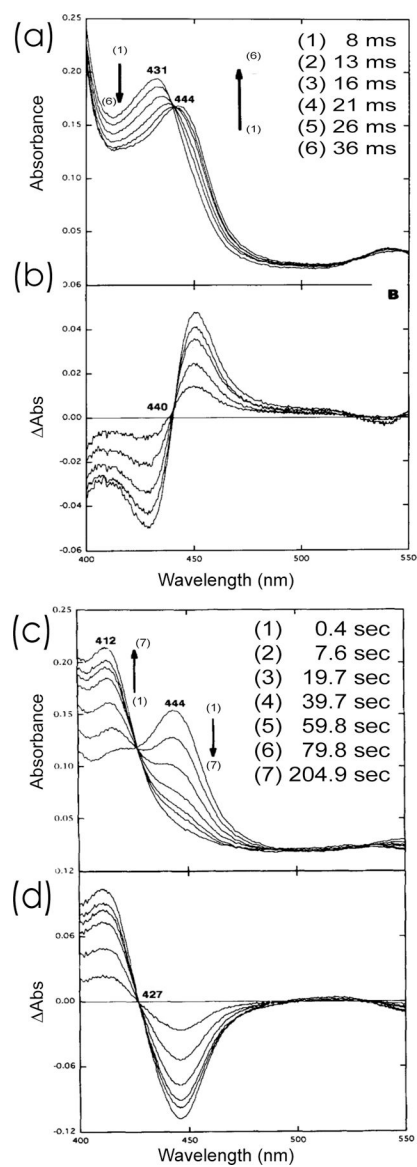


Figure 14.

(a) Time-resolved spectral traces and (b) difference spectra of the reaction between the ferric nitrosyl P450nor with nicotinamide adenine dinucleotide (NADH) at 10°C. These show the isosbestic growth of the characteristic 440 nm Soret peak of Intermediate I. (c) and (d) show analogous spectra monitoring the decay of Intermediate I. Adapted with permission from Reference ¹⁴⁴. Copyright ASBMB.

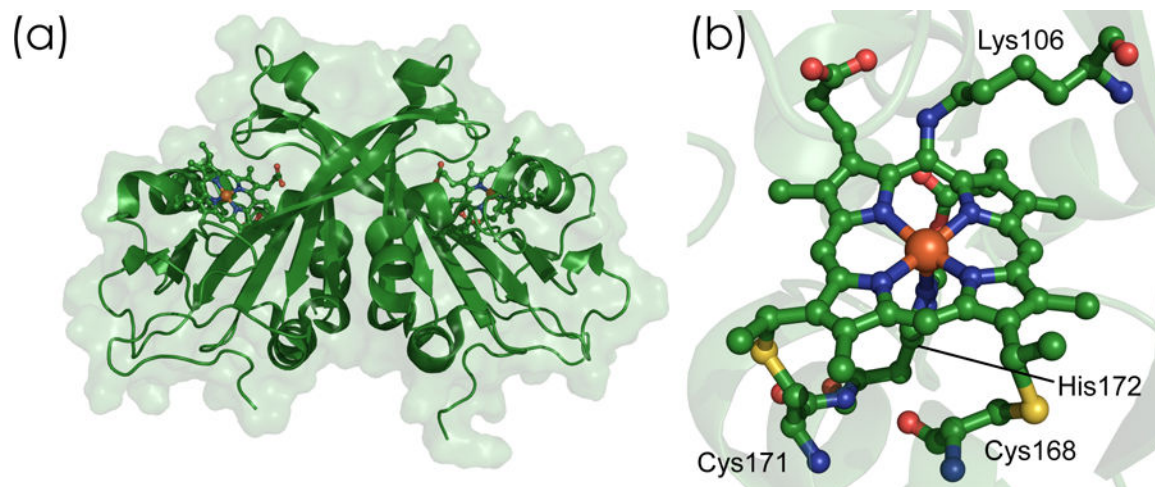


Figure 15.

1.4 Å resolution crystal structure of cyt P460 from the nitrifying bacterium *Nitrosomonas* sp. AL212 (a). The heme P460 cofactor is shown as sticks and is enlarged in (b) with hydrogen atoms omitted for clarity (PDBID: 6AMG). The CXXCH binding residues as well as the cross-linking lysine residue are also shown and labeled.

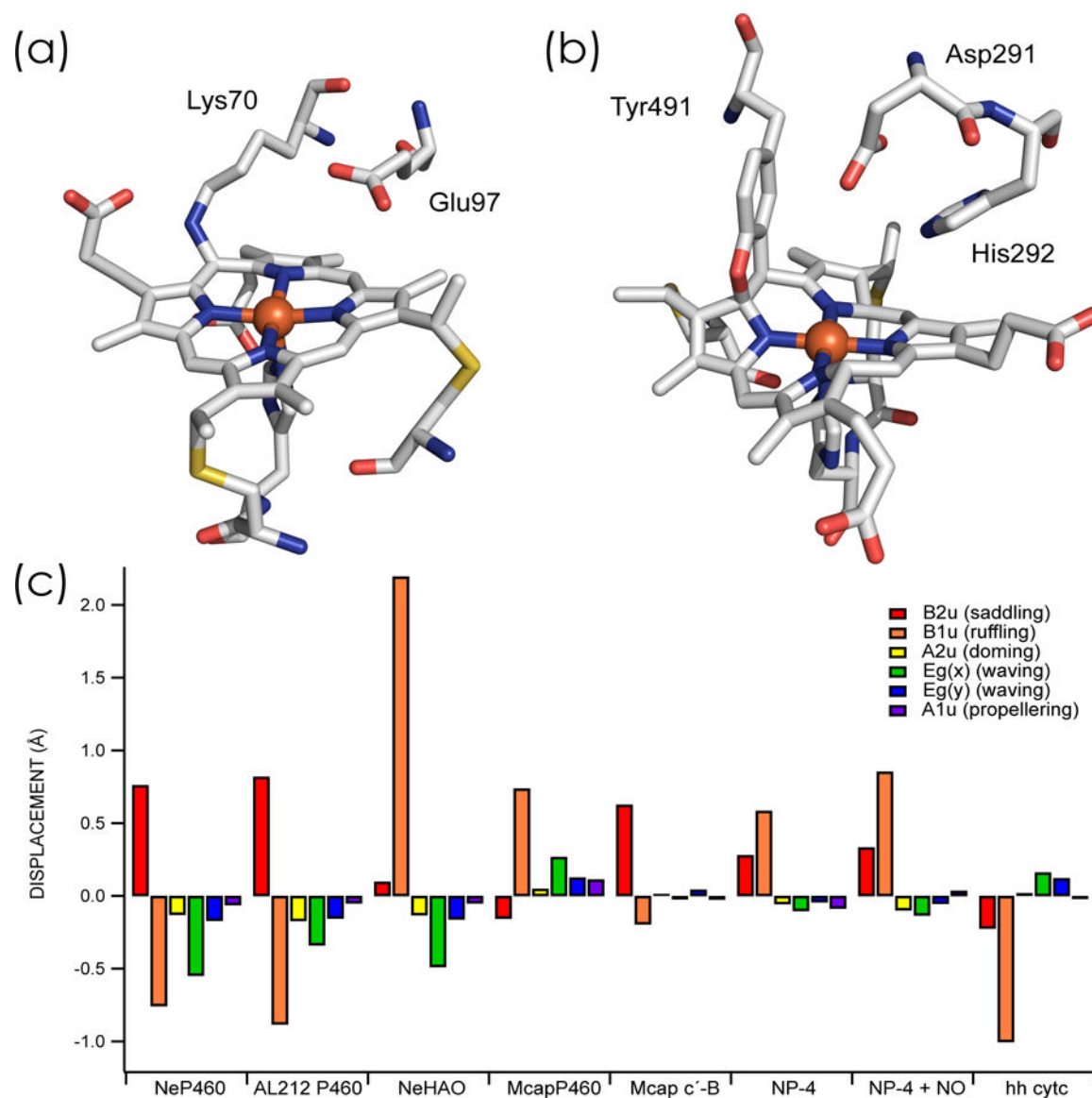


Figure 16.

Comparison of (a) cyt P460 (PDBID: 2JE3) and (b) HAO (PDBID: 4N4N) active sites from the organism *Nitrosomonas europaea*. Residues which have been speculated or proven to be of catalytic importance have also been shown and labeled. The heme planar distortions can be quantified by normal-coordinate structure decomposition calculations,^{200,201} shown here (c) to illustrate the similarities and differences between cyt P460 and related heme proteins (bottom). The heme coordinates were derived from the following proteins: *N. europaea* cyt P460 (NeP460); *N. sp* AL212 cyt P460 (AL212); *N. europaea* HAO (NeHAO); *M. capsulatus* (Bath) cyt P460 (McapP460); *M. capsulatus* (Bath) cyt c'-β (Mcap c'-β); *Rhodnius prolixus* nitrophorin-4 (+NO) (NP-4 (+NO)); horse heart cyt c (hh cyt c).

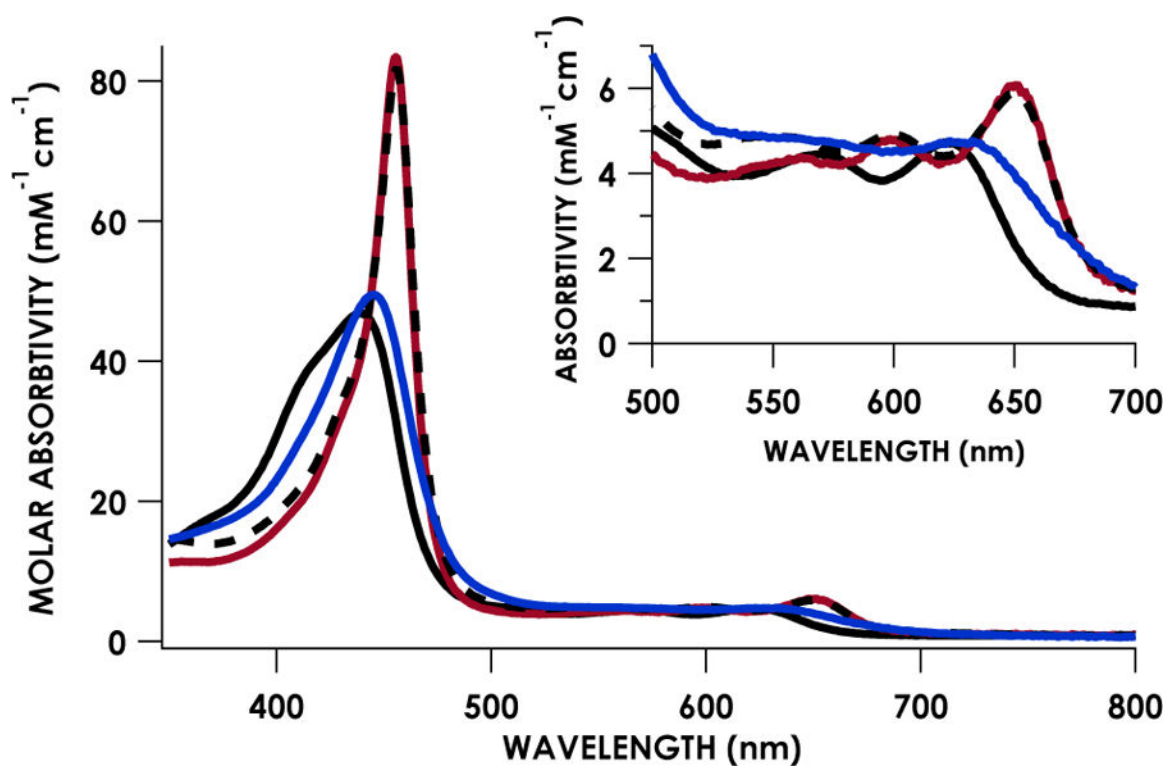


Figure 17.

Optical spectra of catalytic adducts of cyt P460, including Fe^{III}-OH₂ (black), Fe^{III}-NH₂OH (blue), {FeNO}⁶ generated by addition of PROLI-NONOate (red) or by the turnover of NH₂OH in the presence of oxidant (dashed black). Reproduced from Reference 178.

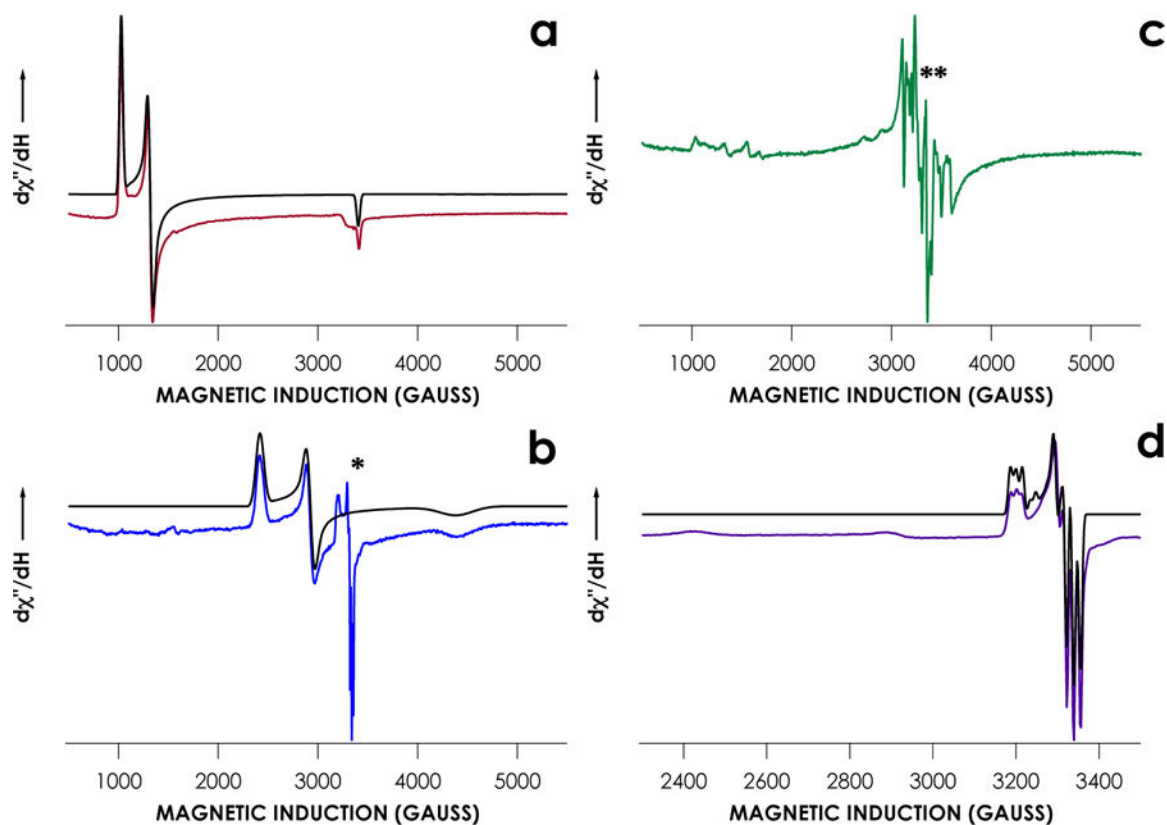


Figure 18.

Representative EPR spectra of catalytically relevant intermediates in cyt P460 NH_2OH oxidation. All spectral fits are in black. The high-spin rhombic signal in (a) represents resting ferric enzyme. (b) is after treating the ferric enzyme with excess NH_2OH . Here the $S = 5/2$ signal is replaced by a low-spin, $S = 1/2$ species. Additionally, the asterisk notes a contamination of the on-path $\{\text{FeNO}\}^7$ species. (c) shows cyt P460 under turnover conditions (excess NH_2OH and oxidant); the double-asterisk notes a Mn^{2+} contamination. (d) is the resulting spectrum after the reaction is allowed to complete after ten minutes and is indicative of a 5-coordinate $\{\text{FeNO}\}^7$ species. Adapted from Reference 178.

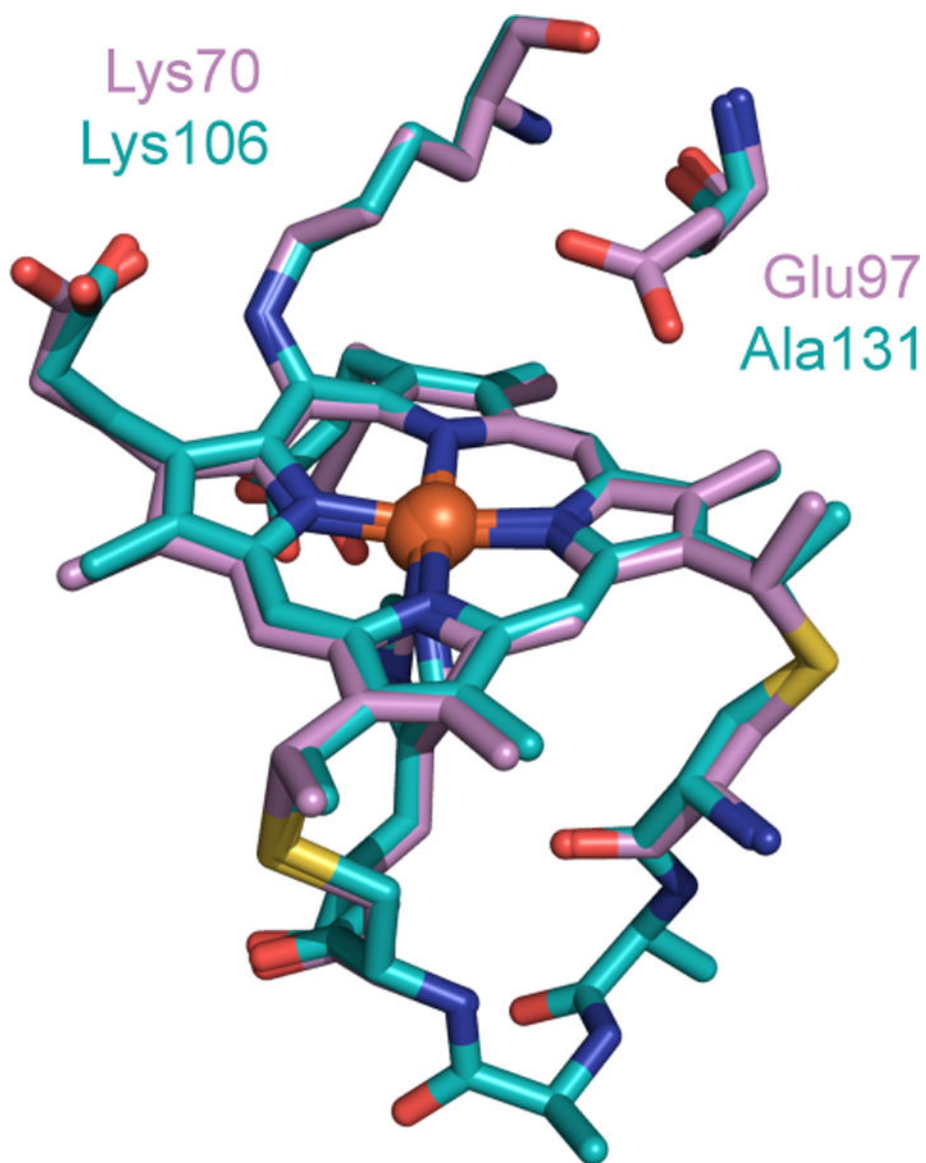
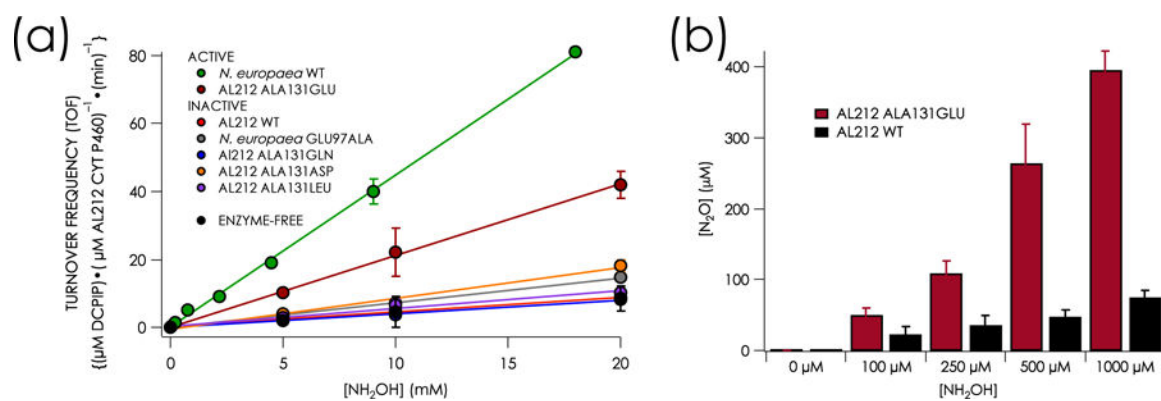


Figure 19.

Overlay of the X-ray crystal structures of cyt P460 from *N. europaea* (PDBID: 2JE3, pink) and *N. sp. Al212* (PDBID: 6AMG, teal). In the former, a distal glutamate (Glu97) is poised to participate in hydrogen-bonding and proton transfer with substrate, while in the AL212 structure this position is occupied by an inactive alanine (Ala131). Adapted from Reference 228.

**Figure 20.**

(a) NH_2OH -oxidase steady-state activity plot of wild-type (WT) *N. europaea* and *Nitrosomonas* sp. AL212 cyt P460 variants. Turnover frequencies, determined by initial rates, represent the average of three trials and were measured by the consumption of the first 10% of oxidant. (b) Plot of N_2O production from AL212 WT cyt P460 as well as the Ala131Glu variant. Adapted from Reference 228.

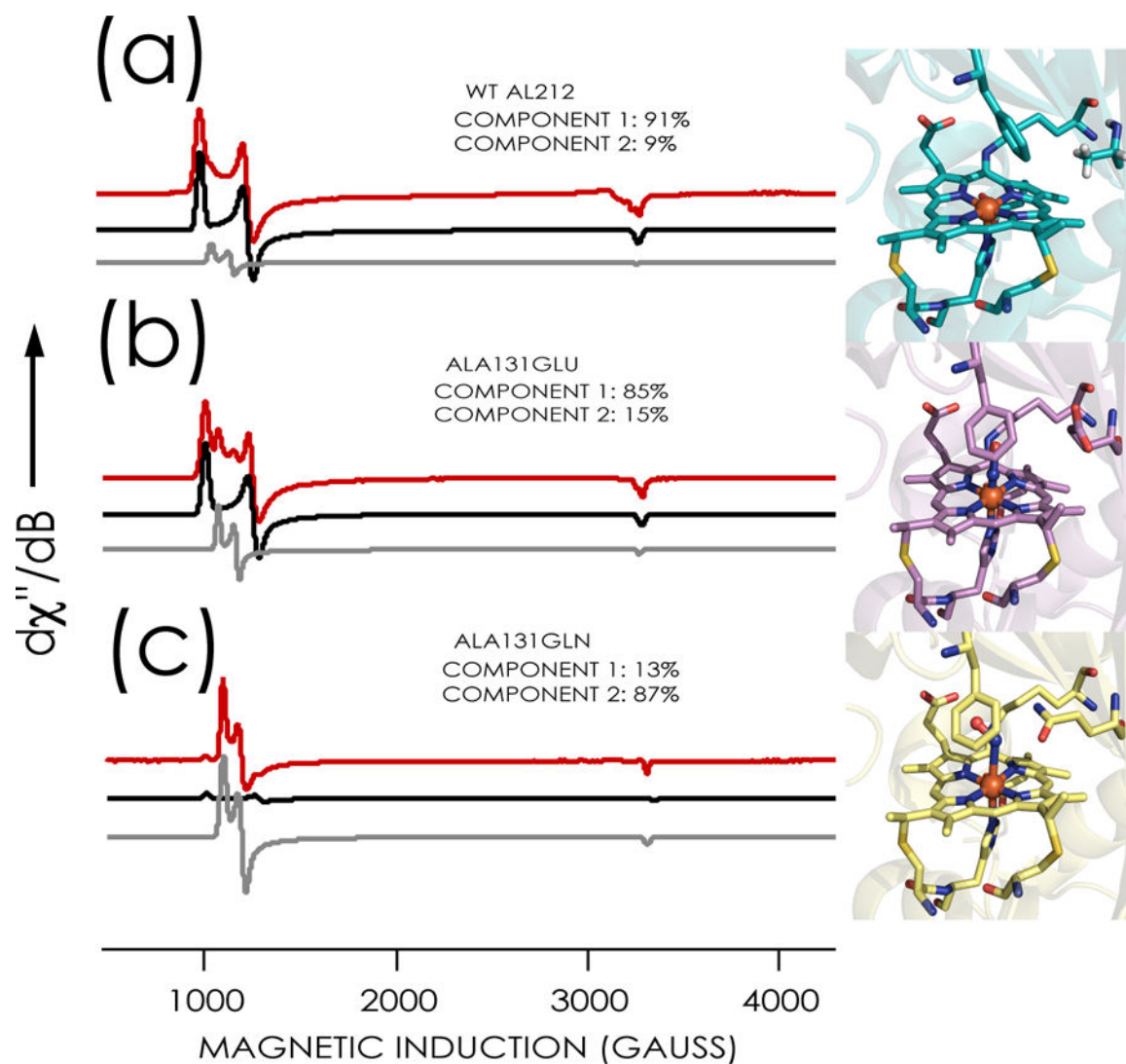


Figure 21.

Representative X-band EPR spectra of *Nitrosomonas* sp. AL212 cyt P460 variants in their resting ferric state (left) and crystal structures of variants with adducts illustrating second sphere dynamics (right). Red lines correspond to experimental data, while the black and gray lines represent fits to those data. (a) WT cyt P460 from *N. sp.* AL212 (PDBID: 6AMG, teal). (b) Ala131Glu variant coordinated with NO (PDBID: 6E17, violet, RMSD = 1.97 Å). Note apparent movement of distal Phe76 upon ligand binding (c) Ala131Gln variant coordinated with NH₂OH (PDBID: 6EOY, yellow, RMSD = 2.26 Å) Here, glutamine is able to participate in hydrogen bonding with the NH₂OH substrate, but notably cannot perform catalysis. Adapted from Reference 228.

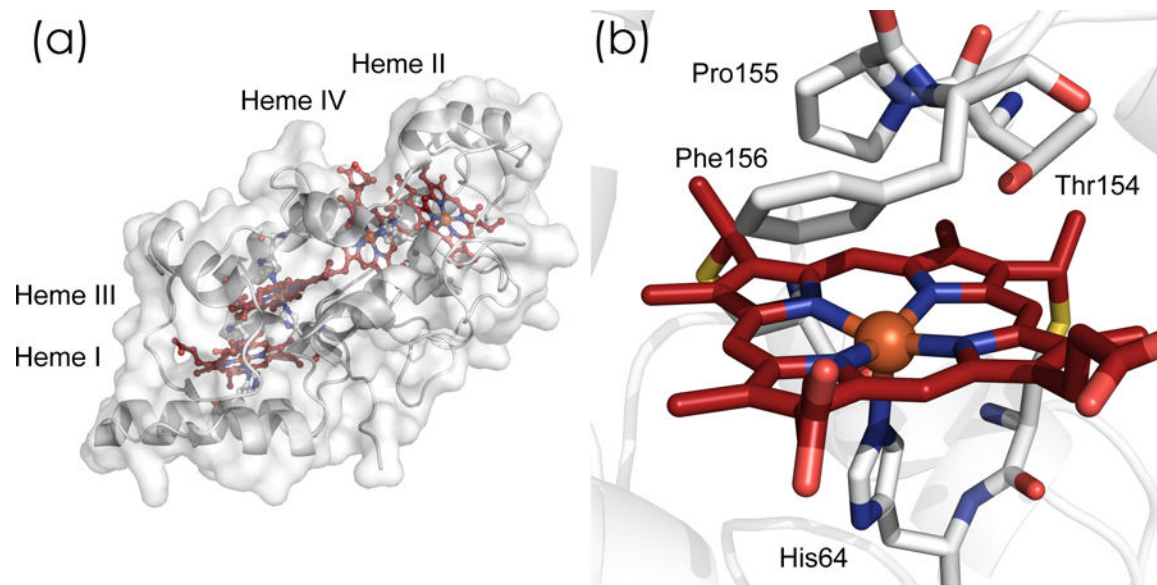


Figure 22.

1.8 Å resolution crystal structure of tetraheme cyt *c*554 from *N. europaea* (PDBID: 1FT6) with labeled *c*-heme cofactors I-IV (a) and an enlargement of the five-coordinate Heme II with distal residues highlighted and labeled, as well as the *c*-heme CXXCH binding motif (b). Hydrogen atoms have been omitted for clarity.

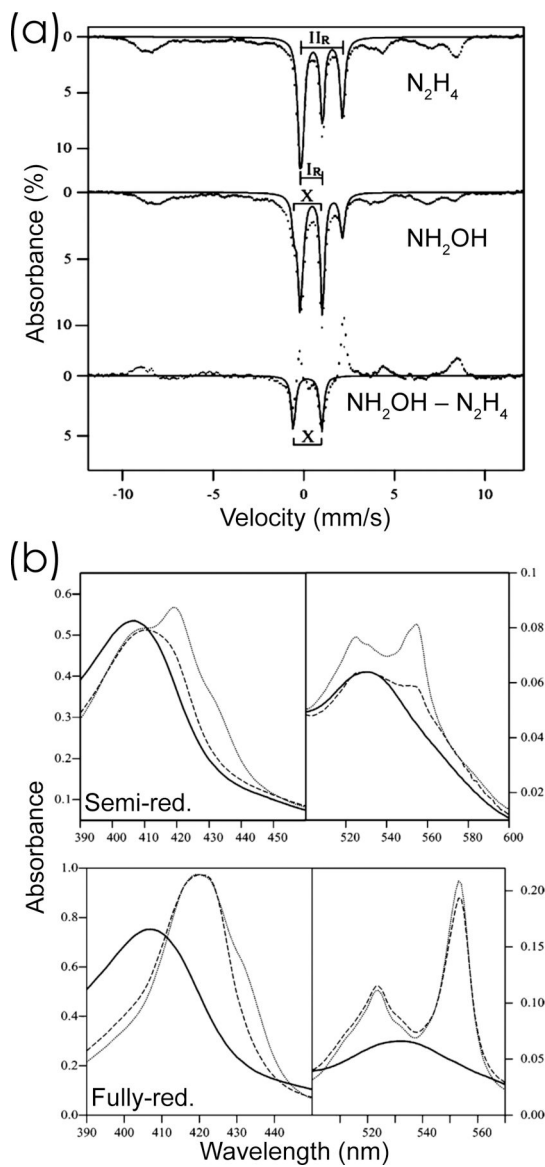


Figure 23.

(a) ^{57}Fe Mössbauer spectra of (top) N_2H_4 /HAO reduced and (middle) NH_2OH /HAO C554 at 4.2 K in the absence of an external magnetic field. “IR and “IIR” indicate the quadrupole doublets of the ferrous low-spin heme I and high-spin heme II, respectively. The bottom spectrum represents the difference spectrum of the top and middle, and “X” is the doublet which is putatively assigned as a $\{FeNO\}^7$. (b) representative changes in the optical spectra of C554. The solid lines represent the ferric state. On top are changes observed for the semi-reduced protein (dotted line) and the semi-reduced protein treated with NO (dashed line). On the bottom are corresponding spectra of the fully-reduced protein (dotted line) and the fully-reduced protein treated with NO (dashed line). Adapted with permission from Reference 247. Copyright 2006, American Chemical Society.

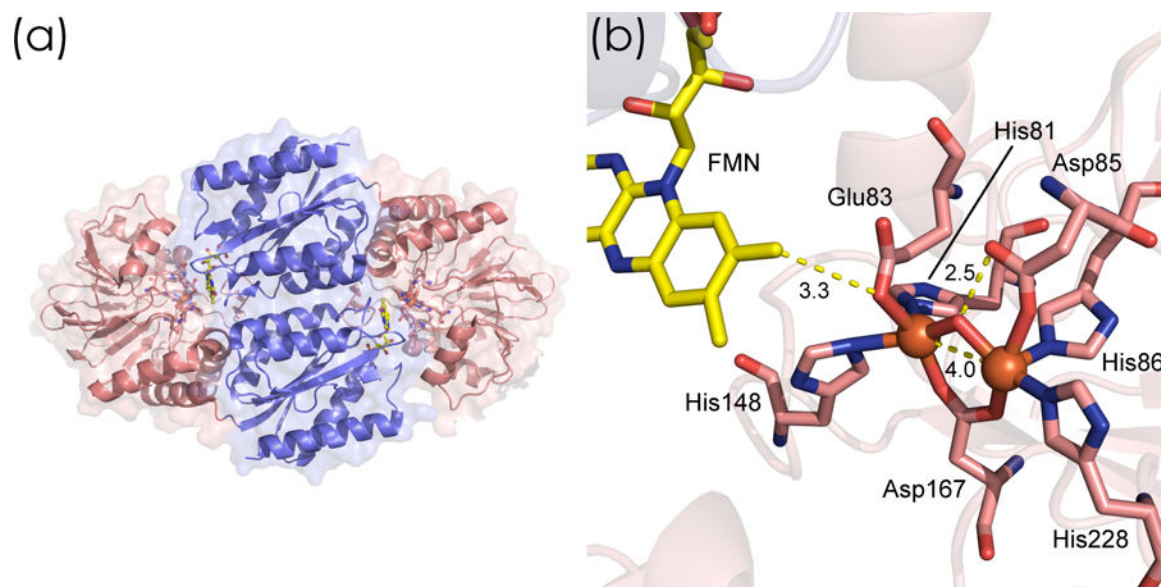


Figure 24.

3.0 Å dimeric crystal structure of the FDP from *Moorella thermoacetica* (PDBID: 1YCF) (a) The flavodoxin domain is shown in pink and the metallo-β-lactamase domain is shown in violet. The subunits are arranged in a “head-to-tail” fashion such that the FMN cofactor (yellow) of one subunit is facing the diiron site of the other subunit. An enlargement of one of these active sites is shown (b) with labeled coordinating residues. Hydrogen atoms are omitted for clarity, and relevant distance measurements are shown in Å as needed.

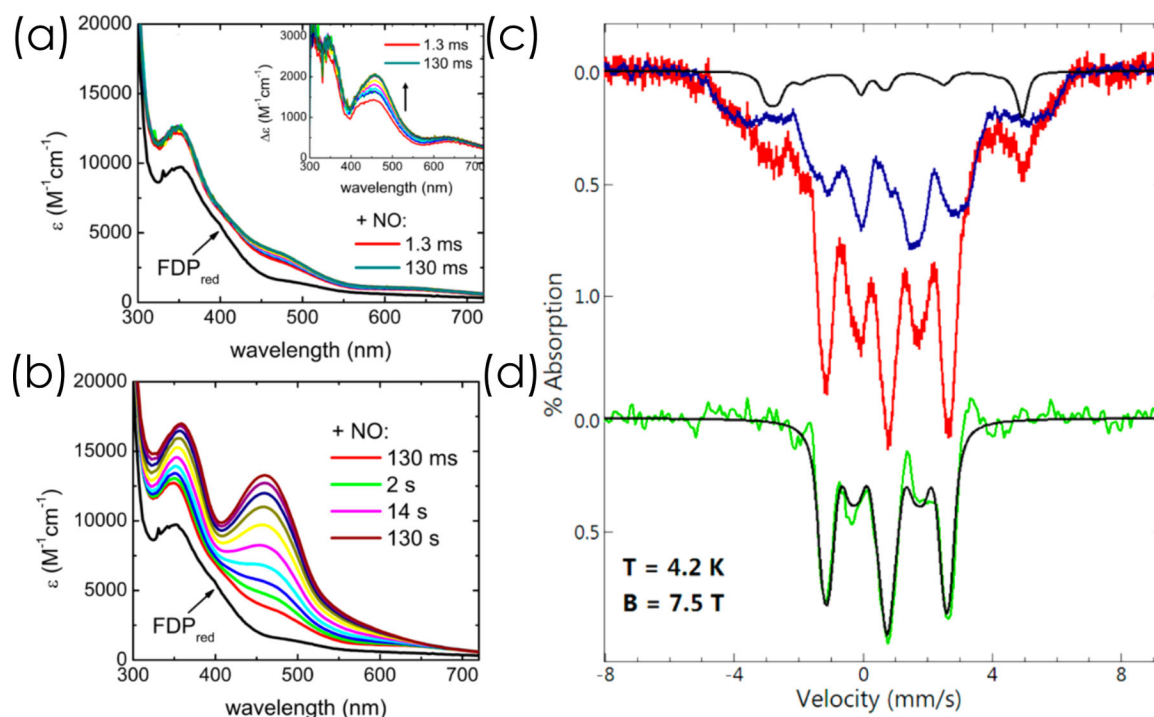


Figure 25.

130 ms (a) and 130 s (b) stopped-flow kinetic optical absorption spectra of fully reduced FDP reacting in the presence of excess NO at 3°C. The inset represents the difference spectra by subtracting out the fully reduced FDP spectra, showing growth of a feature centered at ca. 418 nm, assigned as the $\{FeNO\}^7$. The observed stoichiometry of $\{FeNO\}^7$ under excess NO is much greater than expected for the formation of just $Fe^{2+}\{FeNO\}^7$, which is attributed to the successive formation of $[\{FeNO\}^7]_2$. Also shown are the ^{57}Fe Mössbauer spectra (right panel) at 4 K in the presence of an applied 7.5 T magnetic field of various FDP catalytic intermediates. The red spectrum in (c) shows the rapid freeze quench product between reduced FDP and ca. 3 eq. NO per active site after 200 ms. The blue spectrum in (c) corresponds to the reduced FDP titrated with 2 eq. NO. The black trace in (c) represents a fit to the last species identified by simulation, which is attributed to an $\{FeNO\}^7$ contaminant. In (d), the green trace represents the difference spectrum (red – blue - black), and is best fit by a diamagnetic, $S = 0$ species of exchange-paired $S = 3/2$ $\{FeNO\}^7$ centers. Adapted with permission from Reference 286. Copyright 2014 American Chemical Society.

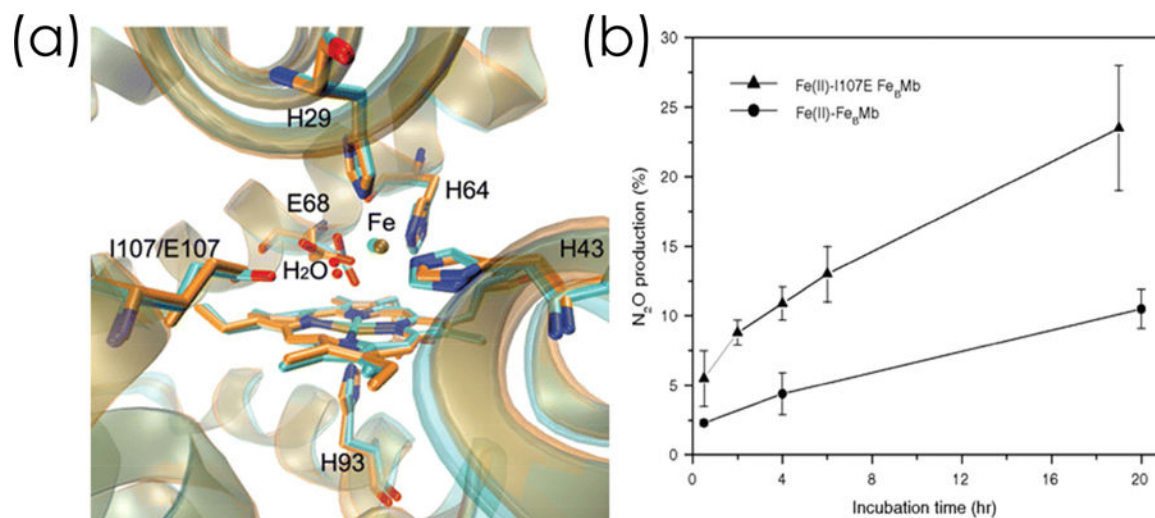
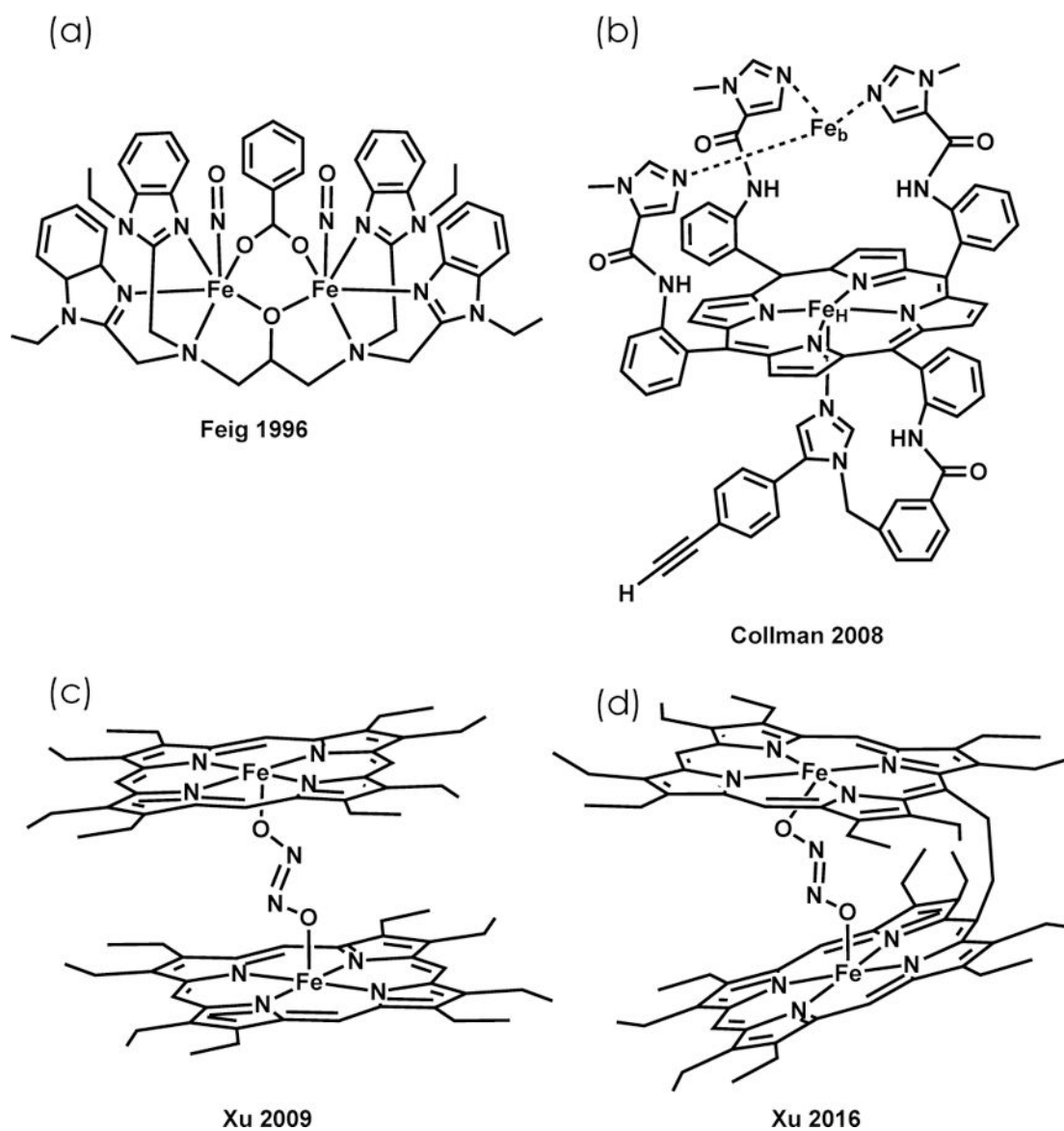
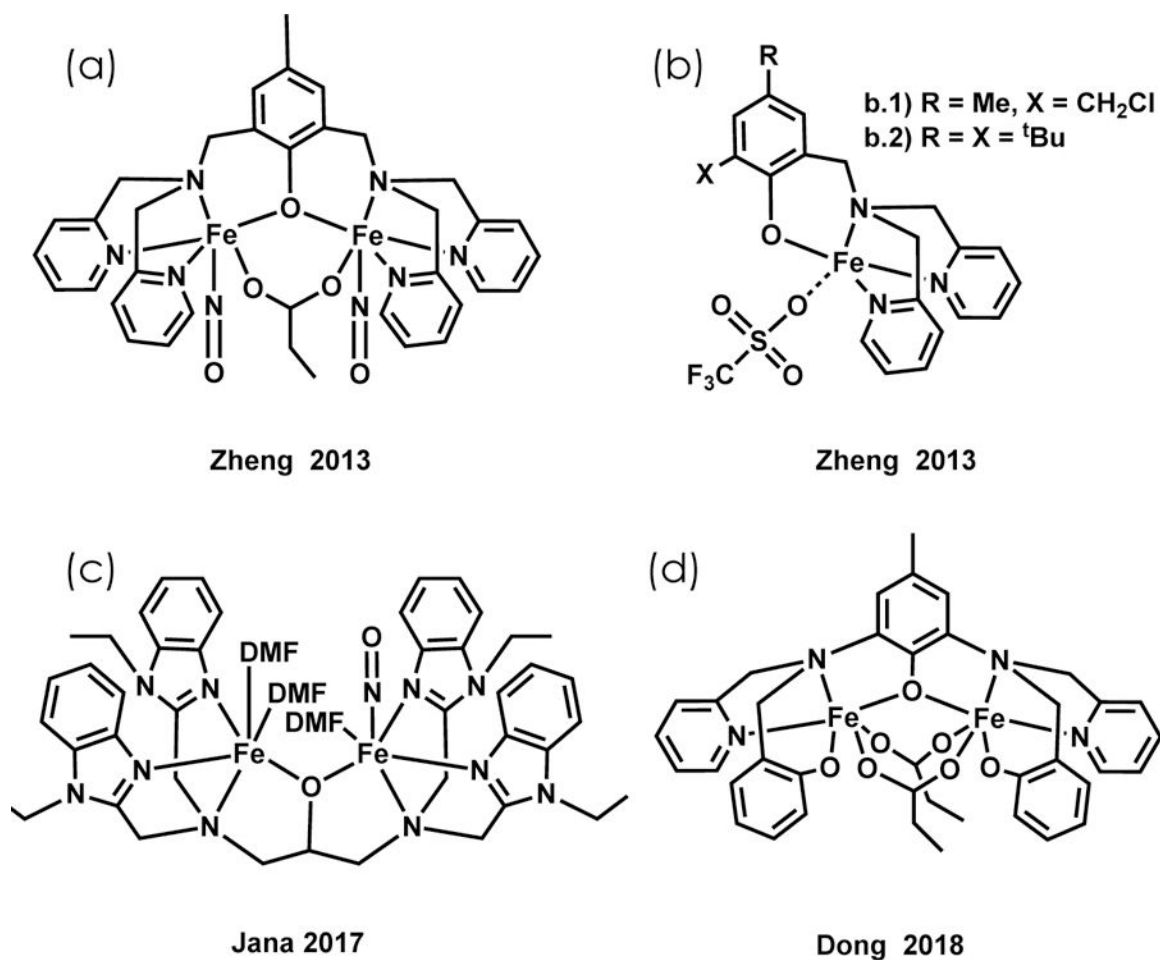


Figure 26.

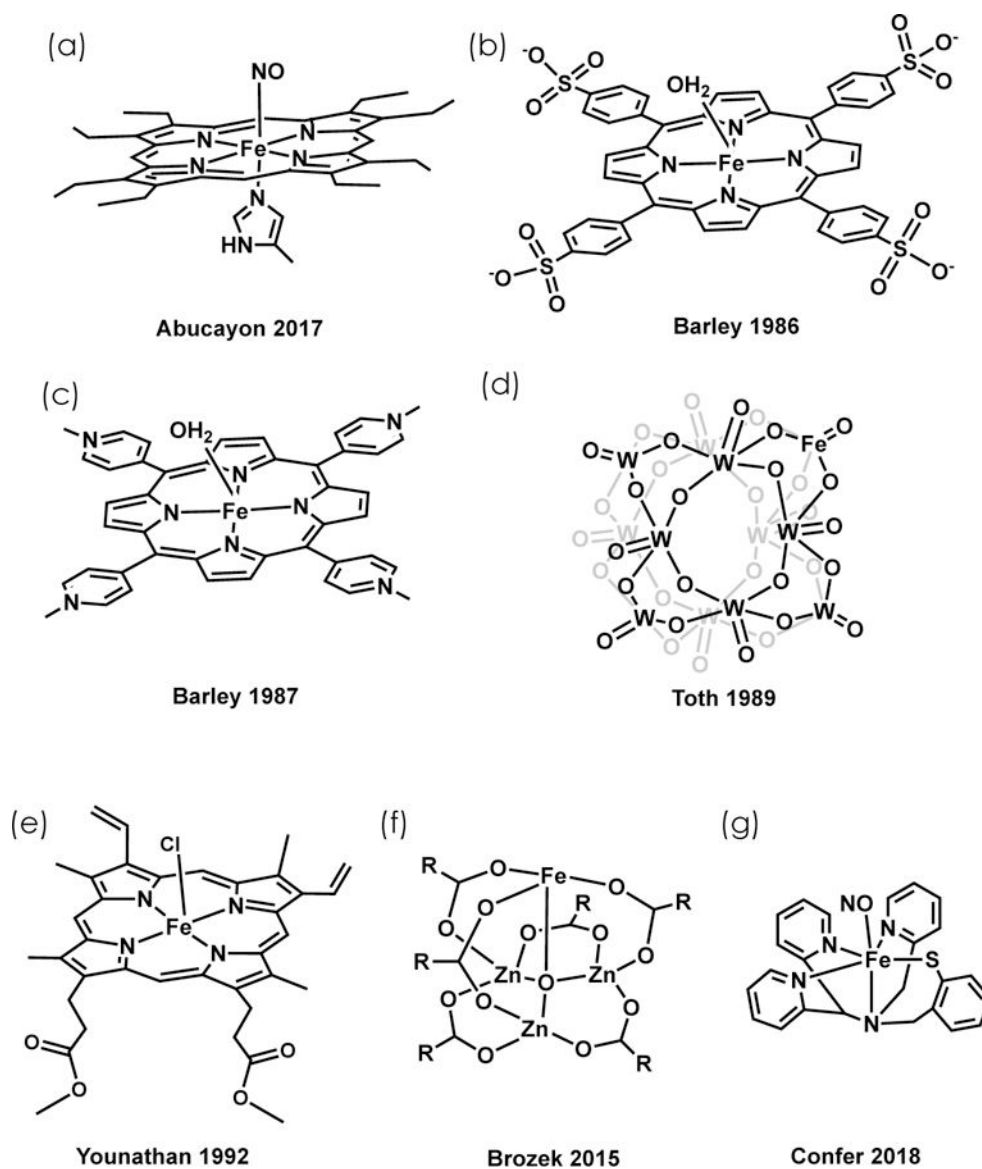
(a) Structural overlay of Fe^{II}-Ile107Glu FeBMb (cyan, PDBID: 3M39) with Fe^{II}-FeBMb (orange, PDBID: 3K9Z). (b) N₂O production efficacy is enhanced by introduction of the Ile107Glu mutation, which presumably is due to its serving as a proton relay for either protonation of nascent N₂O₂²⁻. Adapted with permission from 299. Copyright John Wiley and Sons.

**Figure 27.**

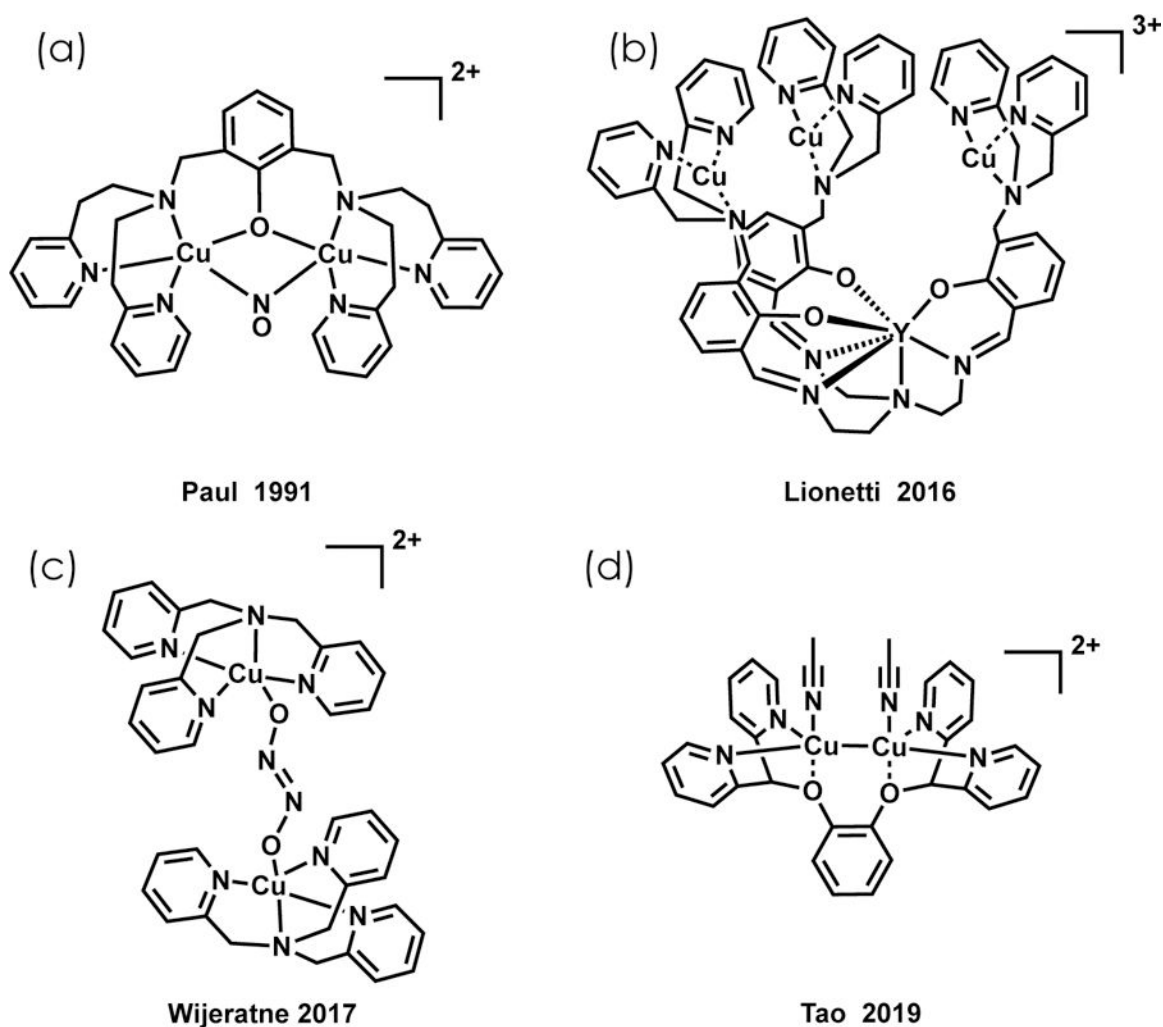
(a) $[\text{Fe}_2(\text{Et-HPTB})(\text{O}_2\text{CPh})](\text{BF}_4)$ (Et-HPTB = *N,N,N',N'*-tetrakis-(*N*-ethyl-2-benzimidazolylmethyl)-2-hydroxy-1,3-diaminopropane),³⁰¹ (b) $\text{LFe}^{\text{II}}\text{H}/\text{Fe}^{\text{II}}\text{B}$,³⁰⁵ (c) $[(\text{OEP})\text{Fe}]_2(\mu\text{-N}_2\text{O}_2)$,³⁰⁶ (d) $(\text{OEP-CH}_2)\text{Fe}]_2(\eta_1, \eta_1\text{-ONNO})$ (OEP = octaethylporphyrin).³⁰⁷

**Figure 28.**

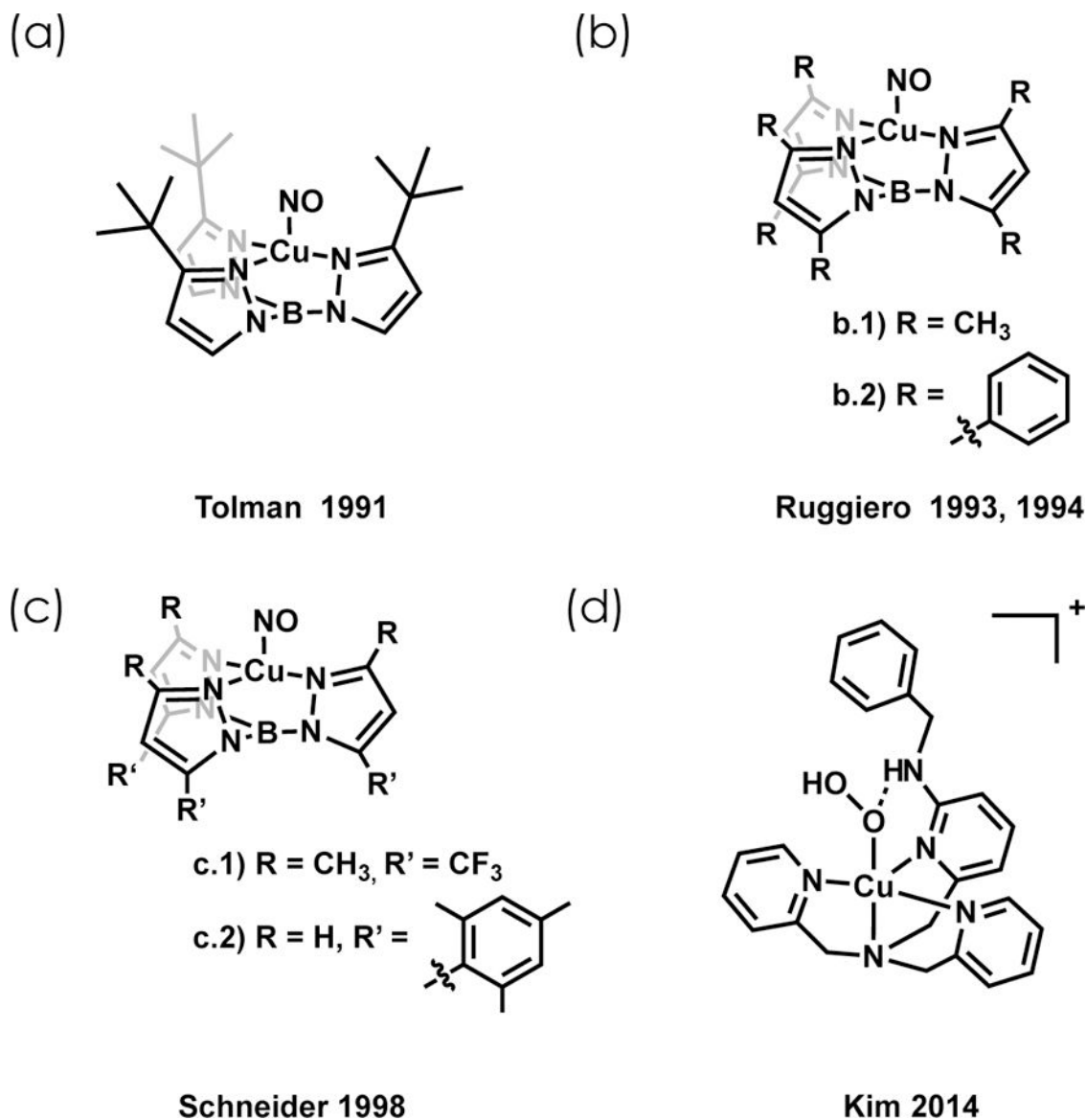
(a) $[\text{Fe}_2(\text{BPMP})(\text{OPr})(\text{NO})_2](\text{BPh}_4)_2$ (BPMP = 2,6-*bis*[*bis*(2-pyridylmethyl)amino)methyl]-4-methylphenol),³⁰⁸ (b) $[\text{Fe}(\text{BMPA-PhO}^{\text{X,R}})(\text{NO})](\text{OTf})$ (BMPA-PhO = *N*-(2-methyl-(2-chloromethyl-6-methylphenolate))-*N,N*-*bis*-(2-pyridylmethyl)amine),³⁰⁸ (c) $[\text{Fe}_2(\text{N-Et-HPTB})(\text{NO})(\text{DMF})_3](\text{BF}_4)_3$ (Et-HPTB = *N,N,N',N'*-*tetrakis*-(*N*-ethyl-2-benzimidazolylmethyl)-2-hydroxy-1,3-diaminopropane),²⁸⁹ (d) $[\text{Fe}_2(\text{Py}_2\text{PhO}_2)\text{MP}(\text{OPr})_2](\text{OTf})$.³¹²

**Figure 29.**

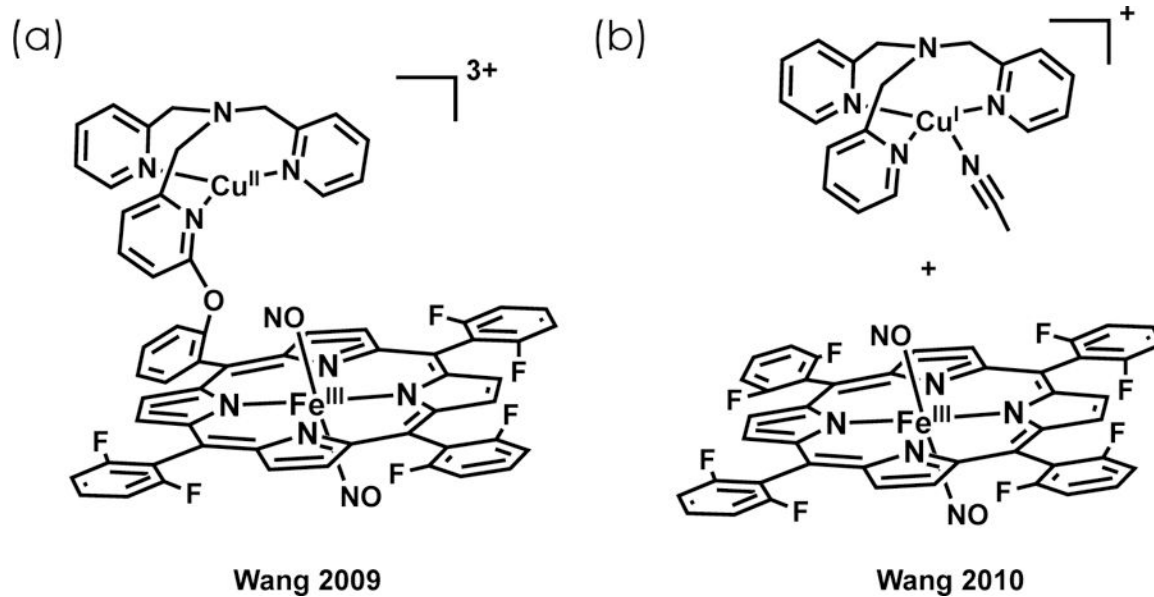
(a) $[(\text{OEP})\text{Fe}-(\text{NO})(5\text{-methylimidazole})]\text{OTf}$ (OEP = octaethylporphyrin),¹⁶¹ (b) $[\text{Fe}(\text{H}_2\text{O})(\text{TPPS})]^{3+}$ (TPPS = *meso-tetrakis(p-sulfonatophenyl)porphine*),³¹⁵ (c) $[\text{Fe}(\text{H}_2\text{O})(\text{TMPyP})]^{5+}$ (TMPyP = *meso-tetrakis(N-methyl-4-pyridyl)porphine*),³¹⁶ (d) Fe-substituted polytungstate,³¹⁷ (e) $\text{Fe}(\text{PP})\text{Cl}$ (PP = protoporphyrin),³¹⁸ (f) Fe^{II} -MOF (MOF = metal-organic framework),³¹⁹ (g) $[\text{Fe}(\text{NO})(\text{N3PyS})]$ (N3PyS = 2-[[di-2-pyridinylmethyl](2-pyridinylmethyl)amino]methyl]benzenethiol).³²⁰

**Figure 30.**

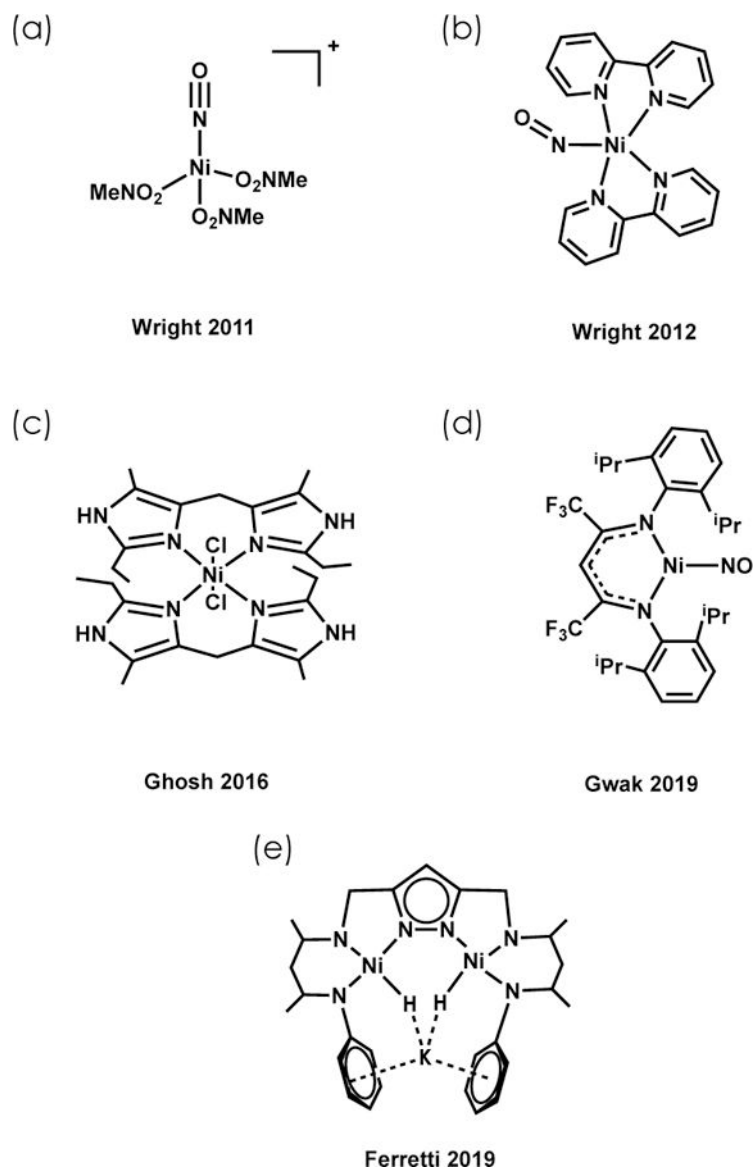
(a) $\text{Cu}_2(\text{XYL-O}^-)(\text{NO})](\text{PF}_6)_2$ (XYL = 2,6-bis[(bis(2-pyridylethyl)amino)methyl]-phenol),³²⁶ (b) $\text{LYCu}_3(\text{OTf})_3$,³²⁷ (c) $\{\text{Cu}^{\text{II}}(\text{tmpa})\}_2(\mu\text{-N}_2\text{O}_2^{2-})](\text{B}(\text{C}_6\text{F}_5)_4)_2$ (tmpa = tris(2-pyridylmethyl)amine),³²⁸ (d) $[\text{Cu}_2(\text{Py}_4\text{DMB})(\text{MeCN})_2](\text{B}(\text{C}_6\text{F}_5)_4)_2$ (Py_4DMB = 1,2-bis(di(pyridine-2-yl)methoxy)benzene).³²⁹

**Figure 31.**

(a) [HB(*t*-Bupz)₃CuNO] (*t*-Bupz = 3-*tert*-butylpyrazole),³³⁰ (b) Tp^{CH₃,CH₃}Cu(NO) (Tp^{CH₃,CH₃} = *tris*(3,5-dimethyl)-pyrazol-1-yl)hydroborate and Tp^{Ph,Ph}Cu(NO) (Tp^{Ph,Ph} = *tris*(3,5-diphenyl)-pyrazol-1-yl)hydroborate,^{332,333} (c) Tp^{CF₃,CH₃}Cu(CH₃CN) (Tp^{CF₃,CH₃} = *tris*(3-(trifluoromethyl)-5-methylpyrazol-1-yl)hydroborate and Tp^{Ms,H}Cu(THF) (Tp^{Ms,H} = *tris*(3-mesitylpyrazol-1-yl)hydroborate,³³⁴ (d) [(BA)Cu^{II}(OOH)](ClO₄) (BA = *tris*-2-pyridylmethylamine with one pyridine decorated with-N(H)CH₂C₆H₅).³³⁷

**Figure 32.**

(a) A binuclear heme/Cu assembly formed after reaction of $({}^6\text{L})\text{Fe}(\text{NO})_2$ with Cu $[\text{Cu}^{\text{I}}(\text{MeCN})_4]\text{B}(\text{C}_6\text{F}_5)_4$ and acid,³⁴² (b) a discrete heme $((\text{F}_8)\text{Fe}(\text{NO}))$ and Cu $[(\text{tmpa})\text{Cu}^{\text{I}}(\text{MeCN})]$ system employed for N_2O production.³⁴³

**Figure 33.**

(a) $[\text{Ni}(\text{NO})(\text{CH}_3\text{NO}_2)_3](\text{PF}_6)$,³⁴⁵ (b) $[\text{Ni}(\text{NO})(\text{bpy})_2](\text{PF}_6)$ (bpy = 2,2′-bipyridine),³⁴⁶ (c) L_2NiCl_2 (L = *bis*(2-ethyl-4-methylimidazol-5-yl)methane),³⁴⁸ (d) $(\text{iPr}_2\text{NNF}_6)\text{Ni}(\text{NO})$ (iPr_2NNF_6 = 1,1,1,5,5,5-Hexafluoro-2-(2,6-diisopropyl)phenylamino-4-(2,6-diisopropyl)phenyliminopent-2-ene,¹⁹ (e) $[\text{KL}(\text{Ni}-\text{H})_2]$.³⁴⁹

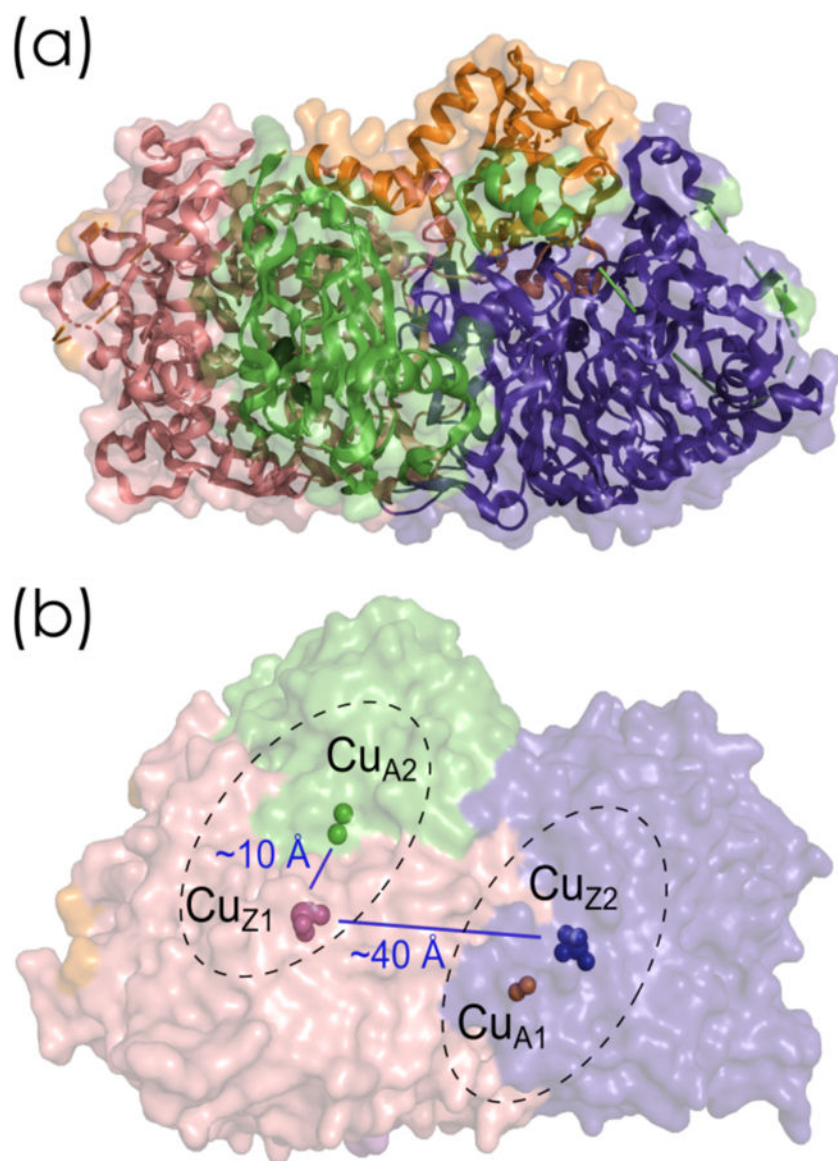


Figure 34.

Structure of the homodimeric N_2OR from *P. denitrificans* (PdN₂OR). (a) surface representation with overlaid cartoon. Pink and blue correspond to the seven-bladed β -propeller domains, while orange and green to the cupredoxin-like domains. Pink and orange domains belong to the same subunit and so is the case for blue and green. All Cu centers are shown as black spheres. (b) surface representation of the dimeric protein with the Cu centers shown as spheres colored as their corresponding domains. Cu_{A1} and Cu_{Z1} belong to subunit 1 and Cu_{A2} and Cu_{Z2} to subunit 2. PDBID: 1FWX.

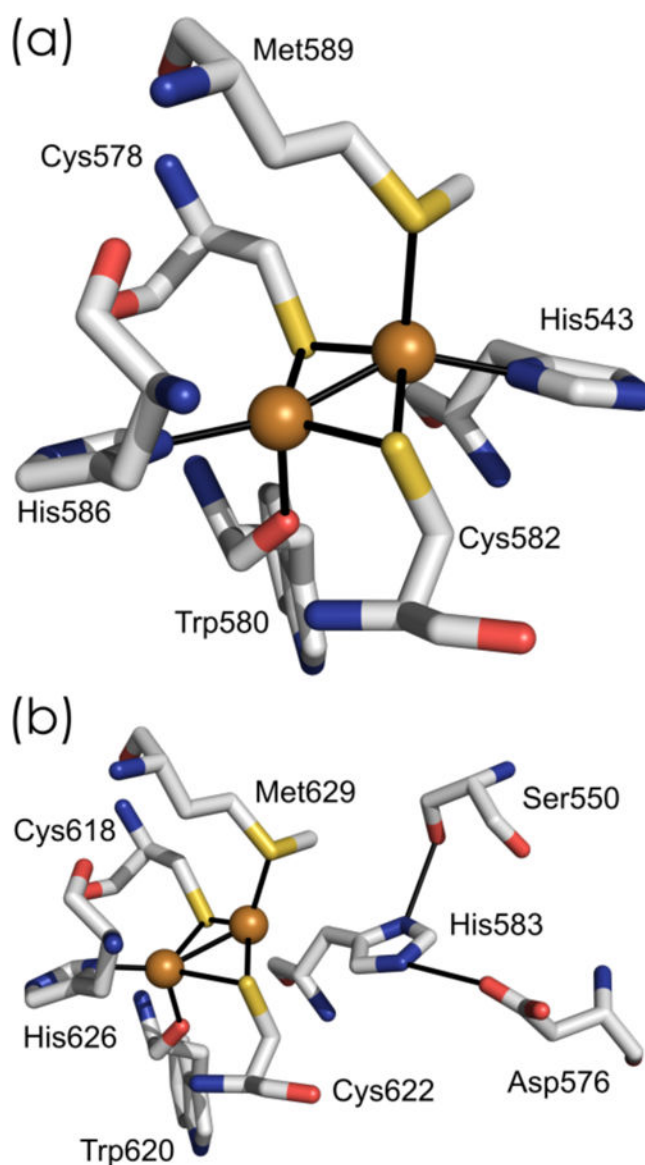


Figure 35.

Cu_A binuclear center from two different N_2OR homologs. (a) Cu_A in *Achromobacter cycloclastes* N_2OR (AcN_2OR). Two fully conserved cysteine residues are the bridging ligands of the two Cu ions that lie about 2.5 Å apart. Each Cu is additionally ligated by a fully conserved histidine, while Cu_{A1} is also bound to Met589 and Cu_{A2} to the backbone carbonyl oxygen of Trp580. PDBID: 2IWF. (b) Cu_A in *P. stutzeri* N_2OR (PsN_2OR). The PsN_2OR structure revealed a slightly different conformation for the Cu_{A1} -ligating His583 that is rotated away from the Cu center and is connected to the neighboring Ser550 and Asp576 via hydrogen-bonding, resulting in a more planar arrangement of Cu_A with respect to the sulfur atoms of the bridging cysteines and Met629. PDBID: 3SBP. Cu atoms are shown as bronze spheres.

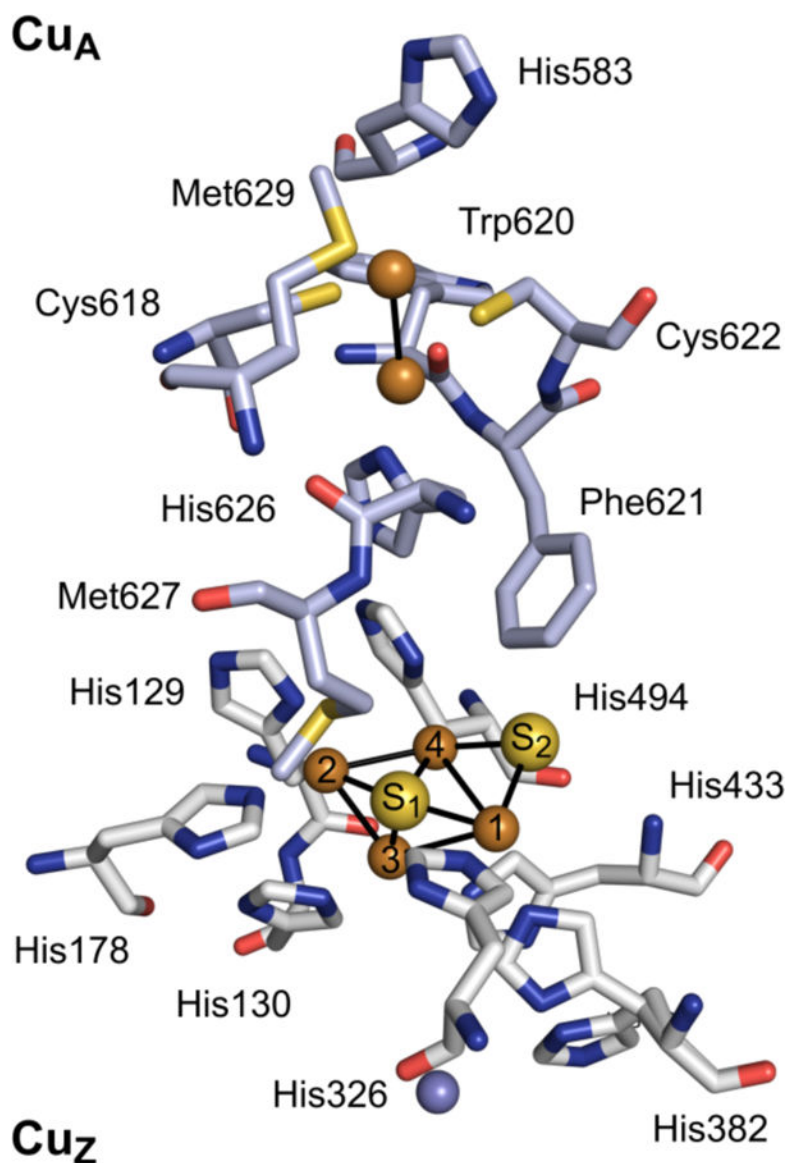


Figure 36.

Catalytic site of PsN₂OR, composed of a Cu_A and a Cu_Z metal center of the different monomers within the dimeric enzyme. The binuclear Cu_A site is shown on top as bronze spheres. The four Cu atoms of Cu_Z (numbered bronze spheres) are coordinated by seven fully conserved histidine residues, a μ₄-sulfido ligand (S₁; yellow sphere), and a μ₂-sulfido (S₂; yellow sphere) bound to Cu_{Z1} and Cu_{Z4}. The ligating histidines participate in an elaborate hydrogen bond network that involves neighboring residues, solvent molecules, and a protein-bound chloride ion (slate sphere). Amino acid residues of different monomers are shown as slate and gray sticks, respectively. PDBID: 3SBP.

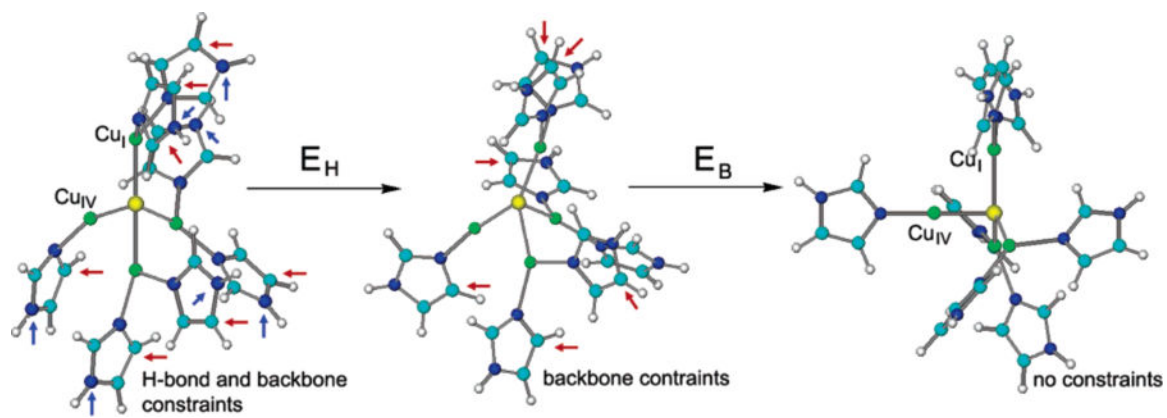


Figure 37.

Rearrangement of the $[\text{Cu}_4\text{S}(\text{im})_7]^{2+/3+}$ complexes upon removal of the protein-imposed constraints. The noncovalent (hydrogen-bond) and covalent (backbone) constraints are indicated by blue and red arrows, respectively. Reprinted with permission from Reference 371. Copyright 2006 American Chemical Society.

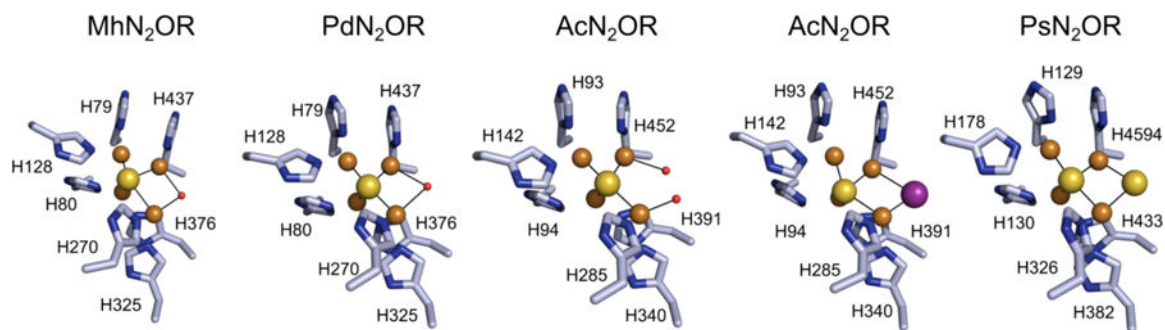


Figure 38.

Stick representation of the Cu_2 sites in five available crystal structures. From left to right: *M. hydrocarbonoclasticus* (MhN_2OR), PDBID: 1QNI; PdN_2OR , PDBID: 1FWX; *A. cycloclastes* (AcN_2OR), PDBID: 2IWF; iodide-bound AcN_2OR , PDBID: 2IWK; *P. stutzeri* (PsN_2OR), PDBID: 3SBP. Water molecules are colored red, Cu bronze, sulfur yellow, and iodide purple. Adapted from Reference 375.

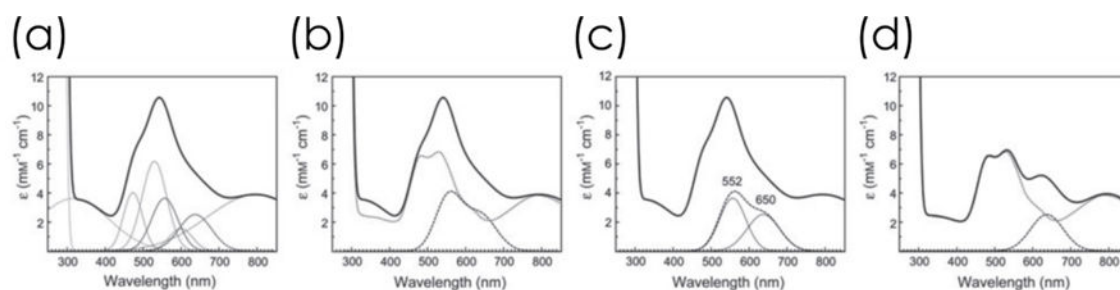


Figure 39.

UV/vis absorption spectra of PsN₂OR. (a) The spectrum of the purple protein as isolated (bold line) can be deconvoluted into individual peaks that can be assigned to either the Cu_A site (dotted) or Cu_Z (dashed). (b) Summation of the bands for each center yield subspectra that very closely match experimental spectra for the individual sites Cu_A (dotted) and Cu_Z (dashed). (c) The spectral features of Cu_Z can be fully explained by two transitions at 552 and 650 nm, with a position and intensity typical for ligand-to-metal charge-transfers in Cu proteins. (d) If the band at 552 nm is lost upon depletion of S₂₂, the remaining band at 640 nm adds up with the signature of Cu_A to yield a typical form II spectrum of N₂OR.

Reprinted with permission from Reference 375. Copyright Walter de Gruyter and Company.

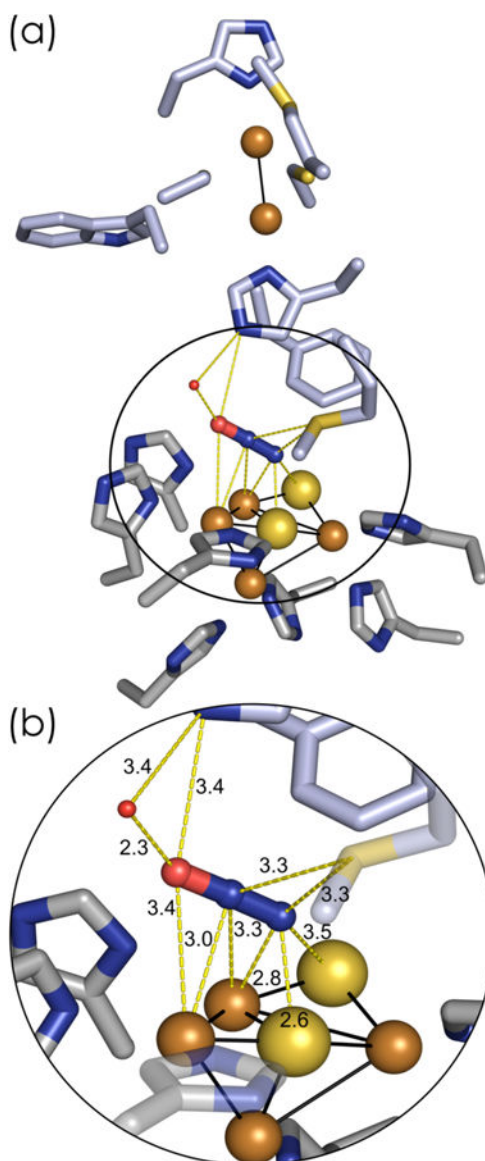


Figure 40.

(a) Stick representation of the N_2O -associated PsN_2OR catalytic site, composed of a CuA and a CuZ metal center of the different monomers within the dimeric enzyme. Crystals of PsN_2OR were pressurized with N_2O gas and an additional structure was obtained, where an N_2O molecule was found within the active site pocket of the enzyme. (b) Close-up of the substrate binding pocket. The binuclear CuA and the tetranuclear CuZ centers are shown as bronze spheres. Amino acid residues of different monomers are shown as slate and gray sticks, respectively. Distances around the N_2O ligand are in Å. PDBID: 3SBR.

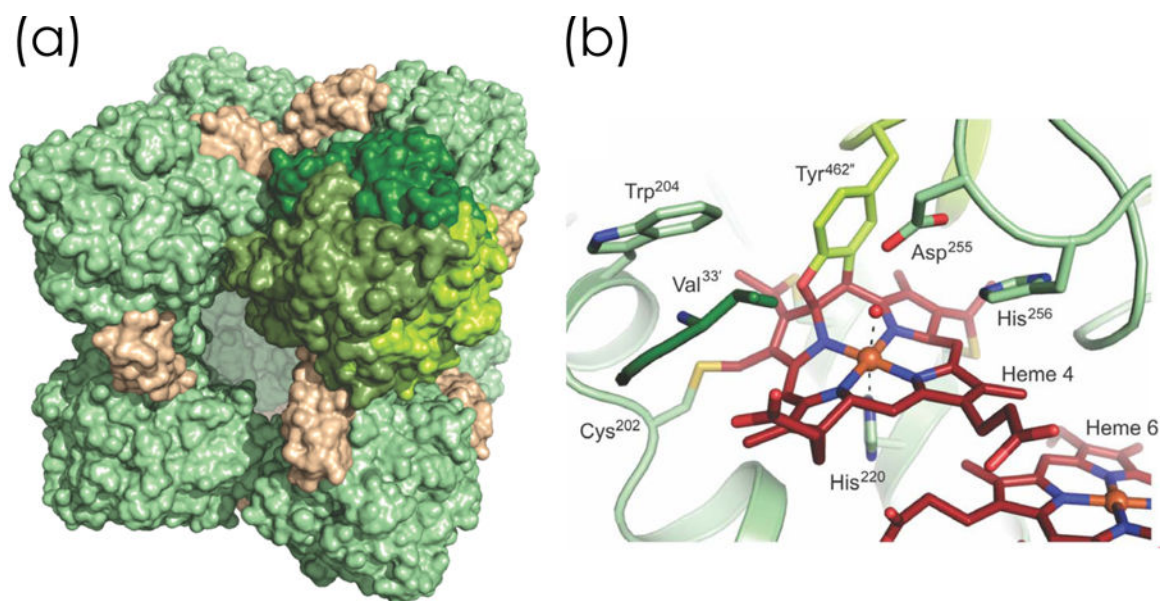
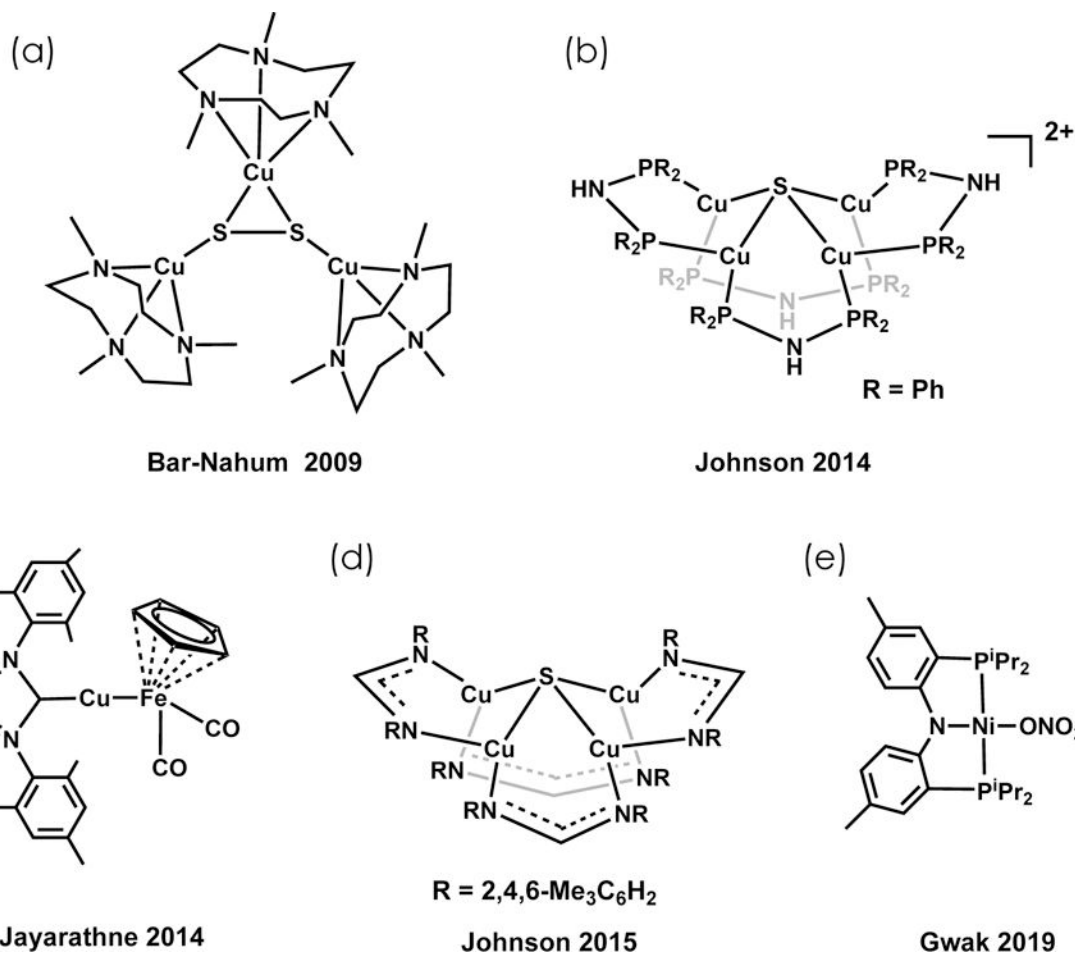


Figure 41.

(a) Quaternary structure of the *Kuenenia stuttgartiensis* HDH determined via cryoelectron microscopy. The α subunits are green, with individual components of one of the 8 homotrimers shown in different shades of green. The β subunits are tan. (b) X-ray crystal structure of one of the putative N_2H_4 -oxidizing P460-like heme cofactors. Adapted from Reference 423.

**Figure 42.**

(a) [(LCu)₃S₂] (L = 1,4,7-trimethyltriazacyclononane),⁴¹¹ (b) [(μ₂-dppa)₄Cu₄(μ₄-S)](PF₆)₂ (dppa = bis(diphenylphosphino)-amine),⁴²⁵ (c) (IMes)CuFp, (IMes = *N,N'*-bis(2,4,6-trimethylphenyl)imidazol-2-ylidene; Fp = Fe(cyclopentadienyl)(CO)₂),⁴²⁶ (d) Cu₄(μ⁴-S),⁴³¹ (e) (PNP)Ni(ONO₂) (PNP = (N[2-PiPr₂-4-Me-C₆H₃]₂)¹⁹).

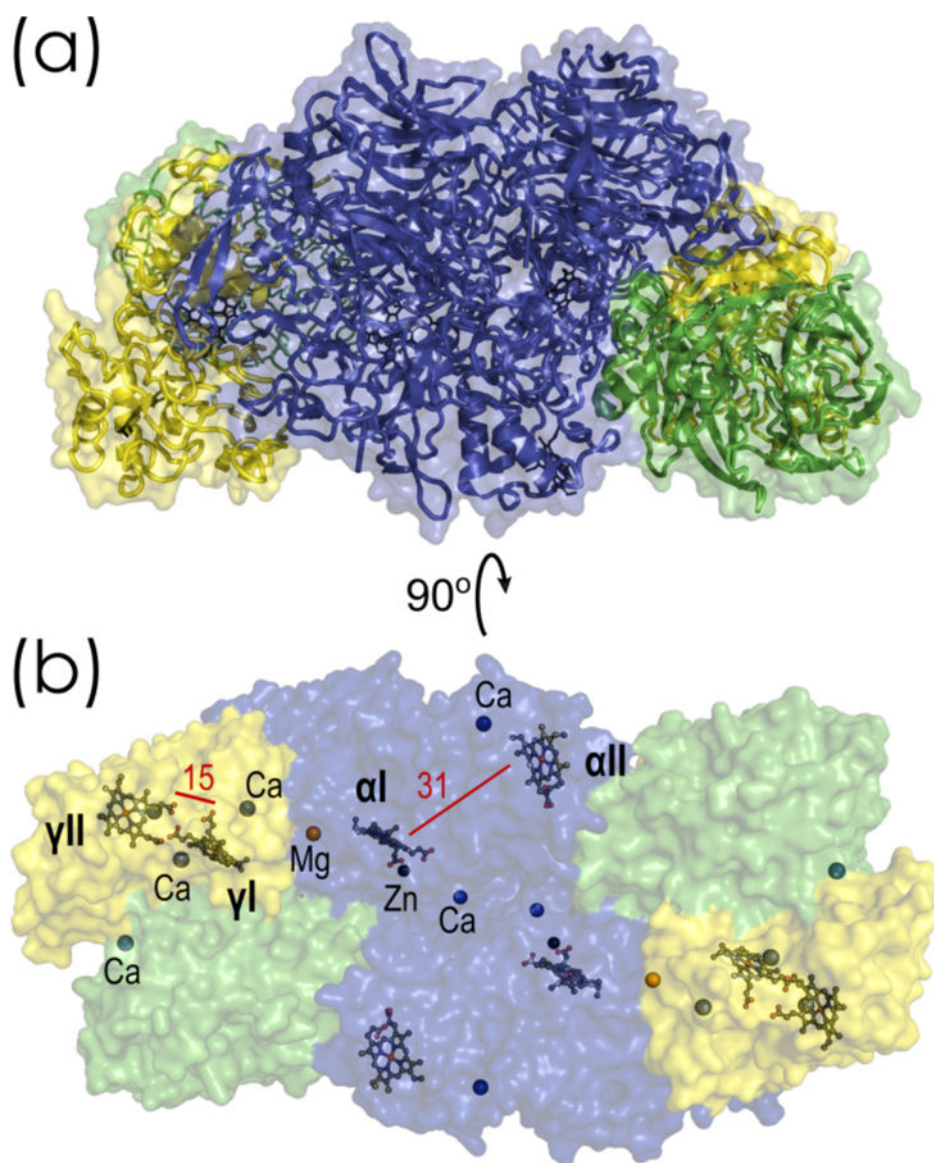


Figure 43.

Structure of the hydrazine synthase (HZS) dimer of heterotrimers. (a) Surface representation with overlaid cartoon. Subunits α , β , and γ are colored blue, green, and yellow, respectively. Heme cofactors are shown as black sticks. (b) Surface representation of the dimeric protein with the heme cofactors shown as sticks. Hemes are named with Greek letters and Latin numerals. Ca, Mg, and Zn are shown as spheres. Distances are indicated in Å. PDBID: 5C2V.

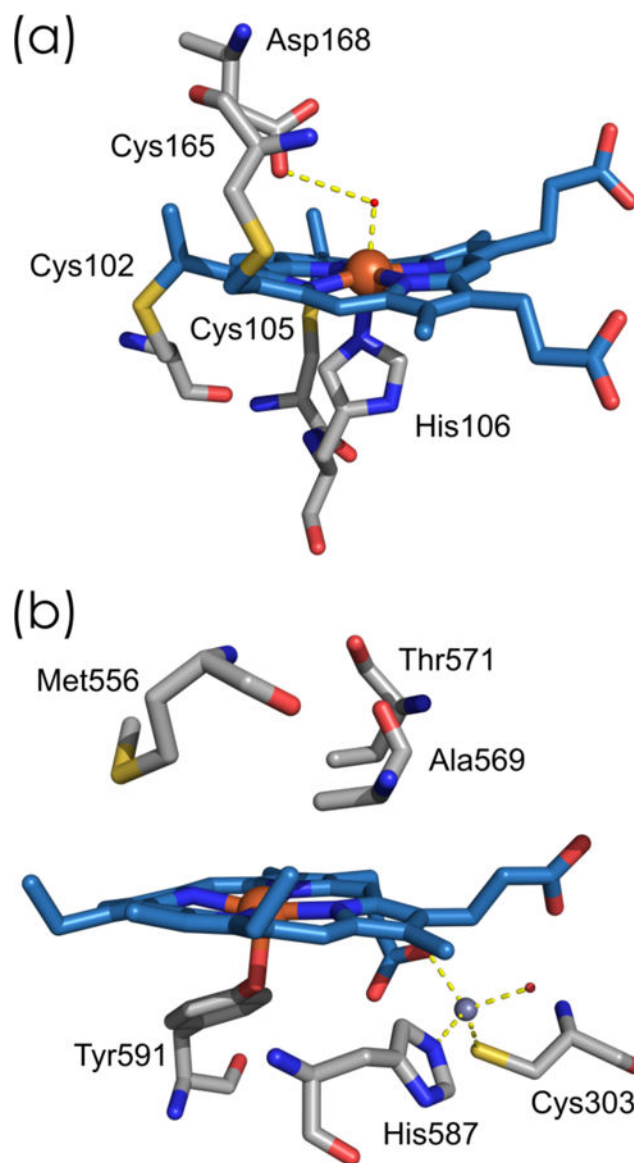
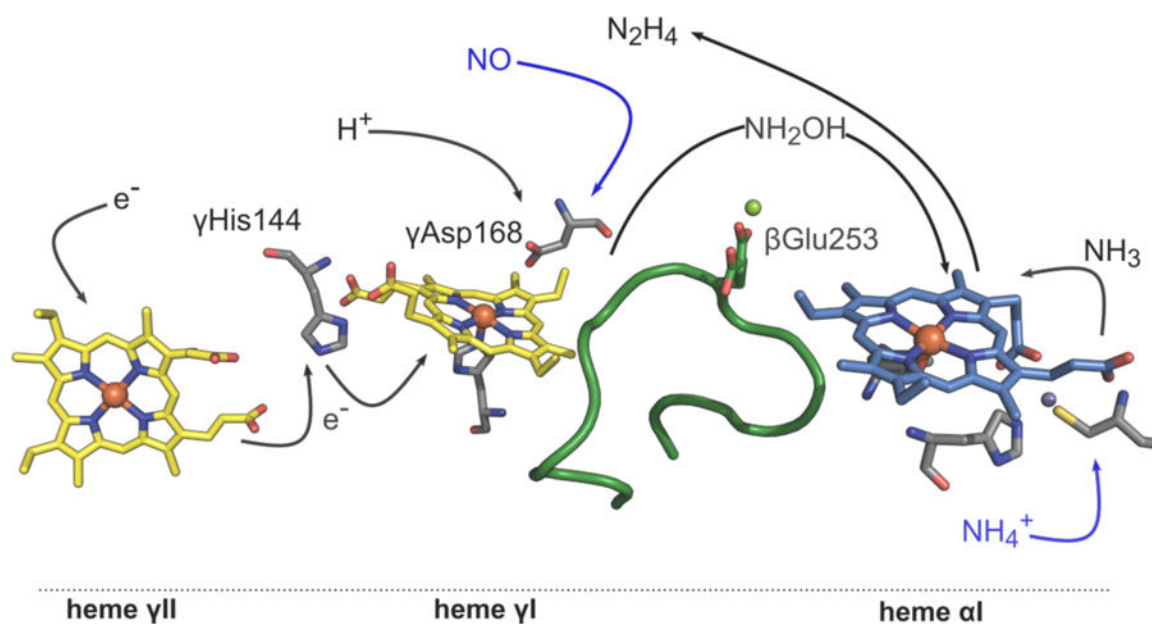


Figure 44.

Stick representation of the putative active site heme cofactors of HZS. (a) Heme γ I, where NO reduction to NH_2OH takes place. Heme γ I is covalently attached to the protein backbone via three cysteine sulfur atoms. Cys102 and Cys105 are part of the CXXCH heme binding motif and are bound to the vinyl groups of the heme moiety, while Cys165 is attached to the C1 porphyrin methyl group of heme γ I. (b) Heme α I, where comproportionation of NH_2OH and NH_3 yields hydrazine. His587 of the CXXCH heme binding motif is rotated away from the heme Fe and the hydroxyl group of Tyr591 is the proximal ligand instead. His587 is bound to a Zn ion (slate sphere). Water molecules are shown as red spheres. PDBID: 5C2V.

**Figure 45.**

Proposed catalytic mechanism for hydrazine synthesis catalyzed by HZS. NO enters the protein complex through a substrate channel that connects the protein surface to heme γ I. Electrons from the external electron donor enter the complex at heme γ II and are shuttled to heme γ I via γ His144. With the input of three protons from the solvent reaching heme γ I via the conserved γ Asp168, the nitrosyl complex undergoes a three-electron reduction to hydroxylamine at the first active site of HZS. NH_2OH is then diffusing to the second active site, heme α I, through an intraprotein tunnel which is possibly controlled by a 15-amino-acid-long loop of the β subunit (shown in green), harboring a conserved glutamate (β Glu253) that binds a magnesium ion (green sphere). A small branch of the identified tunneling system that is reaching heme α I from the proximal side is the assumed entry point of ammonium. An acid/base reaction that would yield ammonia might be taking place at the Zn site (slate sphere), before ammonia would then perform a nucleophilic attack on the nitrogen of NH_2OH , producing N_2H_4 through comproportionation. The latter would then leave the complex via a surface tunnel. PDBID: 5C2V.

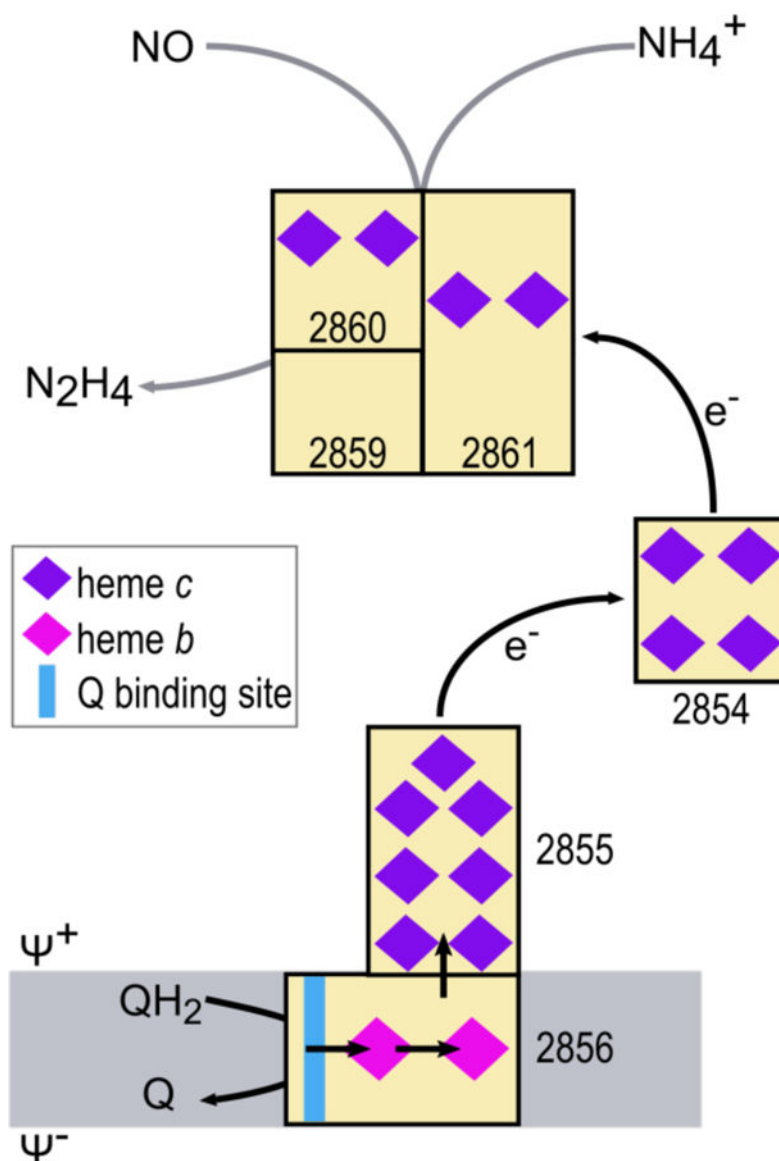
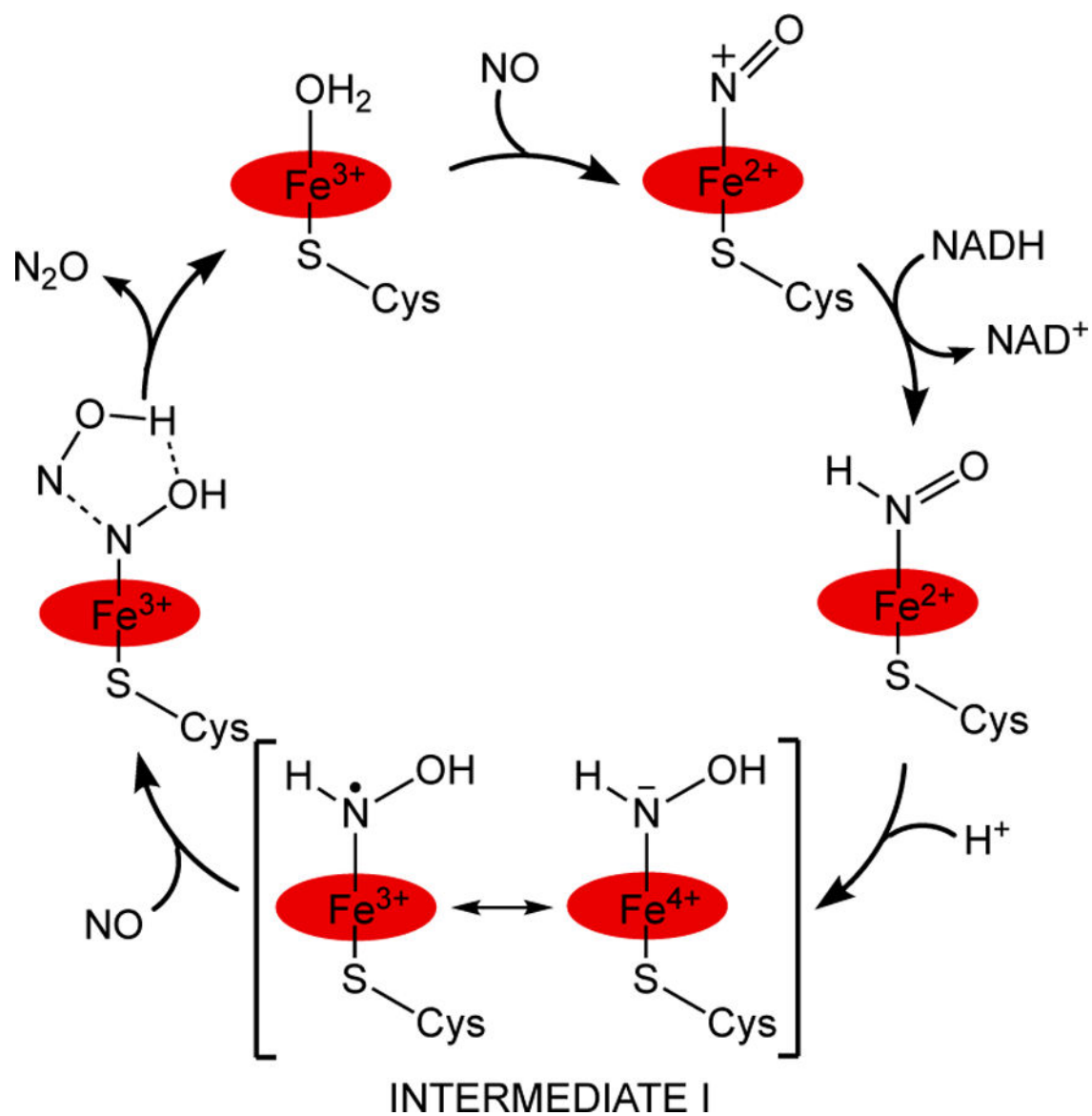
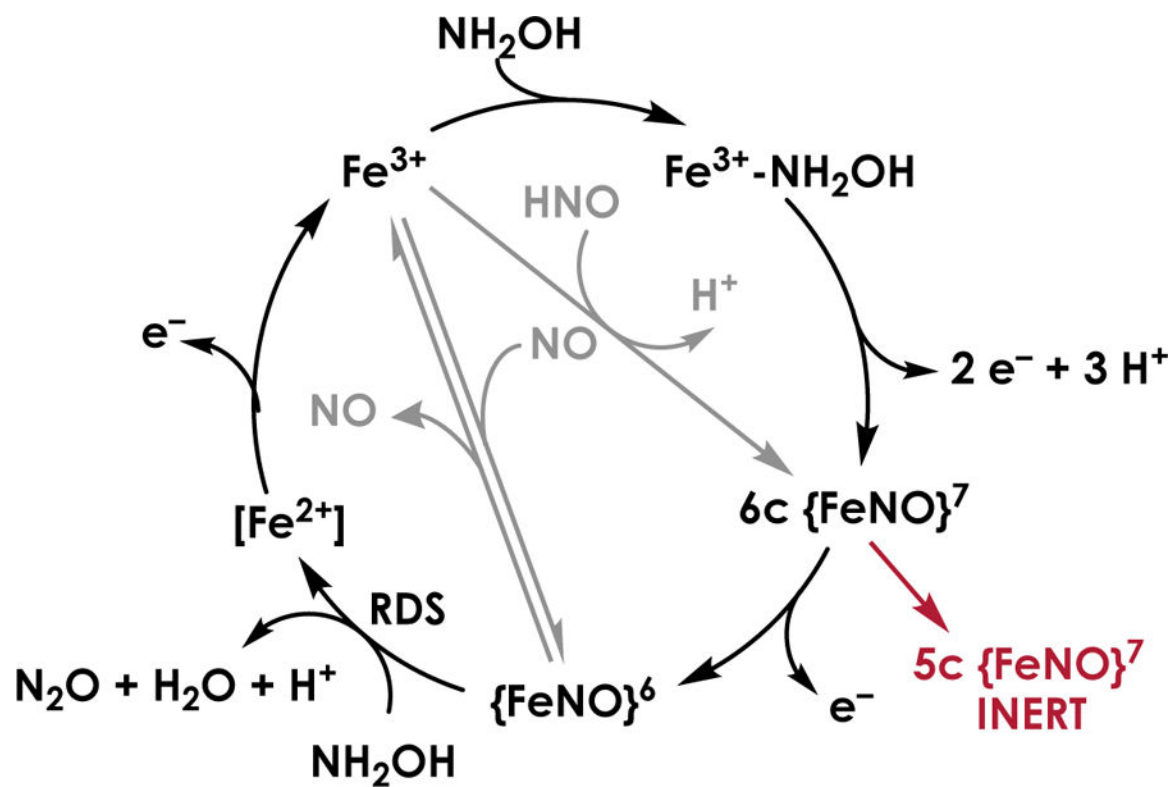


Figure 46. Proposed electron transfer module (ETM) for HZS. The ETM for N_2H_4 synthesis comprises the products of Kuste2854, Kuste2855, and Kuste2856 genes, respectively. An integral membrane protein harboring two *b*-type hemes and one quinone binding site (2856) would transfer the electrons yielded from quinol oxidation to a membrane-anchored heptaheme *c*-type cyt (2855). Subsequently, the soluble tetraheme electron carrier (2854) would donate them to the HZS catalytic complex (2859–2861). Numbers refer to the Kuste open reading frame numbers from the genome of *Kuenenia stuttgartiensis*. QH_2 : quinol; Q: quinone.

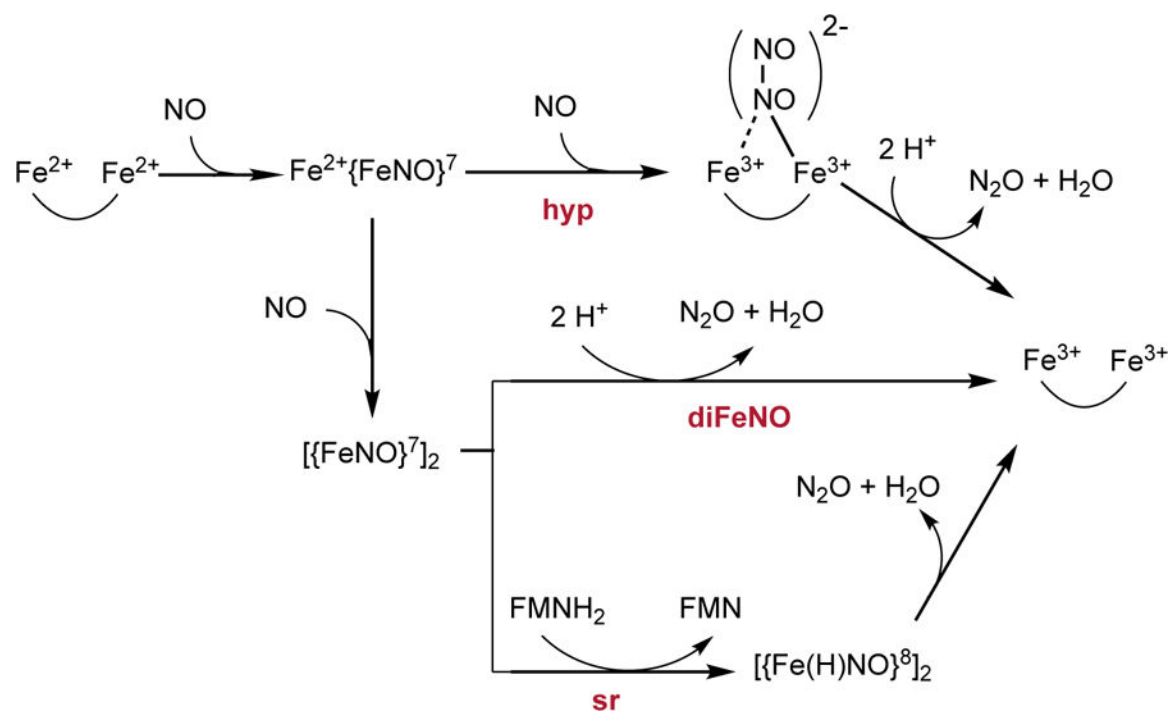


Scheme 2.

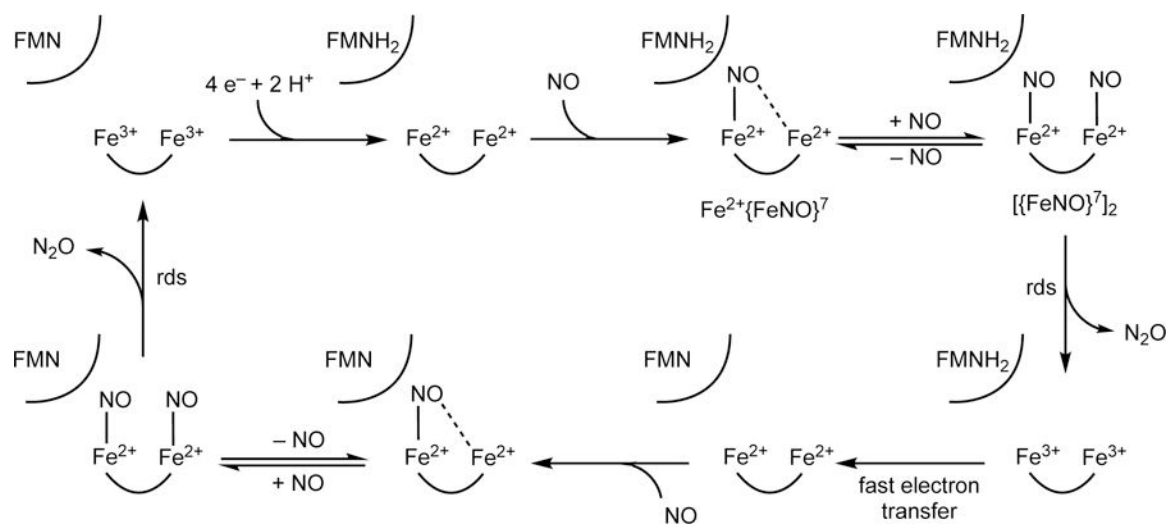
Working mechanism of P450nor catalysis. Adapted from Reference 8.

**Scheme 3.**

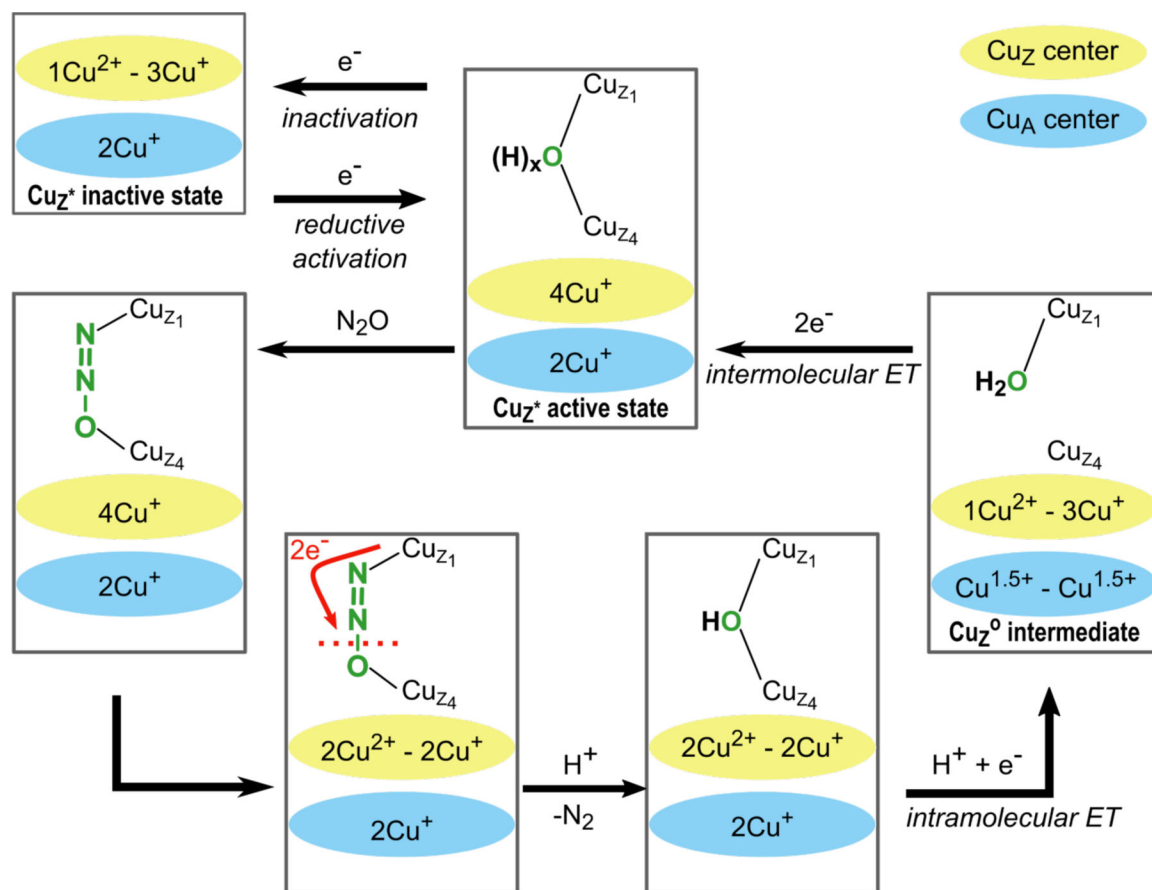
Working mechanism for cyt P460 NH₂OH-oxidase catalysis. Gray steps indicate reactions to shunt to intermediates, while the red step indicates generation of an off-pathway species.

**Scheme 4.**

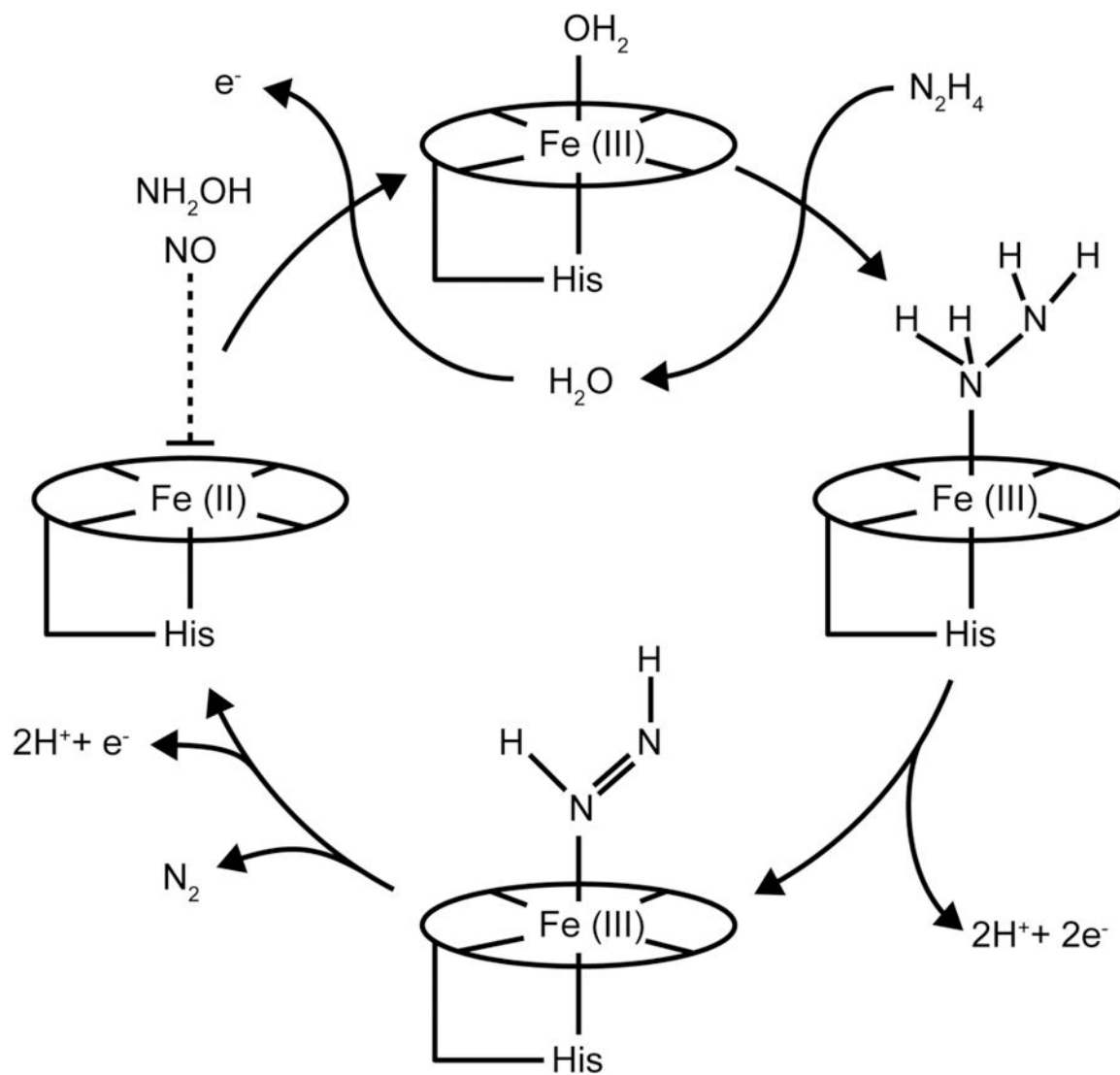
Proposed mechanisms for FDP NOR catalysis. Hyp denotes hyponitrite and sr denotes super-reduced.

**Scheme 5.**

FDP NOR mechanism proposed by Caranto and co-workers. Adapted from Ref ²⁸⁶.

**Scheme 6.**

Proposed mechanism for activation, catalytic redox cycle, and inactivation of N_2OR with the Cu_Z^* center conformation, according to Reference 371. The Cu_A and Cu_Z centers are represented by blue and yellow ovals, respectively. ET = electron transfer.

**Scheme 7.**

Putative mechanism of N_2H_4 oxidation to N_2 by the heme P460-like cofactors in HDH.

Figure reproduced with permission from Reference 424. Copyright ASBMB.

Table 1.

Different forms of N_2OR that have been isolated *in vitro*.

CuA	Redox state		CuZ type	Form	Color	Catalytic competence	Source	PDB ID	References
	CuA	CuZ							
$[Cu_{A1}^{1.5+}; Cu_{A2}^{1.5+}]$	$[2Cu_Z^{2+}; 2Cu_Z^{1+}]$ $[3Cu_Z^{2+}; 1Cu_Z^{1+}]$	Cu_Z	I	purple	inactive (under steady-state)	Anaerobic purification	3SBQ	368,374,376,389,417	
$[Cu_{A1}^{1.5+}; Cu_{A2}^{1.5+}]$	$[1Cu_Z^{2+}; 3Cu_Z^{1+}]$	Cu_Z^*	II	pink	reductive activation	Aerobic purification	2IWF	373,389,416	
$[Cu_{A1}^{1+}; Cu_{A2}^{1+}]$	$[1Cu_Z^{2+}; 3Cu_Z^{1+}]$	Cu_Z^*	III*	blue	Reductive activation	Aerobic purification in the presence of reductant Dithionite reduction of form I Ascorbate or dithionite reduction of form II	IQNI IFWX	389,392,422	
$[Cu_{A1}^{1+}; Cu_{A2}^{1+}]$	$[1Cu_Z^{2+}; 3Cu_Z^{1+}]$	Cu_Z	III	blue	inactive (under steady-state)	Ascorbate reduction of form I	N/A	389,419	
$[Cu_{A1}^{1+}; Cu_{A2}^{1+}]$	$[4Cu_Z^{1+}]$	Cu_Z^*	super reduced	N/A	active	Methyl viologen reduction of either form II or III*	N/A	408,419	